UNIVERSITEIT VAN PRETORIA
UNIVERSITY OF PRETORIA
YUNIBESITHI YA PRETORIA

Spigot Capacity of Dense Medium Cyclones

Mohloana Kwena Magwai

Submitted in partial fulfilment of the requirements for the degree **Master of Engineering (Metallurgical Engineering)** in the Faculty of Engineering, Built Environment and Information Technology, University of Pretoria, Pretoria.

July 2007

Acknowledgements

The author would like to express his gratitude to the following for their contributions to the completion of this work:

- Project supervisor, Mr. Jeremy Bosman, for his guidance throughout the duration of this investigation.
- Prof. Chris Pistorius, for his keen interest and encouragement during the undertaking of the work.
- *Multotec Process Equipments* for funding this project and providing the spigots for the 350mm cyclone.
- Frank van Heerden of *Idwala Magnetite* for the generous donation of magnetite.
- *Mintek* for permission to use their plant for the testwork on the 350mm cyclone.
- Carl Bergman of *Mintek*, for his assistance in executing the testwork on the 350mm cyclones, and Abel Mokwena of *Mintek*, for his assistance with the raw materials.
- Abbey Mahlangu and Kennedy Khwanda for their assistance in carrying out the experiments on the 165mm cyclone.
- Nathan Shago, for his assistance in carrying out some of the experiments on the 165mm cyclone.
- Albert Venter, for technical support.
- My friend, Lesedi Dibakwane, for sacrificing some of his weekends to assist in carrying out some of the tests.

I would like to express great appreciation to my parents, Philemon and Christina Magwai, for their continued support and inspiration over the years. *Ke a le leboga Mokone le Motšhweneng*.

Lastly, I would like to express my deepest gratitude to my love, Mokgadi Pela, for her unwavering love and support.

Spigot Capacity of Dense Medium Cyclones

by

Mohloana Kwena Magwai

Supervisor : Mr. J.B. Bosman

Department : Materials Science and Metallurgical Engineering

Degree : Master of Engineering

Summary

Dense medium cyclones are used extensively in the mineral processing industry to beneficiate various minerals including coal, diamonds and iron ore, amongst others. According to Reeves (2002), "the cyclone has been installed in over one-quarter of the coal preparation plants worldwide". Dense medium cyclones have the ability to achieve high capacities, and simultaneously obtain sharp separations and high separation efficiencies. However, this piece of equipment does have a shortcoming in that its capacity is constrained by the solids carrying capacity of the spigot. This is termed the spigot capacity. There is uncertainty on whether the spigot capacities specified by DSM (Dutch State Mines), the original developers of the dense medium cyclone, can be increased or not, and how these capacities were determined. The purpose of this study is to establish a methodology to determine the spigot capacities of dense medium cyclones, and determine the parameters that influence these capacities.

In order to illustrate the significance of increasing the capacity of dense medium cyclones, the following coal example is used: In 2005, South Africa produced about 245Mt of coal valued at R35.86 billion. A significant proportion of this coal is beneficiated through dense medium cyclones. Therefore, an increase in the cyclone capacity, even if relatively small, represents a large number in terms of tonnages of coal produced or monetary gains.

It has been established clearly in this investigation that the maximum spigot capacity is reached at the onset of roping. A critical sinks ore concentration at which spigot overloading occurs has been observed. The simplest and best indicator of possible spigot overloading has been established to be the sinks ore concentration, measurement of this parameter could, however, prove challenging on most industrial cyclones. Further, spigot overloading of a dense medium cyclone can be detected visually by observing the discharge type at the sinks and monitoring particle misplacement to the floats stream.

A regression model that quantifies the spigot capacity, in terms of ore and slurry, has been developed. Various parameters were considered in the model, these include: cyclone geometry, feed head, medium density, and medium grade. Parameters that influence the spigot capacity of dense medium cyclones have been established, and their effect on the spigot capacity has been quantified.

The spigot capacity values obtained in this investigation were compared with those specified by DSM, and it was concluded that there is large potential to increase the 'spigot capacities' specified by DSM.

Keywords: Dense medium cyclone; Hydrocyclone; Dense medium separation; Spigot capacity; Spigot loading; Roping.

Table of Contents

CHAPTER 1. INTRODUCTION 1
CHAPTER 2. LITERATURE REVIEW 5
2.1. Classification Hydrocyclones 6
2.1.1. Characterisation of Overloading at the Underflow 6
(a) Air Core and Roping 7
(b) Underflow Solids Concentration 10
(c) Effect of Roping on Cyclone Operation 16
2.1.2. The Influence of Cyclone Geometry on the Spigot Capacity 22
(a) Inlet Size 22
(b) Spigot Diameter 23
(c) Vortex Finder Diameter 30
(d) Cone Angle and Barrel Length 31
2.1.3. The Influence of Operational Variables on the Spigot Capacity 33
(a) Feed pressure 33
(b) Ore Size 33
(c) Ore Density 36
(d) 'Overflow Throttling' 37
2.2. Dense Medium Cyclones 38
2.2.1. Characterisation of Overloading at the Sinks 38
(a) Sinks Ore Concentration 38
(b) Effect of roping on cyclone performance 42
2.2.2. Influence of Cyclone Geometry on Spigot Capacity 46
(a) Inlet Size 46
(b) Spigot Diameter 46
(c) Vortex Finder Diameter 50
(d) Cone Angle 51
(e) Barrel Length 52
2.2.3. Influence of Operational Variables on Spigot Capacity 54
(a) Feed pressure 54
(b) Medium Density 56
(c) Medium Grade 57
(d) Ore Size 57

(e) Ore Density 57
2.3. Summary of Literature Review 59
(a) Characterisation of Overloading at the Spigot 59
(b) Influence of Roping on Cyclone Performance 60
(c) Effect of Cyclone Geometry on Spigot Capacity 61
(d) Effect of Operational Variables on Spigot Capacity 62
(e) Classification vs Dense Medium Cyclones 63
CHAPTER 3. EXPERIMENTAL APPROACH 65
3.1. Experimental Set-up - 165mm Cyclone 66
3.1.1. Experimental Procedure: Characterisation of Overloading at Sinks 67
3.1.2. Experimental Procedure: Effect of Variables 69
3.2. Experimental Set-Up and Procedure- 350mm Cyclone 72
3.2.1. Variables Investigated 75
3.3. Experimental Matrix 76
CHAPTER 4. RESULTS AND DISCUSSION 83
4.1. Characterisation of Overloading at the Sinks 84
4.1.1. Spigot Loading 85
4.1.2. The Sinks Ore Concentration 90
4.1.3. Slurry Flow 94
4.1.4. Medium Flow 98
4.1.5. Density Differential 101
4.2. Quantifying the Spigot Capacity 105
4.2.1. Model Development 115
(a) Spigot Capacity 115
(b) Cyclone Capacity 121
(c) Volume Split 122
(d) Sinks Ore Concentration 124
(e) Medium Split to Sinks 125
4.2.2. Comparison with DSM Spigot Capacities 127
4.2.3. Influence of Cyclone Geometry on Spigot Capacity 132
(a) Spigot Diameter 132
(c) Vortex Finder Diameter 137
(d) Inlet Size 139
(e) Cyclone Diameter 140

(f) Cone Angle 140
(g) Barrel Length 140
4.2.4. Influence of Operational Variables on Spigot Capacity 141
(a) Feed Pressure 141
(b) Medium Density 143
(c) Medium Grade 147
(d) Ore Size and Size Distribution 147
CHAPTER 5. CONCLUSIONS AND RECOMMENDATIONS 152
5.1. Conclusions 153
(a) Characterization of Overloading at the Sinks 153
(b) Effect of Cyclone Geometry on Spigot Capacity 155
(c) Effect of Operational Variables on Spigot Capacity 157
(d) Comparison with DSM 157
(e) Model 159
5.2. Recommendations 160
CHAPTER 6. REFERENCES 162
CHAPTER 7. APPENDIX 170
7.1. Appendix A 171
7.2. Appendix B: Processed Data and Experimental Conditions 183
7.2.1. Data for tests performed with 15^{o} cone. 183
7.2.2. Data for tests performed with 20^{o} cone (cone A). 192
7.2.3. Data for tests performed with 20^{o} cone (cone B) 195
7.2.4. Data for tests performed with the 350mm cyclone. 196
7.3. Appendix C. Raw Data and Experimental Conditions 197
7.3.1. Raw data for tests performed with 15^{o} cone. 197
7.3.2. Raw data for tests performed with cone A. 208
7.3.3. Raw data for cyclone operating with cone B 211

List of Figures

Figure. 1.1. Cyclone geometry. (Adapted from Bosman 2003b) 3
Figure 1.2. Milled and atomized ferrosilicon. (Grobler, 2006) 3
Figure 2.1. Schematic diagram showing spray, semi-rope and rope discharges at the underflow of a hydrocyclone. (Neesse et al., 2004a)..... 7
Figure 2.2. Resistivity images showing the air core below the feed inlet of a 44mm diameter hydrocyclone. (Gutiérrez et al. 2000) 7
Figure 2.3. The influence of feed solids' concentration on the air core size. (Gutiérrez et al., 2000)..... 8
Figure 2.4. Angle of discharge for the underflow slurry with changing feed flow-rate and solids concentration. (Gutiérrez et al., 2000) 9
Figure 2.5. The influence of solids concentration on the apparent viscosity of the pulp. Particle size range: -75+50µm. (Aplan, 1985)..... 9
Figure 2.6. The underflow solids concentration at which roping was initiated for ores of different densities. (From Mular and Jull, 1978 adapted in Heiskanen, 2000) 11
Figure 2.7. Influence of feed solids on roping. (Plitt et al., 1987).....12
Figure 2.8. Underflow solids concentration during the transition from spray to rope discharge for (a) a 69mm test cyclone and (b) a 300mm plant cyclone. (Adapted from Fahlstrom, 1963).....13
Figure 2.9. Solids recovery in the underflow as a function of material coarser that the separation size in the feed for a 69mm test cyclone. Fahlstrom (1963). Curve 1: $\%V_{SF}$ = 3.9, 8.4 and 19.6%. Curve 2: $g_u = C_i^+$ 13
Figure 2.10. The influence of feed concentration on the critical underflow concentration at which roping commences. (Flintoff et al., 1987) 15
Figure 2.11. The influence of feed volume concentration on the underflow concentration during roping. The dotted line represents a plot of equation 2.1, and the solid line is equation 2.2. (Heiskanen, 2000).....15
Figure 2.12. Overflow pulp density during the transition from spray to rope discharge. Curve 1: 69mm test cyclone at various $\%V_{SF}$. Curves 2, 3 and 4: $\%V_{SF}$ = 15.1, 21.7 and 37.4%, respectively, with D_c = 300mm. (Fahlstrom, 1963).....16
Figure 2.13. The influence of commencement of roping on the cut-size. (Abbot, 1967a).....17
Figure 2.14. Change in the separation size during roping. Curve 1: $\%V_{SF}$= 3.9, 8.4 and 19.6%. (Fahlstrom, 1963) 17
Figure 2.15. The relationship between separation size and solids recovery in U/F (mass fraction). (Fahlstrom, 1963). 18
Figure 2.16. Influence of roping on cyclone performance at (a) low (~7% by volume) (b) intermediate (~18%) and (c) high (~34%) feed solids concentrations. (Plitt et al., 1987) 19
Figure 2.17. The influence of particle misplacement on the shape of the Tromp curve during rope and spray discharges. (Trawinski, 1976) 20
Figure 2.18. Effect of coarse particles misplacement to the overflow on the partition curve. (Kelly, 1991).....20
Figure 2.19. Influence of roping on cyclone performance. $\%V_{SF}$ = 8.4%, D = 69mm and D_o = 16mm. Curves 1, 2, 3, 4 correspond to D_u = 3, 5, 7,9mm. (Fahlstrom, 1963).....21
Figure 2.20. Effect of the spigot size on spigot capacity. (Tarr, 1985) 24

Figure 2.21. Effect of the spigot size on spigot capacity. (Jull, 1972) 24
Figure 2.22. Spigot capacity under rope and near rope conditions. (Plitt et al., 1987) 25
Figure 2.23. Relationship between spigot diameter and spigot ore capacity. (Heiskanen, 2000) 26
Figure 2.24. (a) Comparison of the spigot size-spigot capacity relationships proposed by various authors. (b) Curve in (a) at smaller spigot sizes on normal scale. 27
Figure 2.25. Underflow solids concentration during roping with changing D_o/D_u. Curves 1, 2 and 3 correspond to $\%V_{SF}$ = 19.6, 8.4 and 3.9%. (Fahlstrom, 1963).....28
Figure 2.26. The influence of the spigot-to-vortex finder diameter ratios on the underflow density. (Heiskanen, 2000) 28
Figure 2.27. The influence of feed concentration on the critical underflow concentration at which roping commences. (Flintoff, 1987) 29
Figure 2.28. D_u/D_o ratios at which roping is likely to occur according to Concha et al. (1996). 30
Figure 2.29. Effect of slurry viscosity on the maximum tangential velocity within a hydrocyclone. (Dyakowski and Williams, 1995) 34
Figure 2.30. Effect of 50% passing particle size on underflow concentration during roping. (Plitt et al., 1987) ..35
Figure 2.31. Effect of median particle size of underflow on $\%V_{MSU}$. (Heiskanen, 2000).....35
Figure 2.32. Effect of the size distribution of particles at the underflow on the underflow solids concentration at which roping commences. (Heiskanen, 2000) 36
Figure 2.33. Effect of particle density on spigot capacity. (Jull, 1972).....36
Figure 2.34. Separation density vs ore recovery in sinks (mass fraction) for coal. (Upadrashta and Venkateswarlu, 1982) 42
Figure 2.35. Separation density vs ore recovery in sinks (mass fraction). (Upadrashta and Venkateswarlu, 1982) 43
Figure 2.36. Influence of spigot overloading on the cyclone performance. Spigot overloaded at D_u = 12.5mm and normal operation at D_u = 19.5mm. (Stas, 1957).....45
Figure 2.37. The spigot overloading on the shape of the partition curve. (Leonard and Leonard, 1983) 45
Figure. 2.38. The relationship between spigot diameter and spigot capacity for coal. (DSM, 1985) 48
Figure 2.39. The relationship between spigot diameter and spigot capacity for coal.....49
Figure. 2.40. The relationship between spigot diameter and spigot capacity for industrial minerals and ores with increasing feed pressure. (DSM, 1985) 49
Figure 2.41. The influence of the barrel length on the spigot capacity. (DSM, 1985) 52
Figure 2.42. The influence of the barrel length on the cyclone capacity. (DSM, 1985) 53
Figure. 2.43. The effect of feed pressure on spigot capacity. (DSM, 1985).....55
Figure 2.44. The effect of ore density on spigot capacity. (DSM, 1985) 58
Figure 3.1. (a) A schematic of the test rig and (b) polyurethane cyclone employed to perform the experiments..66
Figure 3.2. The test rig, with a 165mm cyclone, on which the experiments were performed.....67
Figure 3.3. The 20^o cone with changeable spigots. (Cone A) 70
Figure 3.4. The 200mm long barrel used during the experiments.....70
Figure 3.5 Pictures of the 350mm dense medium cyclone used to perform the validation work.....73
Figure 4.1. Spray discharge at the sinks for the (a) 165mm cyclone, and (b) 350mm cyclone.....85

Figure 4.2. Semi-rope discharge at the sinks for the (a) 165mm cyclone, and (b) 350mm cyclone. 85
Figure 4.3. Rope discharge at the sinks for the (a) 165mm cyclone, and (b) 350mm cyclone.....86
Figure 4.4. Changes in the ore loading at both the floats and sinks streams as ore was added into the cyclone for a 45mm spigot. Data points with white and grey backgrounds were obtained during spray and semi-rope discharges, respectively. While data points with black background were obtained during roping. 86
Figure 4.5. Changes in the ore loading at both the floats and sinks streams as ore was added into the cyclone for a 34mm spigot.....87
Figure 4.6. Changes in the ore loading at both the floats and sinks streams as ore was added into the cyclone for a 25mm spigot.....89
Figure 4.7. Volumetric recovery of ore to sinks during the transition to roping for various spigot diameters.....89
Figure 4.8. The volumetric ore concentration at the sinks for a 45mm spigot. Data points with white and grey backgrounds were obtained during spray and semi-rope discharges, respectively. While data points with black background were obtained during roping.....90
Figure 4.9. The volumetric medium-to-ore ratio at the underflow for a 45mm spigot. Data points with white and grey backgrounds were obtained during spray and semi-rope discharges, respectively. While data points with black background were obtained during roping. 91
Figure 4.10. The volumetric ore concentration at the sinks for the 25 and 34mm spigots.....92
Figure 4.11. The volumetric medium-to-ore ratio at the sinks for the 25 and 34mm spigots during the transition to roping. 92
Figure 4.12. Range of all ore concentrations obtained in this investigation when roping was prevalent at the sinks. 93
Figure 4.13. Range of all the sinks medium-to-ore ratios obtained in this investigation when roping was prevalent at the sinks.....94
Figure 4.14. Slurry loading at the sinks for the 45mm spigot. Data points with white and grey backgrounds were obtained during spray and semi-rope discharges, respectively. While data points with black background were obtained during roping. 95
Figure 4.15. Slurry loading at the sinks for the 25 and 34 mm spigot. 96
Figure 4.16. Cyclone throughput (both ore and slurry) during the transition to rope discharge for the 45mm spigot. Data points with white and grey backgrounds were obtained during spray and semi-rope discharges, respectively. While data points with black background were obtained during roping.....97
Figure 4.17. Cyclone slurry throughput during the transition to rope discharge for the 25 and 34mm spigots. 97
Figure 4.18. Medium flow-rate at the floats and sinks during the transition to rope discharge for the 45mm spigot. Data points with white and grey backgrounds were obtained during spray and semi-rope discharges, respectively. While data points with black background were obtained during roping.....99
Figure 4.19. Medium flow-rate at the sinks during the transition to rope discharge for the 25 and 34mm spigots. 99
Figure 4.20. Medium flow-rate at the floats during the transition to rope discharge for the 25 and 34mm spigots. 100
Figure 4.21. The relationship between R_f and R_m when spray and semi-rope discharges were prevalent at the sinks. 100

Figure 4.22. The relationship between R_f and R_m when rope discharge was prevalent at the sinks.....101
Figure 4.23. Density differential across the cyclone during the overloading of the 45mm spigot. Data points with white and grey backgrounds were obtained during spray and semi-rope discharges, respectively. While data points with black background were obtained during roping. 102
Figure 4.24. Density differential across the cyclone during the overloading of the 25 and 45mm spigots.....102
Figure 4.25. Range of density differential obtained during roping for all the tests performed with fine magnetite. 103
Figure 4.26. Influence of feed concentration on the floats and sinks medium densities for the 45mm spigot. Data points with white and grey backgrounds were obtained during spray and semi-rope discharges, respectively. While data points with black background were obtained during roping. 103
Figure 4.27. Influence of feed concentration on the floats and sinks medium densities for the 34mm spigot.....104
Figure 4.28. Influence of feed concentration on the floats and sinks medium densities for the 25mm spigot.....104
Figure 4.29. The effect of spigot diameter on Q_{USM}.....106
Figure 4.30. The effect of spigot diameter on Q_{UM}. 107
Figure 4.31. The effect of spigot diameter on Q_{USM} (15^o cone angle).....107
Figure 4.32. The effect of spigot diameter on Q_{UM} (15^o cone angle). 108
Figure 4.33. Schematic cross sectional view of the 15^o cone angle for (a) larger spigot and (b) smaller spigot. 109
Figure 4.34. The effect of spigot diameter on Q_{USM}. (Cone A - 20^o) 110
Figure 4.35. The effect of spigot diameter on Q_{UM}. (Cone A - 20^o).....110
Figure 4.36. Schematic cross sectional view of cone A (20^o) for (a) larger spigot and (b) smaller spigot. 111
Figure 4.37. A picture of cone B.....112
Figure 4.38. A schematic diagram of the cross-section through cone B. 112
Figure 4.39. The influence of spigot design on Q_{USM}. (Operating conditions are given in Table A.5).....113
Figure 4.40. The influence of spigot design on Q_{UM}. (Operating conditions are given in Table A.5). 113
Figure 4.41. Configuration of a 350mm DSM cyclone. (Narasimha et al., 2007) 114
Figure 4.42. Predicted versus measured Q_{USM} values for equation 4.3 with parameter values in Table 4.9.....117
Figure 4.43. Predicted versus measured Q_{UM} values for equation 4.4 with parameter values in Table 4.10. 118
Figure 4.44. The effect of medium density on Q_{UM} for the 350mm cyclone. (The plotted lines represent equation 4.5.) 118
Figure 4.45. The effect of D_u on Q_{UM} for the 165mm and 350mm cyclones. 120
Figure 4.46. Predicted versus measured Q_{UM} values for equation 4.5 with parameter values in Table 4.11. 120
Figure 4.47. A closer look at the lower Q_{UM} values in Fig. 4.43.....121
Figure 4.48. Predicted versus measured Q values for equation 4.6 with parameter values in Table 4.12.....122
Figure 4.49. Predicted versus measured S values for equation 4.7 with parameter values in Table 4.13. 124
Figure 4.50. Predicted versus measured C_{mvu} values for equation 4.8 with parameter values in Table 4.14. 125
Figure 4.51. Predicted versus measured R_m values for equation 4.10 with parameter values in Table 4.15.....126
Figure 4.52. Comparison of the spigot diameter-spigot capacity relationship obtained in this study with that by DSM.....127
Figure 4.53. Comparison of Q_{UM} obtained in this study and those specified by DSM. 128

Figure 4.4. Changes in the ore loading at both the floats and sinks streams as ore was added into the cyclone for a 45mm spigot. Data points with white and grey backgrounds were obtained during spray and semi-rope discharges, respectively. While data points with black background were obtained during roping. 129
Figure 4.54. Comparison of Q_{UM} predicted from eq. 4.5 (to correct for effect of D) and those specified by DSM. 130
Figure 4.55. Comparison of Q_{UM} predicted from eq. 4.5 (to correct for effect of D) and those specified by DSM. Dashed line is extrapolation of eq. 4.11. 131
Figure 4.56. The effect of D_u on Q_{UM} for the 165mm cyclone operating with cone A. Plotted lines represent **a.** equation 4.4, and **b**. equation 4.5. 132
Figure 4.57. The effect of D_u on Q_{UM} for both the 165mm (cone A) and 350mm cyclones. Plotted lines represent equations 4.4 ($D_u \leq 45$mm) and 4.5 ($D_u \geq 60$mm). 133
Figure 4.58. The effect of D_u on Q_{UM}. (Jull, 1972) 134
Figure 4.59. The effect of D_u on C_{mvu}. (Cone A - 20^o) 134
Figure 4.60. Porosity in tubes packed with various materials for increasing ratios of particle diameter to tube diameter. (Leva, 1959) 135
Figure 4.61. The effect of spigot diameter on R_m. (Cone A - 20^o) 136
Figure 4.62. Influence of spigot size on volumetric percentage of magnetite particles at the sinks (Cone A –20^o). 137
Figure 4.63. The effect of vortex finder diameter on Q_{USM} (Cone A - 20^o). 137
Figure 4.64. The effect of vortex finder diameter on Q_{UM} (Cone A - 20^o). 138
Figure 4.65. The effect of H on Q_{USM}. (165mm cyclone – cone A) 141
Figure 4.66. The effect of H on Q_{UM}. (165mm cyclone – cone A) 142
Figure 4.67. The effect of H on Q_{UM}. (350mm cyclone). 142
Figure 4.68. The effect of medium density on Q_{USM}. (165mm cyclone – cone A) 143
Figure 4.69. The effect of medium density on Q_{UM}. (165mm cyclone –cone A) 144
Figure 4.44. The effect of medium density on Q_{UM}. (350mm cyclone) 145
Figure 4.70. The effect of medium density on density differential. (The operating conditions are given in Table A.6 in Appendix A.) 145
Figure 4.71. The effect of medium density on density differential. (He and Laskowski, 1995b) 146
Figure 4.72. Influence of feed medium density on the volumetric percentage of magnetite particles at the sinks. 146
Figure 4.73. The effect of ore size on Q_{USM}. (Full details on the operating conditions are given in Table A.7 in Appendix A) 148
Figure 4.74. The effect of ore size on Q_{UM}. (Full details on the operating conditions are given in Table A.7 in Appendix A) 149
Figure 4.75. The effect of ore size on C_{mvu}. (Full details on the operating conditions are given in Table A.7 in Appendix A) 149
Figure 4.76. The effect of ore size on Q_{USM}: -1.8+0.8mm vs –3+1mm. (Full details on the operating conditions are given in Table A.8 in Appendix A). 150

Figure 4.77. The effect of ore size on Q_{UM}: -1.8+0.8mm vs –3+1mm. (Full details on the operating conditions are given in Table A.8 in Appendix A).....150
Figure 4.78. The effect of ore size on C_{mvu}: -1.8+0.8mm vs –3+1mm. (Full details on the operating conditions are given in Table A.8 in Appendix A).....151
Figure 5.1. C_{mvu} expressed in terms of volumetric medium-to-ore ratio at the sinks.....153
Figure 4.55. Comparison of Q_{UM} predicted from eq. 4.5 (to correct for effect of D) and those specified by DSM. Dashed line is extrapolation of eq. 4.11.....158
Figure A.1. The 165mm cyclone with the underflow elbow on.....176
Figure A.2. The pressure gauge used to measure the feed pressure.....177
Figure A.3. SEM image of the magnetite employed during the test-work.....177
Figure A.4. A picture of the dense medium cyclone plant at Mintek, Randburg, South Africa.....178
Figure A.5. The pressure gauge employed during the test-work with the 350mm cyclone. The pressure gauge was 0.915m below the feed inlet.....178
Figure A.6. The Marcy scale and 'density bottle' used to measure the medium density.....179
Figure A.7. The demagnetizing coil at the DMS plant.....179
Figure A.8. The area where the sievebends, receiving the floats and sinks slurries, were removed.....180
Figure A.9. The log-sheet used during flow-rate measurements.....181
Figure A.10. The log-sheet used during analysis of samples from the float and sink streams.....182

List of Tables

Table 2.1. Various $\%V_{MSU}$ obtained by different workers. 14
Table 2.2. The exponent *n* for the relationship between cyclone throughput and inlet diameter. 23
Table 2.3. D_u/D_o ratios at which roping is likely to occur according to Concha et al. (1996). 29
Table 2.4. The exponent *n* for the relationship between Q and D_o ratio. 30
Table 2.5. The exponent *n* for the relationship between S and D_u/D_o ratio. 31
Table 2.6. The exponent *n* for the relationship between cyclone capacity and feed pressure. 33
Table 2.7. Ore concentration at the feed and sinks for coal. Sinks concentrations based on assumption that 40% (v/v) of feed pulp was recovered in sinks. (DSM, 1985) 40
Table 2.8. Ore concentrations in the floats based on the assumption that 40% (v/v) of the feed pulp was recovered at the sinks. 41
Table 2.9. Ore concentrations in the feed when the cyclones were operating at their spigot capacities. (England et al., 2002) 41
Table 2.10. Constants a_o and a_1 for equation 2.10. 44
Table 2.11. The exponent *n* for the relationship between inlet diameter and Q. 46
Table 2.12. The exponent *n* for the relationship between Q and D_u. 47
Table 2.13. The exponent *n* for the relationship between S and D_u. 47
Table 2.14. Dimensions of the cyclones employed by DSM, as a fraction of the cyclone diameter. 50
Table 2.15. The exponent *n* for the relationship between Q and D_O. 51
Table 2.16. Feed concentrations for the curves in Fig. 2.41 and 2.42. (DSM, 1985) 53
Table 2.17. The exponent *n* for the relationship between Q and feed pressure. 54
Table 2.18. The exponent *n* for the relationship between S and head. 54
Table 2.19. The exponent *n* for the relationship between Q and medium density. 56
Table 2.20. The exponent *n* for the relationship between Q and medium density according to Upadrashta and Venkateswarlu (1982). 56
Table 2.21. Comparison of spigot diameter-spigot capacity relationships in the literature. 61
Table 3.1. Screen analysis of the fine magnetite. 67
Table 3.2. The configuration of the cyclone used to perform test-work. 68
Table 3.3. Cyclone dimensions tested during the experimental work. 69
Table 3.4. Operating conditions tested during the experimental work. 71
Table 3.5. The dimensions of the 350mm industrial-scale cyclone. 72
Table 3.6. Conditions tested on the 350mm dense medium cyclone. 76
Table 3.7 Conditions tested when operating with the 15^o cone angle and D_i =0.2D, with silica that had a size range of –1.8+0.8mm. (Roping only) 77
Table 3.8. Conditions tested when operating with the 15^o cone angle and D_i =0.2D, with silica that had a size range of –3+1mm. (Roping only) 78
Table 3.9. Conditions tested when operating with the 15^o cone angle and D_i =0.3D. (Roping only) 79
Table 3.10. Conditions tested when operating with cone A and D_i =0.2D. (Roping only) 80
Table 3.11. Conditions tested when operating with cone A and D_i =0.3D. (Roping only) 81

Table 3.12. Conditions tested when operating with cone B. (Roping only).....82
Table 3.13. Conditions tested when operating the 350mm dense medium cyclone. (Roping only) 82
Table 4.1 The feed ore concentrations at which roping commenced for the various spigot sizes.....88
Table 4.2. Parameter values for equation 4.1. 93
Table 2.21. Spigot diameter-spigot capacity relationships in literature. 105
Table 4.3. Parameter values for equation 4.2 obtained for all the data acquired with the 165mm dense medium cyclone. 105
Table 4.4. Parameter values for equation 2.13 obtained for all the data acquired with the 165mm dense medium cyclone. 106
Table 4.5. Parameter values for equation 4.2 obtained for all the data acquired with the 165mm cyclone when operating with the 15^{o} cone angle. 108
Table 4.6. Parameter values for equation 2.13 obtained for all the data acquired with the 165mm cyclone when operating with the 15^{o} cone angle. 108
Table 4.7. Parameter values for equation 4.2 obtained for all the data acquired with the 165mm cyclone when operating with the 20^{o} cone angle. 110
Table 4.8. Parameter values for equation 2.13 obtained for all the data acquired with the 165mm cyclone when operating with the 20^{o} cone angle. 111
Table 4.9. Summary of statistical results from multiple-regression of Q_{USM} data obtained with the 165mm cyclone (cone A). 116
Table 4.10. Summary of statistical results from multiple-regression of Q_{UM} data obtained with the 165mm cyclone (cone A). 117
Table 4.11. Summary of statistical results from multiple-regression of Q_{UM} data obtained with the 165mm (cone A) and 350mm cyclones. 119
Table 4.12. Summary of statistical results from multiple-regression of Q data obtained with the 165mm cyclone (cone A). 122
Table 4.13. Summary of statistical results from multiple-regression of data obtained with the 165mm cyclone (cone A). 123
Table 4.14. Summary of statistical results from multiple-regression of C_{mvu} data obtained with the 165mm cyclone (cone A). 124
Table 4.15. Summary of statistical results from multiple-regression of R_m data obtained with the 165mm cyclone (cone A). 126
Table 4.16. Comparison of Q_{UM} obtained in this study and those specified by DSM. 128
Table 4.17. Comparison of Q_{UM} predicted with eq. 4.5 and those specified by DSM. 130
Table 5.1. Number of cyclones required to reach the spigot ore capacity of a 350mm cyclone when using a combination of smaller cyclones or those with smaller D_u. 156
Table 5.2. R^2 values for the various equations developed in the current study. 159
Table A.1. Dimensions of the dense medium cyclones employed by DSM. 171
Table A.2. Results obtained when characterizing overloading behaviour of the 45mm spigot. 171
Table A.3. Results obtained when characterizing overloading behaviour of the 34mm spigot. 172
Table A.4. Results obtained when characterizing overloading behaviour of the 25mm spigot. 172

Table A.5. The influence of spigot design on the spigot capacity.....173
Table A.6. The influence of medium density on the density differential. 173
Table A.7. The influence of ore size on the spigot capacity. 174
Table A.8. The influence of ore size on the spigot capacity. 174

Nomenclature

A-inlet – 70x25 mm^2 (D_i = 47mm).

B-inlet – 70x10mm^2 (D_i =30mm).

Bl – barrel length (mm).

C – Coarse grade magnetite with 75% (by mass) passing 45µm.

C_V - the volume fraction of the FeSi and ore in the feed.

C_{vf} – volumetric percentage of ore in the feed (applicable to DMS cyclones).

$C_{vf\,(+\rho 50)}$ – volumetric percentage of ore in the feed with densities above the separation density (applicable to DMS cyclones).

C_{vo} – volumetric percentage of ore in the floats (applicable to DMS cyclones).

C_{vu} – volumetric percentage of ore in the sinks (applicable to DMS cyclones).

C_{mvu} – volumetric percentage of ore in the sinks during roping (applicable to DMS cyclones).

D – cyclone diameter (mm).

D_i – Inlet diameter (mm).

D_o – Vortex finder/overflow diameter (mm).

D_u – Spigot/underflow diameter (mm).

d_{ore} – particle size or size range (mm).

d_u – mass median (50% passing) size of the underflow solids.

d_{50} – cut-size (µm).

EPM - Escart Probable Moyen.

F – Fine grade magnetite with 95% (by mass) passing 45µm.

Gr – medium grade, expressed as mass percentage passing 45µm.

g_u – solids recovery in the underflow/sinks (by mass).

H – Feed Head (D).

M – Medium grade magnetite with 85% (by mass) passing 45µm.

O/F –Overflow or floats.

P – feed pressure (kPa).

Q_O – flow-rate of ore through the floats (l/hr ore).

Q_{OS} – flow-rate of slurry through the floats (l/hr slurry).

Q_U – flow-rate of ore through the sinks (l/hr ore).

Q_{US} – flow-rate of slurry through the sinks (l/hr slurry).

Q_{UM} – the maximum ore carrying capacity of the spigot (l/hr ore).

Q_{USM} – the maximum slurry carrying capacity of the spigot (l/hr slurry).

Q – flow-rate of slurry through the feed (l/hr slurry).

R_f – water split to the sinks.

R_m – volumetric medium split to the sinks.

RD – Relative Density.

S – volume split during spray discharge (Q_{US}/Q_{OS}).

S_R – volume split during roping (Q_{USM}/Q_{OS}).

SG – Specific Gravity.

U/F – Underflow or sinks.

$\%V_{MSU}$ – volumetric percentage of solids in the underflow during roping (applicable to classification cyclones).

$\%V_{SF}$ – volumetric percentage of solids in the feed (applicable to classification cyclones).

C_i^+ – the percentage weight of solids in the feed coarser than the separation size.

α – cone angle (degrees).

ρ_{med} – feed medium density (kg/l).

ρ_{ore} – ore density (kg/l).

$\rho_{OF(med)}$ – floats medium density (kg/l).

$\rho_{UF(med)}$ – sinks medium density (kg/l).

ρ_F – the relative slurry density in the feed.

ρ_O – the relative slurry density in the floats stream.

ρ_U – the relative slurry density in the sinks stream.

σ_{est} – Standard error of the estimate.

CHAPTER 1.

INTRODUCTION

Dense medium cyclones are used extensively in the mineral processing industry to beneficiate various minerals including coal, diamonds and iron ore amongst others. According to Reeves (2002), "the cyclone has been installed in over one-quarter of the coal preparation plants worldwide". Further, de Korte (2000) reported that about 93% of the 58 coal preparation plants in South Africa employed dense medium cyclones. The structure of a dense medium cyclone is illustrated in Fig. 1.1. This equipment separates minerals according to their differences in densities, whereby the heavier particles are sent to the sinks and the light particles to the floats. Feed enters tangentially through the inlet under high pressure so that a vortex is created within the cyclone. Consequently, an air core that extends from the floats through to the sinks along the axis of the cyclone is developed. The inward vortex carries the floats particles to the floats stream and the outward vortex carries the sinks particle to the sinks stream. A slurry mixture of ore particles and an aqueous suspension of very fine medium particles constitute the feed slurry. Cyclone feed is normally de-slimed beforehand to remove fines, typically smaller than 0.5mm, which would have an adverse effect on the medium quality and cyclone performance (Reeves, 2002).

Other centrifugal dense medium separators, which operate on a principle similar to dense medium cyclones, include LARCODEMS, Vorsyl and Dyna Whirlpool separators. LARCODEMS and Dyna Whirlpool separators have been widely used to beneficiate larger particle sizes that are thought to be too large for cyclones (Reeves, 2002).

Dense medium cyclones are usually installed at a near horizontal inclination angle to allow usage of relatively large spigot sizes for sinks removal, and drainage of the cyclone contents during shutdown. This inclination angle is typically 10 degrees to the horizontal.

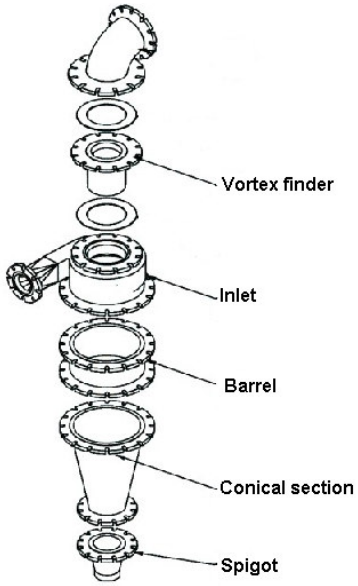
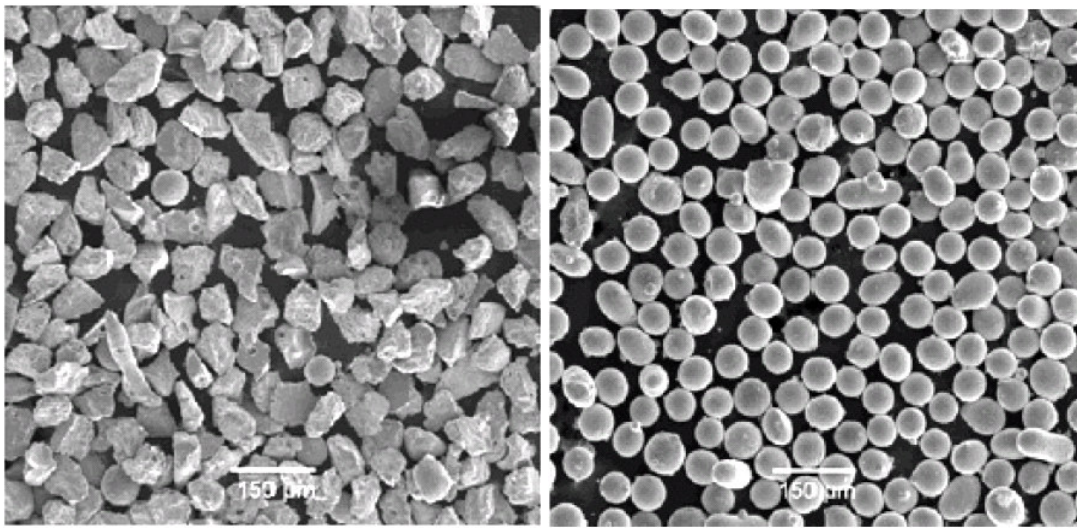


Figure. 1.1. Cyclone geometry. (Adapted from Bosman 2003b)

The medium particles can either be magnetite (SG 5.1) or ferrosilicon (SG 7.0). Magnetite is employed as medium mainly in coal preparation, while ferrosilicon is employed for other minerals/valuables such as diamonds and iron ore. There are two types of ferrosilicon namely: milled and atomized (Fig. 1.2. (a) and (b)). Milled ferrosilicon is used at medium density ranges between 2.0 and 3.0RD, while atomized ferrosilicon is employed at densities between 3.0 and 4.2RD (Smith, 1989 and Grobler, 2006). The application range of magnetite is typically between 1.3 and 2.0RD.



(a) (b)

Figure 1.2. Milled and atomized ferrosilicon. (Grobler, 2006)

Dense medium cyclones have the ability to achieve high capacities, and simultaneously obtain sharp separations and high separation efficiencies. However, this piece of equipment does have a shortcoming in that its capacity is constrained by the solids carrying capacity of the spigot. This is termed the spigot capacity. Once the spigot capacity is exceeded, the separation efficiency of the cyclone suffers. In applications whereby relatively large quantities of the feed material exit through the sinks, the spigot acts as a 'bottleneck' (Bosman, 2003a). In such instances it becomes necessary to install larger or more cyclones in order to achieve the required sinks capacity. According to Peatfield (2003), the capacity of cyclones treating low yield coals is influenced mostly by the medium-to-ore ratio and the rejection capacity of the cyclone spigot.

Manufacturers guidelines such as those provided by the original developers of the dense medium cyclone, Dutch State Mines (DSM) in the so-called DSM handbook, normally specify the spigot capacity for a cyclone of a particular size. Due to the fact that the DSM guidelines "left no issue in doubt" and the dense medium cyclone performed as guaranteed when the DSM guidelines were followed (Moorhead and Schutte, 2005), the specified spigot capacities have been widely accepted; although there is uncertainty with regard to how these capacities were determined and whether they can be increased. The purpose of this study is to establish a methodology to determine the spigot capacities of dense medium cyclones, and determine the parameters that influence these capacities.

In order to illustrate the significance of increasing the capacity of dense medium cyclones, the following coal example is used. In 2005, South Africa produced about 245Mt of coal valued at R35.86 billion according to DME (2005). A significant proportion of this coal is beneficiated through dense medium cyclones. Therefore, an increase in the cyclone capacity, even if relatively small, represents a large number in terms of tonnages of coal produced or monetary gains.

CHAPTER 2. LITERATURE REVIEW

This review aims to discuss and evaluate the current knowledge on the spigot loading and overloading of cyclones. The loading and overloading behaviour of both classification and dense medium cyclones are considered. In order to characterise the spigot overloading behaviour of the cyclone better, classification and dense medium cyclones are considered separately. This way the similarities and differences in behaviour between the two cyclonic devices can easily be identified. The logic followed here is that we first need to characterise and understand the spigot loading and overloading behaviour of the cyclone before investigating (and quantifying) the effects of the various variables on the spigot capacity.

2.1. CLASSIFICATION HYDROCYCLONES

Classification cyclones separate solid particles according to their differences in size. The operation principles for classification cyclones are similar to those of dense medium cyclones, although there are differences in terms of the angle of inclination and cyclone geometry. Classification cyclones make use of water as the separating medium, while a mixture of water and magnetite/ferrosilicon is employed in dense medium cyclones.

2.1.1. Characterisation of Overloading at the Underflow

In tackling this problem it is important to first define what exactly is the maximum spigot capacity, and establish what determines it. Jull (1972), and Mular and Jull (1978) suggested that the spigot capacity of a hydrocyclone was reached at the onset of rope discharge at the underflow. The association of the spigot capacity with roping flow has also been suggested/implied by others, including: Dahlstrom (1949); Fahlstrom (1963); Abbot (1967a); Plitt (1976); Flintoff et al. (1987); Plitt et al. (1987) and Heiskanen (2000). Under the normal operating conditions of the cyclone a ‘cone-shaped’ discharge is prevalent at the spigot, and is referred to as spray discharge. During spray discharge the air core extends across the entire length of the cyclone from the overflow through to the underflow (Fig. 2.1). However, when a rope discharge commences at the spigot the air core in this part of the cyclone collapses. Consequently, the flow at the underflow changes from a ‘cone-shaped’ discharge with an air core in the middle to a ‘rope-shaped’ flow in which the slurry occupies the entire cross-section of the spigot (with no air core at the underflow).

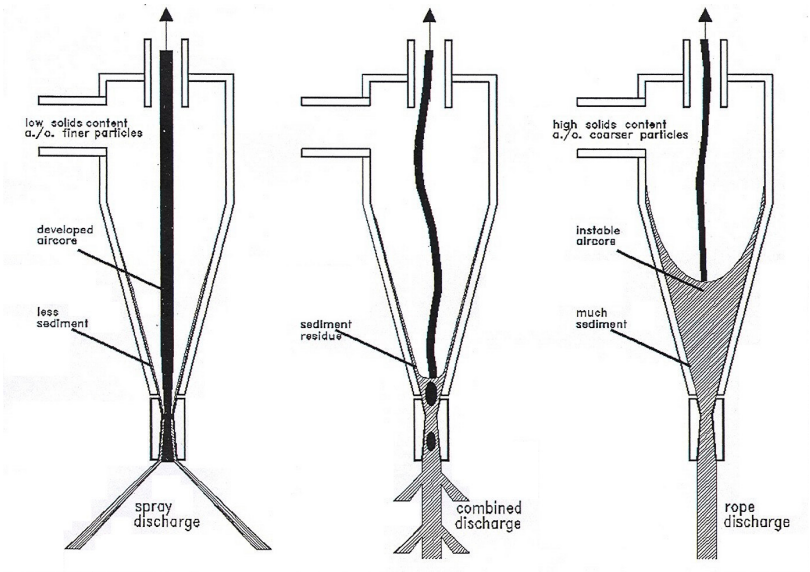


Figure 2.1. Schematic diagram showing spray, semi-rope and rope discharges at the underflow of a hydrocyclone. (Neesse et al., 2004a)

(a) Air Core and Roping

Plitt et al. (1987) proposed, "Roping is initiated by the formation of a bed of solids in the apex (spigot) region of the cyclone. When the viscosity of the slurry increases to the point where the frictional drag of the cyclone wall stops the rotary motion, roping is initiated". Dyakowski and Williams (1995) also proposed that the collapse of the air core during the onset of roping was a consequence of excessive 'fluid' viscosity, which decays the tangential velocity and, consequently, the rotational motion at the underflow.

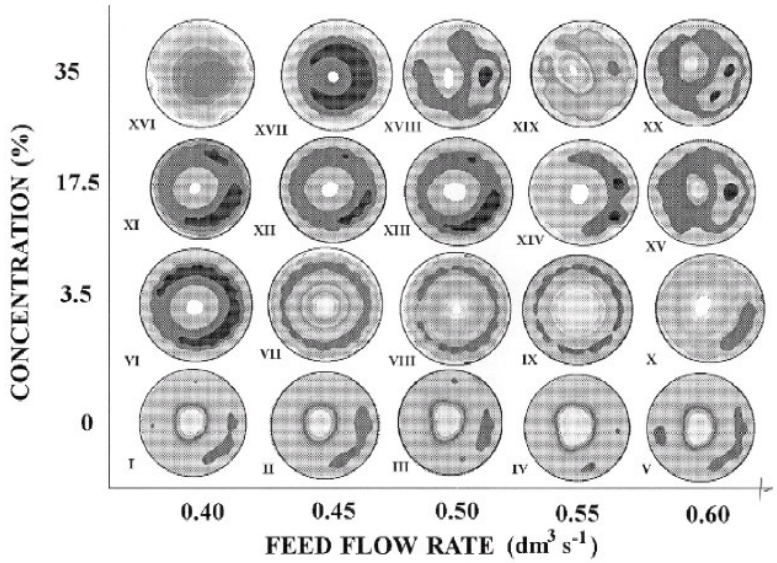


Figure 2.2. Resistivity images showing the air core below the feed inlet of a 44mm diameter hydrocyclone. (Gutiérrez et al. 2000)

Gutiérrez et al. (2000) illustrated the above-mentioned behaviour with their work on the use of electrical impedance tomography to control the underflow discharge of a hydrocyclone (Fig. 2.2). These resistivity images were taken in a single horizontal plane near the feed inlet, and the circular white shapes in the middle of the images represent the air core. The presence of an air core at the underflow can clearly be seen in all images except for image XVI in which rope discharge was obtained at the underflow.

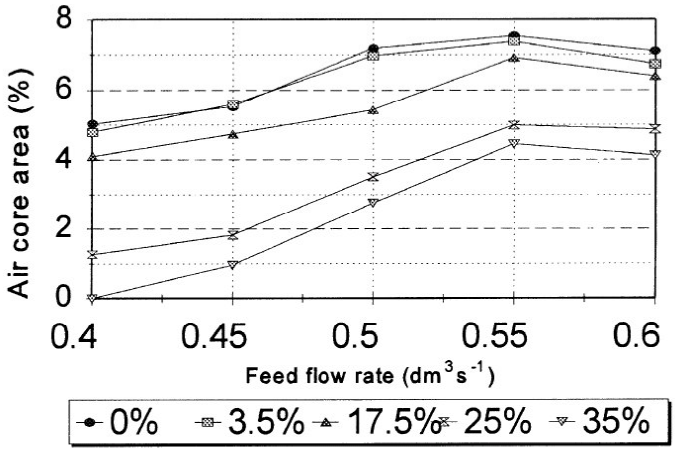


Figure 2.3. The influence of feed solids' concentration on the air core size. (Gutiérrez et al., 2000)

Furthermore, Gutiérrez et al. (2000) studied the effect of the feed flow rate and feed solids concentration on the air core size at the underflow, as shown in Fig. 2.3. The air core size was observed to increase with increasing feed flow-rate up to a certain maximum at various feed solids concentrations. Fig. 2.2 and 2.3 illustrate clearly that the lowest air core sizes were encountered at the highest feed concentration of 35%, and the highest air core sizes were observed at the lowest feed concentration of 0%. Thus, an increase in the feed solids concentration consistently brings about a decrease in the air core size. And the decrease in the air core size with increasing solids concentration is a consequence of increased slurry viscosity, which increases with solids concentration as shown in Fig. 2.5. And once a certain critical underflow solids concentration (and slurry viscosity) is reached the rotational motion of the slurry in the cyclone can no longer be sustained, and as a result the air core collapses and roping commences. This is in agreement with the behaviour postulated by Plitt et al. (1987) as previously mentioned. The critical underflow solids concentration at which roping commences will be discussed in more detail in later parts of this chapter.

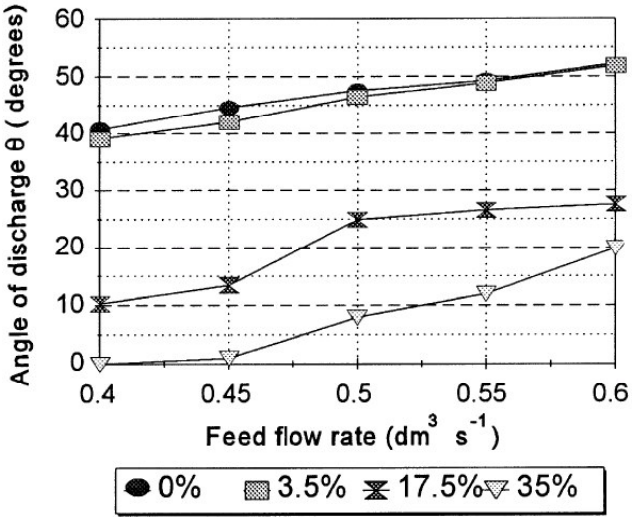


Figure 2.4. Angle of discharge for the underflow slurry with changing feed flow-rate and solids concentration. (Gutiérrez et al., 2000)

The air core area within the hydrocyclone and the angle of discharge at the underflow are shown in Fig. 2.3 and 2.4, respectively. These two figures illustrate clearly that during roping, when the angle of discharge is zero (Fig. 2.4), the air core at the underflow collapsed (Fig. 2.3).

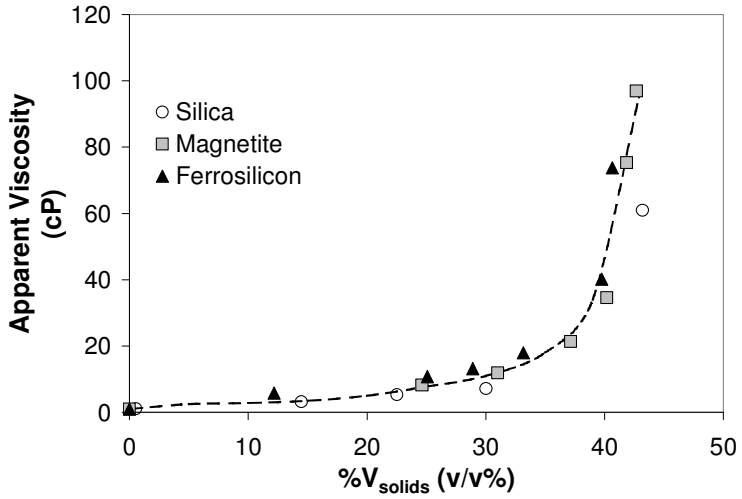


Figure 2.5. The influence of solids concentration on the apparent viscosity of the pulp. Particle size range: -75+50µm. (Aplan, 1985)

The particle size range of the solids used in plotting Fig. 2.5 was –75+50µm for all three material types. It is interesting to note that particle density does not seem to influence the relationship between volumetric solids concentration and apparent viscosity. The abrupt rise

in viscosity with increasing solids concentration was observed to occur at the same concentration of around 37-40% for all three particles types.

(b) Underflow Solids Concentration

According to Neesse et al. (1984) and Neesse et al. (2004a) a 'sediment layer' with high solids concentration forms at the underflow during roping, as illustrated in Fig. 2.1, in which the coarse particles accumulated in the conical section of the cyclone.

As mentioned previously, Plitt et al. (1987) postulated that the collapse of the air core at the underflow during the onset of roping was a consequence of the prevalent high solids concentrations; once a certain critical solids concentration at the underflow is exceeded roping commences. In support of this notion a number of authors established that there is a critical underflow solids concentration beyond which roping flow occurs. These include Dahlstrom (1949), Fahlstrom (1964), Abbot (1967a), Mular and Jull (1978), Plitt et al. (1987), and Heiskanen (2000), amongst others. Thus, the onset of rope discharge could be anticipated/predicted by studying the behaviour of the underflow solids concentration. As a result, some of the authors proposed mathematical expressions that attempted to predict the onset of rope discharge at the underflow. Plitt et al. (1987) refers to the *SPOC* model which makes use of the following expression to predict the onset of roping flow:

$$\%V_{MSU} = \%V_{SU20} + 0.2(\%V_{SF} - 20) \qquad (2.1)$$

where $\%V_{MSU}$ is the %solids by volume in the underflow at which roping is initiated for a feed concentration of $\%V_{SF}$, $\%V_{SF}$ is the volumetric percentage solids in the feed, and $\%V_{SU20}$ is the user defined value for the limiting %solids by volume in the underflow at a feed solids concentration of 20% by volume (default is 56%). Heiskanen (2000) modified the above expression to obtain the following:

$$\%V_{MSU} = 33.8 + \%V_{SF}^{0.098} \qquad (2.2)$$

According to the above-mentioned expressions the critical underflow concentration is dependent only on the feed concentration. It is, however, expected that $\%V_{MSU}$ should not be dependent on $\%V_{SF}$, but rather on the concentration of solids particles in the feed that eventually exit at the underflow. If for instance we have two cyclones (A and B) with same dimensions, operating under the same conditions and at the same $\%V_{SF}$, but say cyclone A has a high proportion of its feed exiting through the underflow and cyclone B has a much smaller proportion of its feed going to the underflow. In such a scenario it is possible for

cyclone A to be roping and for cyclone B to be operating under a spray discharge, even though both cyclone may have the same $\%V_{SF}$. Cyclone B will require a much higher $\%V_{SF}$ than cyclone A in order to exceed $\%V_{MSU}$, assuming that $\%V_{MSU}$ is the same for both cyclones.

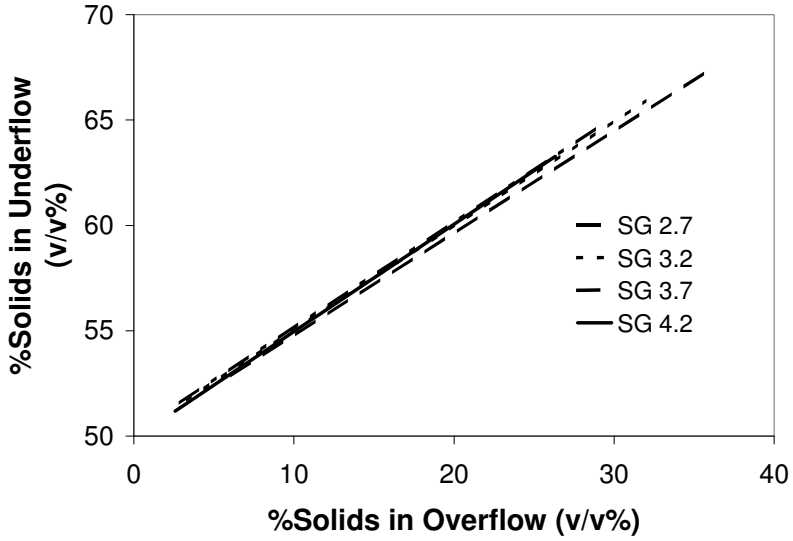


Figure 2.6. The underflow solids concentration at which roping was initiated for ores of different densities. (From Mular and Jull, 1978 adapted in Heiskanen, 2000)

According to Mular and Jull (1978), $\%V_{MSU}$ increased with increasing overflow solids concentration (Fig. 2.6). This behaviour is actually similar to equations (2.1) and (2.2) because the overflow solids concentration increase in accordance with the increase in feed solids concentration. Mular and Jull (1978) attributed the increase in $\%V_{MSU}$ with increasing overflow solids concentration to "filling up of the void space between coarse underflow particles with fine slurry of high percent solids". Thus, $\%V_{MSU}$ increased with increasing overflow solids concentration due to increased short-circuiting of fines to the underflow. In support of this view, Lynch and Rao (1975), and Asomah and Napier-Munn (1997) determined the following relationship between water split to underflow (R_f) and volumetric fraction of solids in the feed slurry ($\%V_{SF}$):

$$R_f \propto \frac{100}{(100 - \%V_{SF})^n}$$

with n = 1.0 according to Lynch and Rao (1975) and n = 0.825 according to Asomah and Napier-Munn (1997). These relationships were determined under normal, spray discharge conditions at the underflow, while Fig. 2.6 was determined under roping conditions. It is assumed that this trend should not change with the discharge type at the underflow.

Plitt et al. (1987), on the other hand, reported that once roping flow had commenced the underflow solids concentrations remained constant with further addition of solids into the cyclone (Fig. 2.7). The dotted line in Fig. 2.7 is a plot of equation 2.1. Abbot (1967a), Heiskanen (2000) and Neesse et al. (2004) also reported the same behaviour.

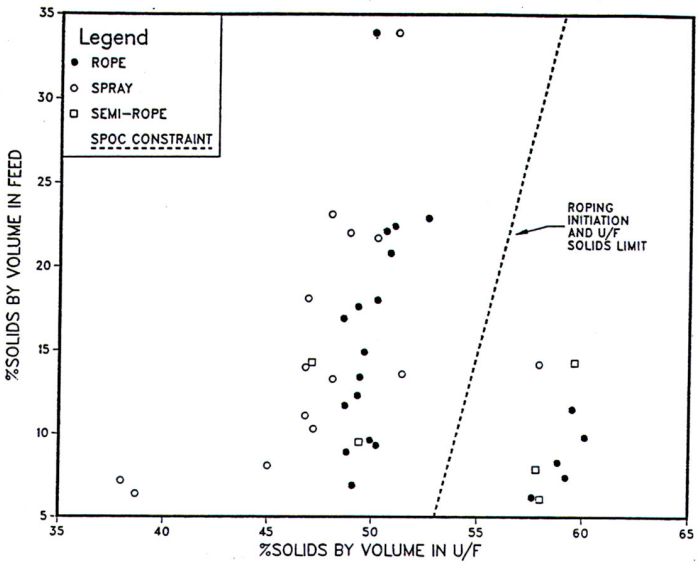


Figure 2.7. Influence of feed solids on roping. (Plitt et al., 1987)

Fahlstrom (1963) also observed $\%V_{MSU}$ to be constant once roping commenced at the underflow; this is shown in Fig. 2.8 (a) and (b). Curves 1, 2 and 3 in Fig. 2.8(a) correspond to volumetric feed concentrations of 19.6, 8.4 and 3.9%, respectively. And curves 6, 7 and 8 in Fig. 2.8(b) correspond to volumetric feed concentrations of 15.1, 21.7 and 37.4%, respectively.

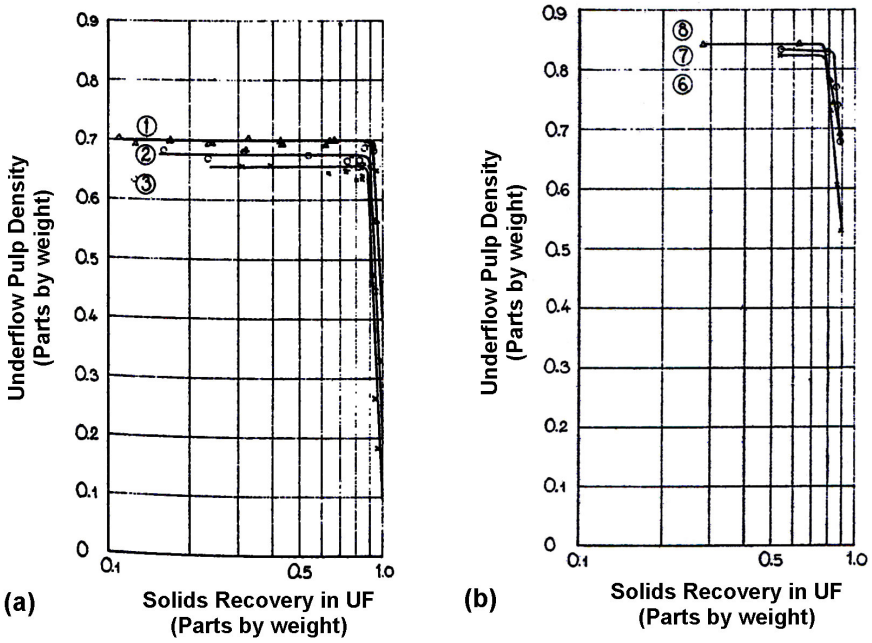


Figure 2.8. Underflow solids concentration during the transition from spray to rope discharge for (a) a 69mm test cyclone and (b) a 300mm plant cyclone. (Adapted from Fahlstrom, 1963).

Fahlstrom (1963) reported the solids recovery in the underflow (g_u) to be a function of C_i^+, the percentage weight of solids in the feed coarser than the separation size (Fig. 2.9). g_u increased with increasing C_i^+ as shown in Fig. 2.9. Obviously the feed solids concentration at which roping commences decreases with increasing C_i^+.

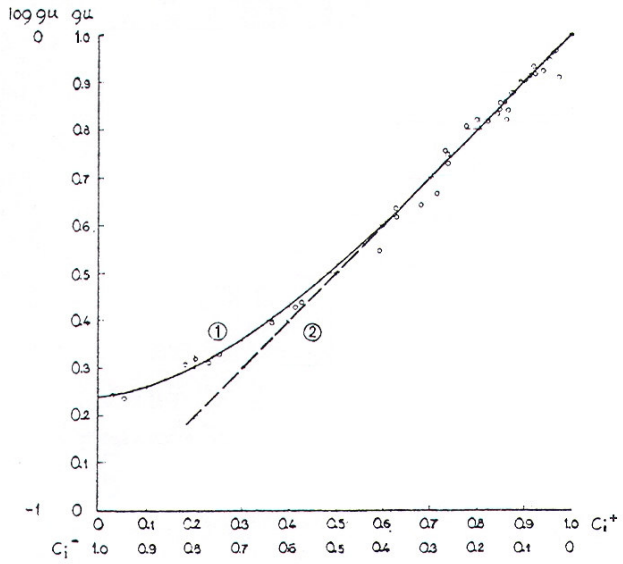


Figure 2.9. Solids recovery in the underflow as a function of material coarser that the separation size in the feed for a 69mm test cyclone. Fahlstrom (1963). Curve 1: $\%V_{SF}$ = 3.9, 8.4 and 19.6%. Curve 2: $g_u = C_i^+$.

Table 2.1 shows $\%V_{MSU}$ obtained from various sources in which hydrocyclones of different sizes and configurations, and ores of different densities and sizes were used. It is shown clearly in Table 2.1 that $\%V_{MSU}$ is generally around 50% solids (by volume) for most hydrocyclones; a minimum of 39% and a maximum of 68% have been reported.

Table 2.1. Various $\%V_{MSU}$ obtained by different workers.

Source	$\%V_{MSU}$ (v/v%)	Material Treated	Particle Size (µm)	D (mm)
Abbot (1967)	48	Coal	-	-
Concha et al. (1996)	49-60	-	-	-
Dahlstrom (1949)	~56[a]	Coal	-	356
Fahlstrom (1963)	41-47	Flotation tails	150[b]	69
Fahlstrom (1963)	54-57	Sulphide ore	1500[b]	300
Heiskanen (2000)	39-46	Limestone	95-212[d]	-
Mular and Jull (1978)	51-68	Various	-	Various
Neesse et al. (2004b)	52	Quartz	1000[b]	150
Plitt et al. (1987)	49-60	Sand	53-151[c]	146
Plitt (1983)*	53-62	-	-	150
Yianatos et al. (2002)	56-59	-	-	-

*As reported in Flintoff *et al*. (1987).
[a]Density of the coal assumed to be 1.5SG.
[b]Particle top size in feed.
[c]Median particle size in feed.
[d]Median particle size in the underflow.

The maximum value for $\%V_{MSU}$ of 68% was obtained by Mular and Jull (1978), who treated ores with specific gravities ranging from 2.7 up to 4.2 and employed much larger hydrocyclones with spigot sizes ranging from about 50 up to 200mm. As mentioned previously, the high $\%V_{MSU}$ is a consequence of increased fines in the underflow product due to increased short-circuiting of fines to the underflow. The same rationale could be used to explain the relatively high value of 62% reported by in Flintoff et al. (1987), shown in Fig. 2.10.

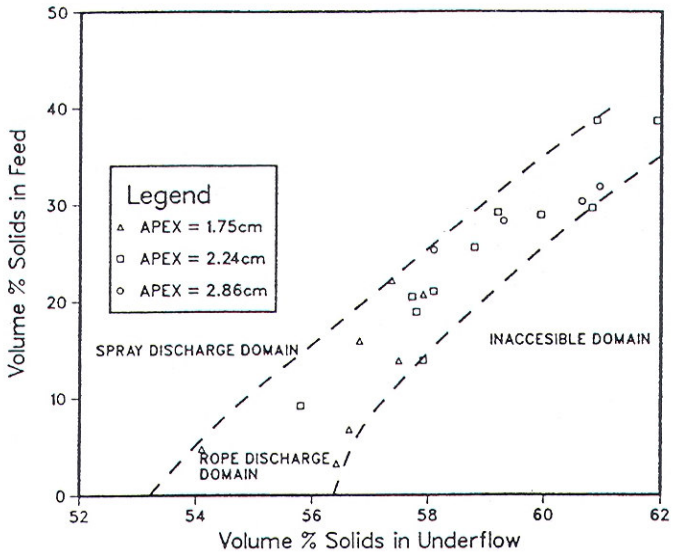


Figure 2.10. The influence of feed concentration on the critical underflow concentration at which roping commences. (Flintoff et al., 1987)

The lowest value for $\%V_{MSU}$ obtained in Table 2.1 was 39% reported by Heiskanen (2000). This minimum value of 39% was obtained when the feed solids concentration was the lowest (6.6% solids by volume), and the highest $\%V_{MSU}$ of 46% (obtained by Heiskanen) was observed at the highest feed concentration (Fig. 2.11). The effect of the feed concentration on $\%V_{MSU}$, as reported by Mular and Jull (1978) and Flintoff et al. 1987 (Fig. 2.6 and 2.10, respectively), is further confirmed by these observations.

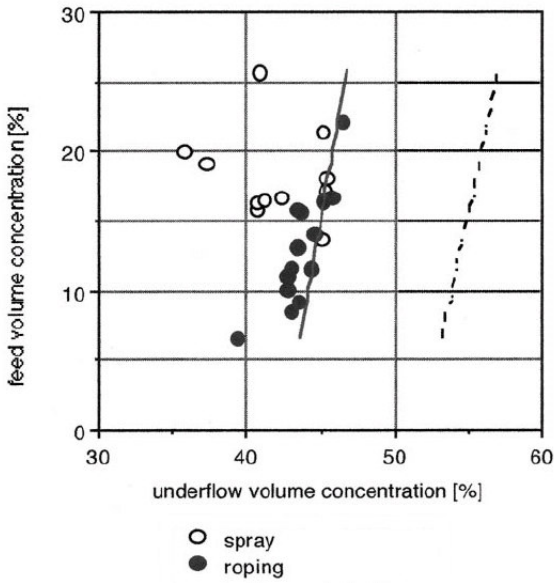


Figure 2.11. The influence of feed volume concentration on the underflow concentration during roping. The dotted line represents a plot of equation 2.1, and the solid line is equation 2.2. (Heiskanen, 2000)

(c) Effect of Roping on Cyclone Operation

Fahlstrom (1963) reported an abrupt increase in the overflow solids concentration at the onset of rope discharge (Fig. 2.12); this is due to misplacement of coarse particles to the overflow. Curve 1 in Fig. 2.12 was obtained with a 69mm test cyclone at various feed solids concentrations, while curves 2, 3, and 4 correspond to volumetric feed concentrations of 15.1, 21.7 and 37.4%, respectively, on the 300mm plant cyclone.

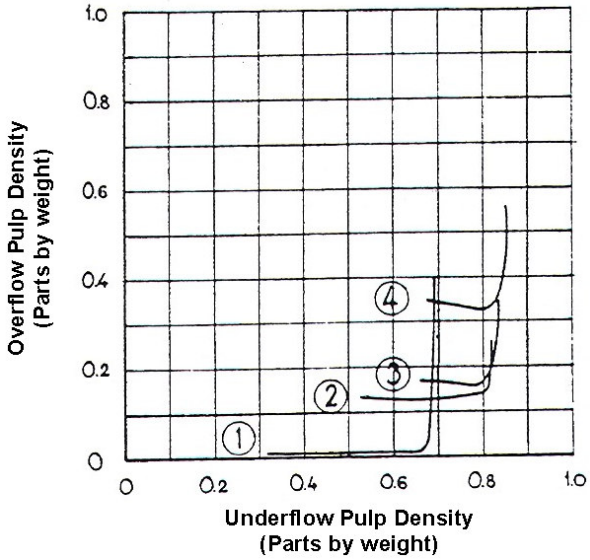


Figure 2.12. Overflow pulp density during the transition from spray to rope discharge. Curve 1: 69mm test cyclone at various $\%V_{SF}$. Curves 2, 3 and 4: $\%V_{SF}$ = 15.1, 21.7 and 37.4%, respectively, with D_c = 300mm. (Fahlstrom, 1963)

Roping or spigot overloading has widely been established to result in an increase in cut-size as a consequence of misplacement of coarse particles to the overflow (Dahlstrom, 1949; Abbot, 1967a; Trawinski, 1976; Mular and Jull, 1978; Plitt et al., 1987; Heiskanen, 2000; Neesse et al., 2004, etc.). This behaviour is illustrated in Fig. 2.13, 2.14 and 2.15.

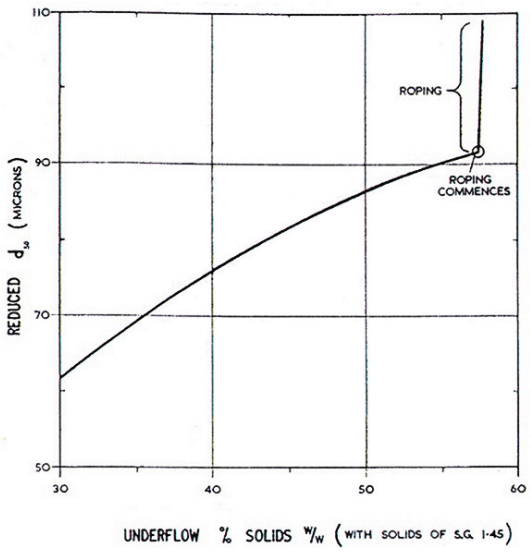


Figure 2.13. The influence of commencement of roping on the cut-size. (Abbot, 1967a)

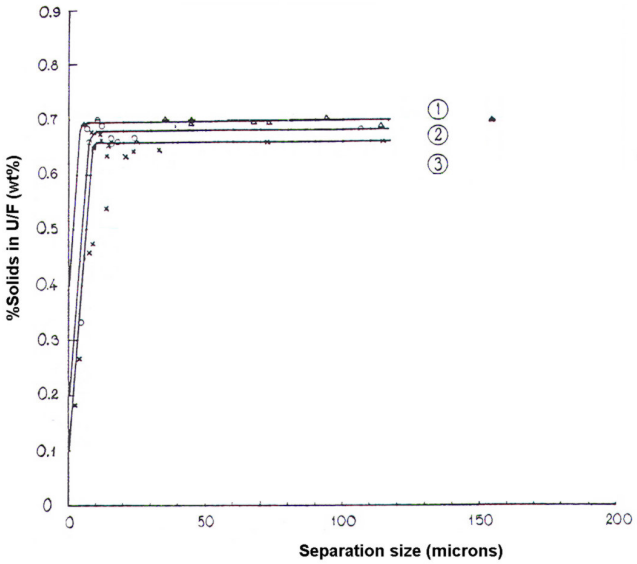


Figure 2.14. Change in the separation size during roping. Curve 1: $\%V_{SF}$= 3.9, 8.4 and 19.6%. (Fahlstrom, 1963)

Roping occurred at lower g_u values and spray discharge was encountered at higher g_u values. According to Fahlstrom (1963) the following relationship is valid (for a 69mm test cyclone), within the range $0.4 < g_u < 1$:

$$d_{50} = -196\log(g_u) \tag{2.3}$$

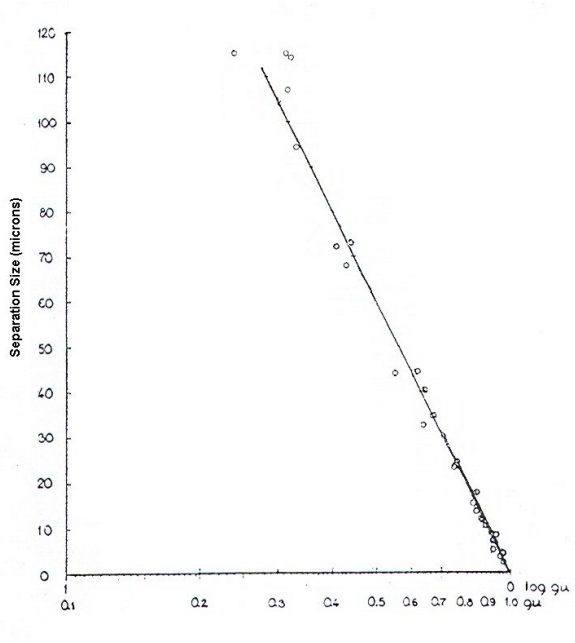
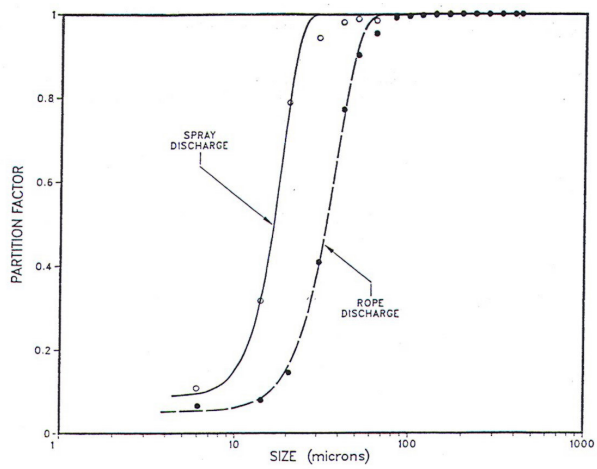
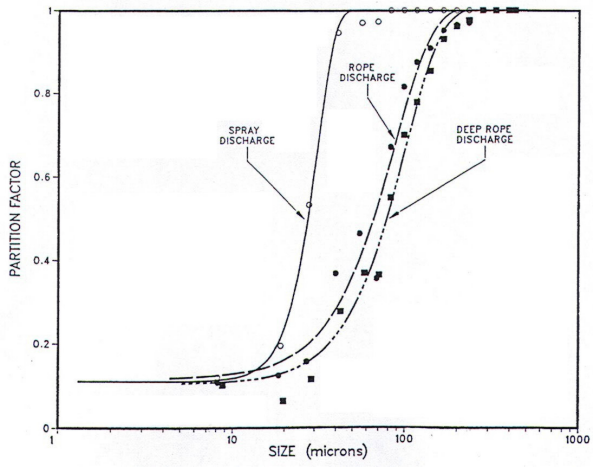


Figure 2.15. The relationship between separation size and solids recovery in U/F (mass fraction). (Fahlstrom, 1963).

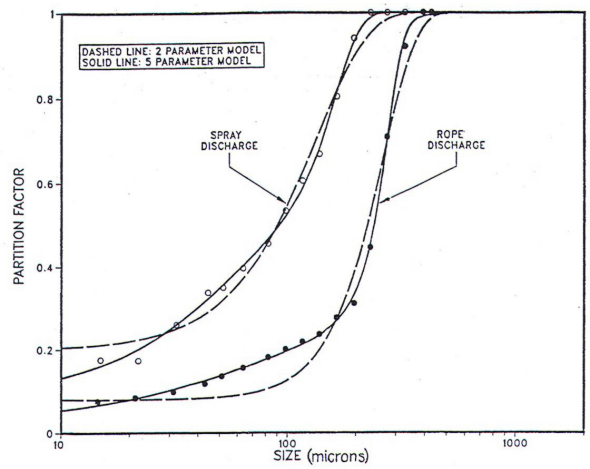
Plitt et al. (1987) reported that the impact of roping on the performance of a cyclone is dependent on the feed solids concentration. They distinguished between three categories of feed solids concentrations, namely: low, intermediate, and high; the partition curves obtained under these three solid concentrations are shown in Fig. 2.16. The feed concentrations were kept relatively constant for each set of the partition curves in Fig. 2.16; roping was induced by decreasing D_u. The increase in the cut-size in Fig. 2.16 is partly a consequence of the decrease in D_u, which was decreased from 25mm for both Fig. 2.16 (a) and (c) to 17 and 14mm, respectively. While D_u was decreased from 25mm to 20mm (roping) and then to 15mm (deep roping) in Fig. 2.16 (b). The effect of roping on the sharpness of separation was reported to be dependent on the feed solids concentration by Plitt et al. (1987). It is interesting to note that there wasn't much misplacement of coarse particles to the overflow in Fig. 2.16.



(a)



(b)



(c)

Figure 2.16. Influence of roping on cyclone performance at (a) low (~7% by volume) (b) intermediate (~18%) and (c) high (~34%) feed solids concentrations. (Plitt et al., 1987)

Fahlstrom (1963), on the other hand, reported the sharpness of separation to initially increase with decreasing g_u up to a maximum, and at low g_u values the sharpness of separation decreased with decreasing g_u. It is known that roping was prevalent at low g_u values, and it is thought that the decrease in the sharpness of separation with decreasing g_u is a consequence of roping.

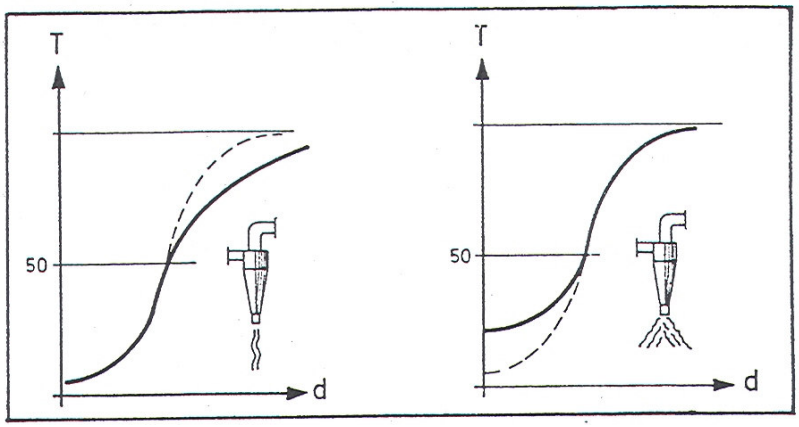


Figure 2.17. The influence of particle misplacement on the shape of the Tromp curve during rope and spray discharges. (Trawinski, 1976)

Trawinski (1976) illustrated the effect of particle misplacement to the overflow during roping as shown in Fig. 2.17, in the curve on the left; a disturbance on the upper part of the Tromp curve is observed during roping. A similar curve was presented by Kelly (1991) as shown in Fig. 2.18. According to Kelly (1991) there are two major causes of coarse particles misplacement to the overflow namely: roping and damaged vortex finder.

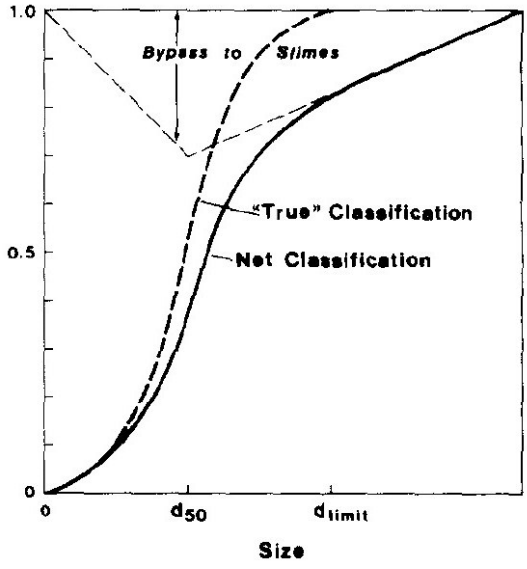


Figure 2.18. Effect of coarse particles misplacement to the overflow on the partition curve. (Kelly, 1991)

Fahlstrom (1963) encountered a similar type of disturbance on the upper part of the Tromp curve (as in Fig. 2.17); this is illustrated in Fig. 2.19. As the spigot diameter was decreased from 9mm down to 5mm (curves 4, 3 and 2) the cut-size increased consistently and the shape of the Tromp curve remained relatively unchanged; short-circuiting of fines to the underflow decreased steadily with decreasing spigot diameter. When the cyclone was operated with the smaller 3mm spigot, excessive short-circuiting of coarse particles to the overflow took place as illustrated by curve 1 (Fig. 2.19). It can be observed that close to 50% of the coarsest particles by-passed the separation process within the cyclone and went straight to the overflow stream.

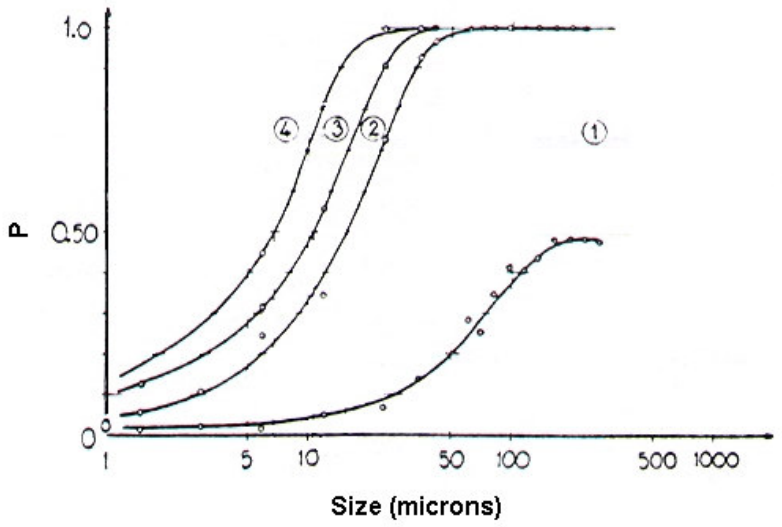


Figure 2.19. Influence of roping on cyclone performance. $\%V_{SF}$ = 8.4%, D = 69mm and D_o = 16mm. Curves 1, 2, 3, 4 correspond to D_u = 3, 5, 7,9mm. (Fahlstrom, 1963)

2.1.2. The Influence of Cyclone Geometry on the Spigot Capacity

Cyclone geometry includes inlet size, overflow diameter, underflow diameter, cone angle and barrel length (Fig. 1.1). Fig. 1.1 is repeated here for convenience. It is assumed that the influence of a particular variable on Q_U during spray discharge should give us an indication of that variables' effect on Q_{UM}.

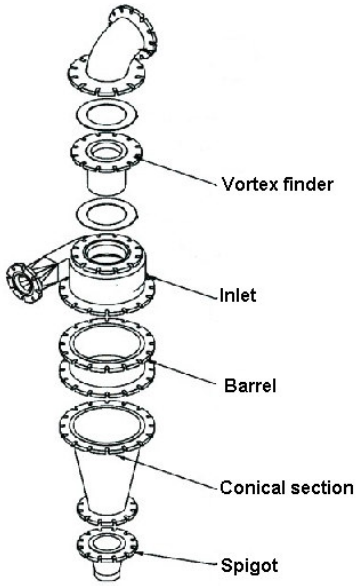


Figure 1.1. Cyclone geometry. (Adapted from Bosman 2003b)

(a) Inlet Size

At constant feed pressure, an increase in the inlet size is expected to increase the cyclone flow-rate. A number of correlations that relate the cyclone throughput to the inlet size have been proposed and they are of the following form:

$$Q_f\,(=Q_{OS}+Q_{US}) \propto D_i^n$$

The various quantities obtained for the exponent n above are shown in Table 2.2. D_i has a significant effect on Q as evident from the exponent n that ranged from 0.77 to 2.0 in the literature.

Table 2.2. The exponent *n* for the relationship between cyclone throughput and inlet diameter.

Source	exponent *n*
Bradley (1965)	0.9-2.0
Rao, Lynch and Nageswararao (1976)	0.85
Plitt (1976)	0.84
Svarovsky (1984)	0.85-0.94
Asomah and Napier-Munn (1997)	0.77

The inlet has previously been reported to have very little influence on the volume split (S) within the cyclone (Svarovsky, 1984). Thus, increasing the inlet size should generally increase the flow-rates of slurry through both the spigot and the vortex finder, more or less equally. The inlet increases the flow-rate of slurry exiting through the outlets by increasing their exit velocities.

(b) Spigot Diameter

A number of authors have proposed various relationships between the spigot diameter and spigot capacity for hydrocyclones. The relationship proposed by Tarr (1965) is shown in Fig. 2.20. The relevant data points used to plot the curves were unfortunately not given, and the spigot capacities were stated to be approximate. Tarr (1965) proposed a number of exponential curves, each at a specific underflow solids concentration, relating the spigot capacity to spigot diameter. The volumetric underflow solids concentrations ranged about 20% to 53% (by volume). It is not clear how these spigot capacities were defined or what the determining factor for these spigot capacities was. Volumetric underflow solids concentrations as low as 20% suggest that the hydrocyclone was not operating with a rope discharge at the spigot, and that spigot capacity was not defined according to the presence or absence of rope discharge at the underflow. It is interesting to note that the underflow concentrations were as high as 53% (by volume), whereby roping would be expected, yet the relationship between the spigot size and spigot capacity was similar to that of low underflow concentrations where roping should not have been taking place.

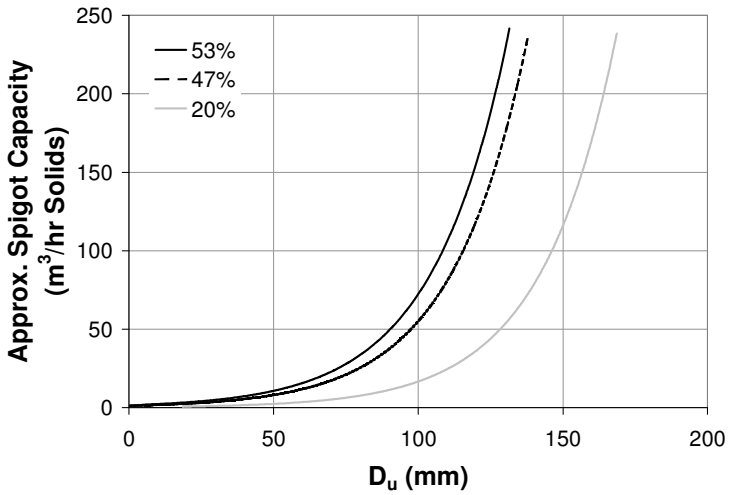


Figure 2.20. Effect of the spigot size on spigot capacity. (Tarr, 1985)

Mular and Jull (1978) also proposed a relationship between spigot capacity and spigot diameter; a similar relationship was reported in Jull (1972) as shown in Fig. 2.21. This curve was used to recommend an appropriate spigot size for a particular hydrocyclone with a specific spigot capacity. The spigot capacities were measured on cyclones operating just "short of roping". Just as with Tarr (1965), the spigot capacities are said to be approximate and no data points were presented.

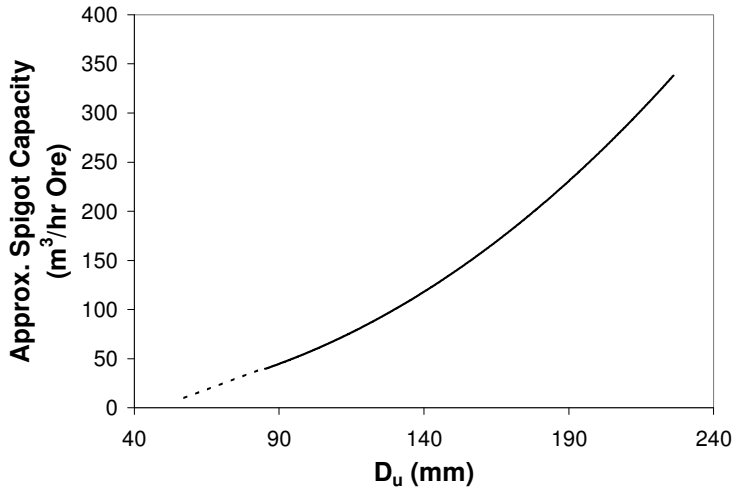


Figure 2.21. Effect of the spigot size on spigot capacity. (Jull, 1972)

The fact that these spigot capacities were obtained just "short of roping", and not during roping is not expected to influence the reliability of these spigot capacities values considerably. This is because a semi-rope discharge precedes the onset of roping, and during

semi-roping the flow at the underflow switches continuously between spray and rope discharges. Closer to the onset of roping the flow at the underflow is predominantly in the form of a rope discharge, occasionally switching to spray discharge (Neesse, 2007). Thus, the slurry occupies the entire cross-section of the spigot for a significantly large proportion of the time just "short of roping", such that the flow rates measured at this point should represent a reasonable approximation of the spigot capacity. The spigot ore loading during semi-roping, just 'short of roping', should therefore not differ too much from the actual spigot capacity.

A regression of the curve in Fig. 2.21 gives the following mathematical expression:

$$Q_{UM} = (2.3\times10^{-3})D_u^{2.19} \tag{2.4}$$

with Q_{UM} the solids capacity of the underflow in m^3/hr and D_u the spigot diameter in mm. This relationship was observed to be variable at small spigot diameters; hence, the dotted line in Fig. 2.21 at small spigot sizes. This variability was not incorporated into equation 2.4.

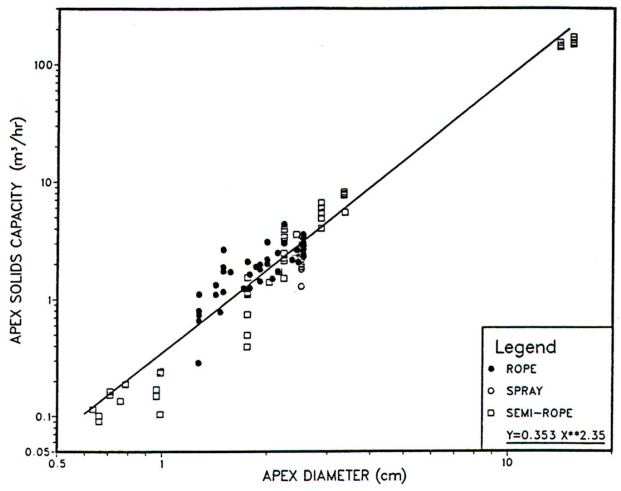


Figure 2.22. Spigot capacity under rope and near rope conditions. (Plitt et al., 1987)

A similar expression was obtained by Plitt et al. (1987):

$$Q_{UM} = 0.35D_u^{2.35} \tag{2.5a}$$

with D_u in cm and Q_{UM} in m^3/hr. A plot of equation 2.5a is shown in Fig. 2.22. This expression can be rearranged so that the D_u is in mm not cm, which gives the following expression:

$$Q_{UM} = (1.563\times10^{-3})D_u^{2.35} \tag{2.5b}$$

This relationship was based on a hydrocyclone operating in the semi-roping and roping regimes; data from spray discharge was not incorporated into equation 2.5. Equations 2.4 and 2.5 seem to suggest that, as expected, the spigot capacity is mainly a function of the cross-sectional area of the spigot. The dependence of the spigot capacity on the cross-sectional area of the spigot was also reported by Fahlstrom (1963); who quoted an expression for spigot capacity of 2.5ton/hr/cm^2. The expression by Plitt et al. (1987) has been validated by Heikanen (2000) as shown in Fig. 2.23. In validating Plitt et al.'s expression Heiskanen used data obtained during roping only.

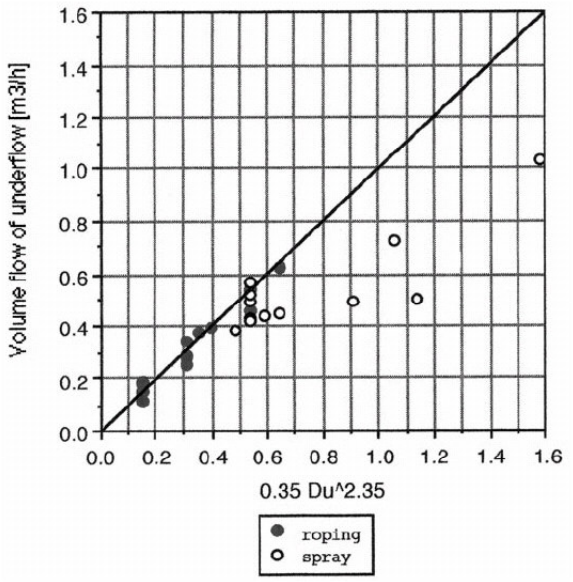
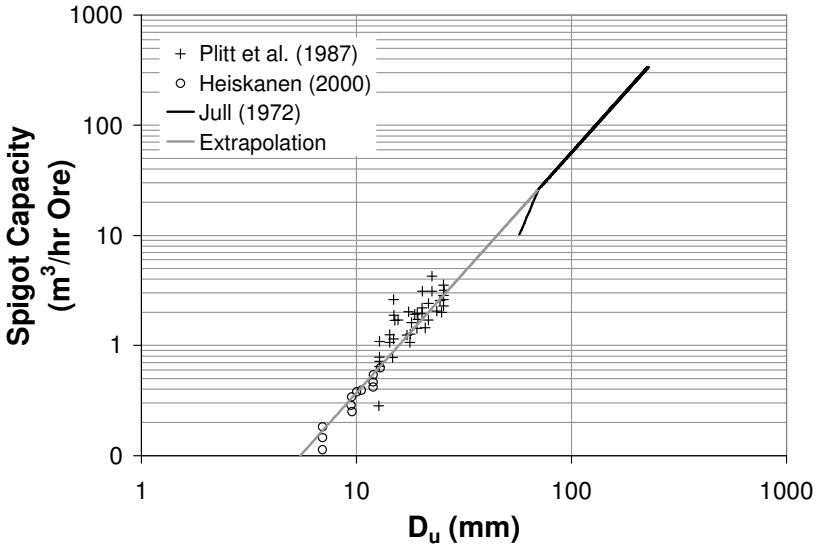
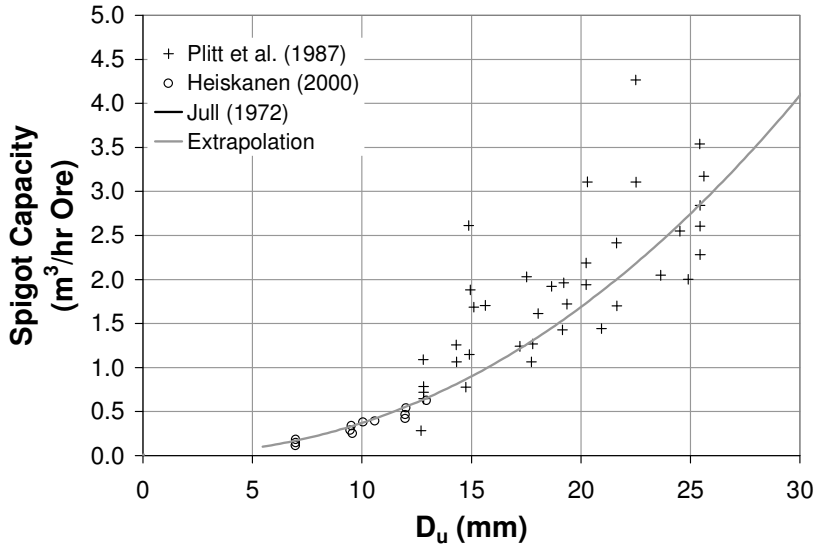


Figure 2.23. Relationship between spigot diameter and spigot ore capacity. (Heiskanen, 2000)

The level of agreement between the various relationships between spigot diameter and spigot capacity proposed by various authors is illustrated in Fig. 2.24. The curve obtained by Jull (1972) was extended down to much lower spigot diameters than those that he investigated. There is some agreement between this curve and the data points reported by Plitt et al. (1987) and Heiskanen (2000), although there is a considerable amount of scatter.



(a)



(b)

Figure 2.24. (a) Comparison of the spigot size-spigot capacity relationships proposed by various authors. (b) Curve in (a) at smaller spigot sizes on normal scale.

Fahlstrom (1963) reported $\%V_{MSU}$ to change with D_o/D_u at constant $\%V_{SF}$ as shown in Fig. 2.25; an increase in D_o/D_u appears to slightly decrease $\%V_{MSU}$. At low D_o/D_u values roping was not prevalent at the underflow. Heiskanen (2000) also reported a similar trend (Fig. 2.26).

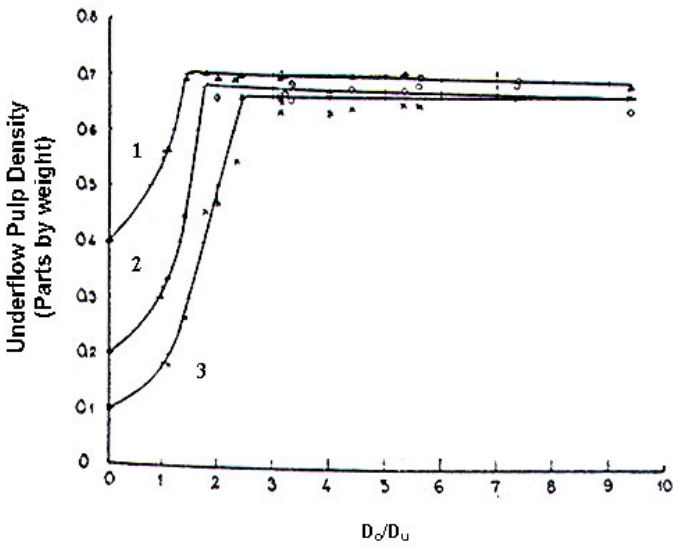


Figure 2.25. Underflow solids concentration during roping with changing D_o/D_u. Curves 1, 2 and 3 correspond to $\%V_{SF}$ = 19.6, 8.4 and 3.9%. (Fahlstrom, 1963)

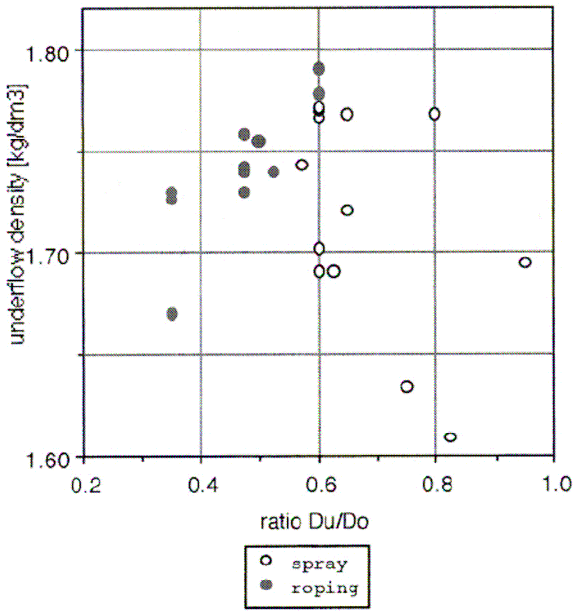


Figure 2.26. The influence of the spigot-to-vortex finder diameter ratios on the underflow density. (Heiskanen, 2000)

A clear distinction between $\%V_{MSU}$ for the 1.75cm and 2.86cm spigots can be made in Fig. 2.27, and the trend is consistent with that reported by Fahlstrom (1963) and Heiskanen (2000). The data points for the 2.24cm spigot, however, do not seem to be following the same trend.

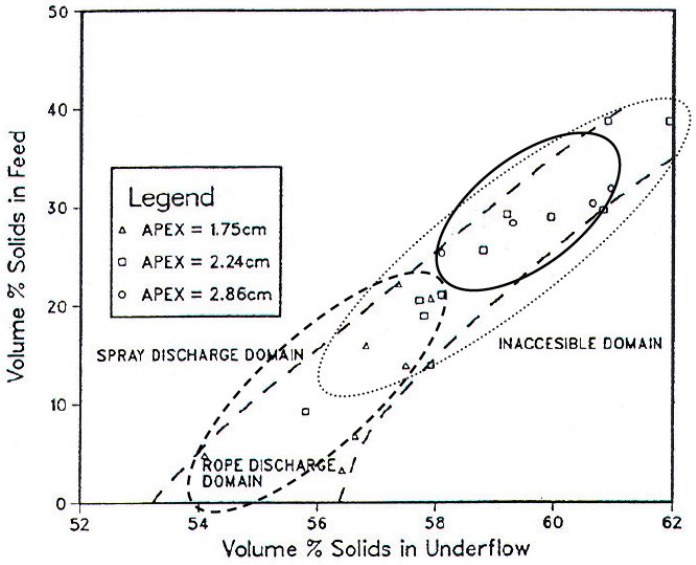


Figure 2.27. The influence of feed concentration on the critical underflow concentration at which roping commences. (Flintoff, 1987)

The above-mentioned observations that the onset of roping (expressed in terms of $\%V_{MSU}$) is dependent on the D_u/D_o ratio, is in agreement with the findings of Concha et al. (1996). They proposed that the "…underflow concentrations alone (do) not determine the type of discharge in a hydrocyclone…" instead the "…ratio of apex to vortex diameters separates the regions of rope and spray discharge". Furthermore, Concha et al. (1996) proposed that there is a specific range of underflow-to-overflow diameters ratios in which a rope discharge will be obtained at the underflow (Table 2.3 and Fig. 2.28).

Table 2.3. D_u/D_o ratios at which roping is likely to occur according to Concha et al. (1996).

D_u/D_o ratio	**Flow type at UF**
More than 0.56	Spray discharge only
Between 0.45 and 0.56	Spray, semi-rope, rope
Less than 0.45	Roping only

It is the author's opinion that although the D_u/D_o ratio influences the point at which roping commences; the onset of roping is determined mainly by the solids concentration within the cyclone. Therefore, it is expected that roping can occur at any D_u/D_o ratio provided the solids concentration within the cyclone is sufficiently high. At low D_u/D_o ratios roping takes place more readily (at lower feed solids concentrations) than at high D_u/D_o ratios.

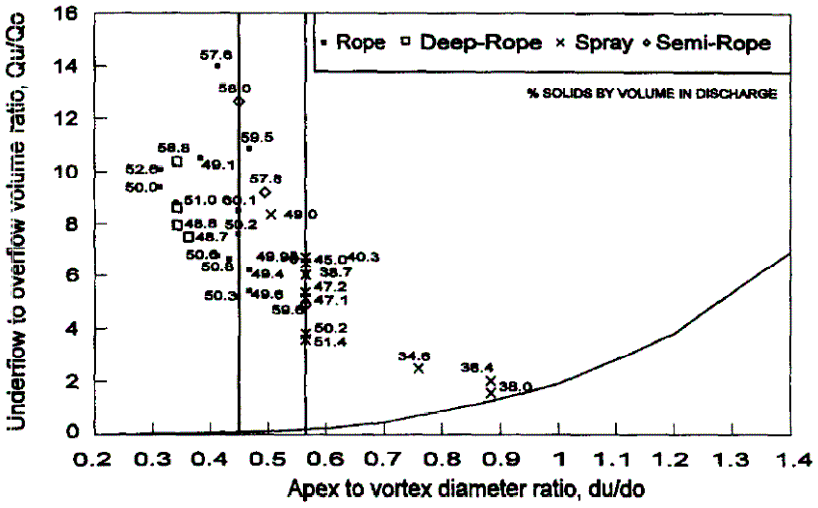


Figure 2.28. D_u/D_o ratios at which roping is likely to occur according to Concha et al. (1996).

(c) Vortex Finder Diameter

According to Plitt (1976), D_o and D_u influence Q as follows:

$$Q \propto (D_u^2 + D_o^2)^{0.49}$$

While other authors proposed a relationship of the following form:

$$Q \propto D_o^n$$

Values obtained for the exponent *n* are given in Table 2.4; Q increases significantly with increasing D_o.

Table 2.4. The exponent *n* for the relationship between Q and D_o ratio.

Source	**exponent** *n*
Lynch and Rao (1975)	0.68-0.73
Lynch and Rao (1968)	1.0
Asomah and Napier-Munn (1997)	0.77

A decrease in D_o, with all other variables constant, increases the proportion of the feed slurry that exits at the underflow and decreases slurry flow at the overflow; this behaviour has been quantified by a number of authors as follows:

$$S = \frac{Q_{US}}{Q_{OS}} \propto \left(\frac{D_u}{D_o}\right)^n$$

Some of the values obtained for the exponent *n* are shown in Table 2.5. It can be inferred from the behaviour of S and Q with changing D_o that the spigot capacity should increase with decreasing vortex finder diameter.

Table 2.5. The exponent *n* for the relationship between S and D_u/D_o ratio.

Source	**exponent** *n*
Bradley (1965)	1.75-4.4
Plitt (1976)	3.31

Furthermore, Concha et al. (1996) reported that roping flow tends to occur more readily at larger vortex finder sizes (and smaller spigot sizes), as shown in Table 2.3.

(d) Cone Angle and Barrel Length

According to van Duijn and Rietema (1983), the residence times for hydrocyclones with smaller cone angles are smaller than those of large cone angle cyclones. Further, Bradley (1965) and Svarovsky (1984) reported that an increase in the overall length of the cyclone, either through a larger cylindrical section or a smaller cone angle, increases the capacity of the cyclone. In agreement with this view Plitt (1976) made use of the so-called free vortex height (h), which is defined as the distance from the bottom of the vortex finder to the top of the spigot, to embody the effect of the barrel length and cone angle. The following relationship between the cyclone capacity and free vortex height was proposed by Plitt (1976):

$$Q(= Q_{OS} + Q_{US}) \propto h^{0.16}$$

with Q the volumetric flow-rate through the cyclone and h the free vortex height. This is in agreement with the behaviour reported by Asomah and Napier-Munn (1997).

Plitt (1976) further reported S to be related to the free vortex height as follows:

$$S = \frac{Q_{US}}{Q_{OS}} \propto h^{0.54}$$

Therefore, an increase in h should result in an increase in both Q and S, and accordingly, an increase in the spigot capacity.

Plitt (1976), however, proposed that there is a loss of rotational energy in the underflow region with increasing cone length (or decreasing cone angle), which implies a decrease in the

air core size. Further, Mular and Jull (1978) proposed, “The action of the cone is to squeeze coarse solids towards the centre to obtain a concentrated underflow product”. As a result roping would tend to occur at lower solids concentrations with smaller cone angles.

2.1.3. The Influence of Operational Variables on the Spigot Capacity

(a) Feed pressure

Feed pressure increases the cyclone capacity in accordance with the following relationship:

$$Q \propto P^n$$

Various values for the exponent n obtained by different authors are shown in Table 2.6.

Table 2.6. The exponent n for the relationship between cyclone capacity and feed pressure.

Source	exponent n
Bradley (1965)	0.38-0.5
Rao, Lynch and Nageswararao (1976)	0.49
Plitt (1976)	0.56
Svarovsky (1984)	0.42-0.56
Asomah and Napier-Munn (1997)	0.5

According to Svarovsky (1984) an increase in the feed pressure, with all other variables constant, is associated with a more concentrated underflow and a decrease in the proportion of feed material that exits at the underflow. Plitt (1976) also reported a decrease in S with increasing feed pressure:

$$S = \frac{Q_{US}}{Q_{OS}} \propto P^{-0.25}$$

The effect of feed pressure on S is not too strong. Accordingly the spigot capacity should increase with increasing feed pressure, although the effect should not be a major one due to the effect of pressure on S.

(b) Ore Size

Roping occurs at high solids concentrations within the cyclone, especially at the underflow, it follows then that slurry with finer particles in these conditions will tend to be more viscous than that with coarser particles. Hydrocyclones typically treat particles as large as about 1mm down to zero depending on the application in which they are employed. According to Plitt et al. (1987) higher slurry viscosities retard the rotational motion of the slurry. In agreement with this view, Concha et al. (1996), Davidson (1995), and Dyakowski and Williams (1995) reported increased slurry viscosity to bring about a decrease in the size of the air core. The influence of slurry viscosity on the maximum tangential velocity within a hydrocyclone

reported by Dyakowski and Williams (1995) is shown in Fig. 2.29. Further, Lynch and Rao (1975) reported the cyclone throughput to decrease with increasing fines content in the cyclone feed; they defined fines to be particles passing 53µm.

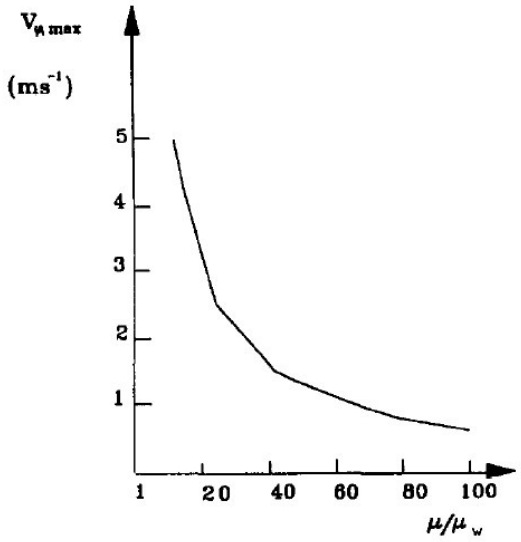


Figure 2.29. Effect of slurry viscosity on the maximum tangential velocity within a hydrocyclone. (Dyakowski and Williams, 1995)

It is therefore expected that the percent solids at which roping commences should be shifted to lower quantities at higher slurry viscosities (finer particle sizes). Plitt et al. (1987) illustrated this behaviour (Fig. 2.30), and proposed the following expressions to show the relationship between the size of the particles in the underflow and $\%V_{MSU}$:

$$\%V_{MSU} = 62.3\left(1 - \exp\left[\frac{-d_u}{60}\right]\right) \qquad (2.6)$$

where d_u is the mass median (50% passing) size of the underflow solids, and $\%V_{MSU}$ is the "percent solids by volume at which the underflow begins to rope and remain during roping". Equation 2.6 and Fig. 2.30 clearly show that at finer particle sizes roping is initiated at lower solids concentrations; hence, the increase in $\%V_{MSU}$ with particle size.

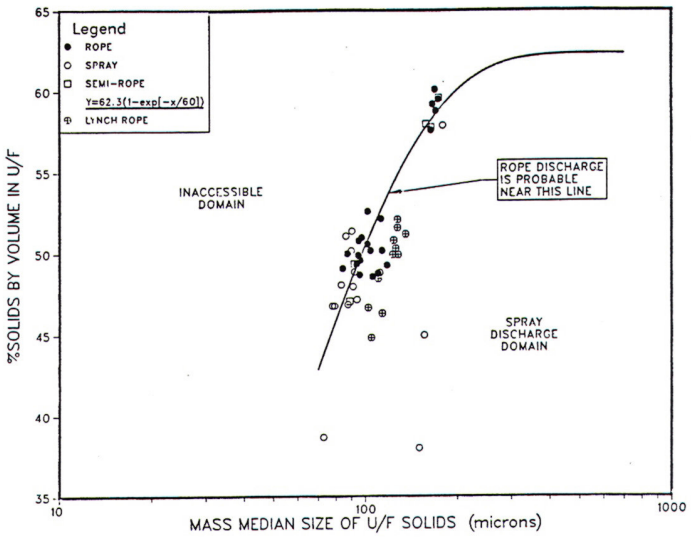


Figure 2.30. Effect of 50% passing particle size on underflow concentration during roping. (Plitt et al., 1987)

Heiskanen (2000), on the other hand, did not observe any relationship between $\%V_{MSU}$ and the 50% passing size (Fig. 2.31). It is expected that particle size influences $\%V_{MSU}$ by changing the packing characteristics of the particles, and the packing characteristics of the particles are more dependent on the size distribution rather than 50% passing size of the material. In agreement with this view Heiskanen (2000) observed, "there is a relationship between roping tendency and the width of particle size distribution" (Fig. 2.32).

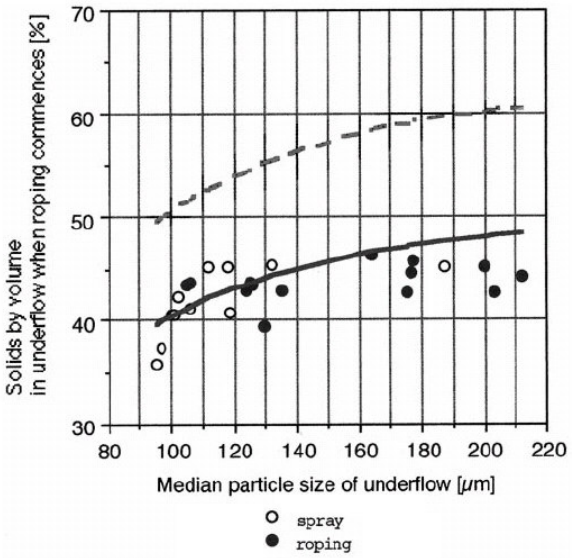


Figure 2.31. Effect of median particle size of underflow on $\%V_{MSU}$. (Heiskanen, 2000)

It remains to be seen whether the behaviour of $\%V_{MSU}$ with changing particle size described above has a significant influence on the spigot capacity.

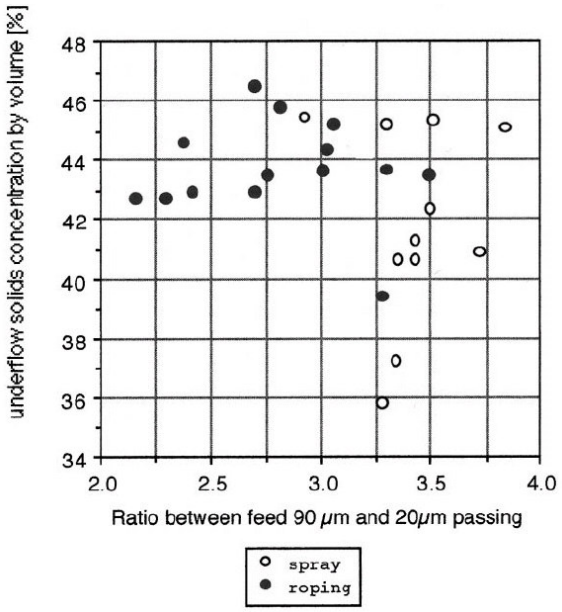


Figure 2.32. Effect of the size distribution of particles at the underflow on the underflow solids concentration at which roping commences. (Heiskanen, 2000)

(c) Ore Density

Particle density does not seem to have any significant influence on the spigot capacity; the effect of particle density on the spigot capacity is illustrated in Fig. 2.33.

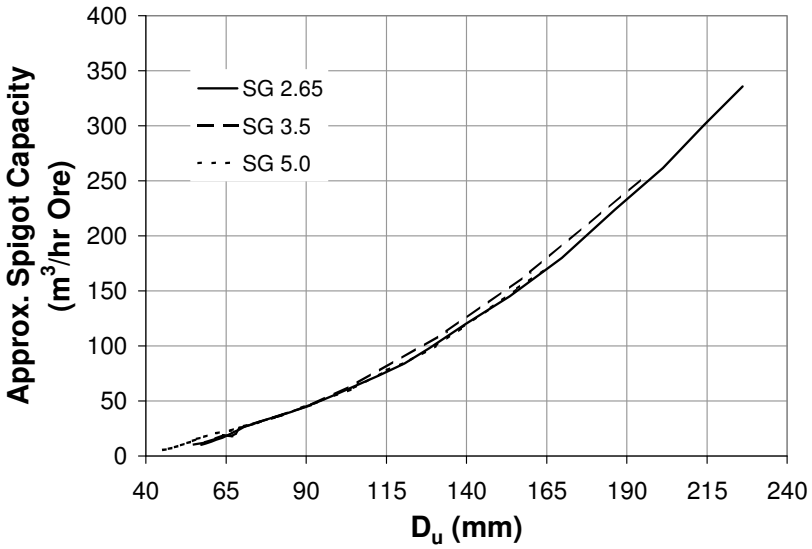


Figure 2.33. Effect of particle density on spigot capacity. (Jull, 1972)

Furthermore, Mular and Jull (1978) reported that particle density does not influence $\%V_{MSU}$; this was illustrated previously in Fig. 2.6.

(d) 'Overflow Throttling'

Neesse et al. (2004c) and Neesse et al. (2007) reported that the discharge capacity of the underflow can be increased by controlling the volume split of a battery of hydrocyclones. They proposed a volume split control method in which a control (or 'throttle') valve at the hydrocyclone overflow is used to regulate the split. By adjusting the 'throttle' valve and the feed pump speed simultaneously, the pressure within the cyclone is intensified resulting in increased underflow discharge capacity. This effect is due to a combination of increased feed pressure (due to feed pump speed) and increased counter-pressure in the overflow (due to 'throttling' valve). The effect of feed pressure on the spigot capacity has been described previously in this chapter, while the effect of the counter-pressure in the overflow on the spigot capacity is very similar to that of the vortex finder diameter. Throttling the overflow, through the control valve, influences the spigot capacity in a similar manner as reducing the overflow diameter.

2.2. DENSE MEDIUM CYCLONES

2.2.1. Characterisation of Overloading at the Sinks

Roping in dense medium cyclones has not been as widely researched as in classification cyclones. None of the literature (referenced in this report) intentionally investigated the overloading behaviour of the dense medium cyclone: roping and spigot overloading were stumbled upon while investigating other phenomena. Some of the interesting papers include those by van der Walt (1950), Stas (1957), Cohen and Isherwood (1960), and Upadrashta and Venkateswarlu (1982).

Both van der Walt (1950), and Cohen and Isherwood (1960) established that there was a maximum sinks ore carrying capacity. While Stas (1957) identified that the cyclone was operating in an "overloaded" condition when a rope discharge was prevalent at the sinks. Upadrashta and Venkateswarlu (1982) proposed that the sinks discharge capacity was exceeded when a rope discharge was encountered at the sinks, but without any evidence to support this notion. Further, Symonds and Malbon (2002) stated, "Apart from the feed capacity, the cyclone has a limit to how much reject material it can handle. This is due to the restriction caused by the apex".

Stas (1957) observed that the "angle of dispersion" of the sinks slurry was reduced with increasing feed solids concentration. In addition he also reported an increase in the thickness (of the annulus) of sinks slurry with increasing feed solids concentration, and therefore a reduction in the air core size. The decrease in the air core size is a consequence of excessive solids concentration at the sinks. Additional increase in the feed concentration resulted in the collapse of the "conical jet" at the sinks (spray discharge) and, as a result, a collapse of the air core. Consequently, the sinks stream was straightened so that the slurry occupied the entire cross section of the spigot (rope discharge).

(a) Sinks Ore Concentration

According to van der Walt (1950), "the quantity of coal which can pass through the (spigot) in unit time, without overloading it, will determine the percentage of coal permissible in the pulp". Peatfield (2003) recommended a medium-to-ore ratio of 3.5:1 (v/v), which is equivalent to 22% coal (v/v), in the feed for typical South African coals with high amounts of near gravity material. Further, Peatfield reported that the minimum recommended feed

medium-to-ore ratio could be as low as 2.5:1; this ratio is, however, applicable only for coal ores with low amounts of near-gravity material. DSM operated with medium-to-coal ratios ranging from 2.2:1 up to 2.7:1 in the feed for coal (Table 2.7). Peatfield proposed that the medium-to-ore ratio in the feed must be increased where the yields (to product of coal) are below 50% in order for the cyclone to be able to handle rejects. Thus, an increase in the proportion of ore in the feed that exits at the sinks necessitates a decrease in the recommended feed concentration to avoid spigot overloading. This implies that it is the sinks ore concentration rather than the feed concentration that is related to overloading at the sinks.

In support of this notion Stas (1957) proposed a mathematical expression that predicts the onset of spigot overloading by expressing it in terms of the sinks slurry density:

$$\rho_U = \rho_F + (\rho_F - \rho_O)\left(\frac{0.921 D_o}{D_u}\right)^{3.5} \qquad (2.7)$$

with ρ_U the relative slurry density in the sinks stream; ρ_F the relative slurry density in the feed and ρ_O the relative slurry density in the floats stream. Equation 2.7 makes use of the sinks slurry density as an indicator of when roping will occur; this expression is not expected to be of much value for two reasons:

- It is based on the expression

$$\frac{Q_{OS}}{Q_{US}} = \left(\frac{0.921 D_o}{D_u}\right)^{3.5},$$

  determined with a cyclone operating with clear water.
- The sinks slurry density at which roping occurred is specific to the conditions under which the tests were performed. Any variation in medium density or ore particle density cannot be taken account with this kind of expression.

What is interesting about equation 2.7, however, is that it is based on the premise that there is a critical sinks ore concentration beyond which roping takes place. Clarkson and Wood (1993) used a similar criterion, in which they propose that spigot overloading can be avoided by not exceeding the volumetric sinks ore concentration of 40% (medium to ore ratio of 1.5:1). Although Wood (1990) also recommended a minimum sinks medium-to-ore ratio of 1.5:1 to avoid spigot overloading, he reported a case in which the volumetric sinks medium-to-ore ratio was 0.9:1 (53% ore by volume) and no serious symptoms such as gross

misplacement of sinks particles to floats stream was observed. Further, he reported that only a 'little disruption to efficient separation' was encountered.

Table 2.7. Ore concentration at the feed and sinks for coal. Sinks concentrations based on assumption that 40% (v/v) of feed pulp was recovered in sinks. (DSM, 1985)

	Feed		Sinks		
D (mm)	C_{vf} (v/v%)	Med:ore Ratio (v/v)	C_{vu} (v/v%)	Med:ore Ratio (v/v)	R_m (v/v)
200	31.3	2.2	39.1	1.6	0.35
250	30.0	2.3	35.0	1.9	0.37
350	26.8	2.7	31.3	2.2	0.38
400	29.9	2.3	29.2	2.4	0.40
500	29.6	2.4	28.0	2.6	0.41
550	29.0	2.4	27.4	2.6	0.41
600	28.9	2.5	26.3	2.8	0.41
650	28.9	2.5	26.7	2.8	0.41
700	29.1	2.4	25.5	2.9	0.42
750	29.0	2.4	25.8	2.9	0.42
800	28.8	2.5	24.0	3.2	0.43

The sinks ore concentrations and medium-to-ore ratios at which DSM possibly operated the cyclones when determining their capacities are shown in Table 2.7. These values are based on the assumption that 40% (v/v) of the feed pulp was recovered at the sinks for all the cyclones. This assumption seems reasonable because R_m obtained with this assumption is in agreement with the maximum R_m of 0.4 as specified by DSM. The maximum R_m of 0.4 was actually specified for the high capacity spigot (D_u/D_o = 0.85), at which the sinks ore concentration should be the highest. Further, the medium-to-ore ratios in the floats stream (Table 2.8), based on the above assumption, appear to suggest that the sinks ore concentrations in Table 2.7 are generally conservative. This is because the recommended minimum medium-to-ore ratio in the floats of 2.5:1 to avoid overloading the vortex finder (Clarkson and Wood, 1993) is exceeded for all the cyclones larger than 350mm in diameter. (The C_{vu} values of 35 and 39% are probably an over-estimation of the values that DSM operated at, given the relatively low floats ore concentrations.) The medium-to-ore ratios given in Table 2.7 are in agreement with the minimum sinks medium-to-ore ratio of 1.5:1 to avoid spigot overloading recommended by Clarkson and Wood (1993). It is, therefore, expected that the spigot capacities specified by DSM were not obtained during roping conditions.

Table 2.8. Ore concentrations in the floats based on the assumption that 40% (v/v) of the feed pulp was recovered at the sinks.

	Floats	
D mm	**C_{vf} (v/v%)**	**Med:ore ratio**
200	26.0	2.8
250	26.7	2.8
350	23.8	3.2
400	30.3	2.3
500	30.7	2.3
550	30.1	2.3
600	30.7	2.3
650	30.4	2.3
700	31.4	2.2
750	31.1	2.2
800	32.0	2.1

As mentioned previously, DSM operated the cyclones at feed medium-to-ore ratios ranging from 2.2 to 2.7:1. England et al. (2002), on the other hand, quoted spigot capacities equivalent to those by DSM but the applicable feed medium-to-ore ratios ranged from 3.42-3.51:1 (Table 2.9). The data reported by England et al. (2002) was for 'relatively difficult to treat South African coal'. This is in agreement Peatfield (2002) who recommended a feed medium-to-ore ratio of 3.5:1 for typical South African coals with high near-gravity material.

Table 2.9. Ore concentrations in the feed when the cyclones were operating at their spigot capacities. (England et al., 2002)

D (mm)	**Feed Med:Ore Ratio (v/v)**	**C_{vf} (v/v%)**
360	3.42	22.6
420	3.44	22.5
510	3.51	22.2
610	3.50	22.2
710	3.51	22.2
800	3.49	22.3
900	3.50	22.2
1000	3.49	22.2
1150	3.50	22.2
1300	3.50	22.2

Stas (1957) observed that once roping commenced the sinks slurry density remained constant with further increase in the feed solids concentrations. Cohen and Isherwood (1960) reported that the sinks slurry density obtained when the spigot was overloaded is dependent on the specific gravity and packing characteristics of the sinks solids. They further postulated that

the sinks slurry density should be relatively high when the spigot capacity has been reached or exceeded.

(b) Effect of roping on cyclone performance

Stas (1957) observed that the floats slurry density increased with increasing feed ore concentration when roping was prevalent at the spigot. The increase in the floats slurry density is due to misplacement of some of the sinks particles to the floats. According to Cohen and Isherwood (1960) this misplacement of sinks particles to the floats occurs because of "lack of accommodation" in the sinks. Upadrashta and Venkateswarlu (1982) proposed the following expressions:

$$S = \frac{Q_{US}}{Q_{OS}} = 1.44(1 - C_V)^{-0.18} Q^{-0.44} \left(\frac{D_u}{D_o} \right)^{2.32} \quad \text{(Spray discharge)} \qquad (2.8)$$

$$S_R = \frac{Q_{USM}}{Q_O} = 1.91(1 - C_V)^{1.1} Q^{-0.44} \left(\frac{D_u}{D_o} \right)^{2.32} \quad \text{(Rope discharge)} \qquad (2.9)$$

with C_V the volume fraction of the FeSi and ore in the feed. The increase in S with increasing C_V during spray discharge was explained to be a consequence of the reduction of the air core size at the sinks, which resulted in an increase in the proportion of material exiting through the spigot. The decrease in S_R with increasing C_V during rope discharge is a result of misplacement of the sinks particles to the floats stream due to the overloaded spigot.

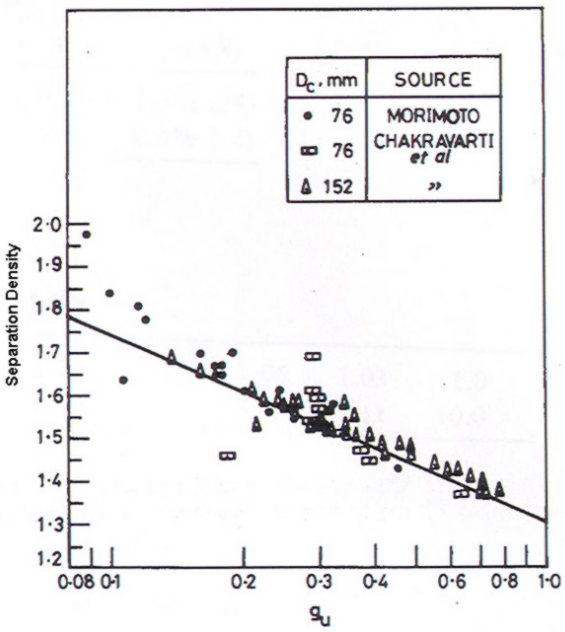


Figure 2.34. Separation density vs ore recovery in sinks (mass fraction) for coal. (Upadrashta and Venkateswarlu, 1982)

Upadrashta and Venkateswarlu (1982) reported the separation density to increase with a decrease in the ore recovery in the sinks for coal and other minerals (Fig. 2.34 and 2.35). Although Upadrashta and Venkateswarlu did not distinguish between separation densities obtained during roping and those obtained with a spray discharge (in Fig. 2.34 and 2.35), it is known that some of their results were obtained during roping. When roping is prevalent at the sinks stream the ore recovery in the sinks should generally be low due to misplacement of sinks particles to the floats. As illustrated in Fig. 2.34 and 2.35 the highest separation densities were obtained at the lowest ore recoveries in the sinks. It can therefore be deduced from this that the separation density should increase when the spigot is overloaded. In support of this view van der Walt (1950) and Cohen and Isherwood (1960) also reported the separation density to increase when the spigot was overloaded.

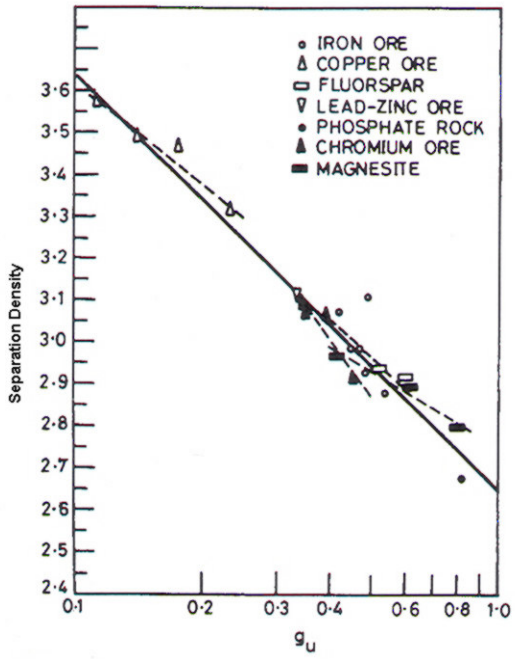


Figure 2.35. Separation density vs ore recovery in sinks (mass fraction). (Upadrashta and Venkateswarlu, 1982)

Upadrashta and Venkateswarlu (1982) proposed the following relationship between ore recovery in the sinks (g_u) - mass fraction - and separation density (ρ_{50}):

$$\rho_{50} = a_o \log(g_u) + a_1 \qquad (2.10)$$

with a_o and a_1 constants. The value of a_1 is said to correspond to the relative density of the lightest constituent of the feed material. The values of constants a_o and a_1 for coal and other ores (as listed in Fig. 2.35) are given in Table 2.10.

Table 2.10. Constants a_o and a_1 for equation 2.10.

	Constant a_o	**Constant** a_1
Coal	-0.48	1.304
Other ore	-0.984	2.654

Stas (1957) also observed the separation density to increase when the spigot was overloaded, as illustrated in Fig. 2.36. Stas induced roping at the sinks by changing the spigot diameter from 19.5mm, at which a spray discharge was prevalent, to 12.5mm, at which a rope discharge was observed. The increase in the separation density observed in Fig. 2.36 when the spigot diameter was reduced from 19.5 to 12.5mm is partly due to the decrease in spigot diameter and partly due to spigot overloading. The most notable change on the partition curve obtained during roping is that on its shape (Fig. 2.36). During roping there is increased misplacement of sinks particles to the floats stream. The separation efficiency clearly suffers when the spigot is overloaded. This view has been expressed by a number of authors including: van der Walt (1950), King and Juckes (1984), Wood et al. (1989) and Sripriya et al. (2001).

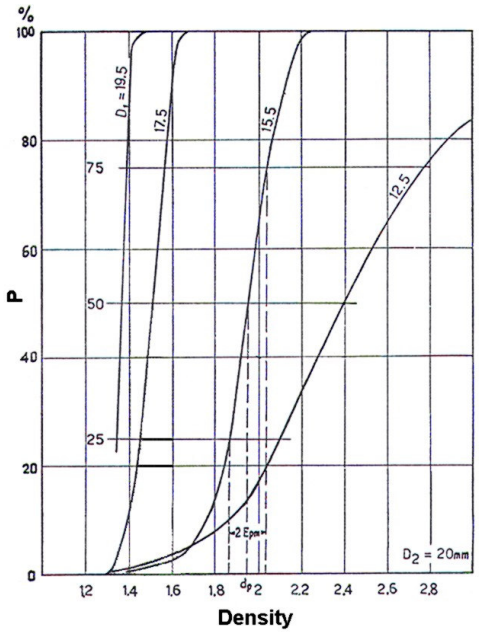


Figure 2.36. Influence of spigot overloading on the cyclone performance. Spigot overloaded at D_u = 12.5mm and normal operation at D_u = 19.5mm. (Stas, 1957)

Leonard and Leonard (1983) illustrated the effect of spigot overloading on the partition curve as shown in Fig. 2.37. Short-circuiting of sinks particles to the floats is illustrated to take place when the spigot is overloaded.

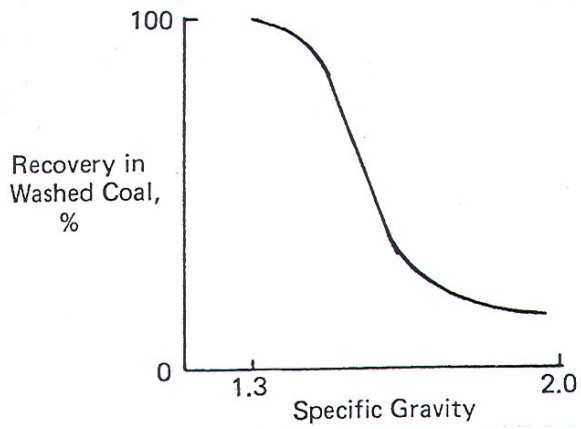


Figure 2.37. The spigot overloading on the shape of the partition curve. (Leonard and Leonard, 1983)

According to King and Juckes (1984) when the volumetric medium-to-coal ratio approaches 1:1 the coal particles interact with each other and this interaction changes the medium properties. As a result of this interaction the performance of the dense medium cyclone as a separating device is significantly affected. King and Juckes further reported that there is a lower limit for EPM of 0.01 when the volume proportion of coal in the slurry increased to values that are relevant to industrial practice, presumably at medium-to-ore ratios around 3:1.

2.2.2. Influence of Cyclone Geometry on Spigot Capacity

(a) Inlet Size

Q is related to the inlet diameter in accordance with the following relationship:

$$Q \propto D_i^n$$

Various values for the exponent *n* obtained in the literature are given in Table 2.11. There is agreement in the literature that D_i has a strong influence on Q. Upadrashta and Venkateswarlu (1982) determined this relationship during spray and rope discharges, and Q was reported to be more sensitive to D_i during roping than when a spray discharge was prevalent.

Table 2.11. The exponent *n* for the relationship between inlet diameter and Q.

Source	Exponent *n*
DSM (1985)	1.0
Dunglison (1991)	1.0
Upadrashta and Venkateswarlu (1982)	1.0*
Upadrashta and Venkateswarlu (1982)	1.8#

*Spray discharge.
#Rope discharge.

The inlet is not expected to have a significant influence on the volume split within the cyclone. Thus, increasing the inlet size should generally increase the flow-rates of slurry through both the spigot and the vortex finder, more or less equally. The inlet increases the flow-rate of material exiting through the outlets by increasing their exit velocities. Accordingly, the spigot capacity should increase with increasing inlet size.

(b) Spigot Diameter

The spigot diameter influences Q in accordance with the following relationship:

$$Q \propto D_u^n$$

The values of the exponent *n* obtained by various sources in the literature are given in Table 2.12. D_u has a relatively small effect on Q.

Table 2.12. The exponent *n* for the relationship between Q and D_u.

Source	Exponent *n*
Clarkson and Wood (1993)	0.15
Dunglison (1991)	0.308
Verghese and Rao (1994)	0.185
Wood et al. (1989)	0.15

Upadrashta and Venkateswarlu (1982), on the other hand, related Q with spigot diameter and vortex finder diameter as follows:

$$Q \propto (D_u^2 + D_o^2)^n$$

with n = 0.30 during spray discharge and n = 0.26 during rope discharge. According to Upadrashta and Venkateswarlu the nature of the influence of D_u and D_o on Q changes slightly with the change in flow type from spray to rope discharge.

Further, the volume split is related to the spigot and vortex finder diameters as follows:

$$\frac{Q_{US}}{Q_{OS}} \propto \left(\frac{D_u}{D_o}\right)^n$$

The values of the exponent *n* obtained by various sources in the literature are given in Table 2.13. Upadrashta and Venkateswarlu (1982) reported the effect of D_u on S to be the same during spray and rope discharges. This is surprising considering that there is an air core at the sinks during spray discharge and none during rope discharge.

Table 2.13. The exponent *n* for the relationship between S and D_u.

Source	Exponent *n*
Stas (1957)	3.5[a]
Upadrashta and Venkateswarlu (1982)	2.32[b]

[a]Cyclone operated with water only.
[b]Valid for spraying and roping conditions.

Spigot diameter generally has a small but significant influence on Q. However, D_u does have a very strong influence on the slurry split to the sinks as shown in Table 2.13. In fact, it is expected that the spigot capacity should be determined mainly by the dimensions of the spigot diameter.

The relationship between spigot diameter and spigot ore capacity obtained by the original developers of the dense medium cyclone, Dutch State Mines (DSM), is illustrated in Fig. 2.38. This figure shows the spigot capacities for dense medium cyclones beneficiating coal whereby the medium was magnetite. The cyclone was operated at a head of 9D.

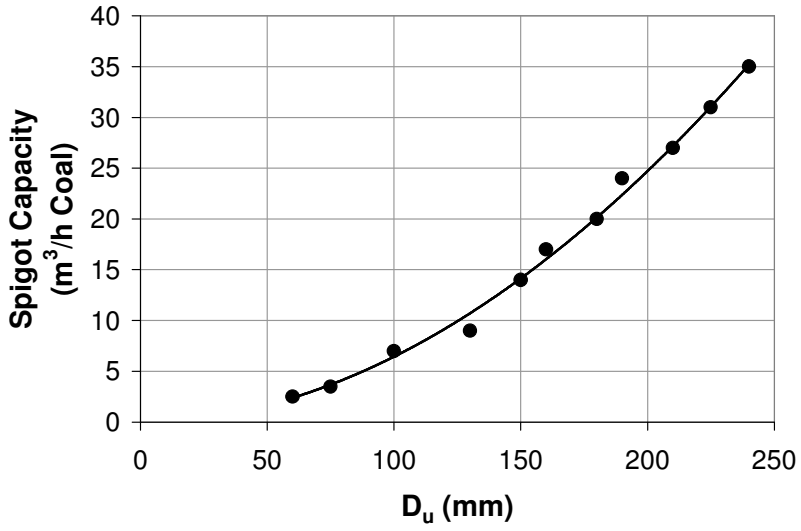


Figure. 2.38. The relationship between spigot diameter and spigot capacity for coal. (DSM, 1985)

A regression of the data in Fig. 2.38 gives the following relationship:

$$Q_{UM} = (0.9\times10^{-3})D_u^{1.94} \qquad (2.11)$$

with D_u in mm and Q_{UM} (ore only) in m^3/hr (R^2 = 0.9944). The spigot capacity for dense medium cyclones appears to depend mainly on the cross-sectional area of the spigot. As previously illustrated, it is thought that these spigot capacities were determined under conditions in which roping was not prevalent at the sinks stream. England et al. (2002) reported spigot capacities that were equivalent to those specified by DSM; these are shown in Fig. 2.39. It appears that the spigot capacities specified by England et al. were actually based on DSM data.

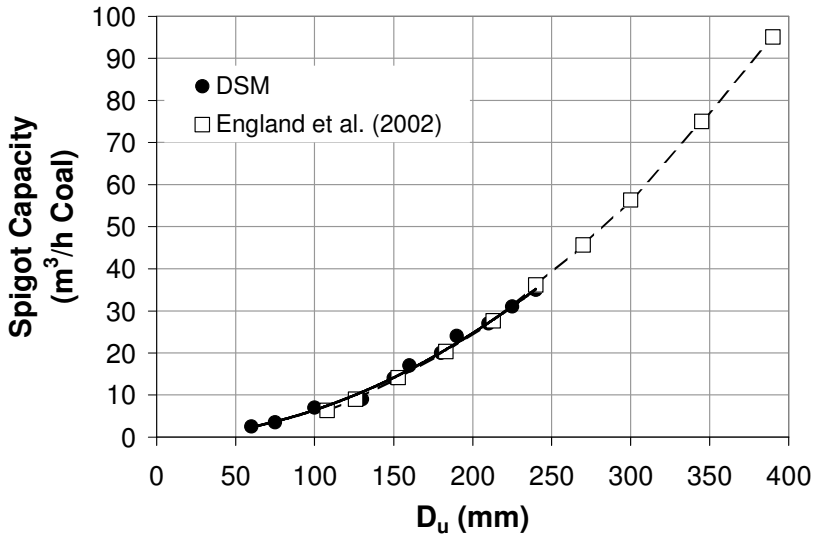


Figure 2.39. The relationship between spigot diameter and spigot capacity for coal.

The relationship between spigot diameter and spigot capacity for industrial minerals and ores at various feed pressures are shown in Fig. 2.40. Regression analysis of the data in Fig. 2.40 yielded the following expression:

$$Q_{UM} = (0.17\times10^{-3})D_u^{2.05}H^{0.19} \qquad (2.12)$$

with H the feed head in D (cyclone diameter) and $R^2 = 0.9911$. This expression is consistent with equation 2.11 above.

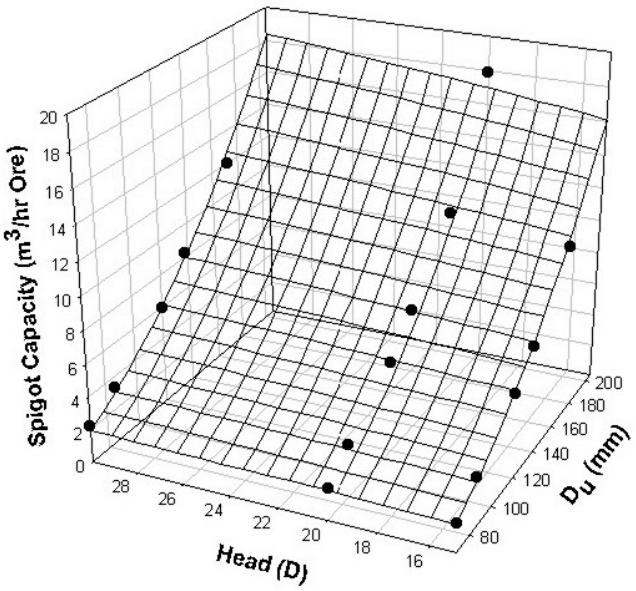


Figure. 2.40. The relationship between spigot diameter and spigot capacity for industrial minerals and ores with increasing feed pressure. (DSM, 1985)

Equation 2.11 was obtained from geometrically similar dense medium cyclones ranging from 200 to 800mm in diameter. The same can be said of equation 2.12, although the cyclone diameters ranged from 200 to 600mm. Each of the cyclones employed had a standard DSM configuration as shown in Table 2.14. The standard D_u size for other minerals (not being coal), which are separated at higher feed pressures, is $0.8D_o$ and not $0.7D_o$ as is the case for coal. The actual dimensions (in mm) are given in Table A.1 in the Appendix. According to DSM (1985), the maximum allowable spigot diameter on a dense medium cyclone is 85% of the vortex finder diameter; beyond this separation efficiency suffers.

Table 2.14. Dimensions of the cyclones employed by DSM, as a fraction of the cyclone diameter.

D_i/D	0.20
D_o/D	0.43
D_u/D	0.3
α (deg.)	20
Bl/D	0.6-0.7

Furthermore, Stas (1957) illustrated that larger spigot-to-vortex finder diameters ratios tend to shift the onset of roping to commence at much higher flow-rates (of slurry and ore) at the sinks. Although Stas (1957) did not measure the spigot capacity, his observations support the notion that spigot capacity increases with increasing spigot size.

(c) Vortex Finder Diameter

The vortex finder diameter has been reported to influence Q in accordance with the following relationship:

$$Q(= Q_{OS} + Q_{US}) \propto D_O^n$$

The values of the exponent *n* obtained by various sources in the literature are given in Table 2.15. The decrease in Q with increasing vortex finder diameter, reported by Clarkson and Wood (1993), and Wood et al. (1989), is counter-intuitive. Like Verghese and Rao (1994), Restarick and Krnic (1991) also observed Q to increase with the vortex finder diameter, although they did not quantify the effect.

Table 2.15. The exponent *n* for the relationship between Q and D_O.

Source	Exponent *n*
Clarkson and Wood (1993)	-0.15
DSM (1985)	1.0
Verghese and Rao (1994)	0.414
Wood et al. (1989)	-0.15

As shown previously, Upadrashta and Venkateswarlu (1982) related Q with spigot diameter and vortex finder diameter as follows:

$$Q \propto (D_u^2 + D_o^2)^n$$

with $n = 0.30$ during spray discharge and $n = 0.26$ during rope discharge.

It is, therefore, expected that Q should increase with increasing D_o. With all other conditions being the same, D_o strongly increases the slurry flow through the vortex finder at the expense of slurry flow at the sinks. The effect of the vortex finder diameter on S was illustrated previously in Table 2.13. According to Cohen and Isherwood (1960) overcrowding at the floats forces some of the floats material to exit at the sinks. Further, Stas (1957) reported larger spigot-to-vortex finder diameters ratios to shift the onset of roping to commence at much higher flow-rates (of slurry and ore) at the sinks. Therefore, the spigot capacity should increase with decreasing vortex finder diameter. However, it is not clear to what extent the vortex finder will have an effect on the spigot capacity (Q_{USM} and Q_{UM}).

(d) Cone Angle

Van der Walt (1950) observed that the rate of flow through the cyclone increases as the cone angle decreases. This trend was generally true when operating the cyclone with water only and with pulp. Further, van der Walt determined that the actual volume of the cyclone increases with decreasing cone angle. The proportion of feed water exiting at the sinks was observed to increase with decreasing cone angle when operating the cyclone with water only. Thus, according to van der Walt (1950) a decrease in the cone angle should increase the slurry flow through the spigot and therefore the spigot capacity as well.

Cohen and Isherwood (1960), on the other hand, observed that at a given feed solids density, "a 15^o cone would be completely choked, a 30^o cone would give a 'ropey discharge' and a

60^{o} cone would spray freely, all other conditions being equal". Thus, an increase in the cone angle shifted the onset of roping to commence at higher feed solids contents.

(e) Barrel Length

The effect of the length of the cylindrical section on the spigot capacity is illustrated in Fig. 2.41; an increase in the barrel length did not influence spigot capacity in anyway. The standard/normal cylindrical section had a length of about 0.6D, and the extra long cylindrical section was 2.5D long.

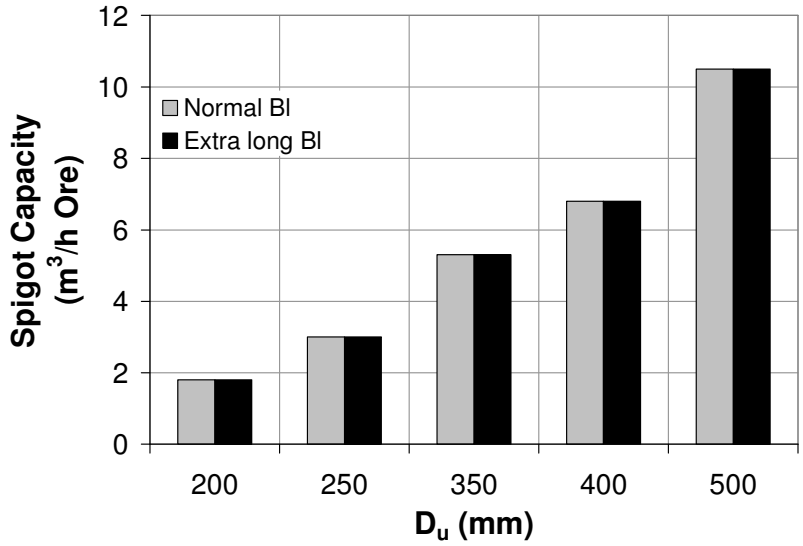


Figure 2.41. The influence of the barrel length on the spigot capacity. (DSM, 1985)

An increase in the cyclone capacity, however, accompanied the increase in the length of the cylindrical section (Fig. 2.42).

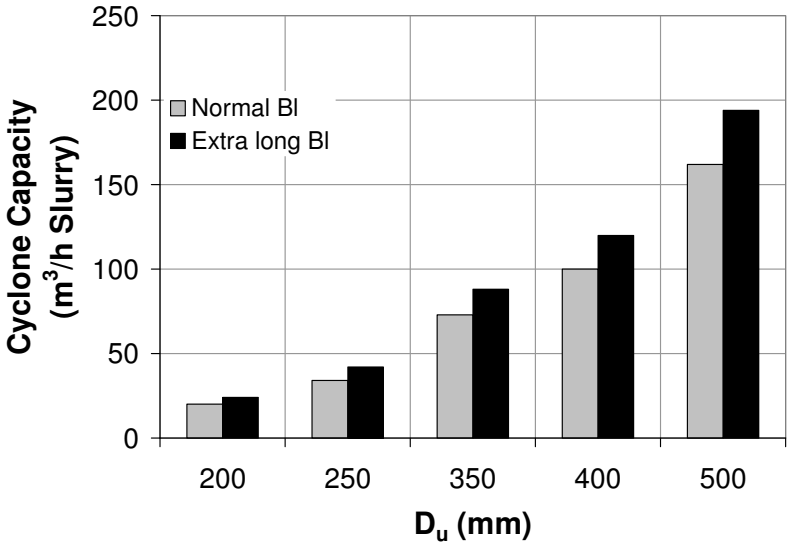


Figure 2.42. The influence of the barrel length on the cyclone capacity. (DSM, 1985)

The solids concentrations for the data presented in Fig. 2.41 and 2.42 are given in Table 2.16. The cyclones with the normal barrel length were operated with lower medium-to-ore ratios ranging from 3.49 to 4.27:1 (18.98 – 22.27% vol. feed concentrations), while those with the extra long barrel were operated at higher medium-to-ore ratios ranging from 4.33 to 5.16:1 (16.24 – 18.75% vol. feed concentrations). These differences in the feed medium-to-ore ratios are possibly due to the fact that the extra long cylindrical sections are used mainly for difficult-to-separate ores. Cyclones generally separate more efficiently at higher feed medium-to-ore ratios. Assuming that S is not influence by Bl, it would be expected that a cyclone with a longer barrel length should have a higher spigot capacity for constant medium-to-ore ratios in the feed when treating the same ore.

Table 2.16. Feed concentrations for the curves in Fig. 2.41 and 2.42. (DSM, 1985)

		Normal barrel		Extra long barrel	
D_c (mm)	H (D)	Feed Med:Ore ratio (v/v)	C_{vf} (v/v%)	Feed Med:Ore ratio (v/v)	C_{vf} (v/v%)
200	15	3.49	22.27	4.33	18.75
250	15	3.82	20.75	4.60	17.86
350	15	4.09	19.64	4.87	17.05
400	15	3.84	20.67	4.71	17.50
500	15	4.27	18.98	5.16	16.24

2.2.3. Influence of Operational Variables on Spigot Capacity

(a) Feed pressure

Feed pressure /head has been reported to influence Q as follows:

$$Q \propto H^n$$

Various values of the exponent *n* in the literature are given in Table 2.17. As expected, an increase in the feed pressure results in an increase in Q. Upadrashta and Venkateswarlu (1982) reported Q to be slightly more sensitive to changes in pressure during roping than when a spray discharge was prevalent at the sinks.

Table 2.17. The exponent *n* for the relationship between Q and feed pressure.

Source	Exponent *n*
Clarkson and Wood (1993)	0.15
DSM (1985)	0.5
Upadrashta and Venkateswarlu (1982)	0.41*
Upadrashta and Venkateswarlu (1982)	0.58#
Wood et al. (1989)	0.45
Wood (1990)	0.46

*Spray discharge.
#Rope discharge.

S is influenced by the feed pressure in accordance with the following relationship:

$$\frac{Q_{US}}{Q_{OS}} \propto H^n$$

Various values of the exponent *n* in the literature are given in Table 2.18. An increase in head appears to bring about a decrease in the proportion of the feed slurry that exits at the sinks.

Table 2.18. The exponent *n* for the relationship between S and head.

Source	Exponent *n*
Clarkson and Wood (1993)	-0.37*
Wood et al. (1989)	-0.5*
Wood (1990)	-0.46

*Determined with zero ore loading.

Van der Walt (1950) reported that the 'maximum permissible spigot loading', that is the spigot capacity, increased with increasing feed pressure. The effect of feed pressure (expressed as head) on the spigot capacity, as reported in the DSM handbook for cyclones beneficiating industrial minerals with ferrosilicon as medium, is shown in Fig. 2.43. Spigot capacity increases with increasing feed pressure. Note Fig. 2.43 is the same as Fig. 2.40 above. The effect of feed pressure on the spigot capacity was illustrated previously in equation 2.12, which is repeated here for convenience:

$$Q_{UM} = (0.17\times10^{-3})D_u^{2.05}H^{0.19} \qquad (2.12)$$

Wood (1990) reported head to have a small influence on the sinks flow-rate.

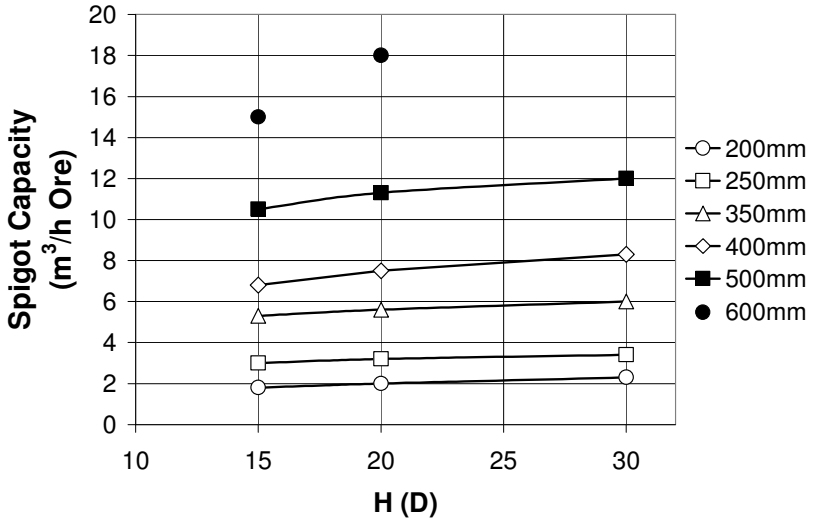


Figure. 2.43. The effect of feed pressure on spigot capacity. (DSM, 1985)

According to Cohen and Isherwood (1960), the effect of pressure on the rate of flow through the spigot is restricted by the high viscosity of the sinks pulp. Napier-Munn (1986) reported that the pressure drop across a dense medium cyclone appears to be a function of the total medium rheology. He proposed that the relationship between flow through cyclone and pressure at low Reynolds numbers is as follows:

$$Q \propto H^{0.59},$$

and medium viscosity plays little or no part in determining the pressure drop. At high Reynolds numbers the relationship between flow through cyclone and pressure can be represented as follows:

$$Q \propto H^{n},$$

with $n < 0.5$. The actual value of the exponent n is related to the prevailing medium viscosity.

(b) Medium Density

Medium density has been reported to influence Q as follows:

$$Q \propto \rho_{med}^{n}$$

The values of the exponent *n* obtained by various sources in the literature are given in Table 2.19; Q decreases with increasing ρ_{med}.

Table 2.19. The exponent *n* for the relationship between Q and medium density.

Source	Exponent *n*
Napier-Munn (1986)	-0.59[a]
Napier-Munn (1986)	-0.79 to -0.99[b]
Verghese and Rao (1994)	-2.17

[a]Low Reynolds number.
[b]High Reynolds number.

Upadrashta and Venkateswarlu (1982), on the other hand, reported medium density to influence Q in accordance with the following relationship:

$$Q \propto (1 - C_V)^m \rho_{med}^{n}$$

with C_V the volume fraction of FeSi and ore in the feed, and ρ_{med} the relative medium density. The values for the exponents *m* and *n* are given in Table 2.20.

Table 2.20. The exponent *n* for the relationship between Q and medium density according to Upadrashta and Venkateswarlu (1982).

Source	Exponent *n*	Exponent *m*
Upadrashta and Venkateswarlu (1982)	-0.41[*]	0.12[*]
Upadrashta and Venkateswarlu (1982)	-0.58[#]	0.56[#]

[*]Spray discharge.
[#]Rope discharge.

ρ_{med} is not expected to influence S and S_R significantly, thus, the spigot capacity should decrease with increasing medium density.

It is interesting to note that DSM does not specify medium densities for the spigot capacities given in the DSM handbook. This omission implies that medium density has no influence on the spigot capacity. Cohen and Isherwood (1960), on the other hand, postulated, "A rise in

flow-rate and a rise in the proportion of ferrosilicon both increase the feed rate of (sink) material and hence both lead to overloading of the apex orifice".

(c) Medium Grade

The medium grade refers to the particle size distribution of the medium particles; finer medium grades tend to be more viscous than coarser grades. He and Laskowski (1995b) reported the cyclone flow-rate, when operated with medium only, to be the highest when operating with the coarsest medium. The medium split was unaffected by changes in the medium grade. Assuming that these trends would still hold at low medium-to-ore ratios, then the spigot capacity should increase when the medium particles are relatively coarse.

Medium segregation within dense medium cyclone is dependent on medium grade, and coarser grades tend to segregate more (He and Laskowski, 1995b).

(d) Ore Size

Of all the literature that has been considered none has proposed or implied any correlation between cyclone flow-rate and particle size. The same can be said of the relationship between S and particle size.

Cohen and Isherwood (1960), on the other hand, reported that the sinks slurry density obtained when the spigot was overloaded is dependent on the specific gravity and packing characteristics of the sinks solids. And the packing characteristics of solids are dependent on the particle size and size distribution.

The effect, if any, of particle size on the spigot capacity is unclear.

(e) Ore Density

The effect of ore density on the spigot capacity is illustrated in Fig. 2.44. Assuming that the use of ferrosilicon as medium does not influence the spigot capacity significantly, then it can be deduced from Fig. 2.44 that ore density significantly decreases the spigot capacity.

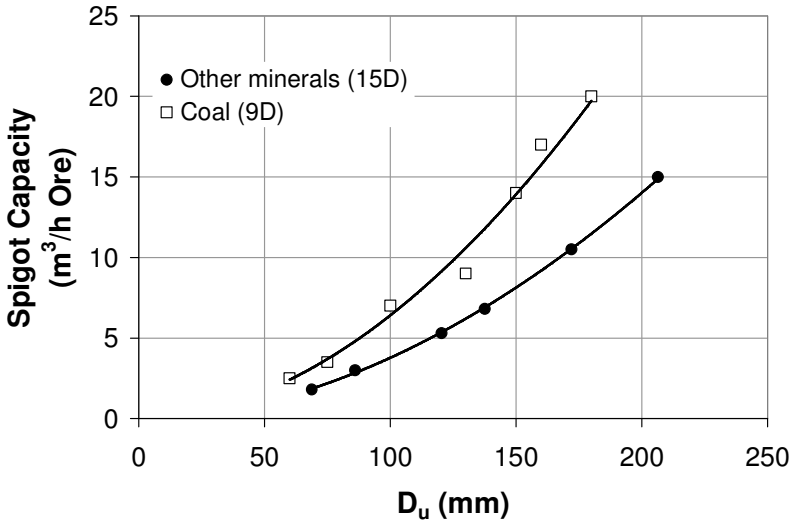


Figure 2.44. The effect of ore density on spigot capacity. (DSM, 1985)

2.3. Summary of Literature Review

(a) Characterisation of Overloading at the Spigot

- There is consensus in the literature that the maximum spigot capacity is reached at the onset of roping, although no clear evidence has thus far been presented to support this notion; this applies to both classification and dense medium cyclones.

- There is a critical underflow/sinks solids concentration beyond which roping commences. The air core at the underflow/sinks has been reported to collapse during the commencement of roping for both cyclonic devices. It has been proposed that excessive solids concentrations at the underflow/sinks are responsible for the collapse of the air core during the onset of roping (Plitt et al., 1987 and Stas, 1957). Before roping commences, an increase in solids content within the cyclone has been reported to steadily reduce the air core size until sufficient solids accumulate at the underflow/sinks to bring about the collapse of the air core (Gutiérrez et al., 2000 and Stas, 1957). The effect of the solids concentration can be explained by considering the effect of the solids concentration on the slurry viscosity. Slurry viscosity increases slightly with increasing solids concentration at relatively low solids loadings; however, once a certain critical solids concentration is reached further increases in the solids concentration result in very sharp increases in the slurry viscosity. Plitt et al. (1987) proposed that once the critical underflow solids concentration is reached the slurry viscosity becomes so high that the rotational motion at the underflow can no longer be sustained, as a result the air core collapses and roping commences. This notion was also proposed by Dyakowski and Williams (1995).

- A number of authors have developed mathematical expressions that attempted to predict the onset of roping. All these expressions make use the underflow/sinks solids concentration as an indicator of the onset of roping; this applies to both dense medium and classification cyclones.

- A number of authors have reported the underflow solids concentration during roping for classification cyclones ($\%V_{MSU}$) to remain constant once roping has been initiated, even with further increase in the feed solids concentration. While, on the other hand, some have reported $\%V_{MSU}$ to increase with further increases in the feed solids concentration. It is

thought that the increase in $\%V_{MSU}$ with increasing feed solids concentration is a consequence of increased short-circuiting of fines to the underflow; water split to the underflow has previously been shown to increase with increasing feed solids concentration (Lynch and Rao, 1975, and Asomah and Napier-Munn, 1997). The volumetric sinks ore concentrations during roping for dense medium cyclones have also been reported to be constant (Stas, 1957).

- Various authors operating classification cyclones of different sizes and configurations under a variety of conditions have reported $\%V_{MSU}$ ranging between 39 and 68% (by volume). Clarkson and Wood (1993) proposed that spigot overloading in dense medium cyclones could be avoided by not exceeding the volumetric sinks ore concentration of 40%. The volumetric sinks ore concentrations inferred from the DSM data are in agreement with this value.

- Once roping commences, misplacement of particles that normally exit at the underflow/sinks to the overflow/floats has been widely reported. In the case of classification cyclones coarse particles are misplaced to the overflow, while with the dense medium cyclones sinks particles are misplaced to the floats stream.

(b) Influence of Roping on Cyclone Performance

- Roping has widely been established to result in an increase in the cut-size of classification cyclones due to of misplacement of coarse particles to the overflow. The separation density has also reported to increase once roping commenced within a dense medium cyclone. The following expressions, in which roping was prevalent at low g_u values, were proposed:

$$d_{50} = -196\log(g_u) \qquad (2.3)$$

$$\rho_{50} = a_o \log(g_u) + a_1 \qquad (2.10)$$

with a_o and a_1 constants; their values are given in Table 2.10. Equation 2.3 is applicable to classification cyclones, while equation 2.10 applies to dense medium cyclones.

- Fahlstrom (1963) reported the sharpness of separation to decrease once roping commenced. Plitt et al. (1987) also reported the same trend, although they reported that the effect of roping on the sharpness of separation was dependent on the feed solids

concentration. There is consensus in the literature that the separation efficiency of a dense medium cyclone suffers when roping is prevalent at the sinks stream.

(c) Effect of Cyclone Geometry on Spigot Capacity

- The nature of the relationship between spigot ore capacity and spigot diameter obtained by Jull (1972), Plitt et al. (1987) and DSM was generally of the following form:

$$Q_{UM} = k_o D_u^n \qquad (2.13)$$

with D_u the spigot diameter in mm; Q_{UM} in m^3/hr of ore. The values for the constant k_o and the exponent *n* are shown in Table 2.21. Heiskanen (2000) validated the expression developed by Plitt et al. (1987). Plitt et al. (1987) operated their cyclone with a rope discharge at the underflow, while Jull (1972) operated theirs "just short of roping". It is thought that DSM did not operate their cyclone under roping conditions. Thus, the 'spigot capacities' specified by DSM do not represent the maximum spigot capacity.

Table 2.21. Comparison of spigot diameter-spigot capacity relationships in the literature.

Source	Cyclone Type	$k_o \times 10^3$	Exponent *n*
Jull (1972)	Classification	2.3	2.19
Plitt et al. (1987)	Classification	1.563	2.35
DSM	Dense medium	0.654	1.99
DSM	Dense medium	-*	2.05

*Dependent on head.

- $\%V_{MSU}$ has been reported to increase with increasing D_u/D_o ratio by Fahlstrom (1963) and Heiskanen (2000). Concha et al. (1996) proposed that there is a specific range of underflow-to-overflow diameters ratios in which a rope discharge will be obtained at the underflow. It is, however, the author's opinion that the onset of roping is determined mainly by the solids concentration, and roping can occur at any D_u/D_o ratio provided the solids concentration within the cyclone is sufficiently high.

- Increasing D_i generally increases the flow-rates of slurry through both the spigot and the vortex finder, more or less equally since S is unaffected by changes in D_i. Thus, the spigot capacity should increase with increasing D_i. This applies to both classification and dense medium cyclones.

- A larger D_o tends to increase Q, and strongly increase the proportion of feed slurry exiting at the overflow/floats at the expense of the underflow/sinks. The spigot capacities of both classification and dense medium cyclones should, therefore, decrease with increasing D_o.

- According to Bradley (1965) and Svarovsky (1984) an increase in the overall length of a classification cyclone, either through a larger cylindrical section or a smaller cone angle, increases the capacity of the cyclone. Further, Plitt (1976) reported S to increase with increasing free vortex height, which is defined as the distance from the bottom of the vortex finder to the top of the spigot. Accordingly, spigot capacity is expected to increase with decreasing cone angle and increasing barrel length.

- Van der Walt (1950) reported the cone angle to have the same effect on a dense medium cyclone as that reported by Bradley (1965), Svarovsky (1984), and Plitt (1976) for the classification cyclone. It can be inferred from the data reported by DSM that the spigot capacity should possibly increase with increasing barrel length. Further, Cohen and Isherwood (1960) reported that at a given feed solids density, "a 15^o cone would be completely choked, a 30^o cone would give a 'ropey discharge' and a 60^o cone would spray freely, all other conditions being equal". Thus, an increase in the cone angle shifted the onset of roping to commence at higher feed solids contents.

(d) Effect of Operational Variables on Spigot Capacity

- An increase in feed pressure is associated with an increase in Q and a relatively small decrease in S. Accordingly, the spigot capacity should increase with increasing feed pressure for both classification and dense medium cyclones. However, the effect of feed pressure on the spigot capacity is expected to be relatively small due to its effect on S. Further, DSM reported spigot ore capacity to increase slightly with increasing feed pressure.

- Plitt et al. (1987) reported $\%V_{MSU}$ to increase with increasing d_u, which is the mass median (50% passing) size of the underflow solids. Heiskanen (2000), on the other hand, observed, "there is a relationship between roping tendency and the width of particle size distribution". Further, Cohen and Isherwood (1960) implied that the sinks ore

concentration during roping is dependent on particle size and size distribution. The effect of particle size on the spigot capacity is, however, unclear from the literature; this applies to both classification and dense medium cyclones.

- Jull (1972), and Mular and Jull (1978) reported particle density to have no influence on the spigot capacity. Further, Jull (1972) reported $\%V_{MSU}$ to be unaffected by changes in particle density. There are indications that the heavier ore particles tend to reduce the spigot capacity.

- Neesse et al. (2004c) and Neesse et al. (2007) reported that the discharge capacity of the underflow can be increased by controlling the volume split of a hydrocyclone through 'overflow throttling'. Throttling the overflow, through the control valve, influences the spigot capacity in a similar manner as reducing the overflow diameter.

- An increase in medium density has been reported to decrease both Q, and S is not expected to be dependent on medium density. The spigot capacity is, therefore, expected to decrease with increasing medium density.

- He and Laskowski (1995b) reported the cyclone flow-rate, when operated with medium only, to be the highest when operating with the coarsest medium. The medium split was unaffected by changes in the medium grade. Assuming that these trends would still hold at low medium-to-ore ratios, then the spigot capacity should increase when the medium particles are relatively coarse.

(e) Classification vs Dense Medium Cyclones

- There are strong indications that the underflow/sinks overloading behaviour of both cyclonic devices are similar:
    - Roping is characterized by excessive solids concentration at the underflow/sinks stream. The value of this solids concentration is around 40% (v/v) and higher, for both devices.
    - The underflow/sinks solids concentration during roping has been reported to be constant for both devices. However, some authors have reported this solids concentration to increase with feed concentration in classification cyclones.

- Misplacement of particles to the overflow/floats stream occurs at the onset of roping.
- Spigot capacity is reported to be associated with roping flow. The exceptions in this regard being Tarr (1965) and DSM (1985).

- The impact of roping on the performance of the two cyclonic devices is also reported to be similar:
  - The onset of roping is reported to be associated with an increase in the separation size and separation density.
  - The separation efficiency of both devices is reported to suffer during roping.

- There are indications that changes in cyclone geometry influences the spigot capacities of classification and dense medium cyclones in a similar manner:
  - Spigot diameter is reported to influence the spigot capacity the most, and the sensitivity of Q_{UM} to D_u is similar for both devices (Table 2.21).
  - D_i, D_o, cone angle and barrel length are expected to influence the spigot capacity in a similar manner for both devices.

- It is anticipated that feed pressure should influence spigot capacity of a classification cyclone in a similar manner to that of a dense medium cyclone.

- There is no reason to expect ore size to influence the spigot capacities of the two devices in a similar manner, given the difference in particle sizes of the solids being beneficiated by classification and dense medium cyclones. However, medium particles have previously been reported to classify in a similar manner to particles being separated in classification cyclones (Verghese and Rao, 1994). Therefore, it is not unexpected that medium grade might influence the spigot overloading behaviour of a dense medium cyclone in a manner that is related/similar to the effect of ore size on the spigot overloading behaviour of a classification cyclone.

CHAPTER 3. EXPERIMENTAL APPROACH

Objective

Experiments were performed on a 165mm dense medium cyclone with the intention to, firstly, characterize the solids loading and overloading behaviour of the spigot, and, secondly, establish the variables that influence spigot capacity. Additional tests were performed with a larger 350mm dense medium cyclone to validate the results obtained with the smaller 165mm cyclone.

3.1. Experimental Set-up - 165mm Cyclone

A polyurethane cyclone with an internal body diameter of 165mm (Fig. 3.1(b)) was used to perform the test work. Fig. 3.1(a) shows a schematic diagram of the test rig used; in which the cyclone was installed at an inclination angle of 20^{o} from the horizontal, and the sump below it had a capacity of about 180 litres. A picture of the cyclone rig with a centrifugal pump is shown in Fig. 3.2. The bypass valve was kept open for all the tests, and the cyclone valve was used to control the feed pressure.

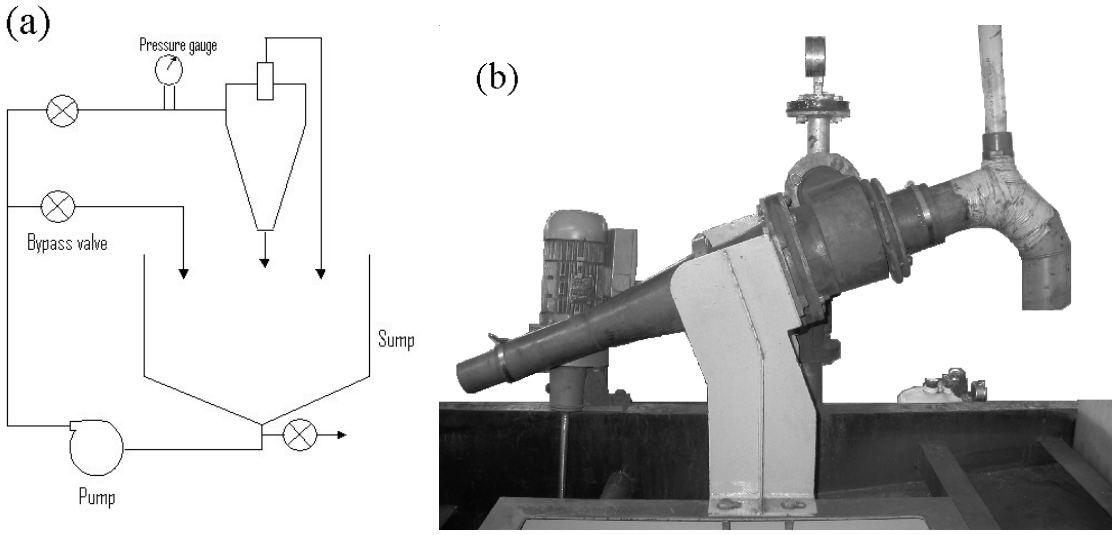


Figure 3.1. (a) A schematic of the test rig and (b) polyurethane cyclone employed to perform the experiments.

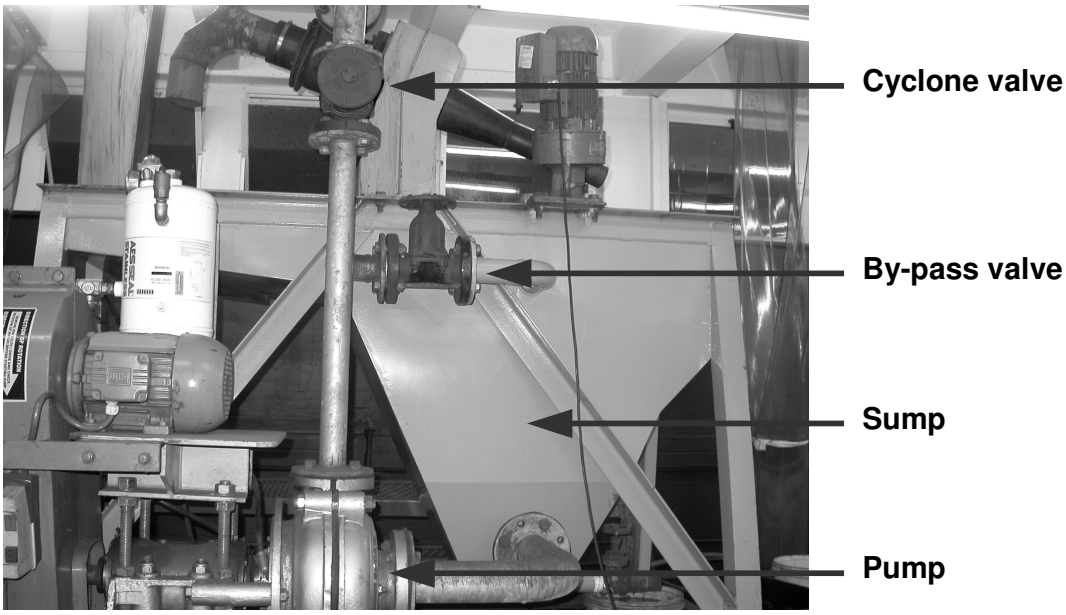


Figure 3.2. The test rig, with a 165mm cyclone, on which the experiments were performed.

3.1.1 Experimental Procedure: Characterisation of Overloading at Sinks

An aqueous suspension of magnetite particles was employed as medium, and the magnetite particles had a particle size distribution shown in Table 3.1. This particle size distribution was determined through wet screen analysis. For each new day of test-work a new batch of medium particles was used, this was done to ensure that medium contamination did not occur. Silica particles (-1.8+0.8mm and 2.65kg/l) were used as ore for all the tests, so that all of the ore was concentrated to the sinks stream and only medium exited at the floats stream when the spigot was not overloaded. A feed pressure of 20kPa, which is equivalent to about 9.5D, was maintained throughout the tests and the medium density was kept at around 1.3kg/l for all the tests. Table 3.2 shows the cyclone configuration adopted for this test-work.

Table 3.1. Screen analysis of the fine magnetite.

Size range (µm)	%Weight (wt%)
-125+90	0.0
-90+63	0.4
-63+45	6.9
-45+38	13.2
-38	79.5

During this test-work silica particles were added into the cyclone in increments until the spigot was overloaded. Spigot overloading was easily recognizable by the change in the type of discharge at the spigot, and the presence of silica particles in the floats stream. Subsequent to every incremental addition of ore particles, flow-rate measurements were performed at both the floats and sinks streams. Flow-rate measurements were performed by taking timed samples with a 25-litre bucket; at least five flow-rates measurements were performed at each outlet per test (See Fig. A.9 in Appendix A). The slurry mass was measured in kg and time in seconds. Between each measurement the cyclone was allowed to stabilize and reach a steady state. This was followed by the taking of simultaneous samples (with 600ml sampling bottles) at both outlets to determine the volumetric percentage of ore and medium. Sampling had the effect of changing the 'equilibrium' state that the cyclone had reached; hence, the samples were taken simultaneously. The sampling bottles had to be large enough to take a representative sample, but small enough not to remove so much solids that the operation state of the cyclone changes from roping to semi-roping. The difference between semi-roping and roping was at times a few handfuls of silica particles added or removed from the sump. Due to the large differences in particle sizes between the magnetite and silica particles, the two could easily be separated out by wet screening to determine the volumetric compositions of the slurry at each outlet (See Fig. A.10 in Appendix A).

Table 3.2. The configuration of the cyclone used to perform test-work.

Cyclone diameter (mm)	165
Inlet area (mmxmm)	70x10
Vortex finder diameter (mm)	64
Spigot diameter (mm)	25,34,45
Cone angle (^{o})	15
Barrel length (mm)	None

3.1.2. Experimental Procedure: Effect of Variables

The experimental procedure followed was similar to that in followed in characterising overloading at the sinks, except that the cyclone was operated with a rope discharge only for all the tests. Once the necessary variable change had been made and the cyclone had reached a 'steady state', flow-rates measurements were performed at both the floats and sinks streams. Flow-rate measurements were repeated five times at each outlet in order to ensure their accuracy. This was followed by taking simultaneous samples with 600ml bottles at both outlets, which were used to determine the solids composition at the floats and sinks streams. Just as in the test-work to characterise overloading at the sinks, a new batch of medium particles was used for each new day of test-work to ensure that there was no medium contamination.

The variables can be divided into two categories, namely: cyclone geometry and operational variables. Cyclone geometry includes: inlet size, vortex finder diameter, spigot diameter, cone angle, and barrel length. The changes in the cyclone dimensions executed during the test-work are shown in Table 3.3.

Table 3.3. Cyclone dimensions tested during the experimental work.

Variable	**Value**
D_i (mm x mm)	70x10, 70x25
D_o (mm)	40, 53, 64
D_u (mm)	20,25,30,34,40,45
α (deg)	15, 20
Barrel length (mm)	None, 200

Pictures of cone A (20^o) and the 200mm barrel employed are shown in Fig. 3.3 and 3.4, respectively.



Figure 3.3. The 20^{o} cone with changeable spigots. (Cone A)



Figure 3.4. The 200mm long barrel used during the experiments.

The operational variables include: feed pressure, medium density, medium grade, and ore size. The changes in the operational variables carried out during the experimental work are shown in Table 3.4. The feed pressure is expressed in terms of head in cyclone diameters. The medium grade is expressed in terms of %passing 45μm, and three grades were tested as shown in Table 3.4. Ore density was also investigated, however, the heavier ore used during the test-work tended to block the spigot and the flow of the slurry was unstable. These results were not included in this report.

Table 3.4. Operating conditions tested during the experimental work.

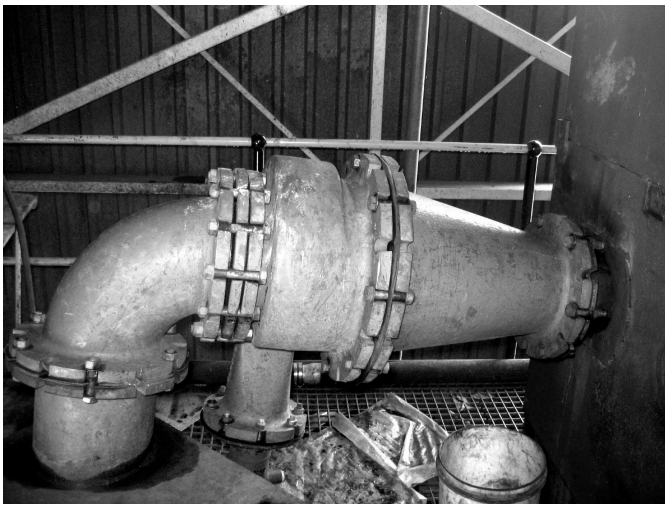
Variable	**Value**
Feed head (D)	9-17
Medium Density (kg/l)	1.3, 1.4, 1.5, 1.7
Medium grade (%Passing 45µm)	75, 85, 95
Ore size (mm)	-1.8+0.8, -3+1, -5+3
Medium Type	Magnetite

3.2. Experimental Set-Up and Procedure- 350mm Cyclone

The 350mm dense medium cyclone employed during the test-work is shown in Fig. 3.5; the cyclone had a standard DSM configuration, and this is shown in Table 3.5. The dimension for the inlet size shown in Table 3.5 is the equivalent inlet diameter; the inlet was rectangular in shape. The spigot diameter is not shown in Table 3.5 because it was varied during the test-work.

Table 3.5. The dimensions of the 350mm industrial-scale cyclone.

Cyclone Dimensions	**Quantity**
D_i (mm)	70
D_o(mm)	151
α (^{o})	20
Bl	None



(a)



(b)

Figure 3.5 Pictures of the 350mm dense medium cyclone used to perform the validation work.

The flow-sheet of the DMS cyclone plant at Mintek is shown in Fig. 3.6; pictures of the plant and various equipment at the plant are shown as Figs. A.4 to A.8 in Appendix A. Medium particles were added directly into the sump and a Marcy scale was used to determine the medium density from the by-pass stream. The fine grade magnetite (95%-45μm) used during the test-work with the 165mm cyclone was employed in this test-work as well. Once the required medium density was achieved the ore particles were fed through a feed hopper into the sump, from where they were pumped together with medium into the cyclone. Silica particles with a size range of –5+3mm were employed as ore. A variable speed pump was used to control the feed pressure. The washed medium re-circulated from the vibrating screens was passed through a demagnetizing coil in order to minimize magnetization of the magnetite and thus viscosity effects.

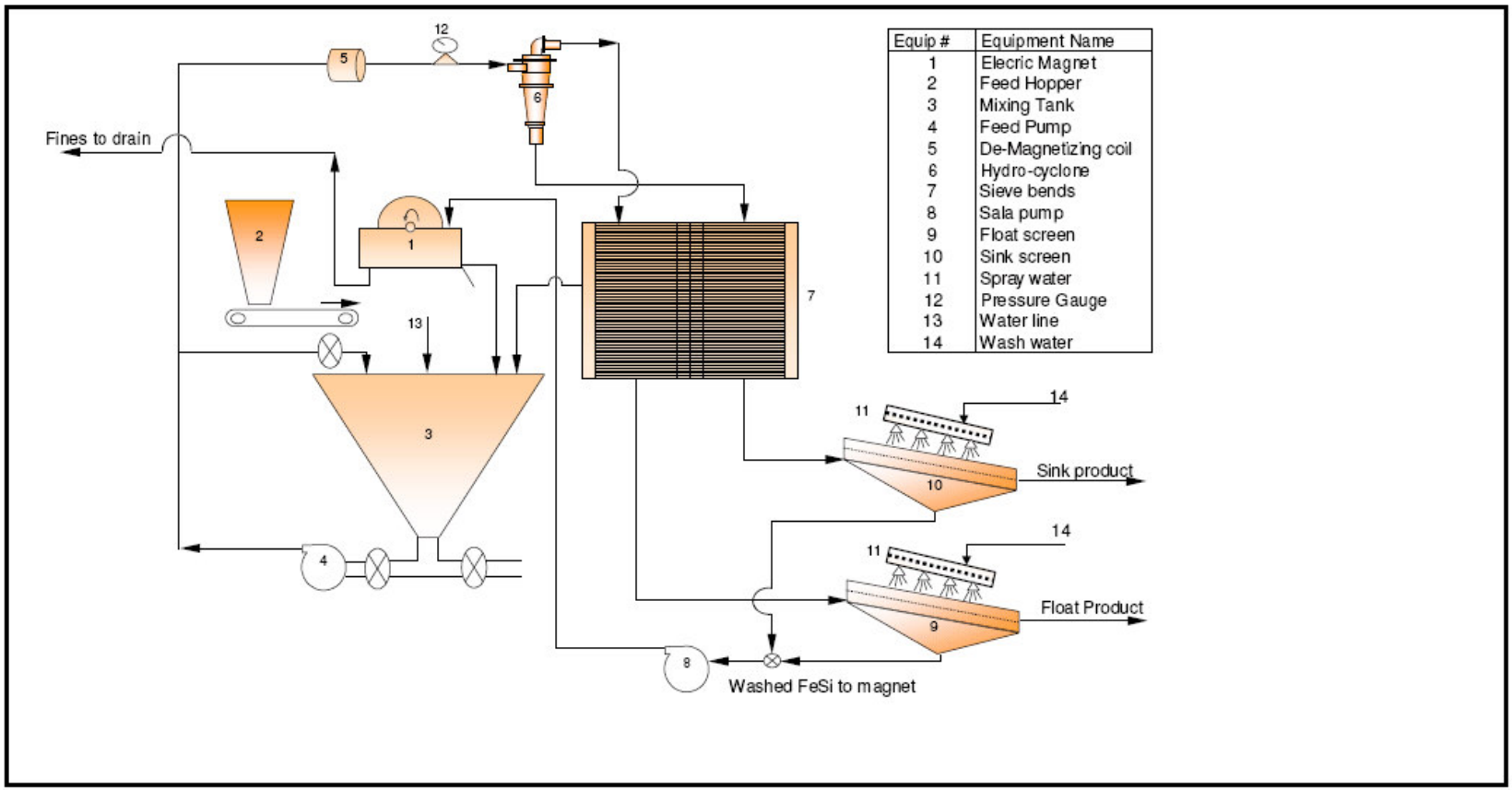


Figure 3.6. The flow-sheet of the DMS plant at *Mintek*.

Normally the slurry from the floats and the sinks streams discharge onto separate sievebends from where the medium particles are washed off on vibrating screens, from which the wet sink and float products can be captured. In this case, just as with the 165mm laboratory cyclone, all of the silica particles were recovered at the sinks (during spray and semi-rope discharges). Spigot overloading could not be achieved with the plant operating in this condition because the ore particles were exiting much quicker than the rate at which they were introduced through the feed hopper. As a result the sievebends were removed so that the slurry from the floats and sinks stream was re-circulated back into the sump; this way sufficient ore particles could accumulate within the system, and overloading of the spigot was achieved.

Spigot overloading could be detected by, firstly, observing the discharge type at the sinks and, secondly, monitoring misplacement of silica particles to the floats stream. Once roping had been achieved and the necessary operating conditions had been set, a timed sample of slurry from the sinks stream was diverted onto the vibrating screen. The washed silica particles were then collected at the end of the screen and the medium particles re-circulated back into the sump. The ore particles were then bagged and kept for drying and weighing at a later stage. Caution was taken not to divert the sinks slurry for too long, otherwise, just as with the smaller 165mm cyclone, the flow at the sinks would revert back to a semi-rope discharge during the flow measurements. This procedure was repeated for each change in the operating conditions and cyclone geometry that was made. Two flow-rate measurements were performed at each test.

3.2.1. Variables Investigated

Only three variables were varied on the 350mm cyclone, namely: spigot diameter; feed pressure and medium density. These parameters were varied as shown in Table 3.6. Initially the plan was to change the feed head (pressure) from 9D up to 18D, however, due to the limitations imposed by the excessive solids concentrations and the pump, the feed head was varied from about 10D and 17D. Below about 10D some of the pipes were blocked due to the relatively high settling rate of the silica particles, especially at the lower medium densities. Above about 17D there was the risk of overloading the pump. The measuring point of the pressure gauge was located 0.915m below the centre line of the cyclone inlet; the pressure read off the gauge had to be corrected by taking this into account.

Table 3.6. Conditions tested on the 350mm dense medium cyclone.

Variable	**Quantity**
D_u (mm)	60, 75, 90, 100
Feed head (D)	13-17
Medium Density (kg/l)	1.3, 1.5, 1.7

3.3. Experimental Matrix

The experimental matrix for all the tests performed under roping conditions are illustrated in Tables 3.7-3.13. The numbers in these tables represent the number of tests performed under those particular conditions.

Table 3.7. Conditions tested when operating with the 15° cone angle and D_i =0.2D, with silica that had a size range of –1.8+0.8mm. (Roping only)

		D_i = 30mm, 15° Cone Angle, d_{ore} =-1.8+0.8mm																																							
		Fine Magnetite Grade																		Medium Magnetite Grade												Coarse Magnetite Grade											
		D_o = 64mm						D_o = 53mm						D_o = 40mm						D_o = 64mm						D_o = 40mm						D_o = 64mm						D_o = 40mm					
	D_u (mm) =	20	25	30	34	40	45	20	25	30	34	40	45	20	25	30	34	40	45	20	25	30	34	40	45	20	25	30	34	40	45	20	25	30	34	40	45	20	25	30	34	40	45
H (D)	ρ_{med} (kg/l)																																										
9D	1.3	1	9	5	11	1	12	1	4		7		6	1	2	2	7		2		1		1		1		1		1		1		1		1		1		1		1		1
	1.4		1		1		1														3		4		1								1		1		1					
	1.5		1		1		1																2																			
	1.6																				1				1								1		1								
	1.7		1		1		1																										1		1		1						
12D	1.3		1		1																																					
	1.4		1		1																																					
	1.5																																									
	1.6																																		1								
	1.7																																									
15D	1.3		1		1																																					
	1.4		1		1																																					
	1.5																																									
	1.6																																		1								
	1.7																																									

Table 3.8. Conditions tested when operating with the 15° cone angle and D_i =0.2D, with silica that had a size range of –3+1mm. (Roping only)

		D_i = 30mm, D_o = 64mm, 15° Cone Angle, d_{ore} = -3+1mm																	
		Fine Grade						Medium Grade						Coarse Grade					
	D_u (mm) =	20	25	30	34	40	45	20	25	30	34	40	45	20	25	30	34	40	45
H (D)	ρ_{med} (kg/l)																		
9D	1.3		2		2		2		1		1		1						
	1.4				1		1		1		2		1						
	1.5	1	1	1	1	1	1		1										
	1.6												1		1		1		1
	1.7																		
12D	1.3																		
	1.4				1														
	1.5				1														
	1.6																1		
	1.7																		
15D	1.3																		
	1.4				1														
	1.5				1														
	1.6																1		
	1.7																		

Table 3.9. Conditions tested when operating with the 15° cone angle and D_i =0.3D. (Roping only)

		D_i = 47mm, 15° Cone Angle, d_{ore} = -1.8+0.8mm, Fine Grade																		D_i = 47mm, 15° Cone Angle, d_{ore} = -5+3mm, Fine Grade															
		D_o = 64mm						D_o = 53mm						D_o = 40mm						D_o = 64mm						D_o = 53mm						D_o = 40mm					
	D_u (mm) =	20	25	30	34	40	45	20	25	30	34	40	45	20	25	30	34	40	45	20	25	30	34	40	45	20	25	30	34	40	45	20	25	30	34	40	45
H (D)	ρ_{med} (kg/l)																																				
9D	1.3																																				
	1.4																																				
	1.5		1		1		1																														
	1.6																																				
	1.7		1		1		1		1		1		1		1		1		1		1		1										1		1		
12D	1.3																																				
	1.4		1		1		1																														
	1.5																																				
	1.6																																				
	1.7																																				

Table 3.10. Conditions tested when operating with cone A and D_i =0.2D. (Roping only)

		D_i = 30mm, Cone A (20°), d_{ore} =-1.8+0.8mm																																							
		Fine Magnetite Grade																		Medium Magnetite Grade																					
		No Barrel																		No Barrel						With Barrel															
		D_o = 64mm						D_o = 53mm						D_o = 40mm						D_o = 64mm						D_o = 64mm						D_o = 53mm						D_o = 40mm					
	D_u (mm) =	20	25	30	34	40	45	20	25	30	34	40	45	20	25	30	34	40	45	20	25	30	34	40	45	20	25	30	34	40	45	20	25	30	34	40	45	20	25	30	34	40	45
H (D)	ρ_{med} (kg/l)																																										
9D	1.3																				1		1		1		2		2		2						1						1
	1.4																														1												
	1.5																																									
	1.6																																									
	1.7																																									
12D	1.3		1		2				1		1				1		1	1			1		1		1																	
	1.4																				1		1		1		1		1													
	1.5		1		1																																					
	1.6																																									
	1.7		1		1																																					
15D	1.3		1		1		1		1		1		1		1		1	1																								
	1.4																										1		1													
	1.5		1		1		1																																			
	1.6						1																																			
	1.7		1		1																																					
17D	1.3		1		1				1		1				1		1	1																								
	1.4																																									
	1.5		1		1																																					
	1.6																																									
	1.7		1		1																																					

Table 3.11. Conditions tested when operating with cone A and D_i =0.3D. (Roping only)

		D_i = 47mm, Cone A (20°), d_{ore} =-1.8+0.8mm, Fine Magnetite Grade																	
		D_o = 64mm						D_o = 53mm						D_o = 40mm					
	D_u (mm) =	20	25	30	34	40	45	20	25	30	34	40	45	20	25	30	34	40	45
H (D)	ρ_{med} (kg/l)																		
12D	1.3		1		1										1		1		
	1.4																		
	1.5																		
	1.6																		
	1.7																		
15D	1.3		1		1										1				
	1.4																		
	1.5																		
	1.6																		
	1.7																		

Table 3.12. Conditions tested when operating with cone B. (Roping only)

D_i = 30mm; D_u = 45mm, $\alpha = 20^o$, Bl = 0mm,
dore =-1.8+0.8mm, Fine Magnetite

	D_o (mm) =	40	53	64
H (D)	ρ_{med} (kg/l) =			
9D	1.3	1		1
	1.4	1	1	1
	1.5			1
	1.7			1

Table 3.13. Conditions tested when operating the 350mm dense medium cyclone. (Roping only)

	H =13D				H =14D				H =15D				H =17D			
D_u (mm) =	60	75	90	100	60	75	90	100	60	75	90	100	60	75	90	100
ρ_{med} (kg/l)																
1.3	1					1	1	1	1	1			1			
1.5	1	1	1	1									1		1	1
1.7	1	1	1												1	

CHAPTER 4. RESULTS AND DISCUSSION

4.1. CHARACTERISATION OF OVERLOADING AT THE SINKS

In order to elucidate on the spigot loading and overloading behaviour of the dense medium cyclone, a number of parameters were studied during the transition to roping. Spigot loading (in l/hr of both slurry and ore) and the volumetric percentage of ore in sinks were monitored during the transition. Spigot overloading is often associated with the misplacement of sinks particles to the floats stream, hence, the amount of silica particles exiting through the floats stream were also monitored. Medium behaviour within the cyclone during spigot overloading was also investigated by monitoring the medium flow (at both the floats and sinks) and the density differential.

The loading and overloading behaviour of the cyclone was characterized for three spigot sizes of 20, 34 and 45mm diameters; the results are given in Tables A.2, A.3 and A.4 (in Appendix A), respectively. The transitional point between spray and semi-rope discharge, and semi-rope and rope discharge were determined experimentally for the 45mm spigot only.

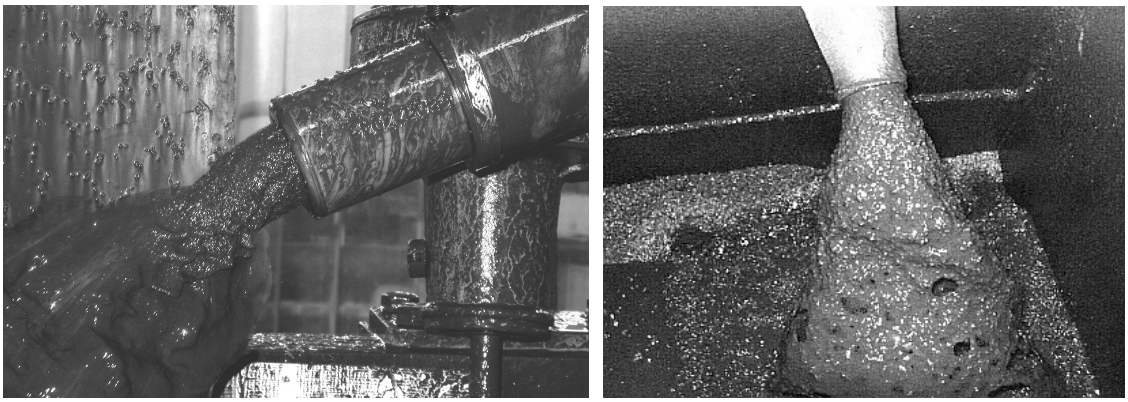
4.1.1. Spigot Loading

Three types of discharges were observed at the sinks depending on the ore concentration within the cyclone, especially at the sinks. At low concentrations a spray discharge was observed at the sinks (Fig. 4.1), a semi-rope discharge was observed at intermediate concentrations (Fig. 4.2) and a rope discharge was encountered at high ore concentrations (Fig. 4.3).



(a) **(b)**

Figure 4.1. Spray discharge at the sinks for the (a) 165mm cyclone, and (b) 350mm cyclone.



(a) **(b)**

Figure 4.2. Semi-rope discharge at the sinks for the (a) 165mm cyclone, and (b) 350mm cyclone.

During semi-roping the flow at the sinks switched continuously between spray and rope discharges; being mostly spray discharge close to about 11% feed ore concentration and predominantly rope discharge at around 21% (Fig. 4.4). This continuous change between spray and rope discharges during semi-roping is shown in Fig. 4.2, where the flow was in the process of switching to roping from a spray discharge.



(a) **(b)**

Figure 4.3. Rope discharge at the sinks for the (a) 165mm cyclone, and (b) 350mm cyclone.

As expected an increase in the feed ore concentration resulted in increased spigot loading, and the relationship appears to be linear (Fig. 4.4). This linear relationship was observed when spray and semi-rope discharges prevailed at the sinks. However, as soon as the sinks stream changed to roping flow further increase in the feed ore concentration did not result in an increase in spigot loading. Instead the spigot loading remained constant and the spigot appeared to have reached its maximum ore carrying capacity! It can therefore be concluded with certainty that the maximum spigot capacity is reached at the onset of rope discharge at the sinks.

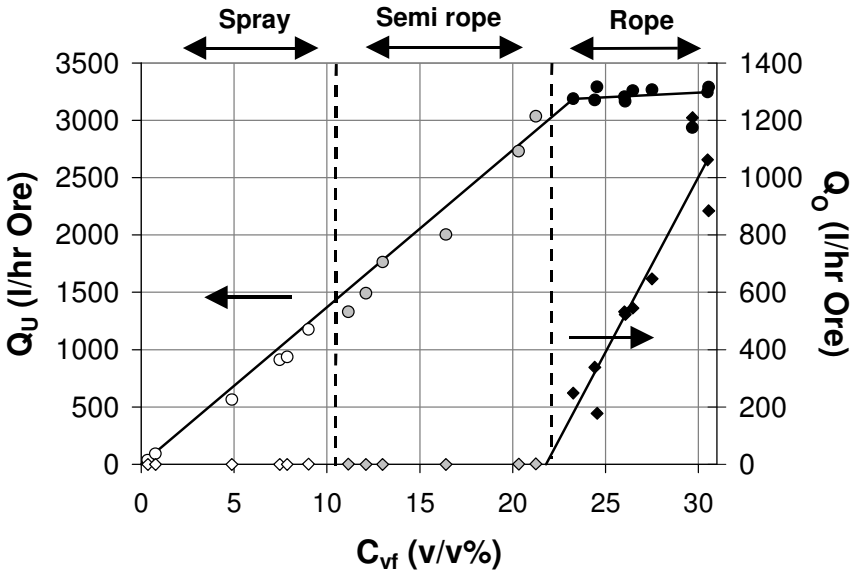


Figure 4.4. Changes in the ore loading at both the floats and sinks streams as ore was added into the cyclone for a 45mm spigot. Data points with white and grey backgrounds were obtained during spray and semi-rope discharges, respectively. While data points with black background were obtained during roping.

The onset of roping flow was also observed to be the point at which silica particles, which were supposed to exit at the sinks stream, were indiscriminately misplaced to the floats stream. The particle size distribution of the silica particles misplaced to the floats stream was exactly the same as that in the sinks stream. This particle misplacement is obviously detrimental to the separation efficiency achieved in the cyclone. Upadrashta and Venkateswarlu (1982) also reported particle misplacement to the floats stream during roping. They proposed the following relationships:

$$S \propto (1 - C_V)^{-0.18} \quad \text{(Spray discharge), and}$$

$$S_R \propto (1 - C_V)^{1.1} \quad \text{(Rope discharge).}$$

The increase in S with increasing C_V during spray discharge was explained to be a consequence of the reduction of the air core size at the sinks, which results in an increase in the proportion of feed material exiting through the spigot. While, on the other hand, the decrease in S_R with increasing C_V during rope discharge is a consequence of misplacement of the sinks particles to the floats stream due to the overloading of the spigot.

It is interesting to note that the misplacement of ore to the floats stream did not actually begin during semi-roping flow, but rather at the commencement of rope discharge. When spray and semi-rope discharges prevailed at the sinks some silica particles of very small quantities were observed to exit at the floats. It is thought this behaviour was due to the probabilistic nature of cyclones.

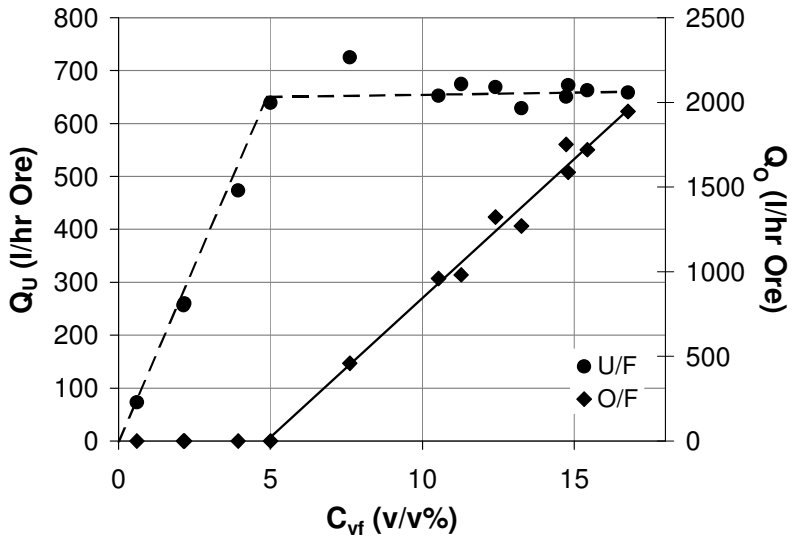


Figure 4.5. Changes in the ore loading at both the floats and sinks streams as ore was added into the cyclone for a 34mm spigot.

Fig. 4.5 and 4.6 show the spigot and vortex finder loading (in l/hr ore) behaviour during the transition to rope discharge for the smaller 25 and 34mm spigots as the feed ore concentration was increased. The point at which the flow changed from spray to semi-rope discharge was not determined for these spigot sizes during the experiments; the same is true for the point of transition to rope discharge. However, just as in Fig. 4.4 above the transitional point from semi-roping to roping flow was easily identifiable from the figure: as soon as roping commenced the spigot loading (in l/hr of ore) did not increase further, and silica particles were misplaced to the floats stream.

Table 4.1 The feed ore concentrations at which roping commenced for the various spigot sizes

D_u (mm)	**C_{vf} at which roping commenced (v/v%)**
25	~3
34	~5
45	~22

Extrapolation of the curve describing the increase in the floats loading during roping, down to the point at which misplacement of the silica particles began appears to give a reasonable estimation of the feed concentration at which roping commenced. The (estimated) feed concentrations at which roping commenced for the 25mm, 34mm and 45mm spigots are shown in Table 4.1. Scrutiny of Fig. 4.4, 4.5 and 4.6 reveals that the feed ore concentration at which roping flow commenced decreased with decreasing spigot size. The spigot capacity is also observed to decrease with decreasing spigot size, however, this will be discussed in more detail later in this chapter.

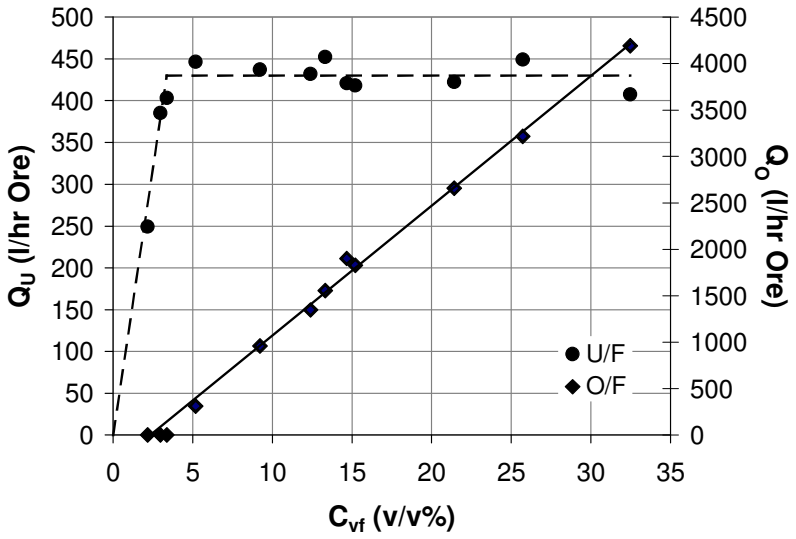


Figure 4.6. Changes in the ore loading at both the floats and sinks streams as ore was added into the cyclone for a 25mm spigot.

The volumetric recovery of both ore to sinks during the transition to roping is shown in Fig. 4.7. All of the ore was recovered in the sinks during spray and semi-rope discharges. Once roping commenced at the sinks there was a reduction in the recovery of ore to sinks, obviously due to ore misplacement to the floats. The feed concentrations at which roping commenced can also be determined from Fig. 4.7.

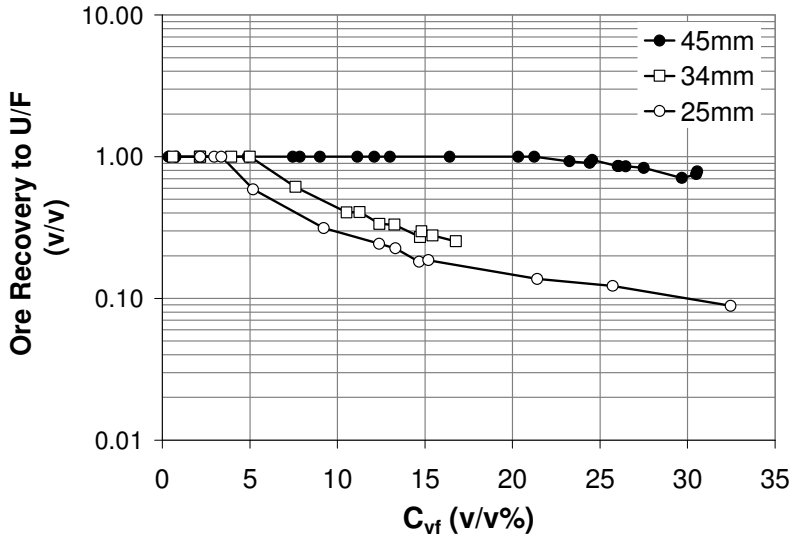


Figure 4.7. Volumetric recovery of ore to sinks during the transition to roping for various spigot diameters.

4.1.2. The Sinks Ore Concentration

The data points obtained during semi-rope discharge were more erratic than those for spray and roping discharge (Fig. 4.8); this behaviour was due to the continuous change in the discharge types at the sinks between spray and rope discharges. The transition from a semi-rope to a rope discharge resulted in a sharp increase in C_{vu}.

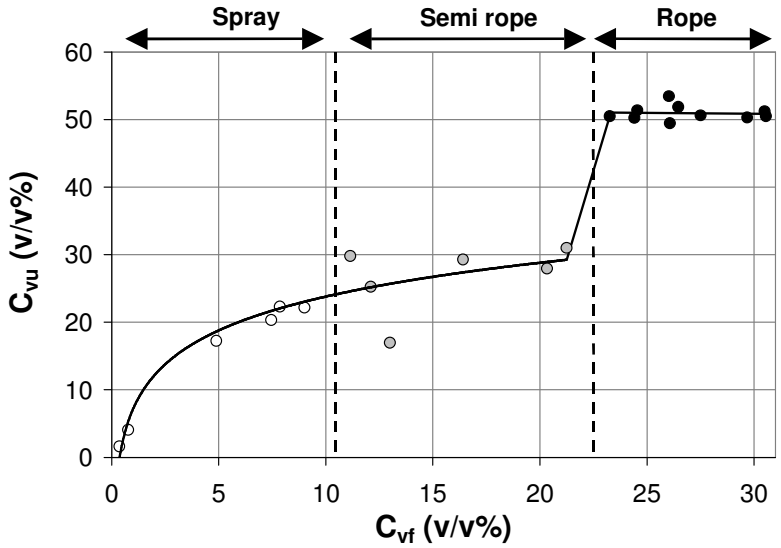


Figure 4.8. The volumetric ore concentration at the sinks for a 45mm spigot. Data points with white and grey backgrounds were obtained during spray and semi-rope discharges, respectively. While data points with black background were obtained during roping.

It was not possible in this study to maintain sinks ore concentrations at values between approximately 31 to 50% for the 45mm spigot; as soon as the ore concentration exceeded about 31% roping commenced. It is thought that this behaviour does not necessarily represent the behaviour of all cyclones. Under overloaded conditions, the sinks ore concentration remained constant at around 50% (for the 45mm spigot) with further increases in the feed ore concentration. It is clear from Fig. 4.8 that the onset of spigot overloading can be anticipated by monitoring C_{vu}. Stas (1957) too observed that when the spigot was overloaded the sinks ore concentration remained constant with further increases in the feed ore concentration. Alternatively C_{vu} could be expressed in terms of volumetric medium-to-ore ratio, which is common practice in industry. Fig. 4.8 in terms of medium-to-ore ratio is shown in Fig. 4.9. During roping the volumetric medium-to-ore ratio at the sinks was generally around 1:1 (for the 45mm spigot).

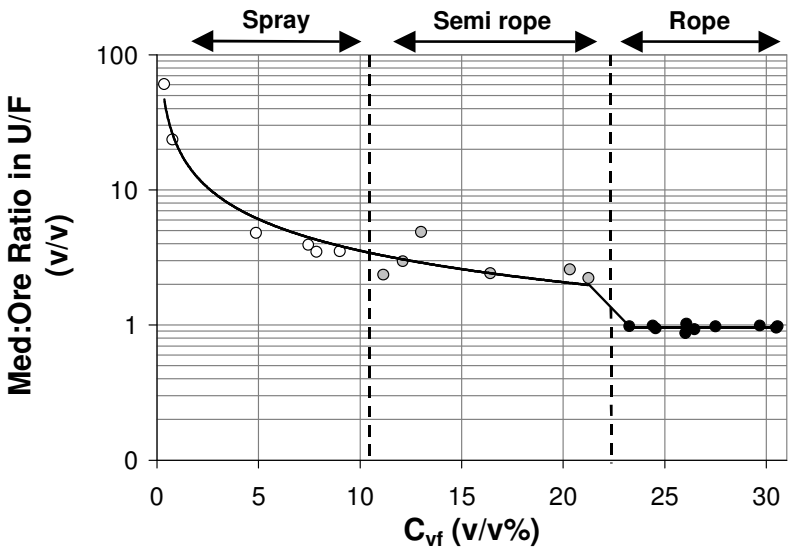


Figure 4.9. The volumetric medium-to-ore ratio at the underflow for a 45mm spigot. Data points with white and grey backgrounds were obtained during spray and semi-rope discharges, respectively. While data points with black background were obtained during roping.

It is not clear whether the presence of coal particles (floats) in the floats stream would change the nature of the relationship between the feed and sinks concentrations as shown in Fig. 4.8. The presence of floats particles in the floats stream is, however, not expected to significantly change the critical sinks ore concentration at which roping is encountered. A regression of Fig. 4.8 during spray and semi-rope discharges gives the following expression:

$$C_{vu} = n \ln[C_{vf(+\rho_{50})}] + k \qquad (4.1)$$

with n = 7.223 and k = 7.165, and R^2 = 0.981. C_{vu} is the volumetric percentage of ore in the sinks stream during spray and semi-roping, and $C_{vf(+\rho 50)}$ is the volumetric percentage of ore in the feed with densities above the cut density at which the cyclone is operating at. It is expected that parameters n and k should change with changes in the cyclone geometry and operating conditions. Note that the two data points that appear to be outliers at semi-roping regime in Fig. 4.8 were not considered in obtaining the above expression. This expression describes how C_{vu} increases with increasing $C_{vf(+\rho 50)}$, for the conditions under which these tests were performed. It does not take into account the onset of roping, thus, prior knowledge of the $C_{vf(+\rho 50)}$ (at which the abrupt jump in C_{vu} occurs) at the onset of roping is required.

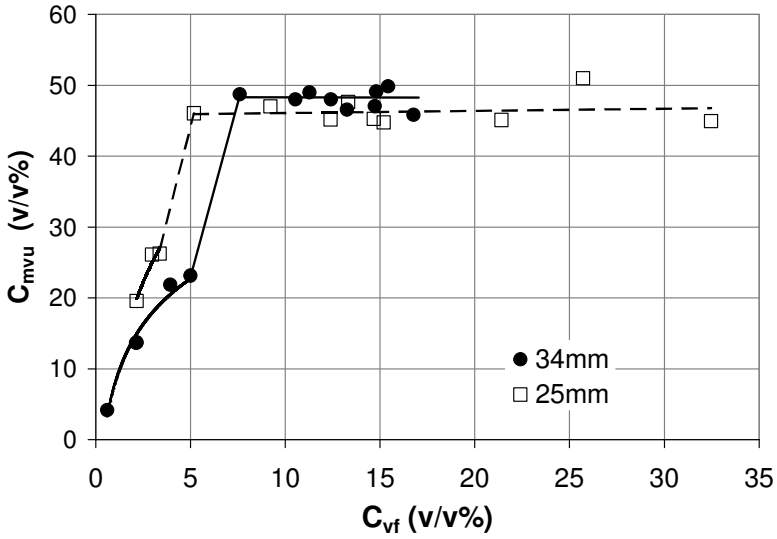


Figure 4.10. The volumetric ore concentration at the sinks for the 25 and 34mm spigots.

Fig. 4.10 shows the change in C_{mvu} with increasing feed concentration during the transition to rope discharge for the 25 and 34mm spigots. The manner in which C_{vu} changed with increasing feed concentration for the 25 and 34mm spigots confirms the results shown in Fig. 4.8. Further, Fig. 4.8 and 4.10 illustrate that C_{mvu} decreased with decreasing spigot size. The decrease in the concentration was, however, relatively small. C_{mvu} values obtained with the 25 and 34mm spigots expressed in terms of volumetric medium-to-ore ratios are shown in Fig. 4.11.

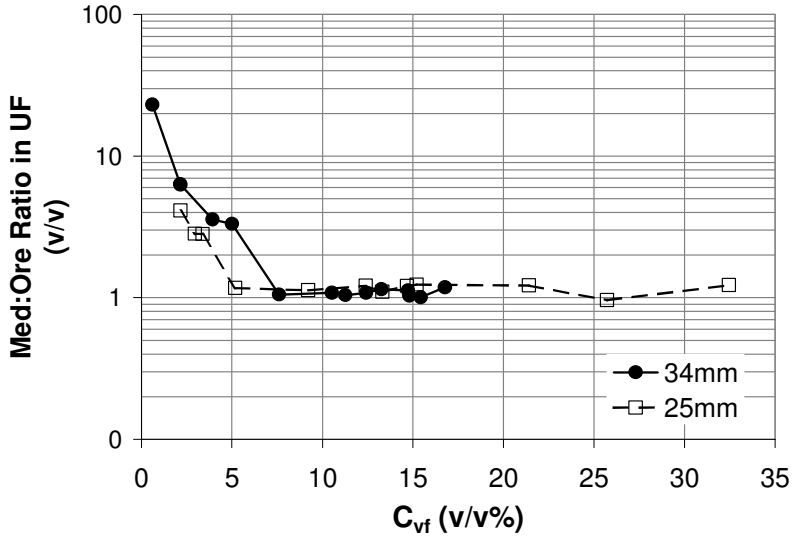


Figure 4.11. The volumetric medium-to-ore ratio at the sinks for the 25 and 34mm spigots during the transition to roping.

The increase in C_{vu} with increasing C_{vf} during spray and semi-rope discharges, for the smaller 25 and 34mm spigots, was also according to a relationship of the form of equation 4.1. Table 4.2 shows the parameters *n* and *k*, and the R^2 values for the 25, 34 and 45mm spigots. The fit of the curves to the data was generally good, and the parameter *k* appears to be relatively unaffected by changes in the spigot diameter. While, on the other hand, parameter *n* appears to be dependent on spigot size.

Table 4.2. Parameter values for equation 4.1.

D_u (mm)	Parameter *n*	Parameter *k*	R^2
25	16.092	7.465	0.928
34	9.216	7.915	0.974
45	7.223	7.165	0.981

The range of C_{mvu} values obtained from all the tests performed in this study is shown in Fig. 4.12; C_{mvu} obtained in this study ranged from 43 up to 54% (v/v). The C_{mvu} values of 56 and 57% shown in Fig. 4.12 are thought to be erroneous because repetition of these tests did not reproduce the same results. The same was true for the C_{mvu} value of 41 in Fig. 4.12. The C_{mvu} values in Fig. 4.12 compares very well with the $\%V_{MSU}$ values (for classification cyclones) reported in the literature, which ranged from 39 to 68% (v/v). They are also in good agreement with Clarkson and Wood (1993)'s proposed sinks ore concentration upper limit of 40% (to avoid spigot overloading).

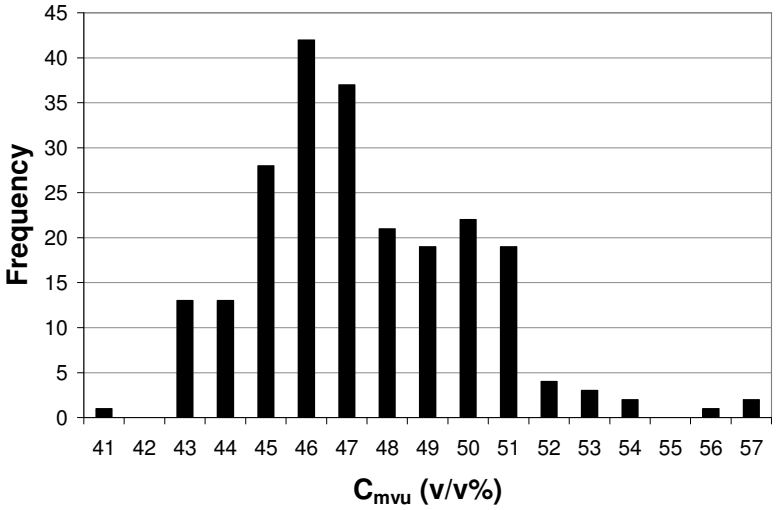


Figure 4.12. Range of all ore concentrations obtained in this investigation when roping was prevalent at the sinks.

Alternatively C_{mvu} can be expressed in terms of volumetric medium-to-ore ratios; the range of sinks medium-to-ore ratios obtained during roping in this study is shown in Fig. 4.13. These ranged mainly from 0.9 to 1.3 (v/v).

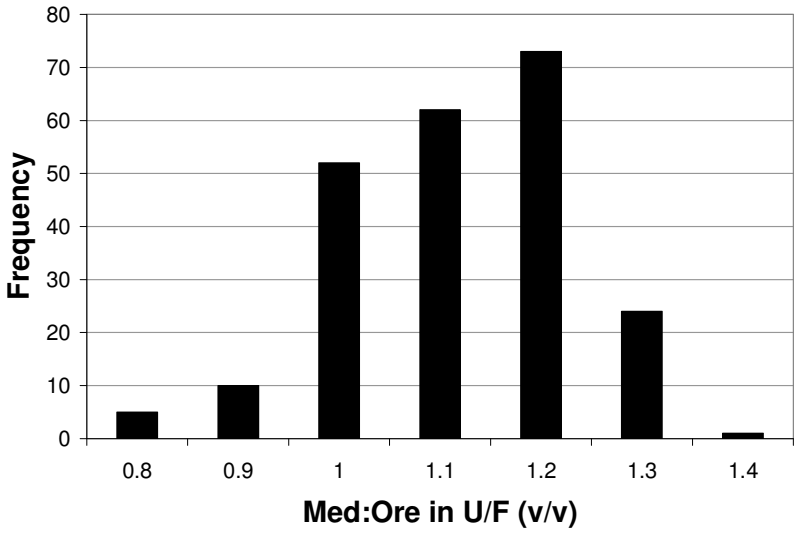


Figure 4.13. Range of all the sinks medium-to-ore ratios obtained in this investigation when roping was prevalent at the sinks.

4.1.3. Slurry Flow

The change in the slurry flow-rate through the 45mm spigot during the transition to roping is shown in Fig. 4.14. The slurry flow-rate at the sinks increased in a similar manner to the ore flow-rate before roping flow commenced (Fig. 4.4 and 4.14). During the transition to roping a drastic drop in the slurry flow-rate occurred, after which the flow-rate remained constant with further addition of ore into the cyclone. The ore flow-rate did not change abruptly during this transition (Fig. 4.4), thus, the abrupt drop in slurry loading at the sinks was a consequence of changes in the behaviour of medium flow which also dropped sharply during the transition to roping (Fig. 4.18). This also accounts for the sudden increase in the sinks ore concentration during the transition to roping flow (Fig. 4.8).

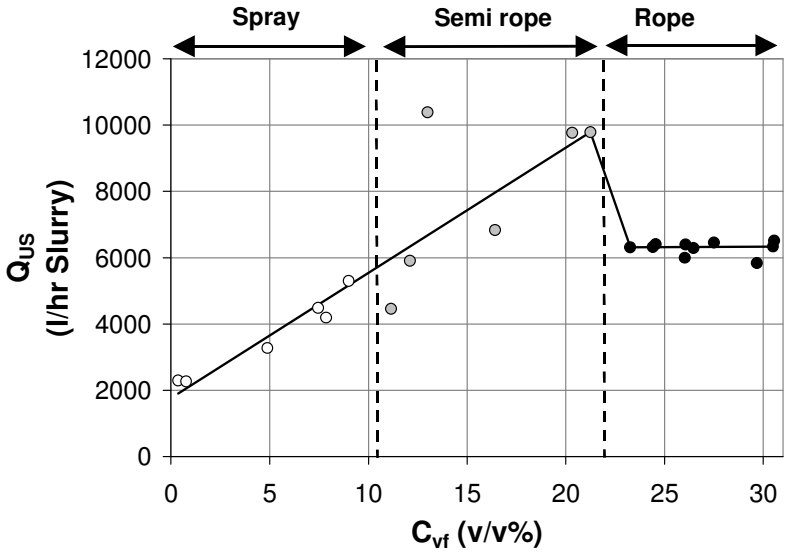


Figure 4.14. Slurry loading at the sinks for the 45mm spigot. Data points with white and grey backgrounds were obtained during spray and semi-rope discharges, respectively. While data points with black background were obtained during roping.

Fig. 4.15 shows the change in the slurry loading at the sinks during the transition to roping flow for the 25 and 34mm spigots. The nature of the influence of the feed concentration on the slurry loading at the spigot for the 25 and 34mm spigot is similar to that of the 45mm spigot reported in Fig. 4.14. It is interesting to note that the slurry flow-rate during roping for the 34mm spigot was below that obtained when only medium was fed into the cyclone. Similarly, the slurry flow-rate during roping for the 25mm spigot was almost equal to that obtained when only medium was fed to the cyclone. This is quite different from the behaviour observed in Fig. 4.14 for the larger 45mm spigot.

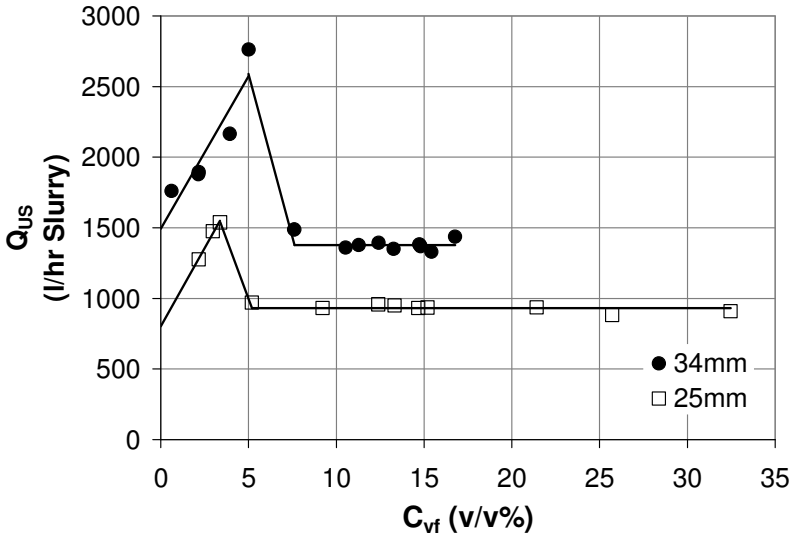


Figure 4.15. Slurry loading at the sinks for the 25 and 34 mm spigot.

Fig. 4.16 shows the influence of increasing feed ore concentration on the cyclone throughput. The slurry throughput through the cyclone increased with increasing feed concentration during spray and semi-rope discharges. Once roping commenced, the throughput decreased with further increase in feed ore concentration. This decrease in the slurry throughput is actually a consequence of the decreasing floats flow-rate during roping; the conditions at the sinks have been established to be constant once roping commences (Fig. 4.4, 4.8 and 4.14). The decrease in the slurry flow-rate at the floats is reflected in the decreasing floats medium flow-rate as shown in Fig. 4.18.

The increase in the ore throughput with increasing feed concentration during spray and semi-rope discharges (Fig. 4.16) is the same as that shown in Fig. 4.4 (for the spigot loading). The ore throughput increase during roping (Fig. 4.16), however, is a reflection of the increase in the ore flow-rate through the floats; the ore flow-rate through the sinks remained constant with further increase in the feed concentration once roping had commenced (Fig. 4.4).

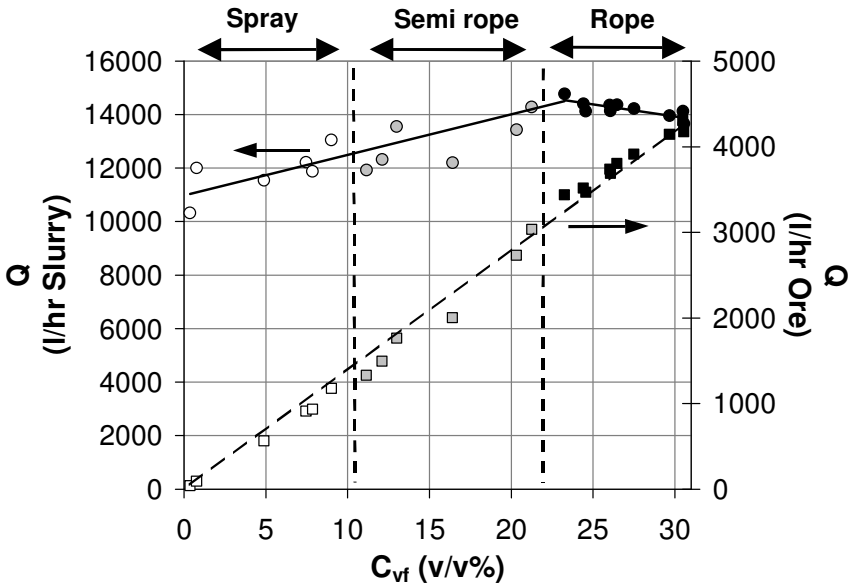


Figure 4.16. Cyclone throughput (both ore and slurry) during the transition to rope discharge for the 45mm spigot. Data points with white and grey backgrounds were obtained during spray and semi-rope discharges, respectively. While data points with black background were obtained during roping.

This decrease in the cyclone slurry throughput with increasing feed concentration during roping (Fig. 4.16) is in agreement with the findings of Upadrashta and Venkateswarlu (1982). They also observed Q to decrease with increasing feed concentration during roping; this behaviour was in accordance with the following relationship:

$$Q \propto (1 - C_V)^{0.56} \quad \text{(Rope discharge)}$$

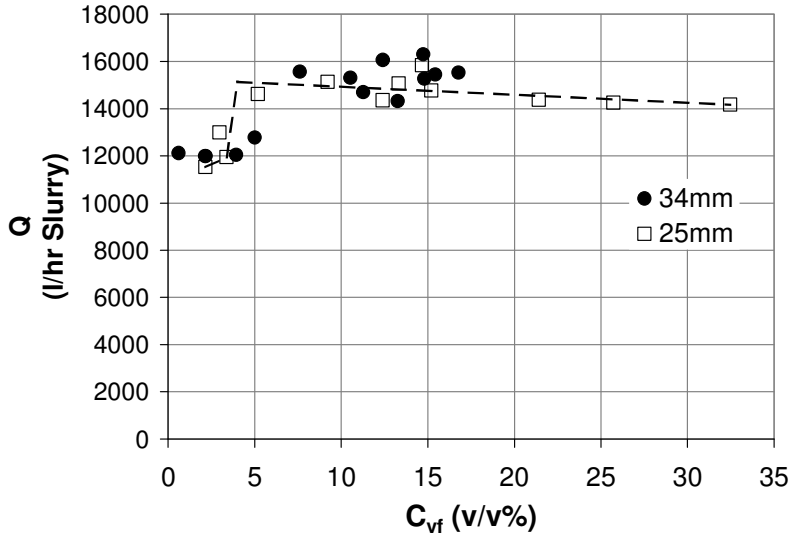


Figure 4.17. Cyclone slurry throughput during the transition to rope discharge for the 25 and 34mm spigots.

A look at the slurry throughput for the 25 and 34mm spigots reveals a different trend (Fig. 4.17): a sharp increase in the slurry throughput was observed at the transition to roping, after which the throughput decreased slightly for the 25mm spigot; the slurry throughput for the 34mm spigot remained relatively constant with further increase in the feed concentration during roping. These results also agree with the findings of Upadrashta and Venkateswarlu (1982). The sudden increase in the cyclone throughput at the onset of roping has also been reported by Plitt et al (1987), who observed a 16% increase in the cyclone flow-rate during the transition to roping.

4.1.4. Medium Flow

During the transition to roping the medium flow-rate at the sinks dropped abruptly, and this coincided with a drastic rise in the medium flow-rate at the floats; indicating that the onset of roping at the spigot resulted in a transfer of medium from the sinks to the floats. The steady drop in medium flow-rate at the floats during roping is a consequence of increased quantities of silica particles that had been misplaced to the floats (Fig. 4.4). Furthermore, there was a transfer of medium from the floats to the sinks with increasing feed ore concentration before roping commenced (Fig. 4.18). This is thought to be a consequence of the interaction between the silica particles and medium, resulting in the 'dragging' of medium to the spigot. This behaviour was also observed by Wood (1990), who observed, "Excessive sinks flow tends to carry additional medium to (sinks stream), rather than displace medium from the (sinks stream)".

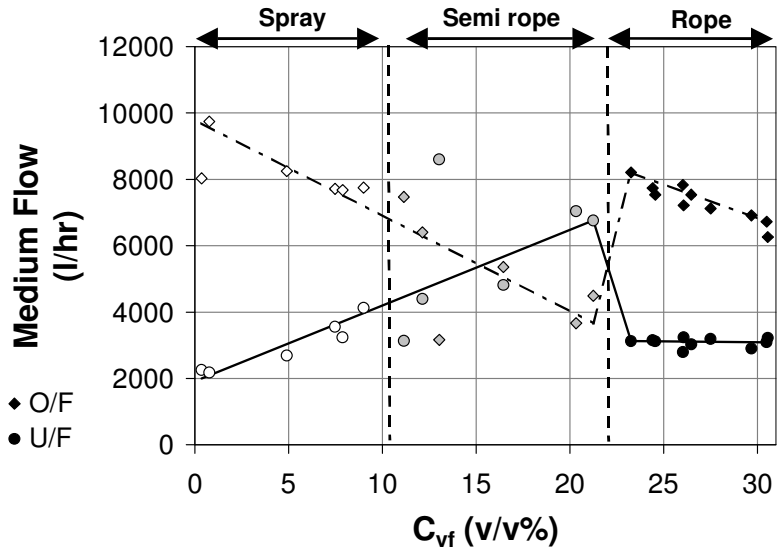


Figure 4.18. Medium flow-rate at the floats and sinks during the transition to rope discharge for the 45mm spigot. Data points with white and grey backgrounds were obtained during spray and semi-rope discharges, respectively. While data points with black background were obtained during roping.

The medium flow-rates at the sinks for the 25 and 34mm spigots during the transition to roping are shown in Fig. 4.19. Again the behaviour for the small spigots (25 and 34mm) mirrors that of the 45mm spigot as shown in Fig. 4.18.

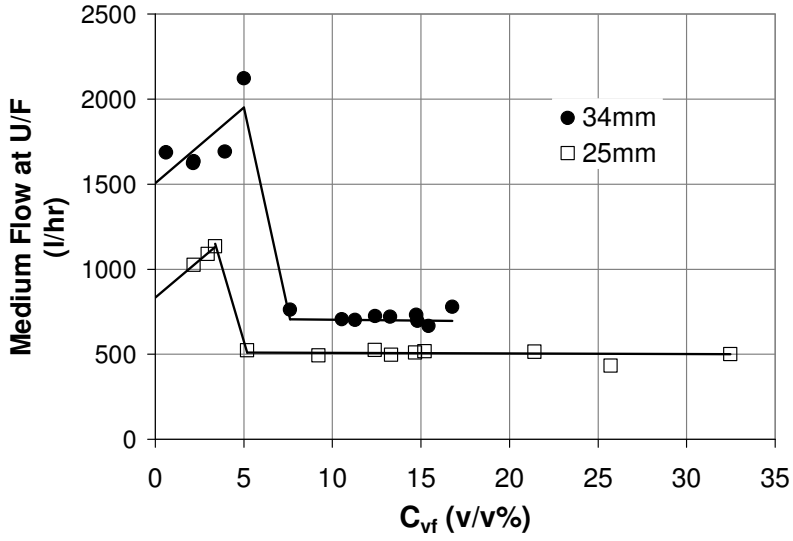


Figure 4.19. Medium flow-rate at the sinks during the transition to rope discharge for the 25 and 34mm spigots.

Fig. 4.20, on the other hand, illustrates the changes in the medium flow-rate at the floats during the transition to roping for the 25 and 34mm spigots.

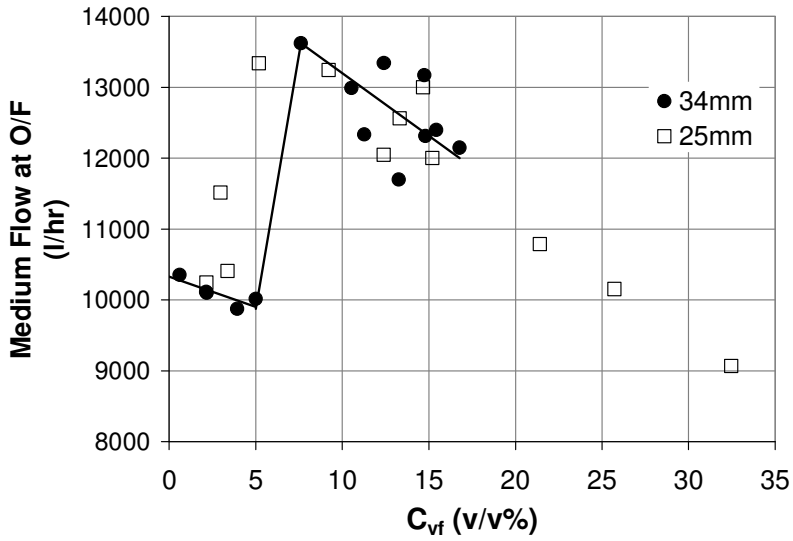


Figure 4.20. Medium flow-rate at the floats during the transition to rope discharge for the 25 and 34mm spigots.

The above-mentioned transfer of medium from the floats to the sinks with increased addition of silica particles into the cyclone, during spray and semi-rope discharges, was further confirmed by the behaviour of the density differential parameter (Fig. 4.23 and 4.24).

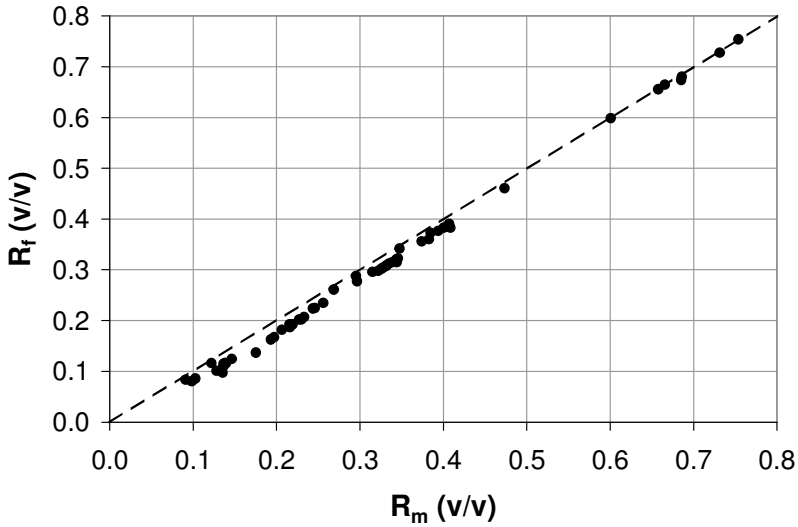


Figure 4.21. The relationship between R_f and R_m when spray and semi-rope discharges were prevalent at the sinks.

Volumetric medium split to sinks (R_m) is illustrated to be very similar to the water split to sinks (R_f) during spray and semi-rope discharges in Fig. 4.21. R_m was consistently higher than R_f at R_f and R_m values below 0.6. The relationship between R_f and R_m during roping is shown in Fig. 4.22, where the R_f and R_m values are almost always equal. The systematic deviation of

R_f from R_m observed during spray and semi-rope discharges was not evident during roping. This is indicative of a stabilized medium during roping conditions.

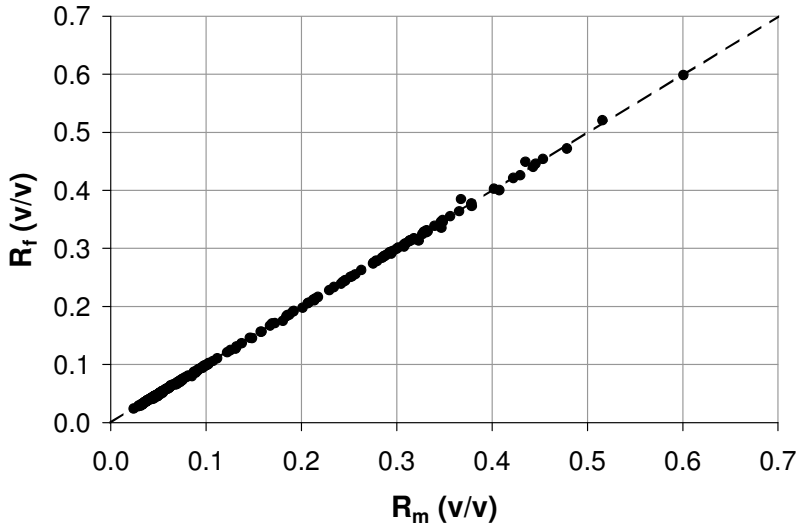


Figure 4.22. The relationship between R_f and R_m when rope discharge was prevalent at the sinks.

4.1.5. Density Differential

Density differential refers to the difference between the sinks and floats medium densities. The decrease in the differential observed in Fig. 4.23 and 4.24 is a consequence of the dilution of the high-density medium at the sinks by the low-density medium from the floats that was carried over to the spigot by the ore particles. According to King and Juckes (1984) when the volumetric medium-to-coal ratio approaches 1:1 the particles interact with each other, and this interaction changes the medium properties. The actual values of the density differentials shown in Fig. 4.23 and 4.24 might change in the presence of floats particles due to the consequent interaction between the floats particles and medium. The trend of the curve in Fig. 4.23 and 4.24 is, however, not expected to change, thus, spigot overloading should always be associated with relatively low-density differentials.

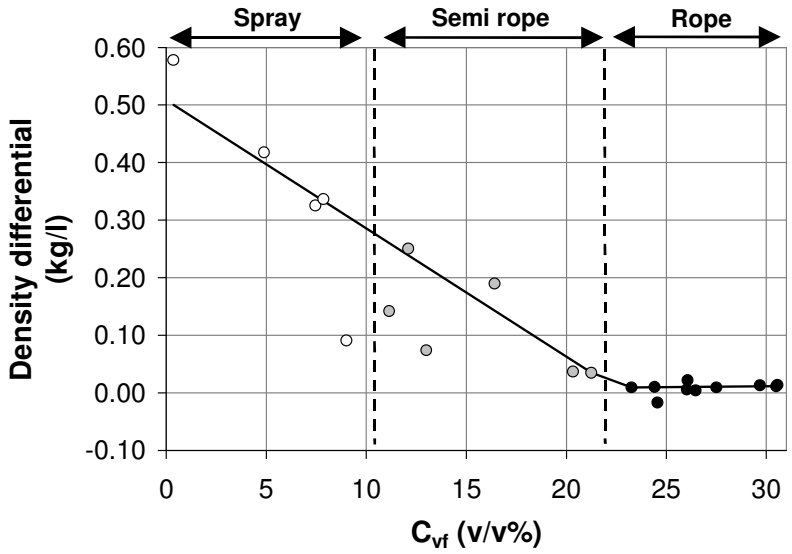


Figure 4.23. Density differential across the cyclone during the overloading of the 45mm spigot. Data points with white and grey backgrounds were obtained during spray and semi-rope discharges, respectively. While data points with black background were obtained during roping.

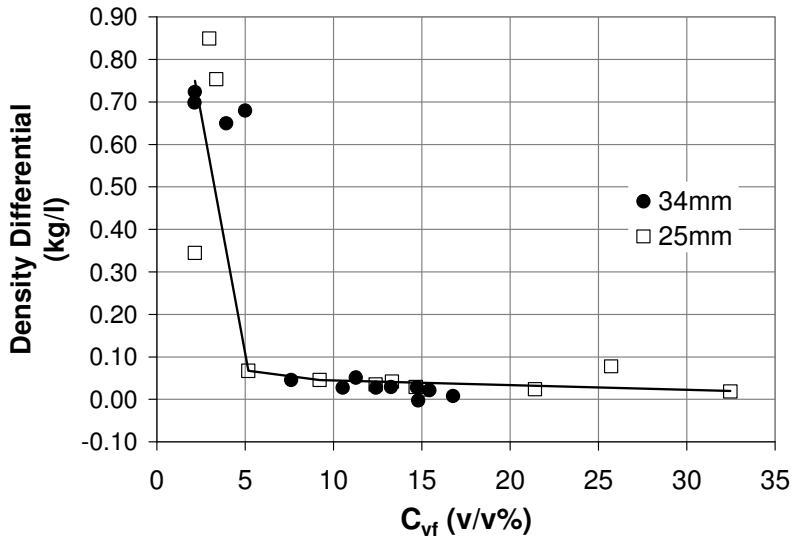


Figure 4.24. Density differential across the cyclone during the overloading of the 25 and 45mm spigots.

The range of density differentials obtained during all the tests performed with fine magnetite (95% -45µm) are shown in Fig. 4.25. This includes data from test-work aimed at determining the effect of various variables on the spigot capacity. The range of density differential obtained with medium and coarse grades ranged from –0.07 to 0.26 and 0.10 to 0.31, respectively.

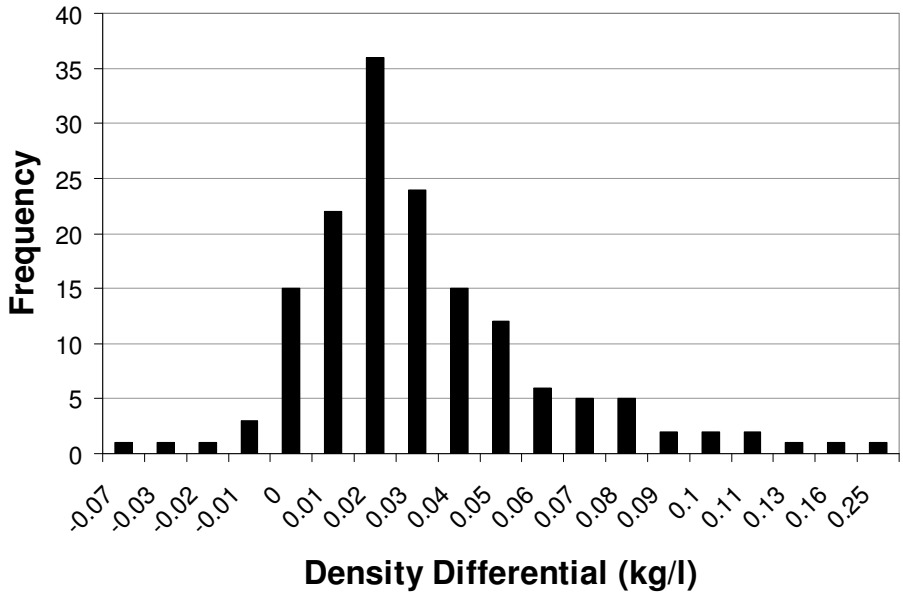


Figure 4.25. Range of density differential obtained during roping for all the tests performed with fine magnetite.

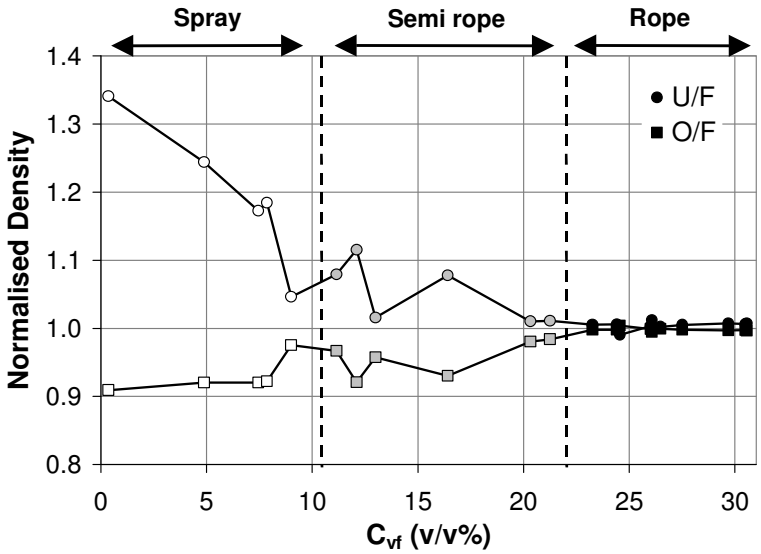


Figure 4.26. Influence of feed concentration on the floats and sinks medium densities for the 45mm spigot. Data points with white and grey backgrounds were obtained during spray and semi-rope discharges, respectively. While data points with black background were obtained during roping.

The floats and sinks medium densities were normalized to the feed density in Fig. 4.26, 4.27 and 4.28; the floats and sinks medium densities were increased and reduced, respectively, to equal the feed density during roping.

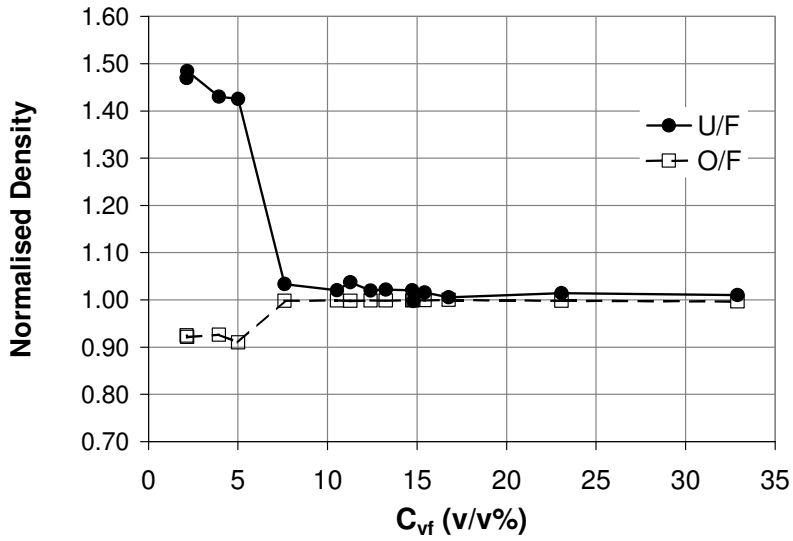


Figure 4.27. Influence of feed concentration on the floats and sinks medium densities for the 34mm spigot.

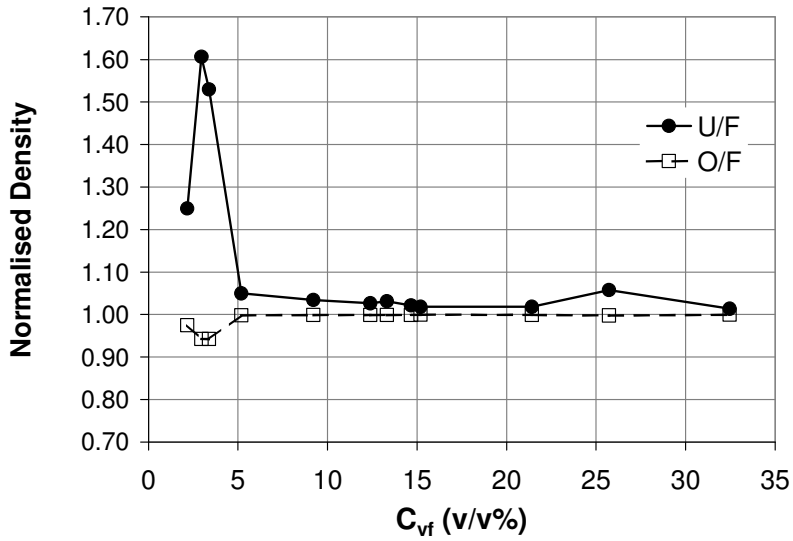


Figure 4.28. Influence of feed concentration on the floats and sinks medium densities for the 25mm spigot.

It is, therefore, expected that monitoring of the density differential could prove to be a useful diagnostic tool in detecting and avoiding spigot overloading in the cyclone.

4.2. QUANTIFYING THE SPIGOT CAPACITY

Jull (1972), Plitt et al. (1987), Heiskanen (2000) and DSM (1985) obtained mathematical expressions describing the relationship between spigot ore capacity and spigot diameter in accordance with the following relationship:

$$Q_{UM} = k_o D_u^{\ m} \qquad (2.13)$$

Heiskanen (2000) did not actually develop his own mathematical expression to quantify the spigot capacity, instead he validated Plitt et al. (1987)'s expression. The values for the constant k_o and exponent m for each of the relationships obtained by the various authors are shown in Table 2.21 (which is repeated here for convenience).

Table 2.21. Spigot diameter-spigot capacity relationships in literature.

Source	**Cyclone Type**	**Parameter** k_o	**Exponent** m
Jull (1972)	Classification	2.3	2.19
Plitt et al. (1987)	Classification	1.563	2.35
DSM (coal)	Dense medium	0.9	1.94
DSM (other minerals)	Dense medium	- *	2.05

*Dependent on head.

It, therefore, seems reasonable to expected Q_{USM} to be related to D_u in accordance with the following relationship:

$$Q_{USM} = kD_u^{\ n} \qquad (4.2)$$

Fitting equation 4.2 to all the data from the 165mm cyclone yielded the parameter values given in Table 4.3. The relationship between Q_{USM} and D_u is illustrated in Fig. 4.29; the plotted line in Fig. 4.29 represents equation 2.13, with the parameter values given in Table 4.3.

Table 4.3. Parameter values for equation 4.2 obtained for all the data acquired with the 165mm dense medium cyclone.

k	n	$\mathbf{R^2}$	$\boldsymbol{\sigma_{est}}$ **(l/hr slurry)**
21.97×10^{-3}	3.31	0.8088	1052.2

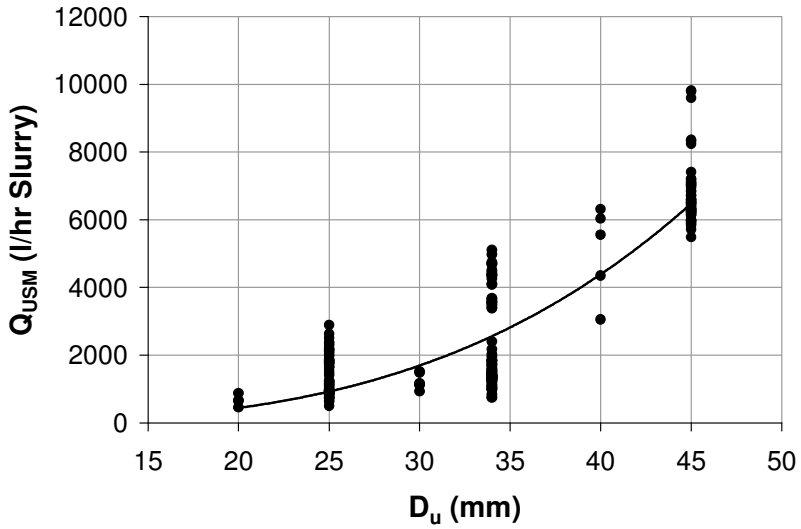


Figure 4.29. The effect of spigot diameter on Q_{USM}.

Fitting equation 2.13 to all the data from the 165mm cyclone yielded the parameter values presented in Table 4.4. The relationship between Q_{UM} and D_u is illustrated in Fig. 4.30; the plotted line represents equation 2.13 with the parameter values given in Table 4.4.

Table 4.4. Parameter values for equation 2.13 obtained for all the data acquired with the 165mm dense medium cyclone.

k_o	m	$\mathbf{R^2}$	$\boldsymbol{\sigma_{est}}$ **(l/hr ore)**
3.18×10^{-3}	3.64	0.8499	454.7

Fitting equations 2.13 and 4.2 to the 165mm cyclone data gave unsatisfactory results as illustrated in Tables 4.3 and 4.4, and Fig. 4.29 and 4.30. The exponent *n* and *m* obtained in both equations 2.13 and 4.2 are much higher than those reported in the literature (Table 2.21). Further, what appears to be an inflection point can be observed at the lower part of both Fig. 4.29 and 4.30, while none is apparent at the upper part of the curve. It was, therefore, decided to analyse the data obtained with the 15^o cone angle separately from those obtained with the 20^o cone angle.

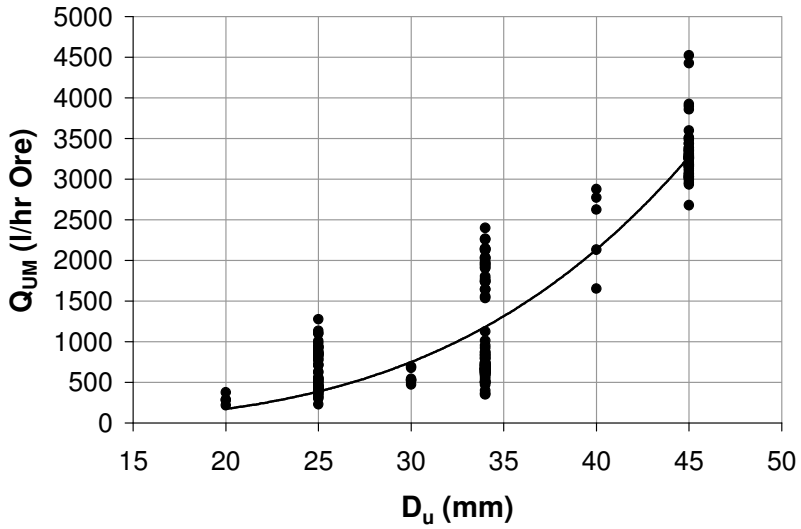


Figure 4.30. The effect of spigot diameter on Q_{UM}.

(a) 15^o Cone

The relationship between Q_{USM} and D_u for the 165mm cyclone when operating with a 15^o cone angle is shown in Fig. 4.31. An inflection point can clearly be observed at D_u is equal to 34mm. It appears that there was a change in 'flow regime' at the 34mm spigot diameter; beyond this spigot diameter Q_{USM} was more sensitive to changes in D_u. The relationship between Q_{UM} and D_u follows the same trend (Fig. 4.32).

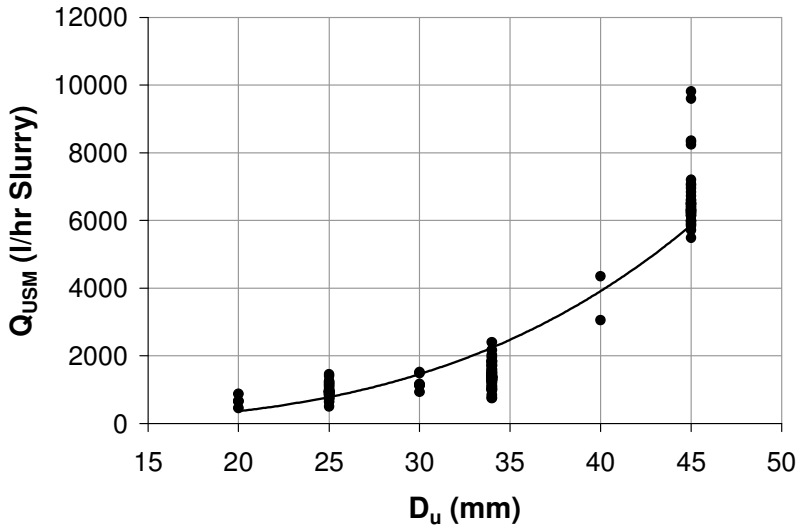


Figure 4.31. The effect of spigot diameter on Q_{USM} (15^o cone angle).

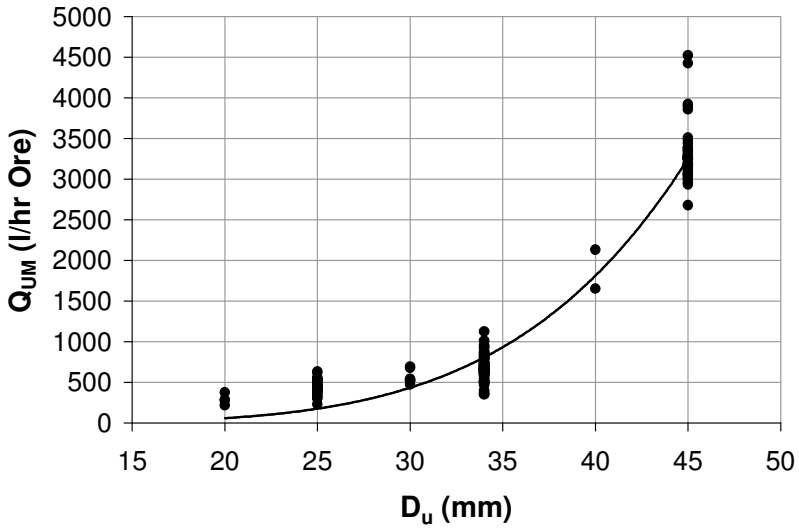


Figure 4.32. The effect of spigot diameter on Q_{UM} (15° cone angle).

Fitting equation 4.2 to all the data obtained with the 15° cone angle yielded the parameter values given in Table 4.5.

Table 4.5. Parameter values for equation 4.2 obtained for all the data acquired with the 165mm cyclone when operating with the 15° cone angle.

k	n	$\mathbf{R^2}$	$\boldsymbol{\sigma_{est}}$ **(l/hr slurry)**
12.63×10^{-3}	3.43	0.8747	895.2

Likewise fitting equation 2.13 to all the data obtained with the 15° cone angle yielded the parameter values given in Table 4.6. Analysis of the data obtained with the 15° cone angle separately from that obtained with the 20° one appears to have improved the quality of the fit, for both equation 2.13 and 4.2.

Table 4.6. Parameter values for equation 2.13 obtained for all the data acquired with the 165mm cyclone when operating with the 15° cone angle.

k_o	m	$\mathbf{R^2}$	$\boldsymbol{\sigma_{est}}$ **(l/hr ore)**
1.95×10^{-5}	4.98	0.9529	268.6

A schematic cross-section of the conical part of the cyclone for the 15° cone with the spigot inserted at the bottom is shown in Fig. 4.33. Fig. 4.33 (a) resembles the 45mm spigot, while the smaller spigots (20, 25, 30 and 34mm) look more like Fig. 4.33 (b). The 40mm spigot, on

the other hand, is in between the two configurations. The cone initially converges to a diameter of 45mm and then extends a length of about 225mm, of which the inserted spigot occupies only approximately 80mm. Thus, the slurry travels a distance of 145mm within 'cylindrical' part (with a diameter of 45mm) of the cone before reaching the inserted spigot. A consequence of this extra length is the accentuation of the effect of friction on the slurry flow at the sinks (increased resistance to flow), giving lower spigot capacities for the 15^o cone.

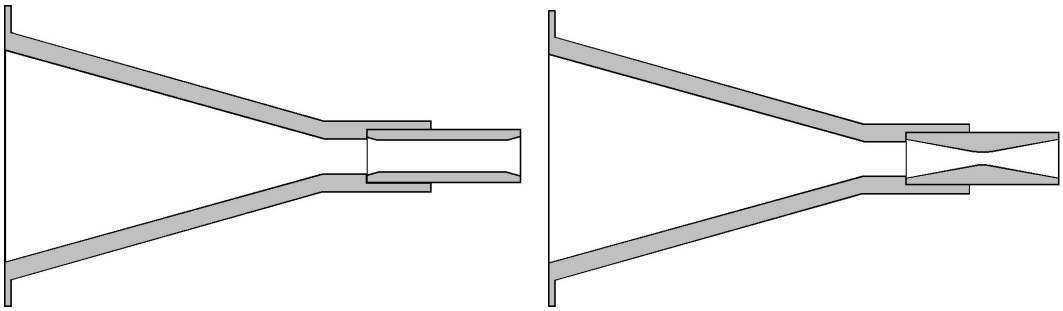


Figure 4.33. Schematic cross sectional view of the 15^o cone angle for (a) larger spigot and (b) smaller spigot.

It is interesting to note that the smaller spigots (20, 25, 30 and 34mm), which have a design resembling that in Fig. 4.33 (b), appear to be following one relationship, and the bigger spigots (40 and 45mm) appear to be following another. It is thought that the observed inflection point in Fig. 4.31 and 4.32 is a consequence of the above-mentioned differences in spigot design.

(b) 20^o Cone

The relationship between D_u and Q_{USM} for a cone angle of 20^o is shown in Fig. 4.34. The inflection point encountered with the 15^o cone was not observed with the 20^o cone. The same is true for the relationship between D_u and Q_{UM} (Fig. 4.35).

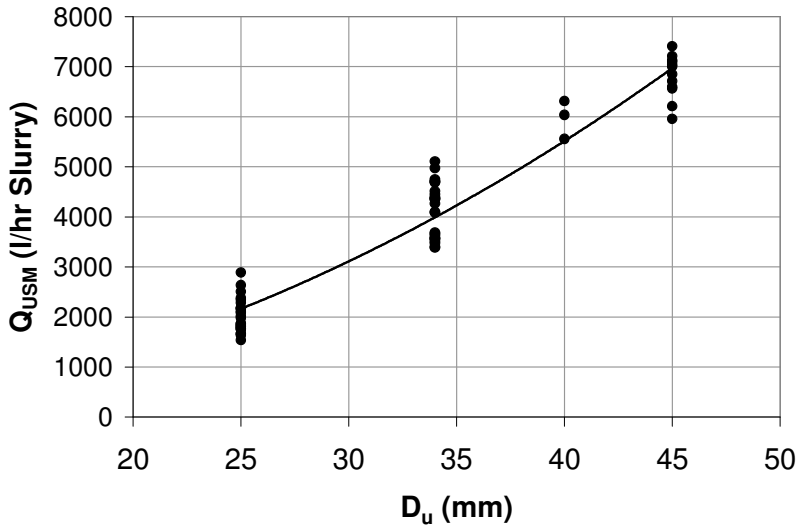


Figure 4.34. The effect of spigot diameter on Q_{USM}. (Cone A - 20°)

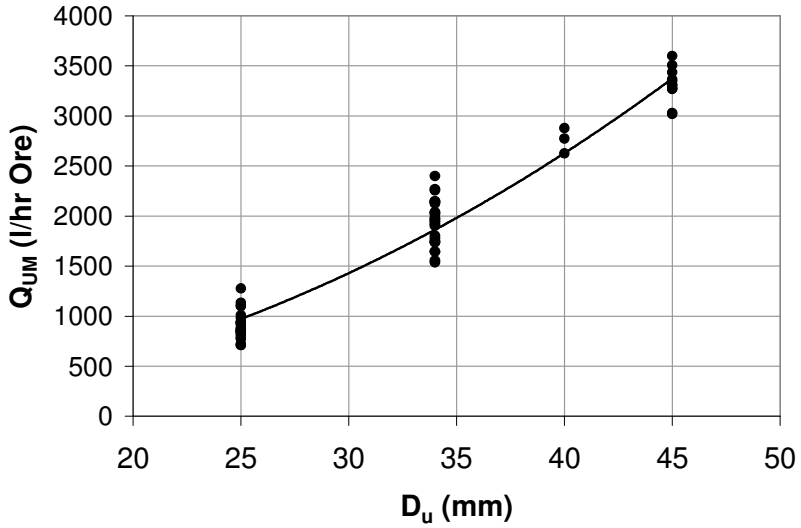


Figure 4.35. The effect of spigot diameter on Q_{UM}. (Cone A - 20°)

Fitting equation 4.2 to all the data obtained with the 20° cone angle yielded the parameter values given in Table 4.7. Likewise fitting equation 2.13 to all the data obtained with the 20° cone angle yielded the parameter values given in Table 4.8.

Table 4.7. Parameter values for equation 4.2 obtained for all the data acquired with the 165mm cyclone when operating with the 20° cone angle.

k	*n*	R^2	σ_{est} (l/hr slurry)
3.57	1.99	0.9361	468.6

Analysis of the data obtained with the 20° cone angle separately from those obtained with the 15° one clearly improved the quality of the fit for both equations 2.13 and 4.2 (Tables 4.7 and 4.8). Further the exponent *n* and *m* obtained in both equations 2.13 and 4.2, for the 20° cone angle, are in agreement with those reported in the literature (Table 2.21).

Table 4.8. Parameter values for equation 2.13 obtained for all the data acquired with the 165mm cyclone when operating with the 20° cone angle.

k_o	m	$\mathbf{R^2}$	$\boldsymbol{\sigma_{est}}$ **(l/hr ore)**
1.07	2.12	0.9548	194.6

A schematic cross-section of the conical part of the cyclone with the spigot inserted at the bottom of cone A is shown in Fig. 4.36. Just as with the 15° cone, Fig. 4.36 (a) resembles the 45mm spigot, while the smaller spigots (20, 25, 30 and 34mm) look more like Fig. 4.36 (b). Unlike the 15° cone, cone A converges down to a diameter of 50mm and the cone converges directly onto the inserted spigot. The extra length of about 145mm, present in the 15° cone-spigot design, was not present in this arrangement. It is thought that this might be the reason for the difference in the nature of the spigot diameter-spigot capacity relationships obtained between the 15° cone angle and cone A (20°).

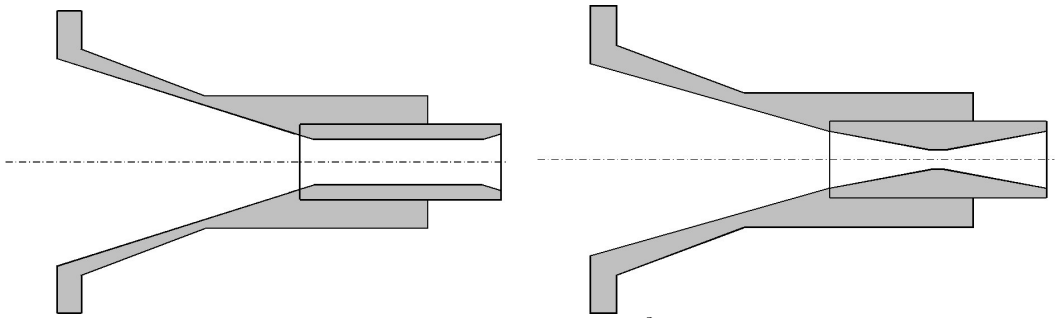


Figure 4.36. Schematic cross sectional view of cone A (20°) for (a) larger spigot and (b) smaller spigot.

In order to elucidate further the effect of the spigot design on the spigot capacities another 20° cone (cone B) with a different design from cone A was employed. Cone B differs from the cone A in that its spigot is not interchangeable; instead it is fixed at 45mm.



Figure 4.37. A picture of cone B.

A picture of cone B is shown in Fig. 4.37, and a schematic diagram of the cross-section through cone B is shown in Fig. 4.38.

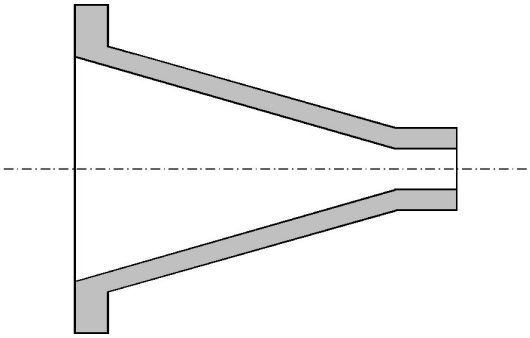


Figure 4.38. A schematic diagram of the cross-section through cone B.

A comparison between Q_{USM} values obtained with cone A and those with cone B is shown in Fig. 4.39. Q_{USM} values obtained with cone B were higher than those obtained with cone A. The differences in the Q_{USM} values were on average about 20%. The conditions under which the results given in Fig. 4.39 and 4.40 were obtained are presented in Table A.5 in Appendix A.

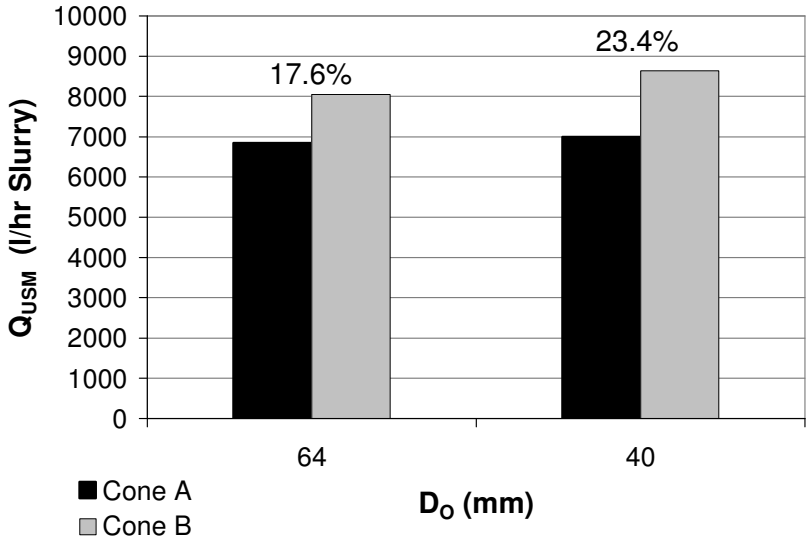


Figure 4.39. The influence of spigot design on Q_{USM}. (Operating conditions are given in Table A.5).

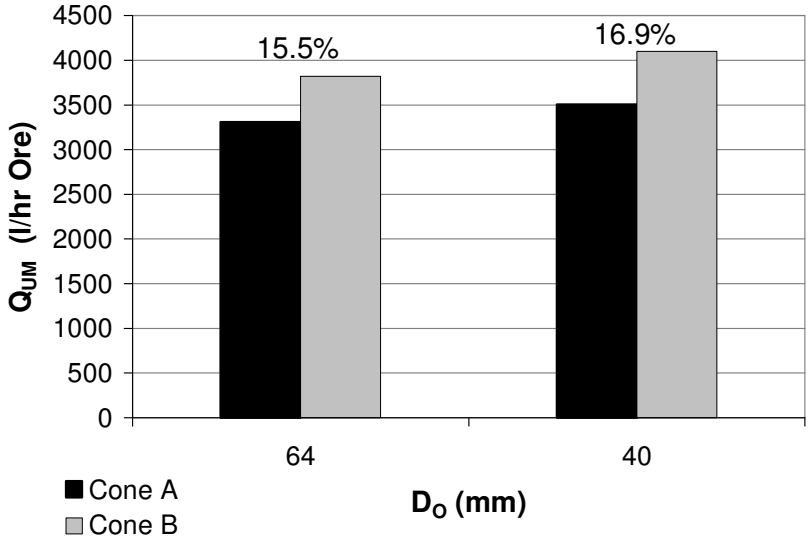


Figure 4.40. The influence of spigot design on Q_{UM}. (Operating conditions are given in Table A.5).

Similarly Q_{UM} values obtained with cone B were higher than those obtained with cone A by about 16% (Fig. 4.40). The main difference between cone A and B is that cone A (with the spigot inserted) is 115mm longer. It is this difference in length (at the sinks) that accounts for the lower spigot capacities obtained with cone A. These observations validate the postulation that the lower Q_{USM} and Q_{UM} values obtained with the 15^o cone angle were, at the least, partly due to the 145mm extra length present within the 15^o cone. It appears that the effect of this extra length is dependent on the size of the inserted spigot. The effect was more pronounced

at the smaller spigot diameters (34mm and less) at which the resistance to flow was the highest; hence, the presence of the inflection point.

It appears, therefore, that the DSM design gives the least resistance to flow; a typical DSM cyclone design is illustrated in Fig. 4.41.

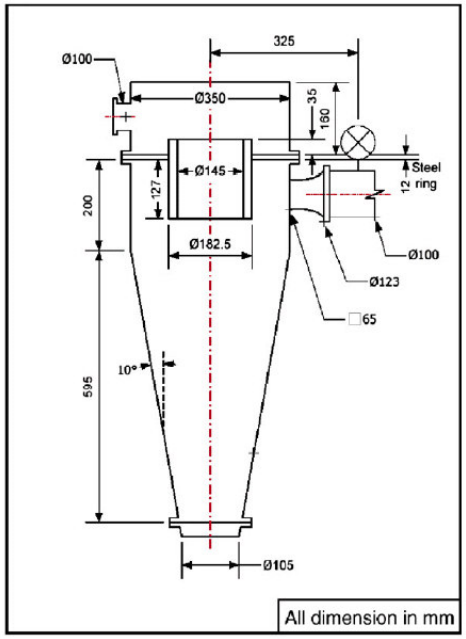


Figure 4.41. Configuration of a 350mm DSM cyclone. (Narasimha et al., 2007)

4.2.1. MODEL DEVELOPMENT

Empirical models quantifying/predicting various parameters including Q_{USM}, Q_{UM}, Q, S_R, C_{mvu} and R_m were developed making use of multiple-regression techniques. Only data obtained when operating the 165mm cyclone with cone A was utilized in developing the mathematical models that follow. None of the data obtained when operating with the 15^o cone angle was used in developing the models due to the presence of an inflection point as previously illustrated (Fig. 4.31 and 4.32). The behaviour encountered when operating with the 15^o cone angle is not well understood; hence, this data is left out in developing the regression models. The data acquired with the smaller 165mm cyclone (cone A only) were initially analysed separately, and then combined with those obtained with the larger 350mm cyclone. The dependent variables considered for the 165mm cyclone data include: Q_{USM}, Q_{UM}, Q, S_R, C_{mvu} and R_m. Only Q_{UM} was measured on the 350mm cyclone.

Multiple-regression procedure was repeated making use of different functional forms of the independent variables, namely: linear, power, exponential, etc. Only variables that were significant at the 95 percent confidence level were added to the regression equations. Although the spigot capacity is dependent mainly on D_u, it is expected that other variables should also have an effect on it. As a result a number of independent variables including D_o, D_i, Bl, H, ρ_{med}, and medium grade were considered.

(a) Spigot Capacity

The spigot capacity and spigot diameter have previously been illustrated in the literature to be correlated according to a power relationship, as in equation 2.12 and 2.13. Feed head has also been shown to correlate with the spigot capacity in accordance with a power relationship (Equation 2.12). Although mathematical correlations between D_o and D_i with spigot capacity have not previously been proposed, it seems reasonable to make use of a power relationship as with D_u and H. The relationship between spigot capacity and medium density appeared to be more complex than that of the other independent variables. Q_{USM} and Q_{UM} decreased with increasing ρ_{med}, and the sensitivity of both Q_{USM} and Q_{UM} to ρ_{med} increased beyond a certain critical value of ρ_{med}. In order to describe this behaviour the exponential term in equation 4.3 and 4.4 was employed. The best fit for both equation 4.3 and 4.4 was obtained when the critical ρ_{med} value was set at 1.45 kg/l; various ρ_{med} values ranging from 1.3 up to 1.7kg/l were attempted.

Hence, the following empirical model, which takes into account other variables other than D_u, to predict Q_{USM} is proposed:

$$Q_{USM} = kD_u^{n_1} D_o^{n_2} D_i^{n_3} H^{n_4} \exp\left[n_5(\rho_{med} - 1.45)^3\right] \quad (4.3)$$

with Q_{USM} in l/hr slurry, D_u in mm, D_o in mm, D_i in mm, H in D and ρ_{med} in kg/l. Fitting equation 4.3 to all the data obtained when operating the 165mm cyclone with cone A gave the parameter values given in Table 4.9. Medium grade and barrel length were found not to be significant at the 95 percent confidence level, and as a result they were left out of the regression equation. The P-value given in Table 4.9 is the probability of falsely rejecting the null hypothesis, or wrongfully concluding that there is an association between the dependent and independent variables.

Table 4.9. Summary of statistical results from multiple-regression of Q_{USM} data obtained with the 165mm cyclone (cone A).

	Coefficient	**Std Error**	**P-value**	**R^2**	**σ_{est} (l/hr slurry)**
k	0.394	0.156	0.0144	0.9805	267.3
n_1	2.09	0.046	<0.0001		
n_2	-0.14	0.045	0.0039		
n_3	0.43	0.070	<0.0001		
n_4	0.36	0.044	<0.0001		
n_5	-5.67	1.362	0.0001		

Equation 4.3 appears to predict Q_{USM} reasonably well. The goodness of fit is illustrated in Fig. 4.42 where the measured Q_{USM} values are compared with those predicted with equation 4.3.

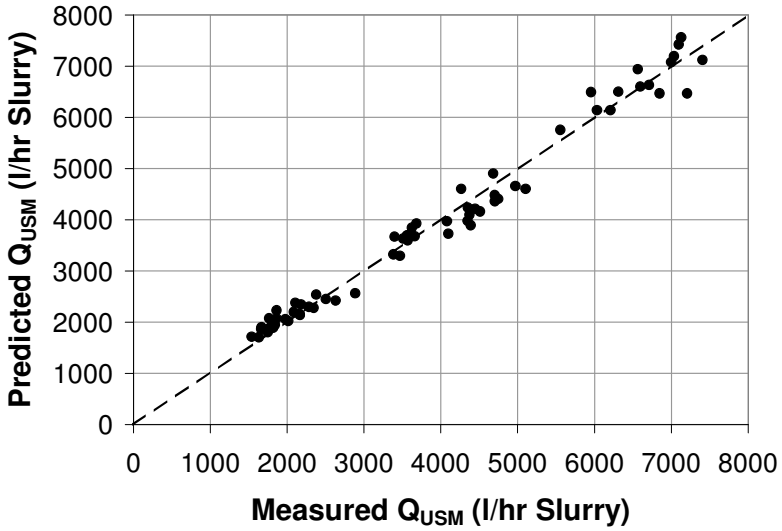


Figure 4.42. Predicted versus measured Q_{USM} values for equation 4.3 with parameter values in Table 4.9.

The following empirical model to predict Q_{UM} is proposed:

$$Q_{UM} = k_o D_u^{m_1} D_o^{m_2} D_i^{m_3} H^{m_4} \exp\left[m_5 (\rho_{med} - 1.45)^3\right] \quad (4.4)$$

with Q_{UM} in l/hr ore, D_u in mm, D_o in mm, D_i in mm, H in D and ρ_{med} in kg/l. Fitting equation 4.4 to all the data obtained when operating the 165mm cyclone with cone A gave the parameter values given in Table 4.10. Just as with Q_{USM}, medium grade and barrel length were found not to be significant at the 95 percent confidence level.

Table 4.10. Summary of statistical results from multiple-regression of Q_{UM} data obtained with the 165mm cyclone (cone A).

	Coefficient	**Std Error**	**P-value**	**R^2**	**σ_{est} (l/hr ore)**
k_o	0.226	0.091	0.0158	0.9821	126.7
m_1	2.16	0.046	<0.0001		
m_2	-0.11	0.046	0.0181		
m_3	0.38	0.072	<0.0001		
m_4	0.20	0.044	<0.0001		
m_5	-7.59	1.447	<0.0001		

Equation 4.4 appears to predict Q_{UM} reasonably well. The goodness of the fit is illustrated in Fig. 4.43, where the measured Q_{UM} values are compared with those predicted with equation 4.4.

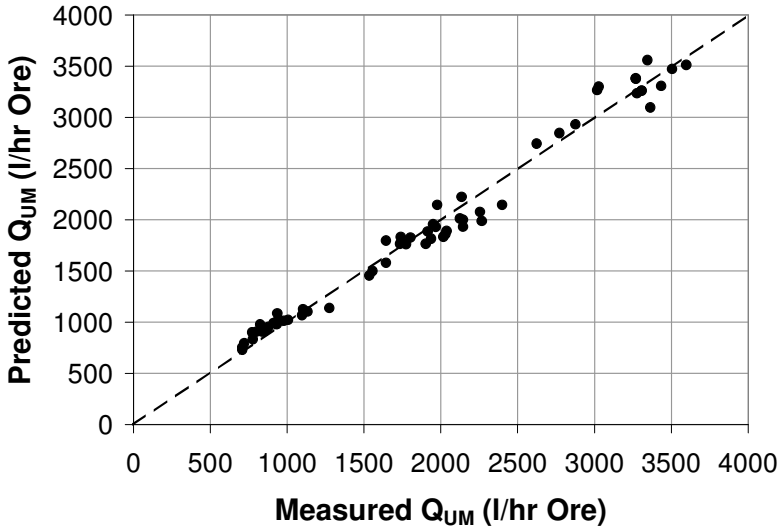


Figure 4.43. Predicted versus measured Q_{UM} values for equation 4.4 with parameter values in Table 4.10.

Inclusion of 350mm cyclone data

Data obtained with the 350mm cyclone showed Q_{UM} to reach a peak at a certain critical value of ρ_{med}, beyond which Q_{UM} decreased with further increases in ρ_{med}. In order to describe this 'peaking' behaviour the exponential term in equation 4.5 was employed; Fig. 4.44 illustrates how well this term describes the 'peaking' behaviour. The best fit for equation 4.5 was obtained when the critical ρ_{med} value was set at 1.45 kg/l just as was the case for equations 4.3 and 4.4; various ρ_{med} values ranging from 1.3 up to 1.7kg/l were attempted.

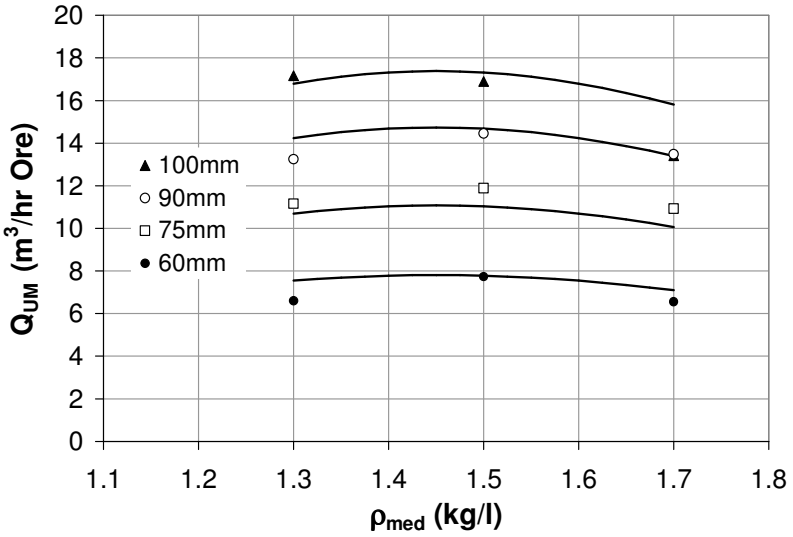


Figure 4.44. The effect of medium density on Q_{UM} for the 350mm cyclone. (The plotted lines represent equation 4.5.)

The following empirical model, which takes into account data from both the 165mm (cone A only) and 350mm cyclones, to predict Q_{UM} is proposed:

$$Q_{UM} = k_o D^{m_1} D_u^{m_2} H^{m_3} \exp\left[m_4 (\rho_{med} - 1.45)^2\right] \quad (4.5)$$

with Q_{UM} in l/hr ore, D_u in mm, D in mm, H in D and ρ_{med} in kg/l. The relevant parameter values for equation 4.5 are given in Table 4.11. It appears that Q_{UM} is less sensitive to changes in D_u for the 350mm cyclone; the exponent m_1 was reduced from 2.16 to 1.53. The exclusion of D_o and D_i from equation 4.5 is a consequence of the fact that these variables were not varied on the 350mm cyclone, rather than an indication of their influence on Q_{UM}.

Table 4.11. Summary of statistical results from multiple-regression of Q_{UM} data obtained with the 165mm (cone A) and 350mm cyclones.

	Coefficient	**Std Error**	**P-value**	**R^2**	**σ_{est} (l/hr ore)**
k_o	0.235	0.063	0.0003	0.991	440.0
m_1	0.63	0.045	<0.0001		
m_2	1.53	0.063	<0.0001		
m_3	0.18	0.063	0.0055		
m_4	-1.58	0.368	<0.0001		

An independent and significant effect of D on Q_{UM} is illustrated in Fig. 4.45. The dashed line in Fig. 4.45 represents Q_{UM} values that have been corrected for spigot design differences by increasing them by 20% (v/v). The figure of 20% is based on the results shown in Fig. 4.39 and 4.40, whereby the effect of spigot design on Q_{USM} and Q_{UM} was quantified. This correction does not entirely account for the differences in the spigot designs of the two cyclones. Although cone B is quite similar to the DSM design, it is not the same as illustrated in Fig. 4.38 and 4.41. Other factors that might possibly also contribute towards a discrepancy between results obtained with the 165mm and 350mm cyclones is their materials of construction and differences in inclination angle. The 165mm cyclone was constructed of polyurethane while the material of construction for the 350mm cyclone was cast iron. Although the afore-mentioned factors influence Q_{UM}, they do not account for the step increase in Q_{UM} values that is observed in Fig. 4.45 when the cyclone diameter is increased from 165mm to 350mm. It is thought that this is a consequence of the cyclone diameter; hence, it is included in equation 4.5.

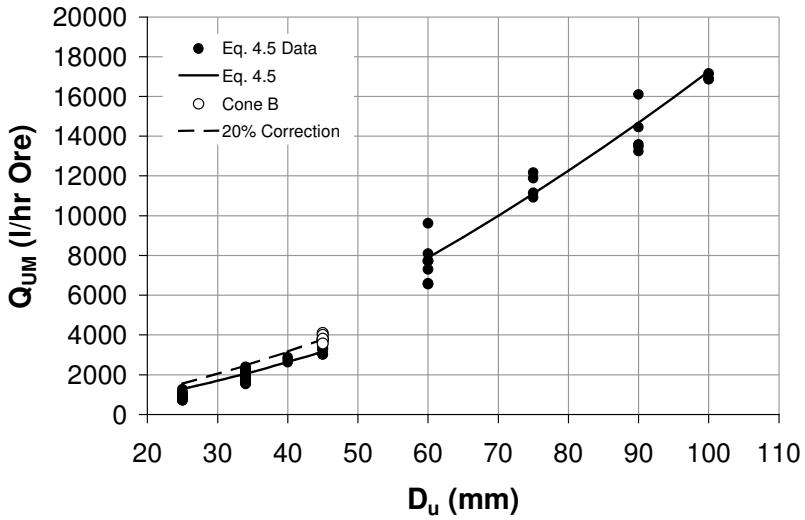


Figure 4.45. The effect of D_u on Q_{UM} for the 165mm and 350mm cyclones.

Equation 4.5 appears to predict Q_{UM} reasonably well. A comparison of the measured Q_{UM} values with those predicted with equation 4.5, for the data obtained with both the 165mm (cone A only) and 350mm cyclones, is shown in Fig. 4.46:

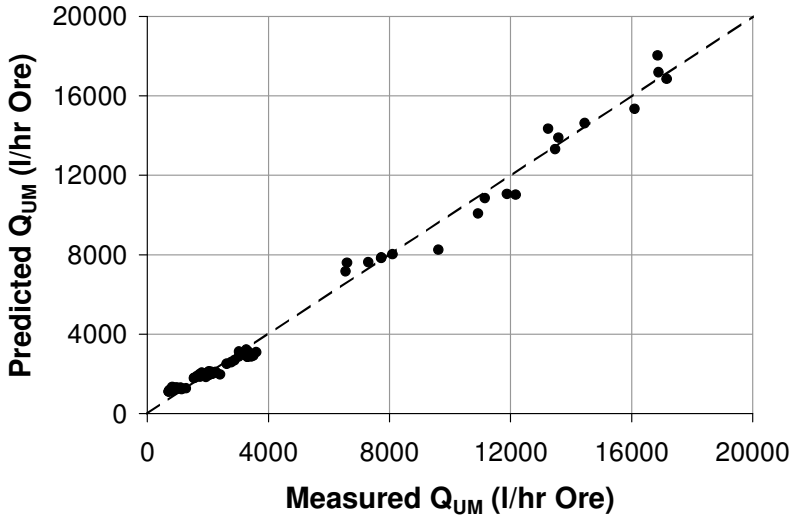


Figure 4.46. Predicted versus measured Q_{UM} values for equation 4.5 with parameter values in Table 4.11.

A closer look at Fig. 4.46 at the lower Q_{UM} values, which were obviously obtained with the 165mm cyclone, indicates that Q_{UM} was systematically over-estimated and under-estimated at the relatively lower and higher Q_{UM} values, respectively (Fig. 4.47). This is due to the differences in the sensitivity of Q_{UM} to D_u for the 165mm and 350mm cyclones.

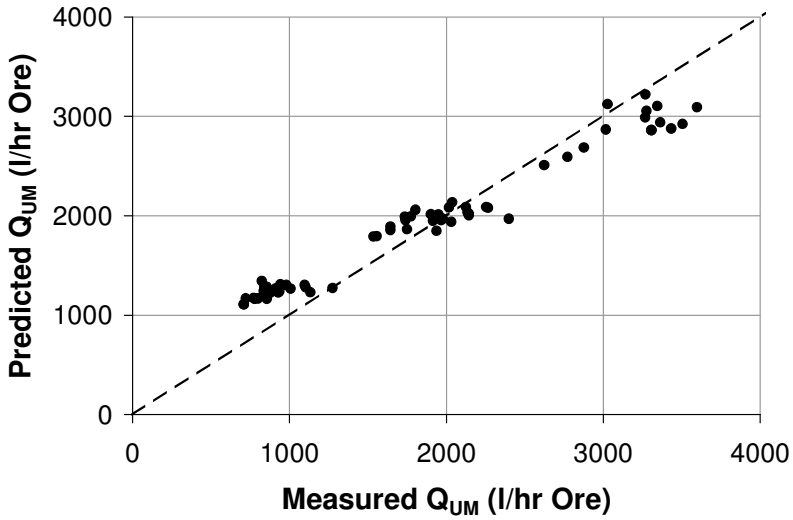


Figure 4.47. A closer look at the lower Q_{UM} values in Fig. 4.43.

(b) Cyclone Capacity

Upadrashta and Venkateswarlu (1982) proposed the following expression, which was determined during roping:

$$Q = K\left(\frac{P}{\rho_{med}}\right)^{0.58}(1-C_v)^{0.56}\left(D_u^2 + D_o^2\right)^{0.26} D_i^{1.8} \qquad \text{(A.2)}$$

Other expressions which were determined under spray discharge conditions are given in Appendix A (Equations A.1 to A.9). The use of the term $\left(D_u^2 + D_o^2\right)^n$ in equation 4.6 yielded the best fit; other functional forms yielded inferior correlations to that presented in Table 4.12. The increase in Q with increasing ρ_{med} is in contradiction with all other relationships reported in the literature. There is consensus in the literature that Q decreases with increasing ρ_{med}. The reasons for this contradiction are not clear.

Based on the expressions in the literature the following empirical model to predict Q seems reasonable:

$$Q = k\left(D_u + D_o\right)^{n_1} D_i^{n_2} H^{n_3} \rho_{med}^{n_4} \qquad \text{(4.6)}$$

with Q in l/hr slurry, D_o in mm, D_i in mm, H in D and ρ_{med} in kg/l. Fitting equation 4.6 to all the data obtained when operating the 165mm cyclone with cone A gave the parameter values given in Table 4.12. Only D_u, D_o, D_i, H and ρ_{med} were found to be significant at the 0.05 significance level.

Table 4.12. Summary of statistical results from multiple-regression of Q data obtained with the 165mm cyclone (cone A).

	Coefficient	Std Error	P-value	R^2	σ_{est} (l/hr slurry)
k	64.72	16.93	0.0003	0.9446	645.4
n_1	0.074	0.026	0.0057		
n_2	0.90	0.032	<0.0001		
n_3	0.62	0.034	<0.0001		
n_4	0.18	0.061	0.0052		

Equation 4.6 appears to give a fair prediction of Q. A comparison of Q values predicted with equation 4.6 and those measured is shown in Fig. 4.48.

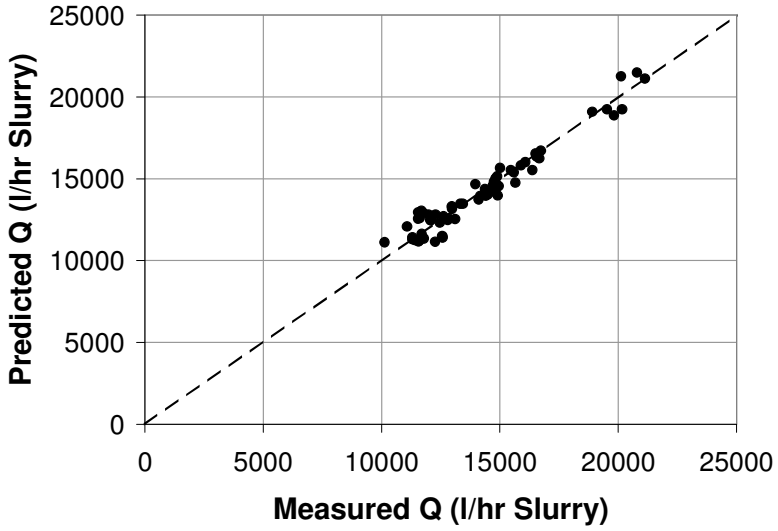


Figure 4.48. Predicted versus measured Q values for equation 4.6 with parameter values in Table 4.12.

(c) Volume Split

Upadrashta and Venkateswarlu (1982) proposed the following expressions, which was determined under roping conditions:

$$S_R = \frac{Q_{USM}}{Q_O} = 1.91(1-C_V)^{1.1} Q^{-0.44} \left(\frac{D_u}{D_o}\right)^{2.32} \qquad (2.9)$$

A combination of equations 2.9 and A.2 give the following expression:

$$S_R = \frac{Q_{USM}}{Q_O} \propto (1-C_V)^{0.85} \left(\frac{P}{\rho_{med}}\right)^{-0.26} \left(D_o^2 + D_u^2\right)^{-0.11} \left(\frac{D_u}{D_o}\right)^{2.32} D_i^{-0.79}$$

Usage of the following terms on the results obtained in this study did not yield an acceptable correlation:

$\left(D_o^2 + D_u^2\right)^{n_1}$ and $\left(\frac{D_u}{D_o}\right)^{n_2}$.

Instead a power relationship was employed to correlate S_R with D_o and D_u. Misplacement of sinks particles to the floats stream did not influence S_R in the same way in the current study as reported by Upadrashta and Venkateswarlu (1982). S_R increased with increasing C_{vf} in the current investigation while Upadrashta and Venkateswarlu reported it to decrease with increasing C_V. A power relationship was used to correlate H with S_R and this gave reasonable results.

The following empirical model to predict S_R is, therefore, proposed:

$$S_R = \frac{Q_{USM}}{Q_{OS}} = 10^k D_u^{n_1} D_o^{n_2} H^{n_3} C_{vf}^{n_4} \qquad (4.7)$$

with Q_{USM} in l/hr slurry, Q_{OS} in l/hr slurry, D_u in mm, D_o in mm, H in D and C_{vf} in %v/v. Fitting equation 4.7 to all the data obtained when operating the 165mm cyclone with cone A gave the parameter values given in Table 4.13. Only D_u, D_o, H and C_{vf} were found to be significant at the 0.05 significance level.

Table 4.13. Summary of statistical results from multiple-regression of data obtained with the 165mm cyclone (cone A).

	Coefficient	**Std Error**	**P-value**	**R^2**	**σ_{est} (v/v)**
k	-4.52	0.3145	<0.0001	0.9637	0.081
n_1	2.76	0.1816	<0.0001		
n_2	-0.25	0.0904	0.0071		
n_3	-0.70	0.0983	<0.0001		
n_4	0.83	0.1564	<0.0001		

Equation 4.7 appears to give a fair prediction of S_R. A comparison of the measured S_R values with those predicted with equation 4.7 is shown in Fig. 4.49.

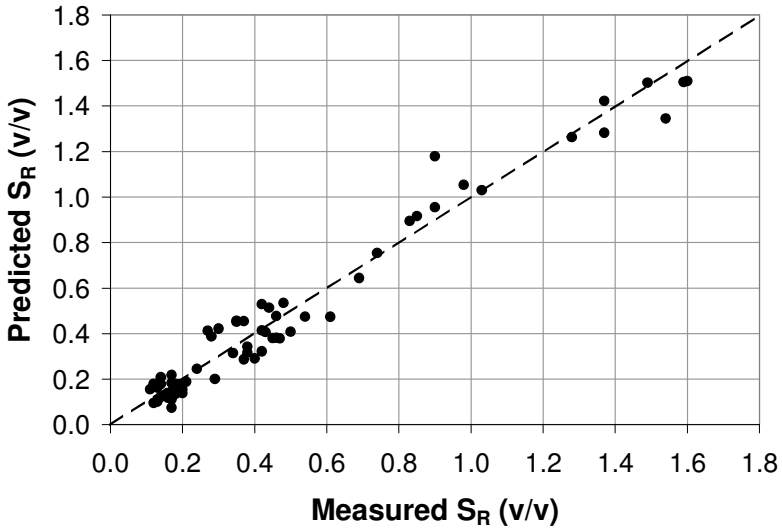


Figure 4.49. Predicted versus measured S values for equation 4.7 with parameter values in Table 4.13.

(d) Sinks Ore Concentration

C_{mvu} was found to be dependent on other independent variables as illustrated in equation 4.8:

$$C_{mvu} = kD_u^{a_1} Gr^{a_2} \qquad (4.8)$$

with C_{mvu} in %v/v, D_u in mm and Gr in mass percentage passing 45µm. Only D_u and medium grade were found to be significant at the 95 percent confidence level, and the correlation was poor (Table 4.14). Parameter values obtained from fitting equation 4.8 to all the data obtained with the 165mm cyclone operating with cone A are given in Table 4.14.

Table 4.14. Summary of statistical results from multiple-regression of C_{mvu} data obtained with the 165mm cyclone (cone A).

	Coefficient	**Std Error**	**P-value**	**R^2**	**σ_{est} (v/v%)**
k	139.34	44.65	0.0028	0.6702	1.38
a_1	0.14	0.017	<0.0001		
a_2	-0.35	0.073	<0.0001		

A comparison of the C_{mvu} calculated with equation 4.8 and those measured during experimental work is shown in Fig. 4.50. The quality of fit is illustrated to be very poor; this correlation is, therefore, of no significance.

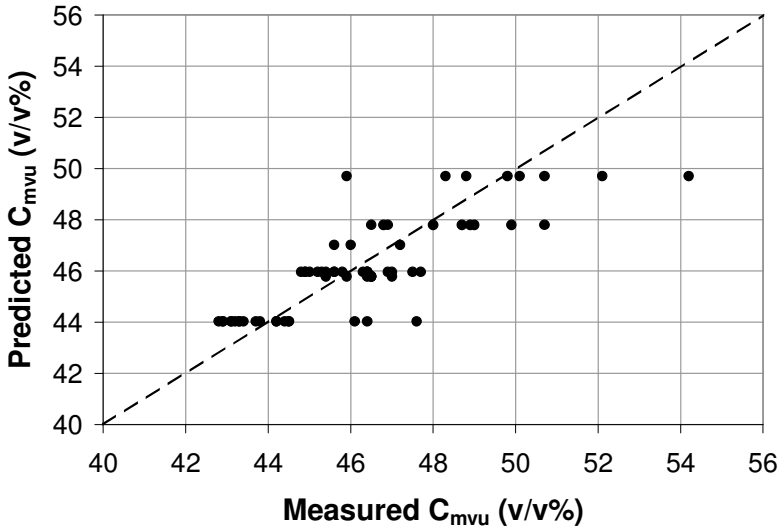


Figure 4.50. Predicted versus measured C_{mvu} values for equation 4.8 with parameter values in Table 4.14.

(e) Medium Split to Sinks

Clarkson and Wood (1993) proposed the following relationship, which was determined with a cyclone operating with medium only:

$$R_m = 0.79\left(\frac{D_u}{D_o}\right)^{4.2} H^{-0.37} \qquad (4.9)$$

Davis and Napier-Munn (1987), on the other hand, reported R_m to be a function of spigot diameter and kinematic viscosity. D_o and D_u were observed not to influence R_m as a ratio in the current study. Further, C_{vf} was observed to influence R_m significantly in the current investigation.

R_m was found to be dependent on other independent variables as illustrated in equation 4.10:

$$R_m = 10^k D_u^{b_1} D_o^{b_2} H^{b_3} C_{vf}^{b_4} \qquad (4.10)$$

with R_m in v/v, D_u in mm, D_o in mm, H in D and C_{vf} in v/v%. D_i, ρ_{med} and medium grade were found not to be significant at the 95 percent confidence level. Fitting equation 4.10 to all the data obtained when operating the 165mm cyclone with cone A gave the parameter values given in Table 4.15.

Table 4.15. Summary of statistical results from multiple-regression of R_m data obtained with the 165mm cyclone (cone A).

	Coefficient	**Std Error**	**P-value**	**R^2**	**σ_{est} (v/v)**
k	-3.78	0.2255	<0.0001	0.9600	0.024
b_1	1.96	0.1104	<0.0001		
b_2	-0.25	0.0716	0.0009		
b_3	-0.17	0.0746	0.0247		
b_4	0.52	0.0983	<0.0001		

Equation 4.9 appears to give a fair prediction of R_m. A comparison of the measured R_m values with those predicted with equation 4.10 is shown in Fig. 4.51.

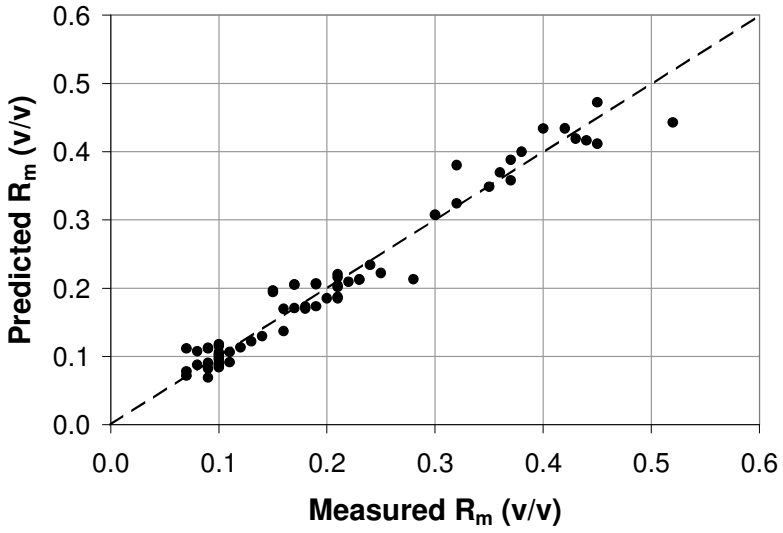


Figure 4.51. Predicted versus measured R_m values for equation 4.10 with parameter values in Table 4.15.

4.2.2. Comparison with DSM Spigot Capacities

A comparison between the spigot ore capacities obtained in this study with those by DSM is shown in Fig. 4.52 and 4.53; a log-log scale is used in Fig. 4.56 for clarity especially at the smaller spigot diameters. The spigot capacities obtained in this study are consistently higher than those by DSM.

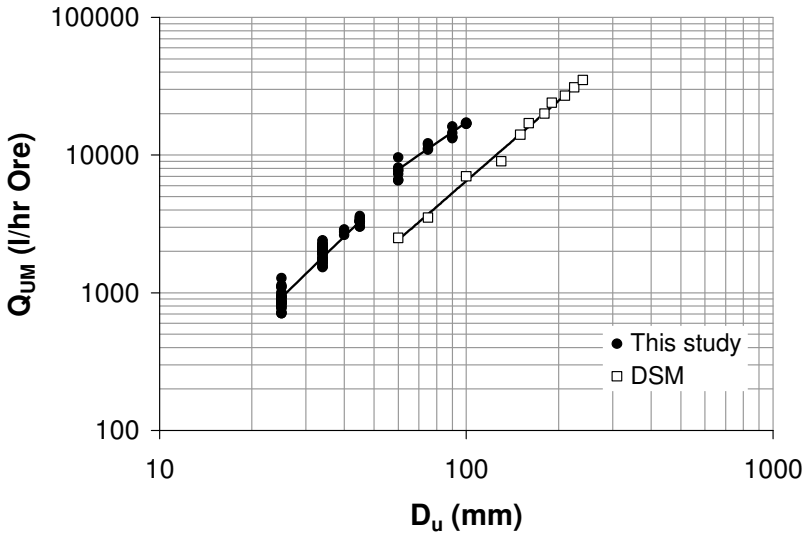


Figure 4.52. Comparison of the spigot diameter-spigot capacity relationship obtained in this study with that by DSM.

The differences between Q_{UM} values obtained in this investigation and those by DSM are quantified in Fig. 4.53 and Table 4.16 for D_u ranging from 60 to 100mm. Q_{UM} values obtained in this study were generally more than double those specified by DSM; a safety factor of around 60% was established. It can, therefore, be concluded that there is large potential to increase the 'spigot capacities' specified by DSM. In support of this view, Wood (1990) previously reported a case in which the volumetric sinks medium-to-ore ratio of a dense medium cyclone was 0.9:1 (53% ore by volume) and no serious symptoms such as gross misplacement of sinks particles to floats stream was observed. Further, he reported that only a 'little disruption to efficient separation' was encountered.

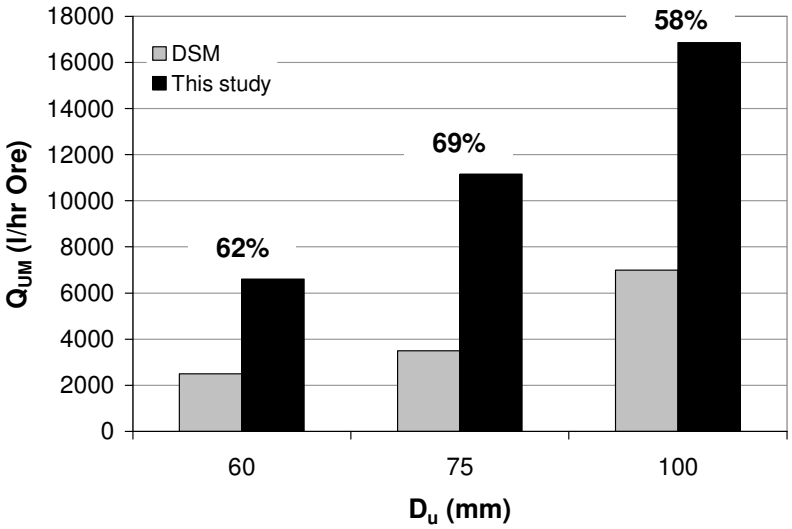


Figure 4.53. Comparison of Q_{UM} obtained in this study and those specified by DSM.

Table 4.16. Comparison of Q_{UM} obtained in this study and those specified by DSM.

D_u (mm)	Q_{UM} (l/hr ore)		
	This study	DSM	Safety Factor
60	6599	2500	0.62
75	11154	3500	0.69
100	16860	7000	0.58

Safety Factor = $(Q_{UM(This\ study)} - Q_{UM(DSM)})/Q_{UM(This\ study)}$

It is interesting to note that the spigot loading (in l/hr ore) at the transition point from a spray to semi-rope discharge is about 40% of the maximum spigot capacity (as shown Fig. 4.4, which is repeated here for convenience), so that the relevant safety factor is as follows:

$$\text{Safety factor} \approx \frac{3200-1350}{3200} = 58\%$$

This value is consistent with the values given in Table 4.16 and Fig. 4.53; implying that DSM possibly defined their 'spigot capacities' as the maximum spigot loading that can be achieved before semi-roping commences. This notion is further supported by the sinks ore concentrations (at the DSM specified 'spigot capacities'), which were inferred from the DSM data; these concentrations largely ranged between 24 and 31% (v/v) as given previously in Table 2.7. As previously mentioned, spigot overloading (or roping) is expected at sinks ore concentrations of 40% (v/v) and above, and semi-roping precedes rope discharge. Thus, the

sinks ore concentrations inferred from the DSM data are consistent with semi-roping conditions.

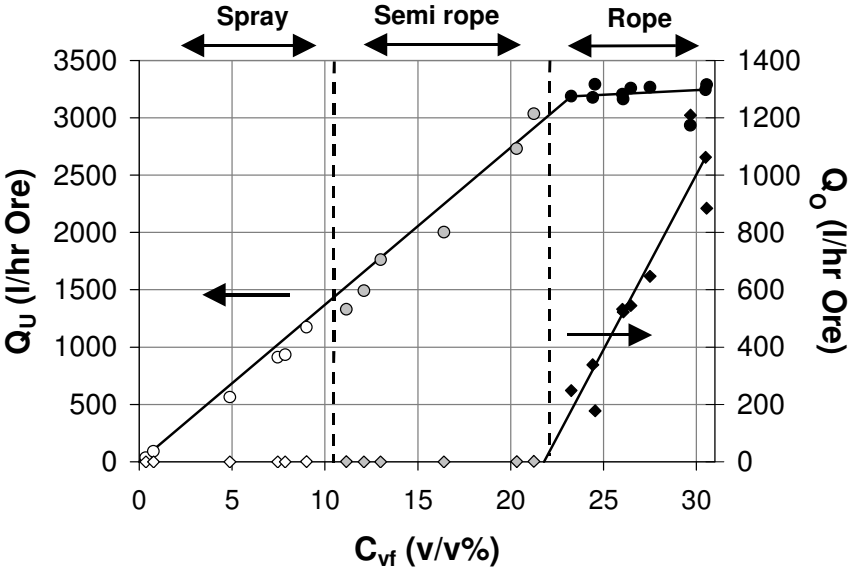


Figure 4.4. Changes in the ore loading at both the floats and sinks streams as ore was added into the cyclone for a 45mm spigot. Data points with white and grey backgrounds were obtained during spray and semi-rope discharges, respectively. While data points with black background were obtained during roping.

The DSM data presented in Fig. 4.52 and 4.53 was determined on geometrically similar cyclones, whilst that was not the case in this study. As previously illustrated, cyclone diameter has an independent and significant influence on Q_{UM}, and the data presented in Fig. 4.52 and 4.53 has not been corrected for this effect. In an attempt to correct this effect of cyclone diameter, equation 4.5 was utilized to predict Q_{UM} values of cyclones with diameters 165, 200, 250 and 350 with standard spigot sizes (D_u/D =0.3). The feed head was kept at 10D and the medium density at 1.5kg/l. The results of this exercise are given in Table 4.17 and Fig. 4.54. This correction gives a slightly lower safety factor of about 55% (Table 4.17).

Table 4.17. Comparison of Q_{UM} predicted with eq. 4.5 and those specified by DSM.

D (mm)	D_u (mm)	Q_{UM} (l/hr ore)		
		Eq. 4.5	DSM	Safety Factor
165	45	3016	–	–
200	60	5290	2500	0.53
250	75	8570	3500	0.59
350	100	16461	7000	0.57

Regression of the data (predicted with eq. 4.5) in Fig. 4.54 gave the following expression:

$$Q_{UM} = 0.642 D_u^{2.20} \quad (R^2 = 0.9997) \qquad (4.11)$$

with Q_{UM} in l/hr ore and D_u in mm. This expression describes the spigot ore capacities of geometrically similar cyclones at specific operating conditions, in this case being at a head of 10D and medium density of 1.5kg/l.

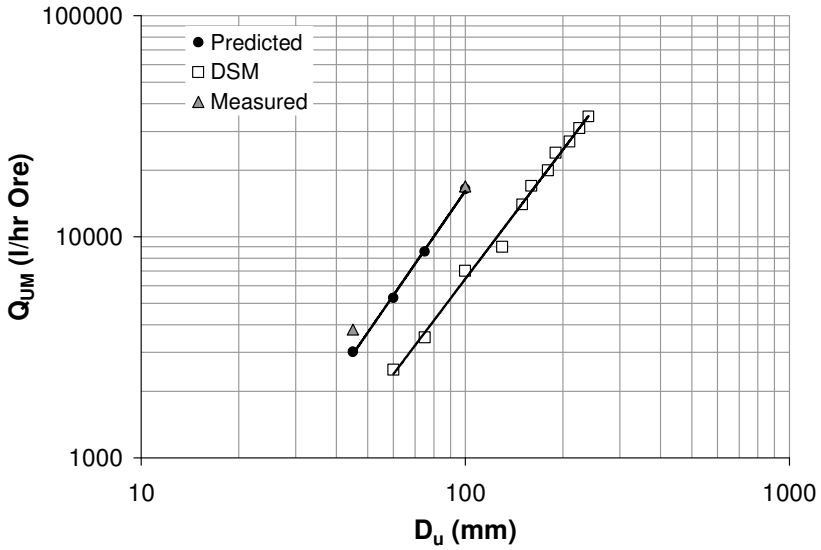


Figure 4.54. Comparison of Q_{UM} predicted from eq. 4.5 (to correct for effect of D) and those specified by DSM.

Assuming that this safety factor of about 50% determined in Table 4.17 holds for all conditions, then the spigot ore capacities for the larger cyclones would be as given in Fig. 4.55. The extrapolated spigot ore capacities in Fig. 4.55 are at best estimates; experimental work is required to valid them.

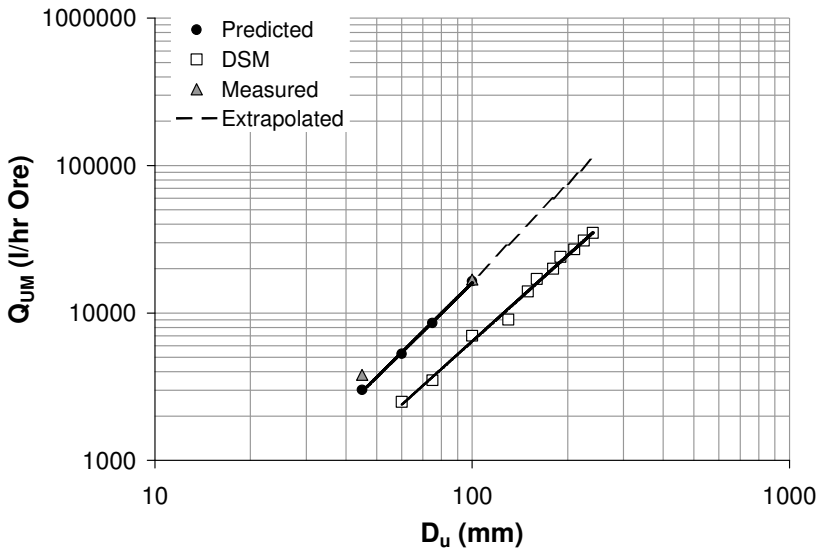


Figure 4.55. Comparison of Q_{UM} predicted from eq. 4.5 (to correct for effect of D) and those specified by DSM. Dashed line is extrapolation of eq. 4.11.

4.2.3. Influence of Cyclone Geometry on Spigot Capacity

(a) Spigot Diameter

As expected D_u was found to be the variable that influenced Q_{USM} the most; the relationship found was of the following form:

$$Q_{USM} \propto D_u^{2.09} \quad \text{(Eq. 4.3)}$$

Q_{UM} was also correlated to D_u in a similar manner:

$$Q_{UM} \propto D_u^{2.16} \quad \text{(Eq. 4.4)}$$

$$Q_{UM} \propto D_u^{1.53} \quad \text{(Eq. 4.5)}$$

The nature of the relationship between Q_{UM} and Q_{USM}, and D_u, especially for the data obtained with the 165mm cyclone operating with the cone A, is in agreement with the literature. Jull (1972) and Plitt et al. (1987) obtained the exponent for the Q_{UM}-D_u relationship to be 2.12 and 2.35, respectively. While DSM obtained the exponent to be 1.94 and 2.05 for coal and other minerals (not being coal), respectively. Q_{UM} was, however, less sensitive to changes in D_u for the relationship that included data from both the 165mm and 350mm cyclones.

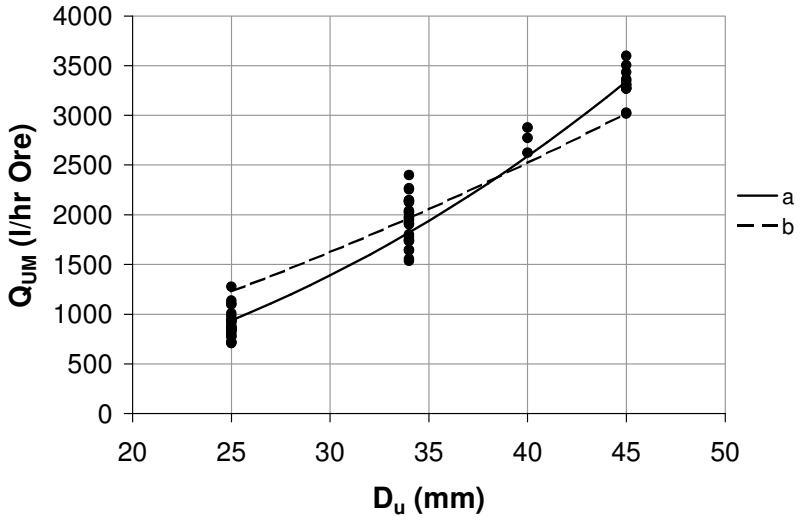


Figure 4.56. The effect of D_u on Q_{UM} for the 165mm cyclone operating with cone A. Plotted lines represent **a.** equation 4.4, and **b**. equation 4.5.

Although Q_{UM} was less sensitive to D_u for the larger 350mm cyclone, D_u still remained the most influential of all the variables tested. The effect of D_u on Q_{UM} is shown in Fig. 4.56 and 4.50. A comparison of equation 4.4 and 4.5 on the data obtained with the 165mm cyclone (cone A only) is shown in Fig. 4.56. The model based on the 165mm cyclone describes this data (shown in Fig. 4.56) much better than that based on both cyclones. The latter does, however, describe the data obtained with the larger 350mm cyclone reasonably well. This is illustrated in Fig. 4.57.

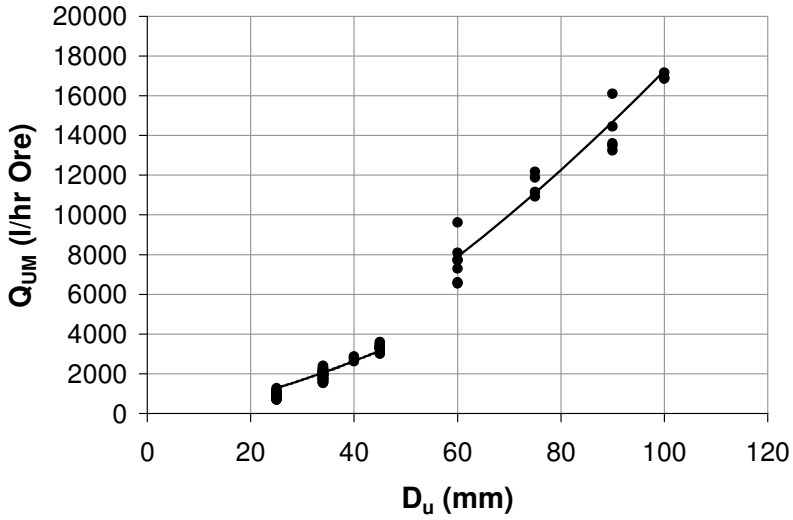


Figure 4.57. The effect of D_u on Q_{UM} for both the 165mm (cone A) and 350mm cyclones. Plotted lines represent equations 4.4 ($D_u \leq 45$mm) and 4.5 ($D_u \geq 60$mm).

The change in the sensitivity of Q_{UM} to D_u at larger cyclone diameters was also reported by Jull (1972), and Mular and Jull (1978) as illustrated in Fig. 4.58. Just as in the current study, Jull (1972) also observed Q_{UM} to be more sensitive to D_u at the smaller spigot sizes. According to Jull (1972) the spigot capacities of smaller cyclones are dependent on the cyclone geometry and certain operating conditions; hence, a range of spigot capacities is given for smaller cyclones in Fig. 4.58.

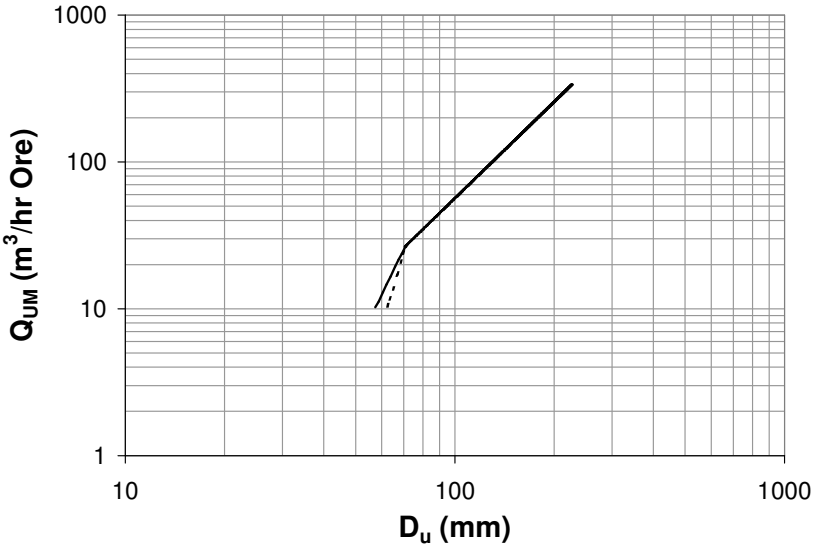


Figure 4.58. The effect of D_u on Q_{UM}. (Jull, 1972)

As previously illustrated, C_{mvu} is an important parameter that determines the onset of roping. It was found to be poorly related to D_u in the following manner:

$$C_{mvu} \propto D_u^{0.14}$$

C_{mvu} increased slightly with increasing D_u; this effect is illustrated in Fig. 4.59. An increase in C_{mvu} means that roping will take place at high ore concentrations at the sinks. This behaviour is in agreement with the literature; a similar trend has also been reported by Fahlstrom (1963) and Heiskanen (2000).

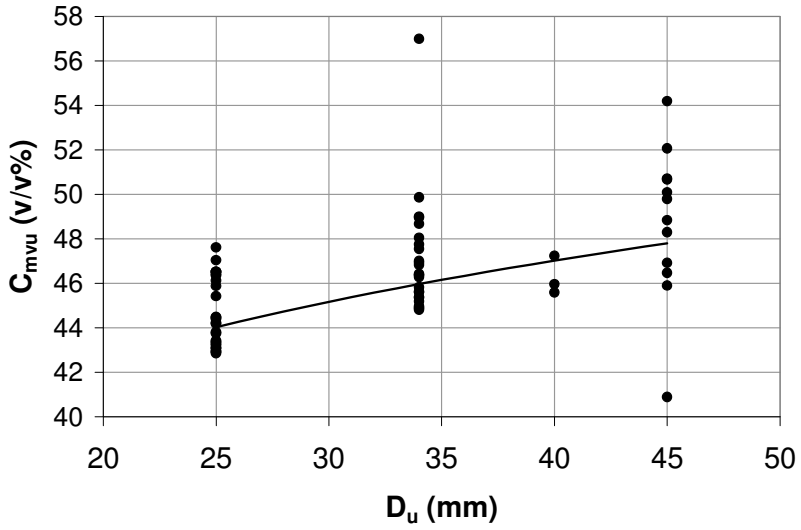


Figure 4.59. The effect of D_u on C_{mvu}. (Cone A - 20°)

Fig. 4.60 shows the change in the porosity of packed beds of various solids in tubes as the ratio of the particle diameter to the vessel diameter is increased. An increase in the particle diameter-to-vessel diameter ratio increases the porosity of packed solid particles, and consequently decreases their packing densities. At the extreme condition when the particle diameter-to-vessel diameter ratio approaches unity, for solids with a very narrow size distribution, the particles arrangement within the vessel would be such that very few particles can be accommodated in a single plane perpendicular to the length of the tube. In such a scenario excessive porosity will be observed, and very low packing densities will be achieved. The porosity of the solids under these conditions is determined not only by the particles' dimensions but also by the effect of the vessel/tube wall, which tends to push the particle inward and, consequently, create more voids closer to the walls. When the particle diameter-to-vessel diameter ratio approaches zero the porosity of the particles would be determined by the dimensions of the particles only, and the effect of the tube wall would be negligible. Thus, under these conditions the highest packing density of solids will be achieved.

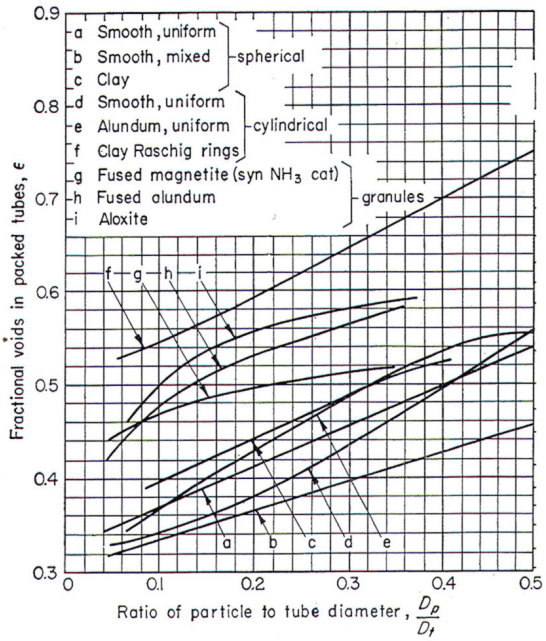


Figure 4.60. Porosity in tubes packed with various materials for increasing ratios of particle diameter to tube diameter. (Leva, 1959)

It is thought that the effect of spigot diameter on the sinks ore concentration is according to the above-mentioned behaviour. Although, strictly speaking, the arrangement of solids at the sinks during roping does not necessarily represent a packed bed, it is expected that the above-mentioned behaviour should be applicable to the conditions in the current investigation.

Particles referred to in Fig. 4.60 ranged from 2.5-18.5mm in size, while the tube diameters were 15.2-101.6mm.

R_m increased with increasing D_u as illustrated in Fig. 4.61. The relationship between R_m and D_u was of the following form:

$$R_m \propto D_u^{1.96}$$

The effect of D_u on R_m appears to be in accordance to D_u's influence on Q_{USM}. Further, the sensitivity of R_m to D_u observed in the current study is much less than that reported by Clarkson and Wood (1993), and Napier-Munn (1987) who reported the exponent to be 4.2 and 4.8, respectively. It is, however, worth noting that both Clarkson and Wood (1993), and Napier-Munn (1987) operated their cyclones with medium only.

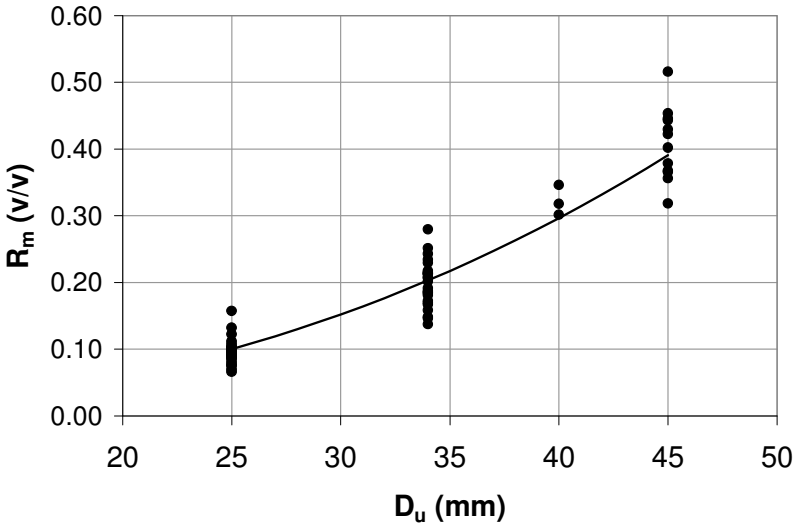


Figure 4.61. The effect of spigot diameter on R_m. (Cone A - 20°)

D_u was also observed to influence the medium density at the sinks. The effect of D_u on the percentage of magnetite particles exiting through the sinks for the cone A is shown in Fig. 4.62. The sinks medium density was diluted as D_u increased.

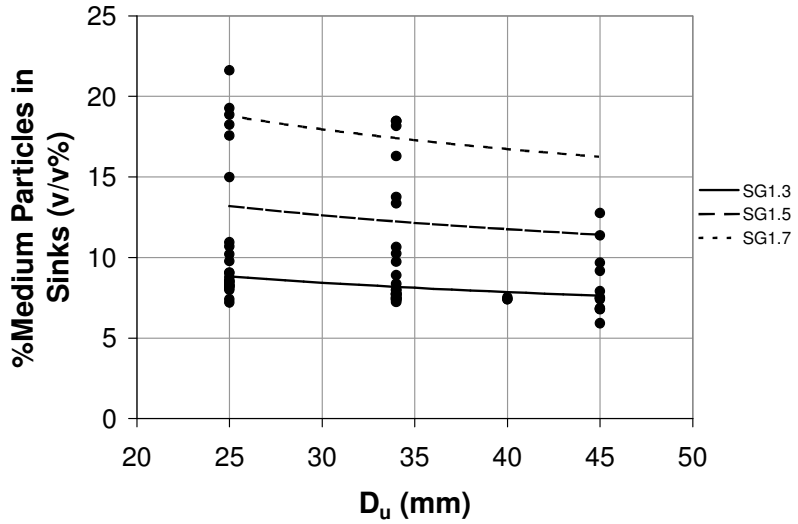


Figure 4.62. Influence of spigot size on volumetric percentage of magnetite particles at the sinks (Cone A –20°).

(c) Vortex Finder Diameter

D_o was observed to influence Q_{USM} in accordance with the following relationship:

$$Q_{USM} \propto D_o^{-0.14}$$

Q_{USM} decreased slightly with increasing D_o, and this is illustrated in Fig. 4.63.

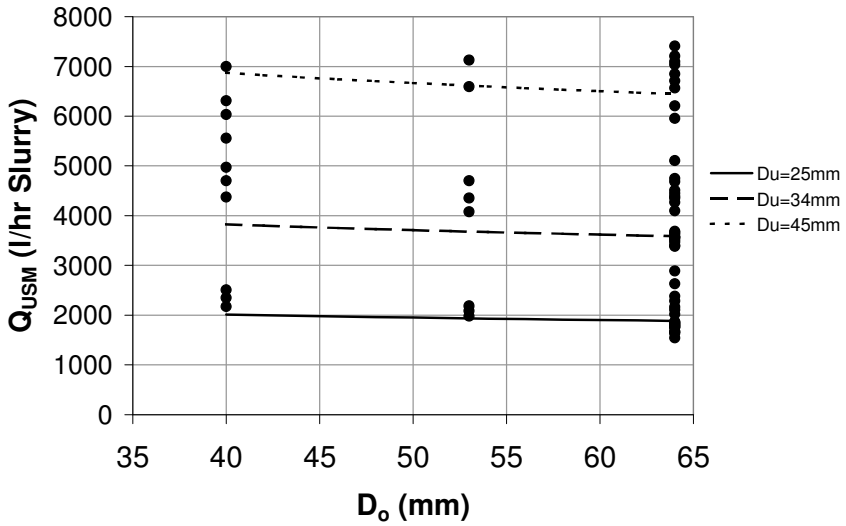


Figure 4.63. The effect of vortex finder diameter on Q_{USM} (Cone A - 20°).

Furthermore, D_o was observed to influence Q_{UM} in accordance with the following relationship:

$$Q_{UM} \propto D_o^{-0.11}$$

Q_{UM} decreased slightly with increasing D_o, and this is illustrated in Fig. 4.64. The effect of D_o on Q_{USM} and Q_{UM} observed in this study is in agreement with the behaviour reported by Stas (1957) that larger spigot-to-vortex finder diameters ratios tend to shift the onset of roping to commence at much higher flow-rates (of slurry and ore) at the sinks.

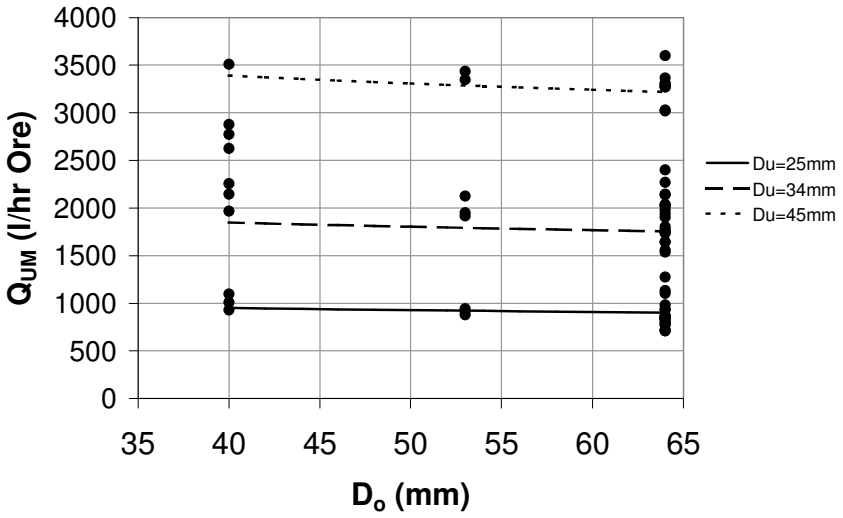


Figure 4.64. The effect of vortex finder diameter on Q_{UM} (Cone A - 20°).

An increase in D_o brought about a slight increase in Q and a decrease in S_R:

$$Q \propto \left(D_u^2 + D_o^2\right)^{0.074}$$

$$S_R = \frac{Q_{USM}}{Q_{OS}} \propto D_o^{-0.25}$$

It is thought that the effect of D_o on Q_{USM} is due to its effect on Q and S_R. Upadrashta and Venkateswarlu (1982), on the other hand, reported S_R to be related to D_o as follows:

$$S_R = \frac{Q_{USM}}{Q_{OS}} \propto D_o^{-2.32}$$

According to Upadrashta and Venkateswarlu, D_o had an equal but opposite effect on S_R as D_u; this behaviour was not observed in the current study. Although D_o and D_u had opposing effects on S_R, their influence on S_R was not in equal in magnitude. Upadrashta and Venkateswarlu (1982) reported S_R to be much more sensitive to D_o than is reported in the current study.

No correlation was found between D_o and C_{mvu}. On the contrary, Fahlstrom (1963) and Heiskanen (2000) observed $\%V_{MSU}$ to increase slightly with increasing D_u/D_o ratio. The

results obtained in the current study seem to suggest that the increase in $\%V_{MSU}$ with increasing D_u/D_o reported by Fahlstrom (1963) and Heiskanen (2000) was probably due to the effect of the spigot diameter only.

Further, R_m was observed to decrease slightly with increasing D_o; the relationship between D_o and R_m found was of the following form:

$$R_m \propto D_o^{-0.25}$$

D_o appears to have a slightly stronger influence on the medium than on the ore particles.

(d) Inlet Size

The inlet size was increased from 70x10 to 70x25 mmxmm; these inlet areas are equivalent to inlet diameters of 30mm (0.2D) and 47mm (0.3D), respectively. The relationship between D_i and Q_{USM} was of the following form:

$$Q_{USM} \propto D_i^{0.43} \quad \text{(Eq. 4.3)}$$

Q_{USM} increased significantly with increasing D_i.

D_i influenced Q_{UM} in accordance with the following relationship:

$$Q_{UM} \propto D_i^{0.38} \quad \text{(Eq. 4.4)}$$

Just as with Q_{USM}, Q_{UM} increased significantly with increasing D_i.

Furthermore, D_i was found to influence Q as follows:

$$Q \propto D_i^{0.90} \quad \text{(Eq. 4.6)}$$

And S_R was observed to be independent of changes in D_i in this study. Thus, the effect of D_i on Q_{USM} and Q_{UM} was due to the increase in Q with increasing D_i. The relationship between Q and D_i obtained in the current study is comparable with those in the literature where the exponent ranged from 1.0 to 1.8 (for dense medium cyclones).

No correlation was found between D_i and C_{mvu}, the same was also true for R_m.

(e) Cyclone Diameter

Cyclone diameter was found to influence Q_{UM} in accordance with the following relationship:

$$Q_{UM} \propto D^{0.63} \quad \text{(Eq. 4.5)}$$

It appears from equation 4.5 that D has a significant and independent effect on Q_{UM}.

(f) Cone Angle

The influence of cone angle on the spigot capacity (Q_{USM} and Q_{UM}) is unclear; the differences in the spigot designs of the 15^o cone and cone A obscured the effect of the cone angle on the spigot capacity. The spigot capacities at the smaller spigot sizes were suppressed by the wall effects, which were enhanced due to the design of the 15^o cone at the spigot as discussed previously. This puts a lot of doubt on whether the behaviour observed in Fig. 4.31 and 4.34 reflects the effect of the cone angle on the spigot capacity, or that of the spigot design as well. Further, an inflection point was encountered in the data obtained with the 15^o cone, while none was observed in the data acquired with 20^o cone angle.

(g) Barrel Length

No correlation was found between Bl, and Q_{USM} and Q_{UM}. Further Q, S_R, C_{mvu}, and R_m were also found to be independent of changes in the barrel length.

4.2.4. Influence of Operational Variables on Spigot Capacity

(a) Feed Pressure

Feed pressure/head was increased only with the 25 and 34mm spigots; at the 45mm spigot diameter the feed head could not be increased significantly due to the constraint on the pump. Q_{USM} was found to be influenced by H as follows.

$$Q_{USM} \propto H^{0.36} \quad \text{(Eq. 4.3)}$$

As expected, Q_{USM} increased with increasing H; the effect of H on Q_{USM} is illustrated in Fig. 4.65.

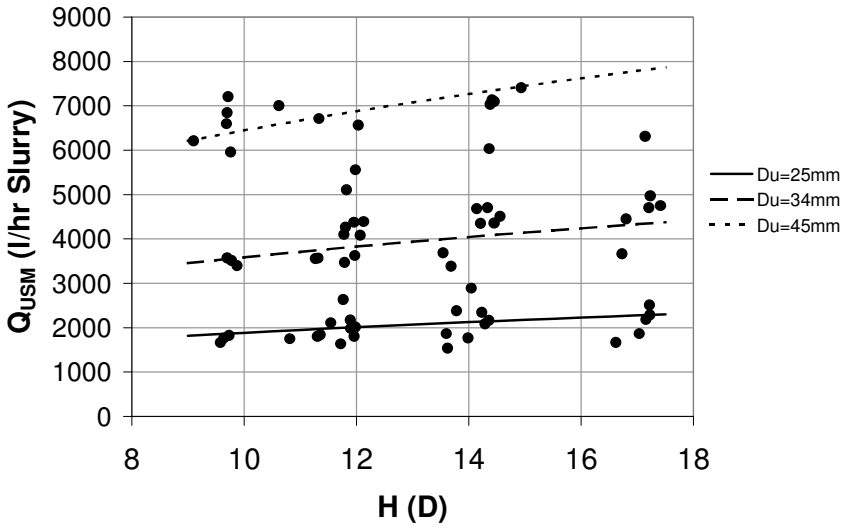


Figure 4.65. The effect of H on Q_{USM}. (165mm cyclone – cone A)

Q_{UM} was found to be influenced by H in accordance with the following relationship:

$$Q_{UM} \propto H^{0.20} \quad \text{(Eq. 4.4)}$$

$$Q_{UM} \propto H^{0.18} \quad \text{(Eq. 4.5)}$$

Q_{UM} increased with increasing H, and the relationship between Q_{UM} and H is shown in Fig. 4.66 and 4.67. This relationship is in good agreement with that reported by DSM, which is as follows:

$$Q_{UM} \propto H^{0.19} \quad \text{(Eq. 2.12)}$$

Van der Walt (1950) also reported the 'maximum permissible spigot loading' that is the spigot capacity, to increase with increasing feed pressure

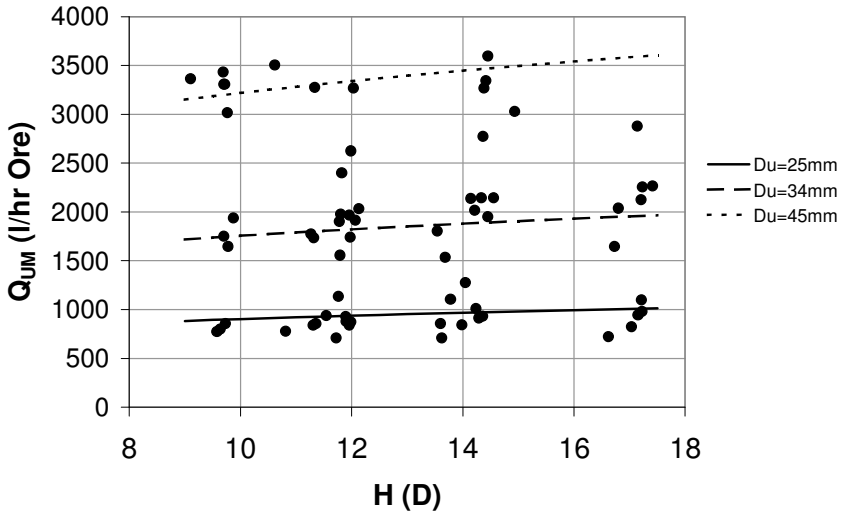


Figure 4.66. The effect of H on Q_{UM}. (165mm cyclone – cone A)

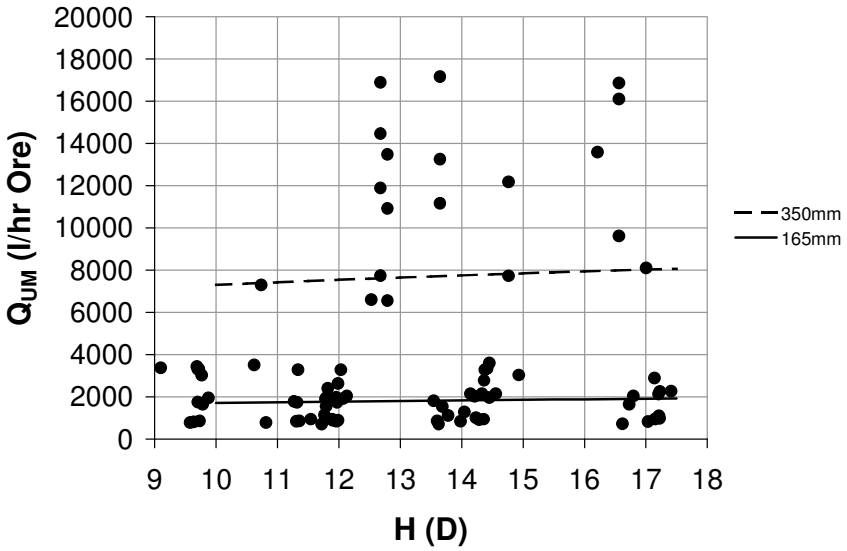


Figure 4.67. The effect of H on Q_{UM}. (350mm cyclone).

It is thought that the effect of H on Q_{USM} and Q_{UM} is a consequence of the influence of H on both Q and S_R:

$$Q \propto H^{0.62} \quad \text{(Eq. 4.6)}$$

$$S_R = \frac{Q_{USM}}{Q_{OS}} \propto H^{-0.70} \quad \text{(Eq. 4.7)}$$

As expected Q increased with increasing H, while S_R decreased with increasing H. Thus, an increase in H increases both the floats and sinks flow-rates, although the floats flow-rate is increased much more strongly than that at the sinks. This accounts for the relatively small influence of H on Q_{USM} and Q_{UM}.

Further, R_m was observed to decrease slightly with increasing D_o; the relationship between D_o and R_m found was of the following form:

$$R_m \propto H^{-0.17} \quad \text{(Eq. 4.10)}$$

The effect of H on R_m appears to be in accordance with the H-Q_{USM} relationship.

The effect of H on C_{mvu} was found not to be statistically significant at the 0.05 significance level.

(b) Medium Density

Q_{USM} decreased with increasing feed medium densities, and the sensitivity of Q_{USM} to ρ_{med} increased significantly at around $\rho_{med} \approx 1.5$RD. Hence, the relationship between Q_{USM} and ρ_{med} was of the following form:

$$Q_{USM} \propto \exp[-5.67(\rho_{med} - 1.45)^3] \quad \text{(Eq. 4.3)}$$

The relationship between feed medium density and Q_{USM} is shown in Fig. 4.68.

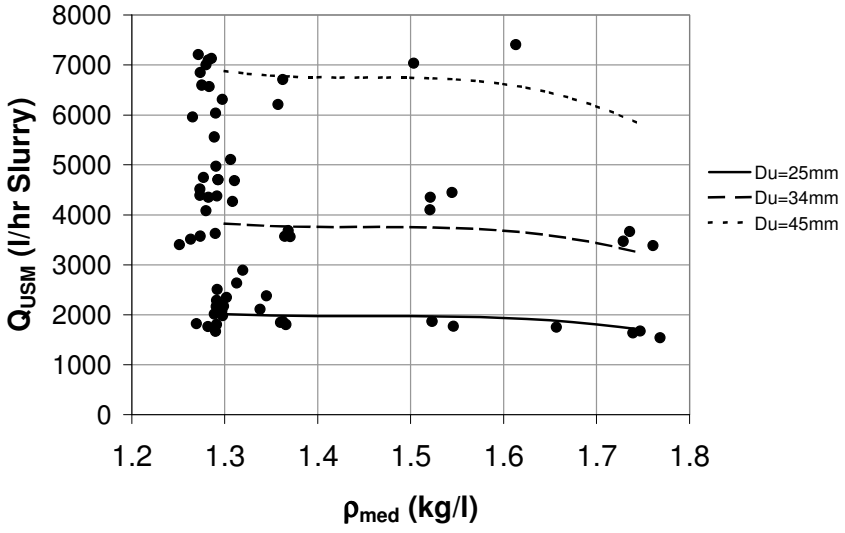


Figure 4.68. The effect of medium density on Q_{USM}. (165mm cyclone – cone A)

Similarly, Q_{UM} was related to the feed medium density in accordance with the following relationship:

$$Q_{UM} \propto \exp[-7.59(\rho_{med} - 1.45)^3] \quad \text{(Eq. 4.4)}$$

Q_{UM} also decreased with increasing ρ_{med} in a similar manner to Q_{USM}; the relationship between ρ_{med} and Q_{UM} is shown in Fig. 4.69.

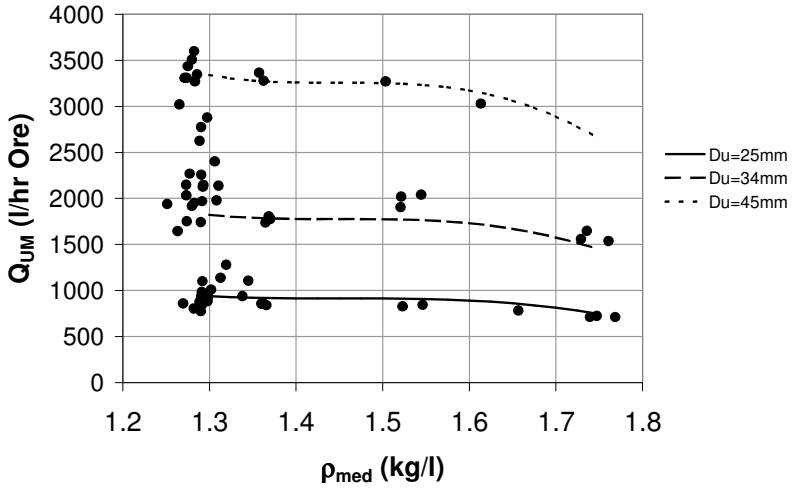


Figure 4.69. The effect of medium density on Q_{UM}. (165mm cyclone –cone A)

Inclusion of the data obtained with the 350mm cyclone in the regression yielded a slightly different relationship:

$$Q_{UM} \propto \exp[-1.58(\rho_{med} - 1.45)^2] \quad \text{(Eq. 4.5)}$$

Q_{UM} increased with increasing ρ_{med} up to a certain critical ρ_{med}, beyond this critical ρ_{med} Q_{UM} decreased with increasing ρ_{med}. This is illustrated in Fig. 4.44 (repeated here for convenience); the plotted lines represent equation 4.5. The best fit was achieved when the value critical ρ_{med} was set at 1.45RD; ρ_{med} values ranging from 1.3 to 1.5 were tried.

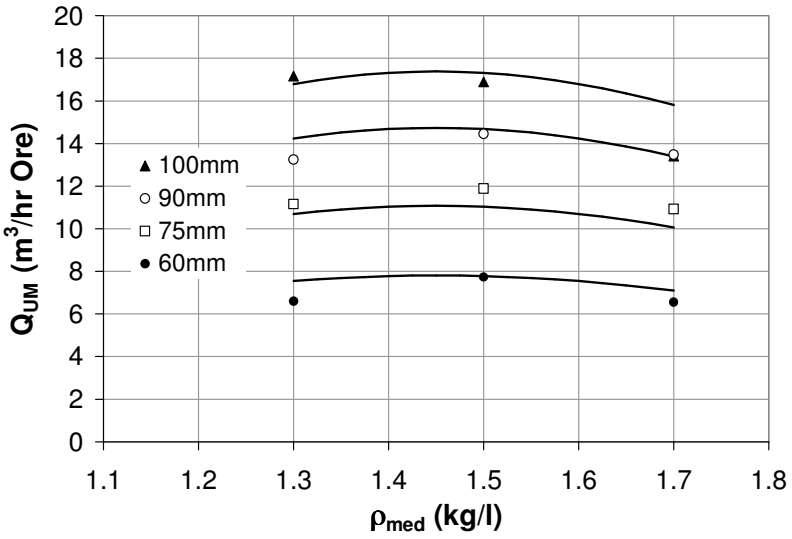


Figure 4.44. The effect of medium density on Q_{UM}. (350mm cyclone)

The effect of ρ_{med} on Q_{USM} and Q_{UM} does not appear to be a consequence of changes in Q and S_R; Q increased with increasing ρ_{med} while S_R was independent of changes in ρ_{med}.

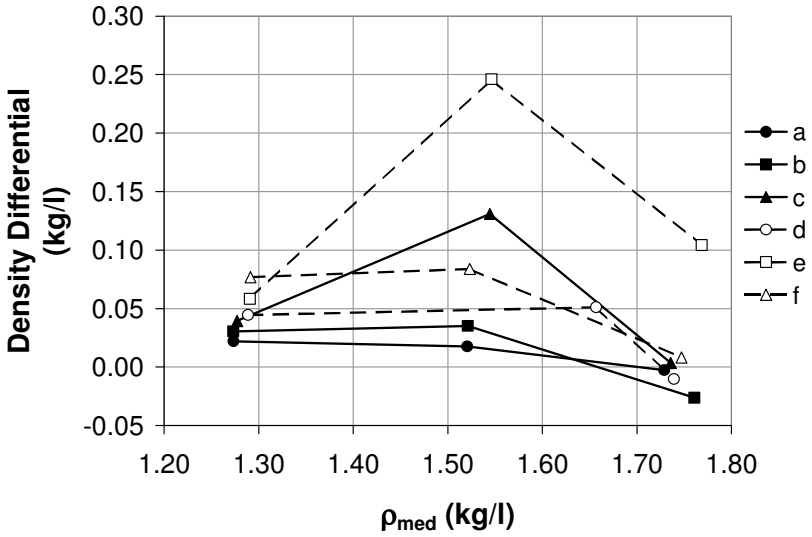


Figure 4.70. The effect of medium density on density differential. (The operating conditions are given in Table A.6 in Appendix A.)

A look at the density differential as ρ_{med} is increased reveals an interesting trend; density differential generally increased with increasing ρ_{med} up to a critical ρ_{med}, beyond which density differential decreased with increasing ρ_{med} (Fig. 4.70). He and Laskowski (1995b), who operated their cyclone with tracers only and magnetite as medium, also reported a similar trend (Fig. 4.71). According to He and Laskowski (1995b), over low medium density ranges

free settling of magnetite particles prevailed and the effect of medium rheology was negligible. While at the high medium density range hindered settling prevailed and the effect of medium rheology was significant. It is thought that the effect of ρ_{med} on Q_{USM} and Q_{UM} is a consequence of changes in the medium rheology with increasing ρ_{med}.

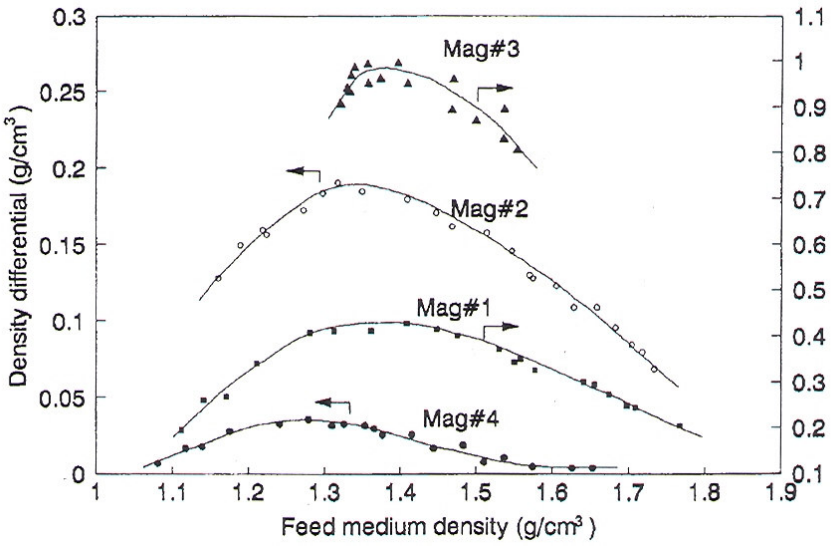


Figure 4.71. The effect of medium density on density differential. (He and Laskowski, 1995b)

The volumetric percent solids in the medium at the sinks with increasing ρ_{med} are shown in Fig. 4.72.

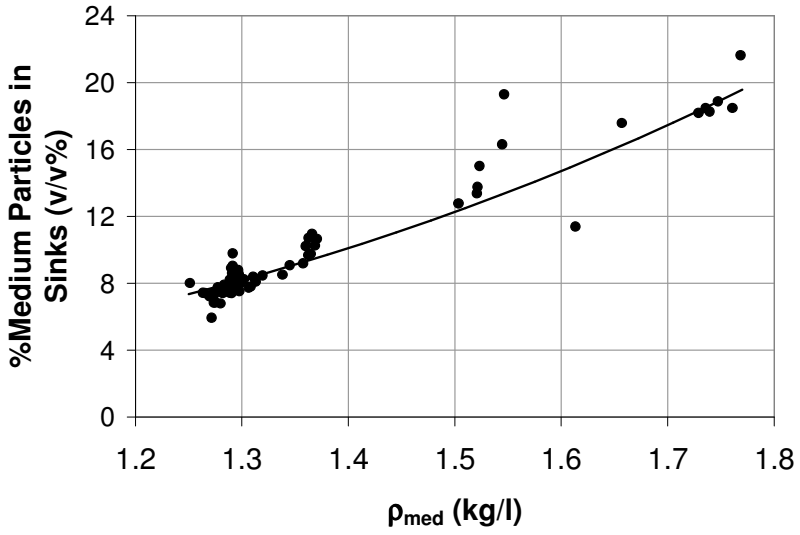


Figure 4.72. Influence of feed medium density on the volumetric percentage of magnetite particles at the sinks.

No correlation was found between medium density and C_{mvu}, the same was also true for R_m. Instead medium density had a strong influence on the volumetric percentage of medium particles exiting at the sinks (Fig. 4.72).

(c) Medium Grade

Medium grade is expressed in terms of percentage magnetite particles passing 45µm. The grade was changed from 95 to 85% passing when operating with cone A; the coarsest magnetite grade was not employed with this cone arrangement. No correlation was found between medium grade and any of the following dependent variables: Q_{USM}, Q_{UM}, Q, S_R and R_m. According to He and Laskowski (1995b) the transition point, beyond which the density differential decreases with increasing ρ_{med}, shifts to higher ρ_{med} values when coarser magnetite medium is used. It is, therefore, expected that medium grade should influence the effect of medium density on Q_{USM} and Q_{UM}. The test-work carried out in the current study was not sufficient to prove or disprove this notion.

Medium grade was, however, found to be poorly correlated to C_{mvu} in accordance with the following relationship:

$$C_{mvu} \propto Gr^{-0.35}$$

C_{mvu} decreased with increasing proportion of the medium particles that were less than 45µm. Thus, the finer the medium particles the lower the C_{mvu} values achieved. This is consistent with the behaviour reported by Plitt et al. (1987) whereby the percent solids at which roping commences decreased with decreasing mass median (50% passing) size of the underflow solids. It is thought that this effect (reported by Plitt et al. and that reported in the current study) is a consequence of increased sensitivity of slurry/medium viscosity to solids concentration when particle sizes are finer. As mentioned previously, it is not unexpected that medium grade should influence spigot overloading behaviour of a dense medium cyclone in a manner that is related/similar to the effect of ore size on the spigot overloading behaviour of a classification cyclone.

(d) Ore Size and Size Distribution

The influence of ore size on the spigot capacity (Q_{USM} and Q_{UM}) is shown in Fig. 4.73 and 4.74; the ore size was changed from –1.8+0.8mm to –5+3mm at vortex finder sizes of 40mm and 64mm. Unfortunately, ore size was changed when operating with the 15° cone, hence it

was not incorporated into equations 4.3 and 4.4. The coarse –5+3mm particles could only be employed with the larger inlet (0.3D) which can take top-sizes of up to 8mm, while the 0.2D inlet can only accommodate a maximum top-size of just over 3mm. All the results shown in Fig. 4.73 and 4.74 were obtained with D_i = 0.3D, and ρ_{med} was maintained at 1.7RD. Q_{USM} and Q_{UM} increased with increasing ore size, although the effect was relatively small at the 25mm spigot. Further, it does not seem as if the influence of particle size on the spigot capacity is related to its influence on Q and S_R. Both of these parameter appear to be unaffected by changes in particle size.

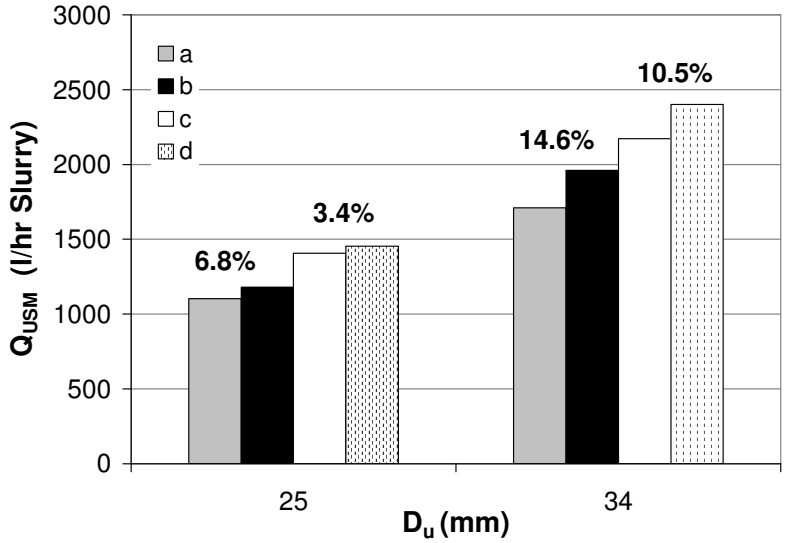


Figure 4.73. The effect of ore size on Q_{USM}. (Full details on the operating conditions are given in Table A.7 in Appendix A).

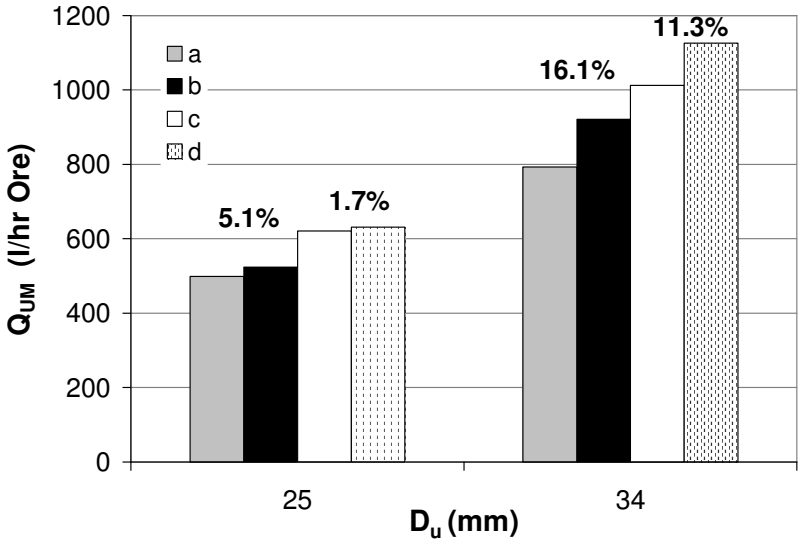


Figure 4.74. The effect of ore size on Q_{UM}. (Full details on the operating conditions are given in Table A.7 in Appendix A).

Ore size did not seem to influence C_{mvu} when the ore size was changed from –1.8+0.8mm to –5+3mm (Fig. 4.75). This was unexpected because it was anticipated that C_{mvu} should be dependent on the packing characteristics of the ore particles. The packing characteristics of the –1.8+0.8mm particles are expected to be considerably different to that of the more coarse –5+3mm particles. This effect is not reflected in Fig. 4.75.

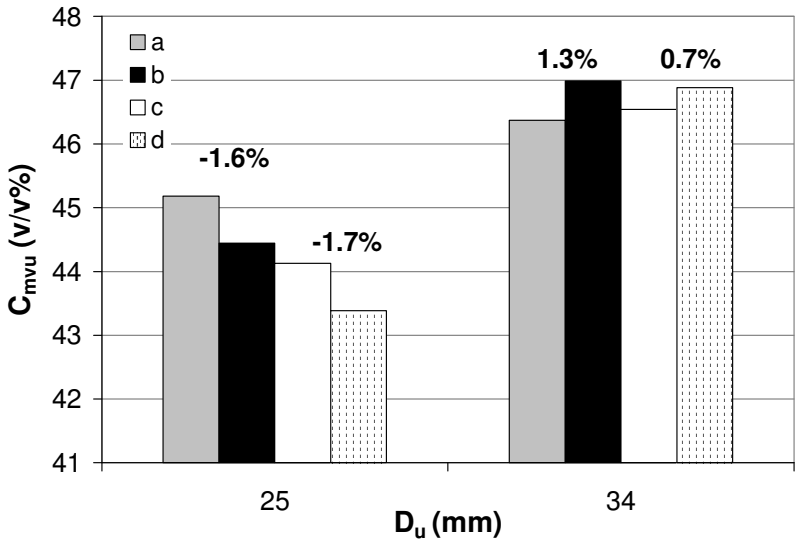


Figure 4.75. The effect of ore size on C_{mvu}. (Full details on the operating conditions are given in Table A.7 in Appendix A).

However, a comparison between the –1.8+0.8mm and the –3+1mm particles indicate that there is a consistent and significant difference between C_{mvu} values obtained for the two size fractions (Fig. 4.78). The –3+1mm size fraction has a wider size distribution than that for the –1.8+0.8mm fraction. It is shown in Fig. 4.78 that –3+1mm size fraction generally obtained higher C_{mvu} values that the –1.8+0.8mm fraction. These observations are in agreement with the findings of Plitt et al. (1987), and Heiskanen (2000) who reported that size distribution of the particles at the underflow to have an effect on the underflow concentration during roping. This, however, did not translate into an increase in Q_{USM} and Q_{UM}, as illustrated in Fig. 4.76 and 4.77. There are strong indications that particle size has an influence on the spigot capacity and none on C_{mvu}, whilst the width of the particle size distribution has no influence on the spigot capacity but has an effect on C_{mvu}.

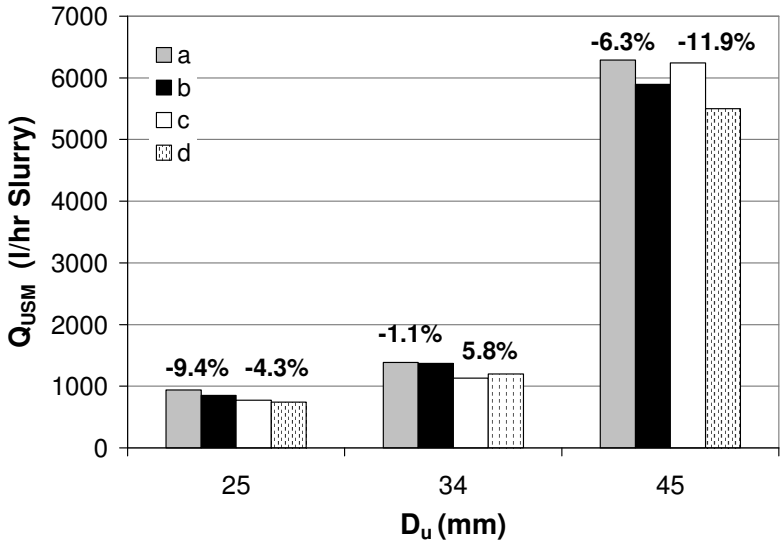


Figure 4.76. The effect of ore size on Q_{USM}: -1.8+0.8mm vs –3+1mm. (Full details on the operating conditions are given in Table A.8 in Appendix A).

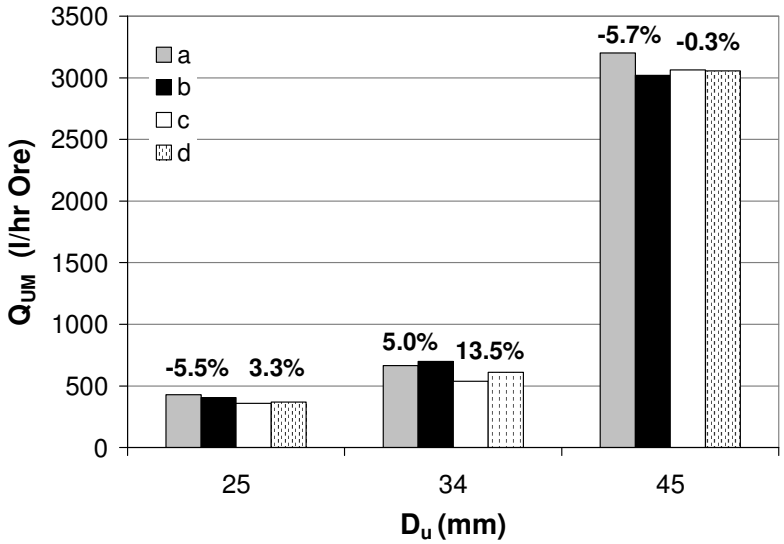


Figure 4.77. The effect of ore size on Q_{UM}: -1.8+0.8mm vs –3+1mm. (Full details on the operating conditions are given in Table A.8 in Appendix A).

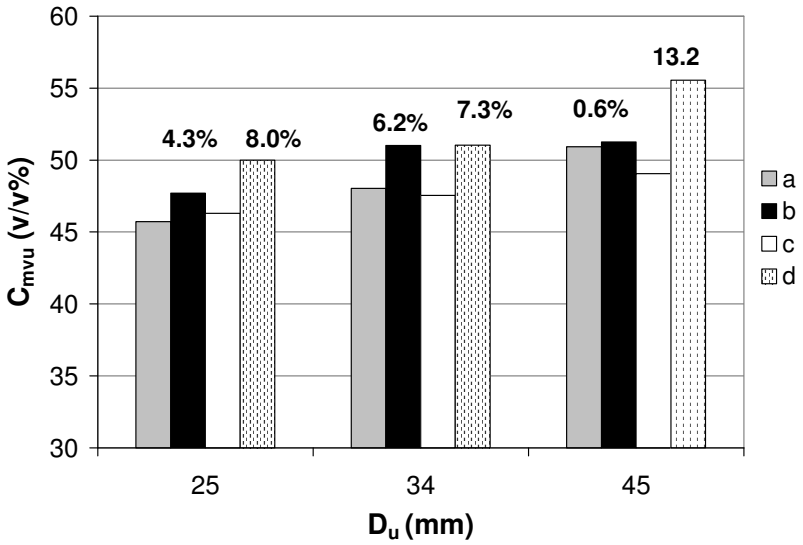


Figure 4.78. The effect of ore size on C_{mvu}: -1.8+0.8mm vs –3+1mm. (Full details on the operating conditions are given in Table A.8 in Appendix A).

CHAPTER 5.

CONCLUSIONS AND RECOMMENDATIONS

5.1. Conclusions

(a) Characterization of Overloading at the Sinks

- This study has established clearly that the onset of rope discharge at the sinks represents the point at which the maximum spigot capacity of the dense medium cyclone is reached.

- A critical sinks ore concentration at which spigot overloading occurs has been observed. The quantity of the sinks ore concentration during roping observed in this study was generally between 43 and 54% (v/v), depending on the spigot diameter and particle size distribution of the medium particles. This equates to sinks medium-to-ore ratios ranging from 0.9 to 1.3 (v/v) (Fig. 5.1). These values are in good agreement with those reported in the literature of 40% (v/v) and higher. Further, $\%V_{MSU}$ values for classification cyclones, ranging from 39% to 68% (v/v), reported in the literature are also in good agreement with those obtained in the current study. It is thought that $\%V_{MSU}$ values of around 60% and higher were probably a consequence of increased short-circuiting of fines to the underflow.

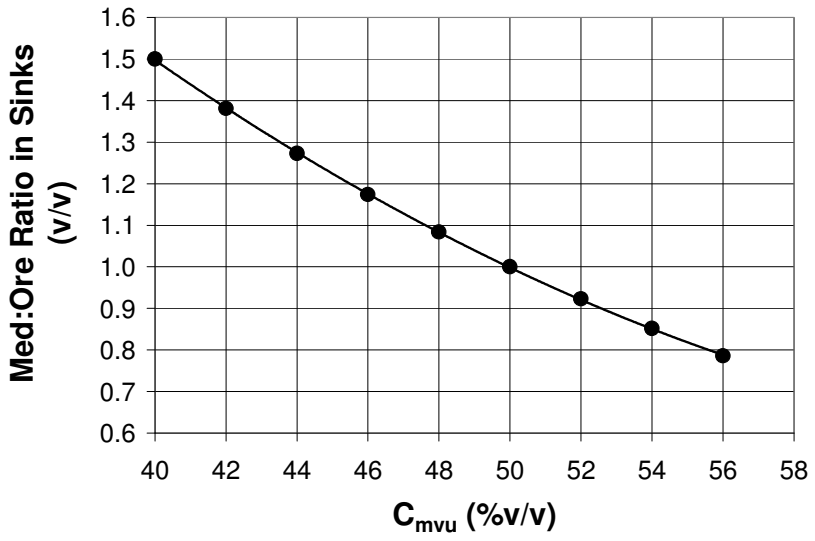


Figure 5.1. C_{mvu} expressed in terms of volumetric medium-to-ore ratio at the sinks.

- The sinks ore concentration during roping remained constant with further addition of ore into the cyclone with all the other variables unchanged. This is consistent with literature on both classification and dense medium cyclones. It has been established that the onset of spigot overloading can be predicted or anticipated by monitoring the volumetric underflow ore concentration.

- An argument that often arises with regard to anticipating the onset of roping is whether the feed ore concentration (or medium-to-ore ratio in the feed) could be used to predict the onset of roping. It is the author's opinion that the best (and simplest) indicator of the onset of roping is the volumetric sinks ore concentration. This can best be illustrated by considering an example of two hypothetical cyclones of the same dimensions, operating under the same conditions except that cyclone A is fed with silica only, and cyclone B with coal and silica. Assume that both cyclones are operating at a medium density above that of the coal and below that of the silica. If the two cyclones are allowed to reach the roping state the following is expected:
  - during roping the volumetric sinks ore concentration for both cyclones should be of similar quantities, however,
  - the feed concentration for cyclone A at the onset of roping would be less than that of cyclone B because of the coal present in the feed. Ideally all the coal should exit at the floats stream.

- During the onset of roping some of the sinks particles were indiscriminately misplaced to the floats stream. The same behaviour has previously been reported in the literature for both classification and dense medium cyclones. Moreover, there was no evidence of significant sinks particles misplacement to the float stream when a semi-rope discharge was prevalent at the spigot of both the 165mm and 350mm cyclones. Before roping commenced at the sinks, the cyclone still operated as a separation device, rather than a mass splitter, even close to the transition point from semi-rope to rope discharge. Further, the particle size distribution of the silica particles misplaced to the floats stream was exactly the same as that in the sinks stream. This behaviour was observed with both 165mm laboratory-scale and 350mm industrial-scale cyclones.

- Medium flow behaviour within the cyclone has been observed to govern the behaviour of various parameters of importance during the transition to roping, namely: the sinks ore concentration, slurry flow through the outlets, and the density differential. This was especially true at the onset of spigot overloading.

- R_m was consistently higher than R_f at R_f and R_m values below 0.6 during spray and semi-rope discharges. However, during roping R_f and R_m values were consistently almost always equal.

- The density differential was diminished during the transition to roping; the density differential was close or equal to zero when the cyclone was operated in roping conditions. The exception, obviously, being when the cyclone was operated with coarse magnetite particles. The density differential could possibly be useful in detecting and/or avoiding overloading of the spigot. Furthermore, the floats and sinks medium densities were observed to equal the feed medium density during roping.

(b) Effect of Cyclone Geometry on Spigot Capacity

- D_u was found to be the variable that influenced Q_{USM} and Q_{UM} the most. The nature of the relationship between Q_{UM} and Q_{USM}, and D_u, especially for the data obtained with the 165mm cyclone operating with the cone A, was in good agreement with the literature. This applies to both classification and dense medium cyclones. Q_{UM} was, however, less sensitive to changes in D_u for the relationship that included data from both the 165mm and 350mm cyclones. The change in the sensitivity of Q_{UM} to D_u at larger cyclone diameters was also reported by Jull (1972), and Mular and Jull (1978). C_{mvu} was found to increase slightly with increasing D_u, although the correlation was poor.

- There are strong indications that the cyclone diameter has a significant and independent influence on Q_{UM}. Thus, for a scenario in which two cyclones have the same D_u but different D, the one with a larger D should have a larger Q_{UM} given that the operating conditions are the same. This has serious implications for the case in which a choice must be made between one large cyclone or two smaller ones. Due to the independent effect of D_u and D, the two parameters that influence Q_{UM} the most (eq. 4.5), larger cyclones are expected to have disproportionally higher spigot capacities as compared to a combination of smaller cyclones. This is illustrated in Table 5.1. N is the number of cyclones required to reach the spigot ore capacity of a 350mm cyclone when using a combination of smaller cyclones or those with same D and a smaller D_u.

Table 5.1. Number of cyclones required to reach the spigot ore capacity of a 350mm cyclone when using a combination of smaller cyclones or those with smaller D_u.

D (mm)	**D_u (mm)**	**Q_{UM} (l/hr ore)**	$\frac{Q_{UM\,(350mm)}}{Q_{UM\,(D)}}$	**N**
165	45	3016*	5.46	6
200	60	5290*	3.11	4
250	75	8570*	1.92	2
350	60	7298	2.26	3
350	75	11884	1.39	2
350	100	16461*	1	1

*Calculated through equation 4.5, with H = 10D and ρ_{med} = 1.5kg/l.

- Spigot design was observed to have a significant effect on the spigot capacity. Q_{USM} and Q_{UM} values obtained with cone B were higher than those obtained with cone A by about 20% and 16%, respectively. Both cones have an angle of 20°, the main difference between cone A and B is that cone A is 115mm longer (which results in increased resistance to flow). DSM design provides the least resistance to flow, and therefore should give higher spigot capacities.

- Q_{USM} and Q_{UM} increased significantly with increasing D_i. The effect of D_i on Q_{USM} and Q_{UM} was due to the increase in Q with increasing D_i. S_R, C_{mvu} and R_m were observed to be independent of changes in D_i in this study.

- Q_{USM} and Q_{UM} decreased slightly with increasing D_o. This effect is thought to be a consequence of the influence of D_o on Q and S_R. No correlation was found between D_o and C_{mvu} in the current study. On the contrary, Fahlstrom (1963) and Heiskanen (2000) observed $\%V_{MSU}$ to increase slightly with increasing D_u/D_o ratio. The results obtained in the current study seem to suggest that the increase in $\%V_{MSU}$ with increasing D_u/D_o reported by Fahlstrom (1963) and Heiskanen (2000) was probably due to the effect of the spigot diameter only.

- Differences in the spigot design of the cones employed obscured the effect, if any, of the cone angle on the spigot capacity. The results obtained to determine the effect of cone angle on spigot capacity were inconclusive.

- No correlation was found between Bl, and Q_{USM} and Q_{UM}. Further Q, S_R, C_{mvu}, and R_m were also found to be independent of changes in the barrel length.

(c) Effect of Operational Variables on Spigot Capacity

- Q_{USM} and Q_{UM} increased with increasing H, and the effect was relatively small. It is thought that the effect of H on Q_{USM} and Q_{UM} is a consequence of its influence on Q and S_R. No correlation was observed between H, and C_{mvu}.

- Q_{USM} and Q_{UM} decreased with increasing feed medium densities, and their sensitivity to ρ_{med} increased significantly at around $\rho_{med} \approx 1.5$RD. This behaviour was observed with data obtained with the 165mm cyclone (cone A only). Data obtained with the 350mm cyclone indicate that Q_{UM} to reach a maximum at around $\rho_{med} \approx 1.5$RD, beyond this medium density Q_{UM} decreased with increasing ρ_{med}. The density differential was also observed to reach a maximum and then decrease as ρ_{med} was increased. It is thought that the effect of ρ_{med} on Q_{USM} and Q_{UM} is related to changes in the medium rheology with increasing ρ_{med}.

- No correlation was found between medium grade and any of the following parameters: Q_{USM}, Q_{UM}, Q, S_R and R_m. Medium grade was, however, found to have a statistically significant effect on C_{mvu} at the 0.05 significance level, although the correlation was poor.

- There are indications that particle size has an influence on the spigot capacity and none on C_{mvu}, whilst the width of the particle size distribution has no influence on the spigot capacity but has an effect on C_{mvu}.

(d) Comparison with DSM

- Q_{UM} values obtained in this study were generally more than double those specified by DSM. A safety factor, defined as the difference between Q_{UM} values between the two investigations divided by the relevant Q_{UM} value from the current study, of about 60% was established. This factor was determined making use of data obtained from cyclones that were not geometrically similar, whilst DSM data was determined on geometrically

similar cyclones. It can, therefore, be concluded that there is large potential to increase the 'spigot capacities' specified by DSM. Especially considering that the cyclone still behaves as a separation device even close to the transition point from semi-rope to rope discharge. It is, however, not advisable to operate too close to this transition point because variations in the feed can easily lead to overloading.

- There are indications that DSM possibly defined their 'spigot capacities' as the maximum spigot loading that can be achieved before semi-roping commences. This notion is supported by the sinks ore concentrations (at the DSM specified 'spigot capacities'), which were inferred from the DSM data and are consistent with semi-roping conditions. Further, the spigot loading (in l/hr ore) at the transition point from a spray to semi-rope discharge was about 40% of the maximum spigot capacity; this gave a safety factor of about 60%, which is consistent with that given above.

- Correction for the independent influence of cyclone diameter on Q_{UM} yielded a safety factor of about 50%, which is applicable to geometrically similar cyclone. Assuming that this safety factor of about 50% holds for all conditions, then the spigot ore capacities for the larger cyclones could be estimated as illustrated in Fig. 4.55 (repeated here for convenience). The extrapolated spigot ore capacities in Fig. 4.55 are at best estimates; experimental work is required to valid them.

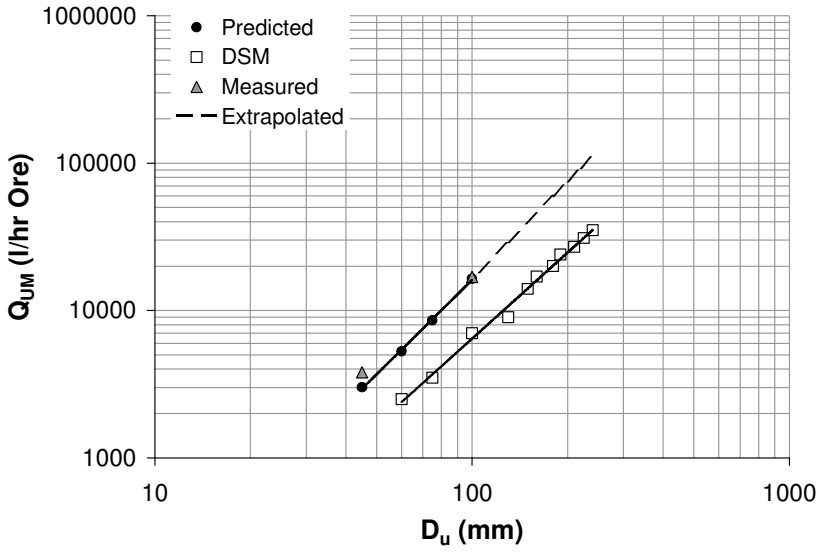


Figure 4.55. Comparison of Q_{UM} predicted from eq. 4.5 (to correct for effect of D) and those specified by DSM. Dashed line is extrapolation of eq. 4.11.

(e) Model

- The following empirical equations, based on a 165mm cyclone (cone A only), to predict spigot capacity (Q_{USM} and Q_{UM}) were developed in this investigation:

$$Q_{USM} = 0.394 D_u^{2.09} D_o^{-0.14} D_i^{0.43} H^{0.36} \exp\left[-5.67(\rho_{med} - 1.45)^3\right] \quad (4.3)$$

$$Q_{UM} = 0.226 D_u^{2.16} D_o^{-0.11} D_i^{0.38} H^{0.20} \exp\left[-7.59(\rho_{med} - 1.45)^3\right] \quad (4.4)$$

Only variables that were significant at the 95 percent confidence level were added to the regression equations. Inclusion of the data obtained with the 350mm dense medium cyclone into the regression analysis yielded the following expression:

$$Q_{UM} = 0.235 D^{0.63} D_u^{1.53} H^{0.18} \exp\left[-1.58(\rho_{med} - 1.45)^2\right] \quad (4.5)$$

The quality of the fit was very good for these three expressions (Table 5.2).

Table 5.2. R^2 values for the various equations developed in the current study.

Equation No.	**R^2**
4.3	0.9805
4.4	0.9821
4.5	0.991
4.6	0.9446
4.7	0.9637
4.10	0.96

Furthermore, expressions to predict Q, S_R and R_m during roping were also developed:

$$Q = 64.72\left(D_u^2 + D_o^2\right)^{0.074} D_i^{0.90} H^{0.62} \rho_{med}^{0.18} \quad (4.6)$$

$$S_R = \frac{Q_{USM}}{Q_{OS}} = 10^{-4.52} D_u^{2.76} D_o^{-0.25} H^{-0.70} C_{vf}^{0.83} \quad (4.7)$$

$$R_m = 10^{-3.78} D_u^{1.96} D_o^{-0.25} H^{-0.17} C_{vf}^{0.52} \quad (4.10)$$

5.2. Recommendations

- Spigot overloading of a dense medium cyclone can be detected visually by observing the discharge type at the sinks and monitoring particle misplacement to the floats stream. The simplest and best indicator of possible spigot overloading is the sinks ore concentration, measurement of this parameter could, however, prove challenging on most industrial cyclones.

- It is important to consider the composition of the ore to be treated in the process of sizing and selection of dense medium cyclones. When the cyclone feed constitutes a high proportion of sinks particles there is a danger of overloading the spigot. It is the sinks ore concentration rather than feed concentration that is of importance in anticipating overloading at the sinks. The higher the proportion of sinks particles in cyclone feed the lower the feed ore concentration must be in order to avoid spigot overloading.

- There are essentially 5 ways in which the spigot capacity can be increased, and that is through D_u, D, D_i, H, and D_o.
    - D_u and D have the strongest influence on the spigot capacity. There is, however, a limitation on how much D_u can be increased; when D_u/D_o ratio is more than 85% the separation efficiency suffers according to DSM (1985).
    - D_i also presents a viable option to increase the capacity of a cyclone that is spigot constraint.
    - Spigot capacity can also be increased through H, although its influence is relatively weak.
    - Increasing the spigot capacity through D_o does not seem to be a reasonable option because this would be at the expense of the floats capacity and D_o's influence on the spigot capacity is small. In cases where only a small portion of the ore in the feed exits through the floats stream, the use of D_o to increase the spigot capacity becomes an option because overloading at the floats would not be a concern any longer.

- There is strong case for the usage of large diameter cyclones because of the relatively strong, independent influence of D_u and D on the spigot capacity. The disproportionately

higher spigot capacities of large diameter cyclones allows for the operation of cyclones at relatively high medium-to-ore ratios while simultaneous achieving high capacities.

- Manufacturing of dense medium cyclones with an adjustable geometry seems to be worth considering given that the spigot capacity is determined mainly by the cyclone geometry. The necessary changes to the cyclone geometry can therefore be made to accommodate the character of the ore being treated.

CHAPTER 6. REFERENCES

Abbott, J. 1967a. The use of Bretby hydrocyclones for the thickening and recovery of fines-Part 1. *Coal Preparation*. March/April, pp. 53-61.

Abbott, J. 1967b. The use of Bretby hydrocyclones for the thickening and recovery of fines-Conclusion. *Coal Preparation*. May/June, pp. 97-104.

Aplan, F.F. 1985. Heavy Media Separations, Chapter. 4 in *SME Mineral Processing Handbook, Vol. 1*, edited by Weiss N.L. New York. SME/AIME. pp. 4-3 – 4-27.

Asomah, A.K. and Napier-Munn, T.J. 1997. An empirical model of hydrocyclones, incorporating angle of cyclone inclination. *Minerals Engineering*. Vol. 10, No. 3, pp. 339-347.

Bosman, J. 2003a. Latest developments in cyclone technology. *Trans. Instn. Min. Metall. (Sect. C: Mineral Process. Extr. Metall.)*. Vol. 112, pp. C10-12.

Bosman, J. 2003b. *Mineral Processing 411-Class Notes*. Department of Materials Science and Metallurgical Engineering. University of Pretoria.

Bradley, D. 1965. *The Hydrocyclone*. Oxford. Pergamon Press.

Clarkson, C.J., and Wood, C.J. 1993. Model of a dense medium cyclone performance. *Coal Preparation*. Vol. 12, pp. 101-115.

Cohen, E. and Isherwood, R.J. 1960. Principles of dense media separation in hydrocyclones. *International Mineral Processing Congress*. London. Inst. Min. Met. pp. 573-591.

Collins, B., Napier-Munn, T.J. and Sciarone, M. 1974. The production, properties, and selection of ferrosilicon powders for heavy-medium separation. *J of S. Afr. Inst. Min. Metall.* Vol. 75, pp. 103-119.

Collins, D.N., Turnbull, T., Wright, B.A. and Ngan, W. 1983. Separation efficiency in dense medium cyclones. *Trans. Instn. Min. Metall. (Sect. C: Mineral Process. Extr. Metall.)*. Vol. 92, pp. C38-51.

Concha, F., Barrientos, A., Montero, J., and Sampaio, R. 1996. Air core and roping in hydrocyclones. *Int. J. Miner. Process*. Vol. 44-45, pp. 743-749.

Dahlstrom, D.A. 1949. Cyclone operating factors and capacities on coal and refuse slurries. *Trans. AIME*. Vol. 184, pp. 331-344.

Darby, R. 1986. Hydrodynamics of slurries and suspensions. *Encyclopaedia of Fluid Mechanics, Vol. 5: Slurry Flow Technology*. Edited by N.P. Cheremisinoff. pp. 49-92.

Davidson, M.R. 1995. An adaptive method of predicting the air core diameter for numerical models of hydrocyclone flow. *International Journal of Mineral Processing*. Vol. 43, No. 3-4, pp. 167-177.

Davis, J.J. and Napier-Munn, T.J. 1987. The influence of medium viscosity on the performance of dense medium cyclones in coal preparation. *3rd Int. Conf. on Hydrocyclones*. Oxford. BHRA. Paper F3, pp. 155-165.

de Korte, J.G. 2000. *Index of South African Coal Preparation Plants*. http://www.sacoalprep.co.za/information.htm (Visited Feb. 2007)

DME, 2005. *Operating and developing coal mines in the Republic of South Africa*. Directorate: Mineral Economics, Department of Minerals and Energy, Republic of South Africa.

DSM. The heavy medium cyclone washery for minerals and coal. Dutch State Mines (DSM) Handbook.

DSM. 1985. Guide to the calculation of h.m. cyclone and w.o cyclone plants. Stamicarbon bv, Netherlands.

Dyakowski, T. and Williams, R. A. 1995. Prediction of air-core size and shape in a hydrocyclone. *Int. J. Miner. Process.* Vol. 43, No. 1-2, pp. 1-14.

Fahlstrom, P.H. 1963. Studies of hydrocyclone as a classifier. *Proc 6th Intnl Min Proc Congress*, Cannes, edited by Roberts, A. Pergamon Press. pp. 87-114.

Flintoff, B.C., Plitt, L.R. and Turak, A.A. 1987. Cyclone modelling: a review of present technology. *CIM Bulletin*. Vol. 80, No. 905, pp. 39-50.

Frankel, N.A., and Acrivos, A. 1967. On the viscosity of a concentrated suspension of solid spheres. *Chem. Eng. Sci*. Vol. 22, pp. 847-853.

Grobler, P.J. 2006. The production and application of ferrosilicon in the mining industry. *DMS and Gravity Concentration Operations and Technology in South Africa*, Edited by M. Dworzanowski. pp. 153-162.

Gutiérrez, J. A., Dyakowski, T., Beck, M. S. and Williams, R. A. 2000. Using electrical impedance tomography for controlling hydrocyclone underflow discharge *Powder Technology.* Vol. 108, Issues 2-3. pp. 180-184.

He, Y.B., and Laskowski, J.S. 1995a. Dense medium cyclone separation of fine particles. Part 1: The effect of medium split ratio on dense medium cyclone performance. *Coal Preparation*. Vol. 16, pp. 1-25.

He, Y.B., and Laskowski, J.S. 1995b. Dense medium cyclone separation of fine particles. Part 2: The effect of medium composition on dense medium cyclone performance. *Coal Preparation*. Vol. 16, pp. 27-49.

Heiskanen, K. 2000. Experimental hydrocyclone roping models. *Chem. Eng. J.* Vol. 80, pp. 289-293.

Jull, N.A. 1972. Parameters for cyclone selection. *Proc. Canadian Mineral Processors.* Ottawa.

Kelly, E. G. and Spottiswood, D.J. 1989. *Introduction to Mineral Processing*. Mineral Engineering Services, Denver. pp. 213-232.

Kelly, E.G. 1991. The significance of by-pass in mineral separators. *Minerals Engineering*. Vol. 4, No. 1, pp. 1-7.

King, R.P. and Juckes, A.H. 1984. Cleaning of fine coals by dense medium hydrocyclone. *Powder Technology*. Vol. 40, pp. 147-160.

Leonard, J.W. IV and Leonard, J.W. 1983. Using Tromp curves to diagnose performance problems in coal cleaning. In *Basic Mathematics and Computer Techniques for Coal Preparation and Mining*, edited by K.K. Humphreys and J.W. Leonard. New York, Marcel Dekker, INC. pp. 71-79.

Leva, M. 1959. *Fluidization*. New York. McGraw-Hill Book Company, Inc. pp. 54 – 56.

Lynch, A.J. and Napier-Munn, T.J. 1986. Dense medium separation research at the Julius Kruttschnitt Mineral Research Centre. *Trans. Instn. Min. Metall. (Sect. C: Mineral Process. Extr. Metall.)*. Vol. 95, pp. C221-225.

Lynch, A.J. and Rao, T.C. 1975. Modelling and scale-up of hydrocyclone classifiers. *11th International Mineral Processing Congress*. Cagliari, Sardinia. pp. 245-269.

Lynch, A.J. and Rao, T.C. 1968. Studies on the operating characteristics of hydrocyclone classifiers. *Indian Journal of Technology*. Vol. 6, pp. 106-114.

Moorhead, R.G. and Schutte, A. 2005. Operating guidelines for low density-density dense-medium cyclone separations. Paper presented at *SA Coal Preparation Conference and Exhibition*.

Mular, A.L. and Jull, N.A. 1978. The selection of cyclone classifiers, pumps and pump boxes for grinding circuits. *Ch. 17 in Mineral Processing Plant Design*. Ed. A.L Mular and R.B. Bhappu. New York. SME/AIME. pp. 376-403.

Narasimha, M., Brennan, M. and Holtham, P.N. 2007. Prediction of magnetite segregation in dense medium cyclone using computational fluid dynamics technique. *Int. J. Miner. Process.* Vol. 82, Issue 1, pp. 41-56.

Napier-Munn, T.J. 1986. Pressure drop in dense medium cyclones. *Int. J. Min. Process*. Vol. 16, pp. 209-230.

Napier-Munn, T.J. 1990. The effect of dense medium viscosity on separation efficiency. *Coal Preparation*. Vol. 8, pp. 145-165.

Napier-Munn, T.J., Morrell, S., Morrison, R.D., and Kojovic, T. 1999. *Mineral Comminution Circuits - Their Operation and Optimisation*. Queensland, Australia. Julius Kruttschnitt Mineral Research Centre.

Neesse, Th., Dallman, W. and Espig, D. 1984. Effect of turbulence on the efficiency of separation in hydrocyclones at high feed solids concentrations. *2nd Int. Conf. on Hydrocyclones*. Bath. BHRA. pp. 51-66.

Neesse, Th., Schneider, M., Golyk, V., and Tiefel, H. 2004a. Measuring the operating state of the hydrocyclone. *Minerals Engineering*. Vol. 17. pp. 697-703.

Neesse, Th., Schneider, M., Dueck, J., Golyk, V. Butenbach, S., and Tiefel, H. 2004b. Hydrocyclone operation at the transition point rope/spray discharge. *Minerals Engineering*. Vol. 17. pp. 733-737.

Neesse, Th., Golyk, V., Kaniut, P., and Reinsch, V. 2004c. Hydrocyclone control in grinding circuits. *Minerals Engineering*. Vol. 17. pp. 1237-1240.

Neesse, Th., Tiefel, H., and Kaniut, P. 2007. Volume split control of a hydrocyclone group. *Minerals Engineering*. Vol. 20. pp. 355 -360.

Peatfield, D. 2003. Coal and coal preparation in South Africa – A 2002 review. *J of S. Afr. Inst. Min. Metall*. Vol. 103, No. 6, pp. 355-369.

Plitt, LR. 1976. A mathematical model of the hydrocyclone classifier. *CIM Bulletin*. Vol. 69, No. 776. pp. 114-123.

Plitt, L.R., Flintoff, B.C. and Stuffco, T.J. 1987. Roping in hydrocyclones. *3rd Int. Conf. on Hydrocyclones*. Oxford. BHRA. Paper A3, pp. 21-34.

Podd, F. J. W., Schlaberg, H. I. and Hoyle, B. S. 2000. Model-based parameterisation of a hydrocyclone air-core. *Ultrasonics.* Vol. 38, No. 1-8, pp. 804-808.

Qian, L. and Ji Run, X. 1992. The effect of the air core on the flow field within hydrocyclones. *Hydrocyclones – Analysis and applications*. Edited by L. Svarovsky and M.T. Thew. London, Kluwer Academic Publishers. pp. 51 – 62.

Reeves, R.A. 2002. Types and characteristics of heavy-media separators and flowsheets. *Mineral Processing Plant Design, Practice, and Control: Proceedings*. Edited by Mular, A.L., Halbe, D.N. and Barrat, D.J. SME, New York. Vol. 1, pp. 962-977.

Restarick, C.J. and Krnic, Z. 1991. The effect of underflow/overflow ratio on dense medium cyclone operation. *Minerals Engineering*. Vol. 4, No. 3/4, pp. 263-270.

Scott, I. A. and Napier-Munn, T.J. 1990. A dense medium cyclone model for simulation. Paper presented at the *4th Samancor Symposium on Dense Media Separation*. Cairns, Australia.

Scott, I. A. and Napier-Munn, T.J. 1992. Dense-medium cyclone model based on the pivot phenomenon. *Trans. Instn. Min. Metall. (Sect. C: Mineral Process. Extr. Metall.).* Vol. 101, pp. C61-76.

Smith, M.R. 1989. Metal powders for use in mineral separation processes. *Powder Metallurgy*, vol 32, No. 1, pp. 41-45.

Stas, M. 1957. The influence of the orifices on the washing characteristics of the hydrocyclone. *International Mineral Dressing Congress*. Stockholm. pp. 161-192.

Svarovsky, L. 1984. *Hydrocyclones*. Pennsylvania. Holt, Rinehart and Winston Ltd.

Symonds, D.F. and Malbon, S. 2002. Sizing and selection of heavy media equipment: Design and layout. *Mineral Processing Plant Design, Practice, and Control: Proceedings*. Edited by Mular, A.L., Halbe, D.N. and Barrat, D.J. SME, New York. Vol. 1, pp. 1011-1033.

Tarr, D.T. 1965. Practical application of liquid cyclone in mineral dressing problems. Preprint Fall Meeting AIME.

Tarr, D.T. 1985. Hydrocyclones, Chapter. 3D in *SME Mineral Processing Handbook, Vol. 1*, edited by Weiss N.L. New York. SME/AIME, pp. 3D-10 – 3D-45.

Trawinski, H. 1976. Theory, applications and practical operation of hydrocyclones. *Engineering and Mining Journal*. Vol. 177, No. 9, pp. 115-127.

Upadrashta, K.R., and Venkateswarlu, D. 1982. Study of hydrocyclone as heavy media separator. *Journal of Powder and Bulk Solids Technology*. Vo1. 6, No. 6, pp. 22-32.

Van der Walt, P.J. 1950. Study of the operation of the cyclone washer and its application to Witbank fine coal. *J. Chem. Met. Min. Soc. S. Afr*. Vol. 51, pp. 19-103.

Van Duijn, G. and Rietema, K. 1983. Performance of a large-cone angle hydrocyclone II: Separation properties. *Chemical Engineering Science*. Vol. 38, No. 10, pp. 1663-1673.

Verghese, P.A., and Rao, T.C. 1994. Modelling of a 76mm diameter dense medium cyclone. *Coal Preparation*. Vol. 15, pp. 71-91.

Williams, R.A., Ilyas, O.M., Dyakowski, T., Dickin, F.J., Guiterrez, J.A., Wang, M., Beck M.S., Shah, C., and Rushton, A., 1995. Air core imaging in cyclonic separators: implications for separator design and modelling. *Chem. Eng. J*. Vol. 56, pp.135-141.

Wills, B. A. 1997. *Mineral Processing Technology: An introduction to the practical aspects of ore treatment and mineral recovery, Sixth Edition*. Butterworth-Heinemann, Oxford. pp. 192-213 and 237-257.

Wood, C.J., Davis, J.J., and Lyman, G. J. 1989. Towards a medium behaviour based performance model for coal-washing dense medium cyclones. *Coal Preparation*. Vol. 7, pp. 183-197.

Wood, C.J. 1990. *Coal-washing dense medium cyclones: A JKMRC Handbook for operators and plant designers*. JKMRC.

Yianatos, J.B., Lisboa, M.A., and Baeza, D.R. 2002. Grinding capacity enhancement by solid concentration control of hydrocyclone underflow. *Mineral Engineering*. Vol. 15, pp. 317-323.

CHAPTER 7.

APPENDIX

7.1. APPENDIX A

7.1.1. Tables

Table A.1. Dimensions of the dense medium cyclones employed by DSM.

D_c mm	D_i mm	D_o mm	D_u mm	α deg.	Bl mm
200	40	85	60	20	120
250	50	110	75	20	165
350	70	150	100	20	230
400	80	170	120	20	250
500	100	215	150	20	295
550	110	235	160	20	330
600	120	260	180	20	355
650	130	280	190	20	385
700	140	300	210	20	395
750	150	320	225	20	440
800	160	350	240	20	470

Table A.2. Results obtained when characterizing overloading behaviour of the 45mm spigot.
D = 165mm; D_i = 30mm; D_o = 64mm; D_u =45mm; $\alpha = 15^o$; Bl = None.
P = 20kPa; Medium grade = F; d_{ore} = -1.8+0.8mm; ρ_{ore} = 2.65kg/l.

C_{vf} (v/v%)	Q_O (l/hr ore)	Q_U (l/hr ore)	C_{mvu} (v/v%)	Q_{OS} (l/hr slurry)	Q_{US} (l/hr slurry)	R_m (v/v)	ρ_{med} (kg/l)	$\rho_{UF(Med)}$-$\rho_{OF(med)}$ (kg/l)	Q (l/hr slurry)
0.4	0.00	37	1.6	8027	2291	0.22	1.32	0.58	10318
0.8	0.00	92	4.1	9741	2264	0.18	-	-	12005
4.9	0.0	564	17.3	8250	3254	0.25	1.29	0.43	11504
7.5	0.0	911	20.4	7717	4462	0.32	1.29	0.33	12179
7.9	0.0	934	22.4	7677	4170	0.30	1.29	0.34	11847
9.0	0.9	1174	22.2	7750	5300	0.35	1.28	0.09	13049
11.1	0.9	1328	29.8	7468	4456	0.30	1.26	0.14	11925
12.1	0.0	1491	25.3	6402	5885	0.41	1.29	0.26	12287
13.0	0.0	1762	17.0	3159	10359	0.73	1.27	0.08	13519
16.5	0.0	2002	29.4	5355	6815	0.47	1.29	0.19	12170
20.3	1.2	2729	27.9	3664	9769	0.66	1.24	0.04	13433
21.3	1.4	3033	31.0	4491	9790	0.60	1.28	0.03	14281
23.3	248.9	3187	50.5	8457	6313	0.28	1.27	0.01	14770
24.4	338.5	3176	50.2	8075	6322	0.29	1.28	0.01	14397
24.6	177.9	3290	51.4	7718	6406	0.29	1.24	-0.02	14124
26.0	532.1	3205	53.5	8364	5996	0.26	1.27	0.01	14360
26.1	522.9	3163	49.4	7742	6399	0.31	1.25	0.02	14141
26.5	545.1	3259	51.8	8084	6287	0.29	1.27	0.00	14371
27.5	646.7	3265	50.6	7770	6453	0.3	1.24	0.01	14223
29.7	1209.1	2934	50.3	8122	5836	0.30	1.27	0.01	13958
30.5	1062.2	3244	51.2	7785	6335	0.31	1.27	0.01	14120
30.6	884.1	3288	50.5	7145	6511	0.34	1.24	0.01	13656

Table A.3. Results obtained when characterizing overloading behaviour of the 34mm spigot.

D = 165mm; D_i = 30mm; D_o = 64mm; D_u =34mm; $\alpha = 15^o$; Bl = None.

P = 20kPa; Medium grade = F; d_{ore} = -1.8+0.8mm; ρ_{ore} = 2.65kg/l.

C_{vf}	Q_O	Q_U	C_{mvu}	Q_{OS}	Q_{US}	R_m	ρ_{med}	$\rho_{UF(Med)}$-$\rho_{OF(med)}$	Q
(v/v%)	(l/hr ore)	(l/hr ore)	(v/v%)	(l/hr slurry)	(l/hr slurry)	(v/v)	(kg/l)	(kg/l)	(l/hr slurry)
2.1	0.0	256	13.6	10111	1880	0.14	1.28	0.70	11991
2.2	0.0	260	13.7	10099	1895	0.14	1.28	0.72	11994
3.9	0.0	473	21.9	9873	2165	0.15	1.29	0.65	12038
5.0	0.0	639	23.2	10015	2762	0.00	1.32	0.68	12777
7.6	459.2	725	48.8	14081	1487	0.05	1.29	0.05	15569
10.5	959.7	653	48.0	13949	1359	0.05	1.29	0.03	15308
11.3	981.8	675	49.0	13315	1377	0.05	1.29	0.05	14692
12.4	1323.5	669	48.0	14667	1393	0.05	1.28	0.03	16060
13.3	1269.7	629	46.6	12968	1350	0.06	1.25	0.03	14318
14.7	1751.3	651	47.1	14924	1382	0.05	1.29	0.03	16305
14.8	1587.6	673	49.1	13900	1370	0.05	1.28	0.00	15270
15.4	1720.8	663	49.9	14119	1329	0.05	1.28	0.02	15448
16.8	1946.2	659	45.8	14094	1437	0.06	1.28	0.01	15531
23.1	2265.5	1218	49.2	12626	2474	0.11	1.28	0.02	15099
32.9	2096.3	2061	49.8	8498	4140	0.25	1.24	0.02	12638

Table A.4. Results obtained when characterizing overloading behaviour of the 25mm spigot.

D = 165mm; D_i = 30mm; D_o = 64mm; D_u =25mm; $\alpha = 15^o$; Bl = None.

P = 20kPa; Medium grade = F; d_{ore} = -1.8+0.8mm; ρ_{ore} = 2.65kg/l.

C_{vf}	Q_O	Q_U	C_{mvu}	Q_{OS}	Q_{US}	R_m	ρ_{med}	$\rho_{UF(Med)}$-$\rho_{OF(med)}$	Q
(v/v%)	(l/hr ore)	(l/hr ore)	(v/v%)	(l/hr slurry)	(l/hr slurry)	(v/v)	(kg/l)	(kg/l)	(l/hr slurry)
2.2	0.0	249	19.5	10243	1275	9.10	1.25	0.34	11518
3.0	0.0	385	26.1	11515	1475	0.09	1.28	0.85	12990
3.4	0.0	403	26.2	10405	1538	9.83	1.28	0.75	11942
5.2	311.9	446	46.0	13650	970	3.77	1.29	0.07	14620
9.2	958.2	437	47.0	14203	930	3.59	1.29	0.05	15133
12.4	1346.0	432	45.2	13393	957	4.17	1.26	0.03	14349
13.3	1554.0	452	47.6	14114	950	3.81	1.29	0.04	15064
14.7	1901.6	421	45.2	14901	930	3.77	1.28	0.03	15832
15.2	1826.6	418	44.7	13829	935	4.13	1.25	0.02	14763
21.4	2656.8	422	45.1	13442	937	4.55	1.24	0.02	14379
25.7	3216.2	449	51.0	13368	881	4.08	1.29	0.08	14248
32.5	4191.0	408	44.9	13257	907	5.22	1.27	0.02	14164

Table A.5. The influence of spigot design on the spigot capacity.

The following conditions were constant during these tests:

- D = 165mm; D_i = 30mm; D_U = 45mm; $\alpha = 20^o$; Bl = 200mm.
- Medium Grade = F; d_{ore} = -1.8+0.8mm; ρ_{ore} = 2.65 kg/l; P = 20kPa.

D_O (mm)	Cone type	ρ_{med} (ton/m^3)	Q_O (l/hr)	Q_{UM} (l/hr)	Q_{OS} (l/hr)	Q_{USM} (l/hr)	R_m (v/v)
64	B	1.29	126	3818	4149	8054	0.51
40	B	1.28	392	4100	5721	8639	0.46
64	A	1.28	192	3307	4460	6848	0.45
40	A	1.27	352	3506	4697	6999	0.45

Table A.6. The influence of medium density on the density differential.

The following conditions were constant during these tests:

- D = 165mm; D_i = 30mm; D_o = 64mm; $\alpha = 20^o$ (cone A); Bl = none.
- Medium grade = F; ρ_{ore} = 2.65 kg/l; d_{ore} = -1.8+0.8mm.

	D_u (mm)	P (kPa)	ρ_{med} (kg/l)	$\rho_{UF(Med)}$-$\rho_{OF(med)}$ (kg/l)
a	34	25	1.27	0.02
	34	29	1.52	0.02
	34	33	1.73	0.00
b	34	30	1.27	0.03
	34	35	1.52	0.04
	34	39	1.76	-0.03
c	34	33	1.28	0.04
	34	42	1.54	0.13
	34	47	1.74	0.00
d	25	25	1.29	0.04
	25	29	1.66	0.05
	25	33	1.74	-0.01
e	25	30	1.29	0.06
	25	35	1.55	0.25
	25	39	1.77	0.10
f	25	33	1.29	0.08
	25	42	1.52	0.08
	25	47	1.75	0.01

Table A.7. The influence of ore size on the spigot capacity.

The following conditions were constant during these tests:

- D = 165mm; D_i = 47mm; $\alpha = 15^o$; Bl = none.
- ρ_{med} = 1.7RD; Medium grade = F; ρ_{ore} = 2.65 kg/l; P = 25kPa.

	D_O (mm)	D_u (mm)	d_{ore} (mm)	C_{mvu} (v/v%)	Q_{UM} (l/hr ore)	Q_{USM} (l/hr slurry)
a	64	25	-1.8 + 0.8	45.2	499	1104
	64	34	-1.8 + 0.8	46.4	793	1710
b	64	25	-5 + 3	44.4	524	1179
	64	34	-5 + 3	47.0	921	1960
c	40	25	-1.8 + 0.8	44.1	621	1406
	40	34	-1.8 + 0.8	46.5	1012	2174
d	40	25	-5 + 3	43.4	631	1455
	40	34	-5 + 3	46.9	1126	2401

Table A.8. The influence of ore size on the spigot capacity.

The following conditions were constant during these tests:

- D = 165mm; D_i = 30mm; D_o = 64mm; $\alpha = 15^o$; Bl = none.
- Medium grade = F; ρ_{ore} = 2.65 kg/l.

	D_u (mm)	ρ_{med} (ton/m^3)	P (kPa)	d_{ore} (mm)	C_{mvu} (v/v%)	Q_{UM} (l/hr ore)	Q_{USM} (l/hr)
a	45	1.26	20	-1.8 + 0.8	50.9	3201	6286
	34	1.28	20	-1.8 + 0.8	48.0	666	1387
	25	1.27	20	-1.8 + 0.8	45.7	430	939
b	45	1.29	20	-3+1	51.2	3020	5893
	34	1.29	20	-3+1	51.0	700	1371
	25	1.30	20	-3+1	47.7	406	851
c	45	1.46	22	-1.8 + 0.8	49.1	3063	6245
	34	1.46	22	-1.8 + 0.8	47.5	538	1131
	25	1.46	22	-1.8 + 0.8	46.3	358	773
d	45	1.49	22	-3+1	55.5	3054	5499
	34	1.50	22	-3+1	51.0	611	1197
	25	1.50	22	-3+1	50.0	370	740

7.1.2. Equations

(a) Throughput

Dense Medium Cyclones

Source: Upadrashta and Venkateswarlu (1982)

$$Q = K\left(\frac{P}{\rho_{med}}\right)^{0.41}(1-C_v)^{0.12}\left(D_u^2 + D_o^2\right)^{0.302} D_i^{1.03} \quad \text{(Spray discharge)} \qquad \text{(A.1)}$$

$$Q = K\left(\frac{P}{\rho_{med}}\right)^{0.58}(1-C_v)^{0.56}\left(D_u^2 + D_o^2\right)^{0.26} D_i^{1.8} \quad \text{(Rope discharge)} \qquad \text{(A.2)}$$

Source: DSM (1985)

$$Q = f \times D_i \times D_o \qquad \text{(A.3)}$$

with f = f(D).

Source: Napier-Munn (1986)

$$Q \propto \left(\frac{P}{\rho_{med}\, g}\right)^{\frac{1}{\alpha}}\left(\frac{\rho_{med}}{\eta}\right)^{\frac{\beta}{\alpha}} \qquad \text{(A.4)}$$

where α =1.7 and $\beta \approx 0$ at low Reynolds numbers, and $\alpha > 2.0$ and $-\beta = 0.2 - 0.4$ at high Reynolds numbers. With Q in l/min, P in kPa, ρ_{med} in kg/m^3 and η the apparent viscosity of the medium in Nsm^{-2}x10^3.

Source: Wood et al. (1989)

$$Q = 0.064 D^{2.3} H^{0.45}\left(\frac{D_u}{D_o}\right)^{0.15} \qquad \text{(A.5)}$$

with Q in m^3/s, D_o in m, D_u in m, D in m and H in D.

Source: Clarkson and Wood (1993)

$$Q = 76 D^{1.93} H^{0.45}\left(\frac{D_u}{D_o}\right)^{0.15} \qquad \text{(A.6)}$$

Source: Verghese and Rao (1994)

$$Q = 7.547 D_o^{0.414} D_u^{0.185} \rho_{med}^{-2.168} CR^{0.4797} \qquad \text{(A.7)}$$

with Q in l/min, D_o in mm, D_u in mm, ρ_{med} in mg/cm^3 and CR the coal feed rate in kg/min.

Classification Cyclones

Source: Flintoff et al. (1987)

$$Q = \frac{KP^{0.56}D^{0.21}D_i^{0.53}h^{0.16}\left(D_u^2 + D_o^2\right)^{0.49}}{e^{0.0031(\%V_{SF})}} \quad \text{(A.8)}$$

Source: Lynch and Rao (1975)

$$Q = 15.63D_o^{0.68}D_i^{0.85}D_u^{0.16}P^{0.49}\left(-53\mu m\right)^{-0.35} \quad \text{(A.9)}$$

Source: Asomah and Napier-Munn (1997)

$$Q = KD^{0.739}\left(\frac{\left(D_oD_i\right)^{1.538}Bl^{0.455}P}{\rho_p\left(1-\frac{\%V_{SF}}{100}\right)^{0.435}\alpha^{0.246}e^{-0.113(\theta/180)}}\right)^{0.5} \quad \text{(A.10)}$$

(b) Volume Split

Source: Flintoff et al. (1987)

$$S = \frac{K\rho_{ore}^{0.24}\left(\frac{D_u}{D_o}\right)^{3.31}h^{0.24}\left(D_u^2 + D_o^2\right)^{0.36}e^{0.0054(\%V_{SF})}}{D^{1.11}P^{0.24}} \quad \text{(A.11)}$$

7.1.3. Pictures

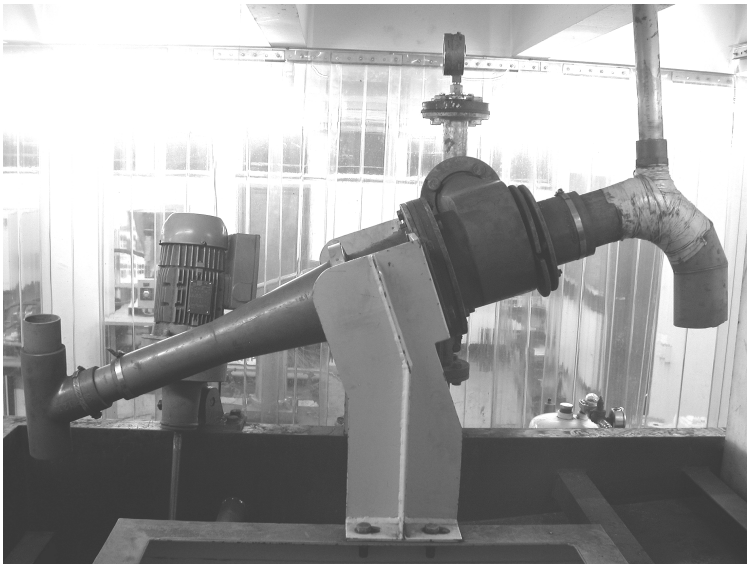


Figure A.1. The 165mm cyclone with the underflow elbow on.



Figure A.2. The pressure gauge used to measure the feed pressure.

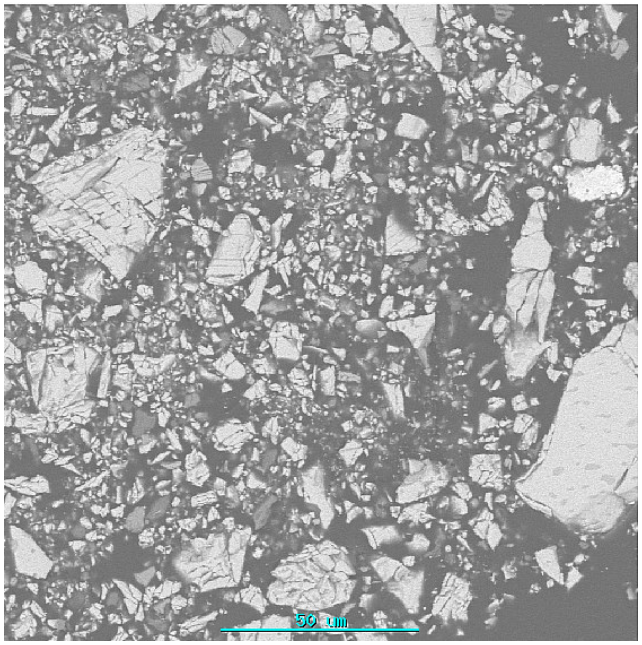


Figure A.3. SEM image of the magnetite employed during the test-work.



Figure A.4. A picture of the dense medium cyclone plant at Mintek, Randburg, South Africa.

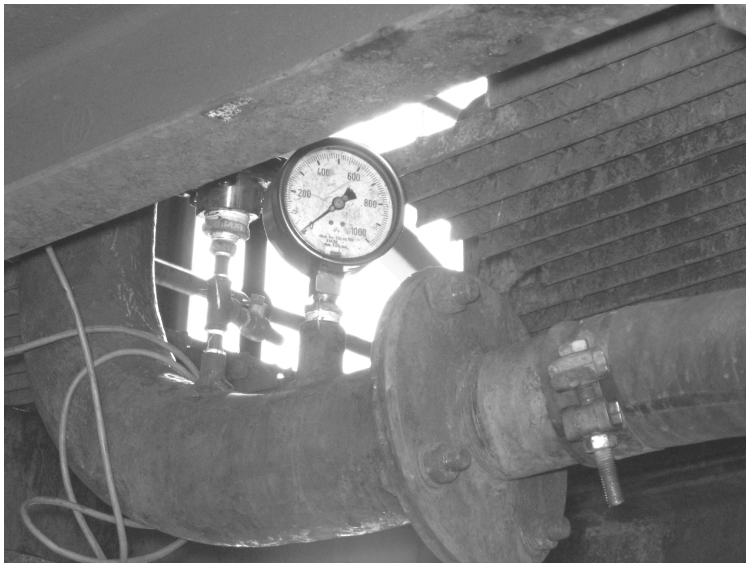


Figure A.5. The pressure gauge employed during the test-work with the 350mm cyclone. The pressure gauge was 0.915m below the feed inlet.



Figure A.6. The Marcy scale and ‘density bottle’ used to measure the medium density.



Figure A.7. The demagnetizing coil at the DMS plant.



Figure A.8. The area where the sievebends, receiving the floats and sinks slurries, were removed.

7.1.4. Others

Sample No				

D_i (mm)	D_o (mm)	D_u (mm)	α (deg.)	Bl (mm)

Grade	P kPa (Set-point)	P kPa(Observed)	ρ_{med} (kg/l)	Ore type	Ore size (mm)

U/F Flow-Rate

Time (s)	Total mass (kg)	Bucket mass (kg)	Flow (kg/s)
		Average	

O/F Flow-Rate

Time (s)	Total mass (kg)	Bucket mass (kg)	Flow (kg/s)
		Average	

Comments

Figure A.9. The log-sheet used during flow-rate measurements.

	Ore + magnetite + water		Solids	
Sample No.	Total mass (g)	Bottle mass(g)	Ore mass (g)	Magnetite mass (g)

Figure A.10. The log-sheet used during analysis of samples from the float and sink streams.

7.2. APPENDIX B: PROCESSED DATA AND EXPERIMENTAL CONDITIONS

7.2.1. Data for tests performed with 15° cone.

D = 165mm; 15° cone

Test No.	D_i	D_o (mm)	D_u (mm)	α (deg.)	BI (mm)	P (kPa)	ρ_{ore} (kg/l)	d_{ore} (mm)	Med grade	C_{vf} (v/v%)	Q_O (l/hr ore)	Q_U (l/hr ore)	C_{mvu} (v/v%)	Q_{OS} (l/hr slurry)	Q_{US} (l/hr slurry)	R_m (v/v)	Q (l/hr)	$\rho_{UF(med)}$ (kg/l)	$\rho_{OF(med)}$ (kg/l)	ρ_{med} (kg/l)
A1	B	64	45	15	0	20	2.65	-1.8 + 0.8	F	0.4	0.0	37.2	1.6	8027	2291	0.22	10318	1.77	1.20	1.32
A2	B	64	45	15	0	25	2.65	-1.8 + 0.8	F	0.7	0.0	78.2	3.4	8921	2269	0.20	11190	1.88	1.18	1.32
A3	B	64	45	15	0	30	2.65	-1.8 + 0.8	F	0.6	0.0	73.9	3.2	10568	2320	0.18	12888	2.15	1.18	1.35
A4	B	64	34	15	0	30	2.65	-1.8 + 0.8	F	0.7	0.0	87.9	4.8	11013	1829	0.14	12842	2.00	1.17	1.29
A5	B	64	45	15	0	20	2.65	-1.8 + 0.8	F	0.2	0.0	25.6	1.0	8353	2565	0.23	10918	1.90	1.39	1.51
A6	B	64	45	15	0	25	2.65	-1.8 + 0.8	F	0.1	0.0	8.3	0.3	9318	2575	0.22	11893	1.97	1.37	1.50
A7	B	64	45	15	0	30	2.65	-1.8 + 0.8	F	1.1	0.0	141.7	5.3	10593	2677	0.19	13269	2.06	1.38	1.51
A8	B	64	45	15	0	20	2.65	-1.8 + 0.8	F	0.0	0.0	3.0	0.1	8201	2645	0.24	10847	1.95	1.59	1.67
A9	B	64	45	15	0	25	2.65	-1.8 + 0.8	F	0.0	0.0	2.4	0.1	9616	2646	0.22	12262	2.04	1.59	1.69
A10	B	64	45	15	0	30	2.65	-1.8 + 0.8	F	0.3	0.0	39.6	1.5	10243	2704	0.21	12947	2.10	1.61	1.71
A11	B	64	20	15	0	20	2.65	-1.8 + 0.8	F	1.6	0.0	203	14	1466	11186	0.10	12652	1.73	1.17	1.23
A12	B	64	34	15	0	20	2.65	-1.8 + 0.8	F	5.0	0.0	639	23	2762	10015	0.17	12777	1.88	1.20	1.32
A13	B	40	20	15	0	20	2.65	-1.8 + 0.8	F	0.8	0.0	60	5.7	6330	1051	0.14	7381	2.37	1.18	1.34
A14	B	40	34	15	0	20	2.65	-1.8 + 0.8	F	0.5	0.0	41	1.2	4847	3388	0.41	8234	1.54	1.15	1.31
A15	B	40	45	15	0	20	2.65	-1.8 + 0.8	F	3.1	0.0	277	4.5	2699	6150	0.69	8849	1.38	1.18	1.31
A16	B	53	20	15	0	20	2.65	-1.8 + 0.8	F	0.4	0.0	39	3.0	8679	1312	0.13	9991	2.08	1.20	1.31
A17	B	53	34	15	0	20	2.65	-1.8 + 0.8	F	1.7	0.0	160	6.9	7260	2327	0.23	9588	1.73	1.15	1.28
A18	B	53	45	15	0	20	2.65	-1.8 + 0.8	F	0.7	0.0	64	1.9	6364	3400	0.34	9764	1.64	1.16	1.33

NB: A-inlet – 70x25 mm^2 and B-inlet – 70x10mm^2.

D = 165mm; 15° cone

Test No.	D_i	D_o (mm)	D_u (mm)	α (deg.)	BI (mm)	P (kPa)	ρ_{ore} (kg/l)	d_{ore} (mm)	Med grade	C_{vf} (v/v%)	Q_O (l/hr ore)	Q_U (l/hr ore)	C_{mvu} (v/v%)	Q_{OS} (l/hr slurry)	Q_{US} (l/hr slurry)	R_m (v/v)	Q (l/hr)	$\rho_{UF(med)}$ (kg/l)	$\rho_{OF(med)}$ (kg/l)	ρ_{med} (kg/l)
B1	B	53	45	15	0	20	2.65	-1.8 + 0.8	F	1.3	0.0	145	4.0	7360	3642	0.32	11002	1.56	1.15	1.28
B2	B	53	45	15	0	20	2.65	-1.8 + 0.8	F	2.1	0.0	237	6.3	7298	3794	0.33	11091	1.55	1.15	1.28
B3	B	53	45	15	0	20	2.65	-1.8 + 0.8	F	3.0	0.4	331	8.7	7221	3818	0.33	11038	1.56	1.15	1.29
B4	B	53	45	15	0	20	2.65	-1.8 + 0.8	F	3.8	0.0	451	10.6	7669	4264	0.33	11933	1.55	1.16	1.29
B5	B	53	45	15	0	20	2.65	-1.8 + 0.8	F	4.3	0.8	488	11.8	7354	4130	0.33	11484	1.55	1.16	1.29
B6	B	53	45	15	0	20	2.65	-1.8 + 0.8	F	4.8	0.4	559	12.8	7253	4359	0.34	11612	1.54	1.16	1.29
B7	B	53	45	15	0	20	2.65	-1.8 + 0.8	F	6.3	1.6	743	16.4	7375	4523	0.34	11897	1.54	1.15	1.28
B8	B	53	45	15	0	20	2.65	-1.8 + 0.8	F	11.3	1.5	1426	25.3	7043	5631	0.37	12674	1.46	1.18	1.28
C1	B	64	45	15	0	20	2.65	-1.8 + 0.8	F	4.9	0.0	564	17.3	8250	3254	0.25	11504	1.61	1.19	1.29
C2	B	64	45	15	0	20	2.65	-1.8 + 0.8	F	7.9	0.0	934	22.4	7677	4170	0.30	11847	1.53	1.18	1.29
C3	B	64	45	15	0	20	2.65	-1.8 + 0.8	F	7.5	0.0	911	20.4	7717	4462	0.32	12179	1.52	1.19	1.29
C4	B	64	45	15	0	20	2.65	-1.8 + 0.8	F	12.1	0.0	1491	25.3	6402	5885	0.41	12287	1.44	1.19	1.29
C5	B	64	45	15	0	20	2.65	-1.8 + 0.8	F	16.5	0.0	2002	29.4	5355	6815	0.47	12170	1.39	1.20	1.29
C6	B	64	45	15	0	20	2.65	-1.8 + 0.8	F	13.0	0.0	1762	17.0	3159	10359	0.73	13519	1.29	1.22	1.27
C7	B	64	34	15	0	20	2.65	-1.8 + 0.8	F	2.1	0.0	256	13.6	10111	1880	0.14	11991	1.88	1.19	1.28
C8	B	64	34	15	0	20	2.65	-1.8 + 0.8	F	2.2	0.0	260	13.7	10099	1895	0.14	11994	1.91	1.18	1.28
C9	B	64	34	15	0	20	2.65	-1.8 + 0.8	F	3.9	0.0	473	21.9	9873	2165	0.15	12038	1.84	1.19	1.29
C10	B	64	25	15	0	20	2.65	-1.8 + 0.8	F	4.4	0.0	524	30.8	10289	1701	0.10	11990	1.89	1.21	1.28
C11	B	64	25	15	0	20	2.65	-1.8 + 0.8	F	3.4	0.0	403	26.2	10405	1538	0.10	11942	1.96	1.21	1.28
D1	B	53	45	15	0	20	2.65	-1.8 + 0.8	F	5.4	0.0	580	14.6	6742	3976	0.33	10718	1.52	1.14	1.26
D2	B	53	45	15	0	20	2.65	-1.8 + 0.8	F	6.7	0.0	719	17.2	6581	4194	0.35	10775	1.52	1.14	1.27
D3	B	53	45	15	0	20	2.65	-1.8 + 0.8	F	5.9	0.0	661	14.1	6496	4688	0.38	11184	1.50	1.14	1.28
D4	B	53	45	15	0	20	2.65	-1.8 + 0.8	F	10.3	0.0	1216	22.6	6411	5379	0.39	11790	1.42	1.15	1.26
D5	B	53	45	15	0	20	2.65	-1.8 + 0.8	F	13.7	0.0	1609	28.4	6086	5673	0.40	11758	1.43	1.15	1.26
D6	B	53	45	15	0	20	2.65	-1.8 + 0.8	F	12.9	0.0	1600	17.7	3401	9031	0.69	12432	1.29	1.19	1.26
D7	B	53	34	15	0	20	2.65	-1.8 + 0.8	F	8.2	424.2	729	45.3	12479	1609	0.07	14088	1.42	1.26	1.27

D = 165mm; 15° cone

Test No.	D_i	D_o (mm)	D_u (mm)	α (deg.)	BI (mm)	P (kPa)	ρ_{ore} (kg/l)	d_{ore} (mm)	Med grade	C_{vf} (v/v%)	Q_O (l/hr ore)	Q_U (l/hr ore)	C_{mvu} (v/v%)	Q_{OS} (l/hr slurry)	Q_{US} (l/hr slurry)	R_m (v/v)	Q (l/hr)	$\rho_{UF(med)}$ (kg/l)	$\rho_{OF(med)}$ (kg/l)	ρ_{med} (kg/l)
D8	B	53	34	15	0	20	2.65	-1.8 + 0.8	F	4.6	0.0	507	15.8	7850	3208	0.26	11058	1.58	1.16	1.27
D9	B	53	34	15	0	20	2.65	-1.8 + 0.8	F	2.6	0.0	271	10.5	7903	2592	0.23	10495	1.68	1.15	1.27
D10	B	53	34	15	0	20	2.65	-1.8 + 0.8	F	1.6	0.0	166	6.8	8199	2448	0.22	10646	1.73	1.14	1.27
D11	B	53	25	15	0	20	2.65	-1.8 + 0.8	F	3.7	0.0	385	21.9	8711	1759	0.14	10471	1.84	1.17	1.26
E1	B	53	45	15	0	20	2.65	-1.8 + 0.8	F	4.4	0.0	477	10.6	6403	4480	0.38	10884	1.39	1.20	1.27
E2	B	53	45	15	0	20	2.65	-1.8 + 0.8	F	22.2	2.0	2922	27.5	2520	10627	0.75	13146	1.26	1.26	1.26
E3	B	53	45	15	0	20	2.65	-1.8 + 0.8	F	24.8	355.8	3168	51.0	7998	6211	0.28	14209	1.27	1.26	1.26
E4	B	53	45	15	0	20	2.65	-1.8 + 0.8	F	27.5	460.0	3321	50.4	7143	6590	0.33	13733	1.26	1.26	1.26
E5	B	53	45	15	0	20	2.65	-1.8 + 0.8	F	25.7	559.6	3104	50.5	8113	6147	0.29	14260	1.26	1.25	1.25
E6	B	53	45	15	0	20	2.65	-1.8 + 0.8	F	24.9	407.4	3152	51.3	8171	6149	0.28	14320	1.27	1.27	1.27
E7	B	53	45	15	0	20	2.65	-1.8 + 0.8	F	23.7	70.1	3272	50.4	7590	6491	0.30	14081	1.27	1.26	1.26
E8	B	53	45	15	0	20	2.65	-1.8 + 0.8	F	24.5	2.7	3282	32.8	3380	10005	0.67	13385	1.27	1.25	1.26
E9	B	53	34	15	0	20	2.65	-1.8 + 0.8	F	16.3	1355.1	1026	49.4	12541	2078	0.09	14619	1.31	1.23	1.24
E10	B	53	34	15	0	20	2.65	-1.8 + 0.8	F	28.0	1803.4	1972	47.4	9346	4157	0.22	13502	1.26	1.26	1.26
E11	B	53	34	15	0	20	2.65	-1.8 + 0.8	F	33.7	2131.9	1956	47.8	8053	4088	0.26	12141	1.27	1.25	1.26
E12	B	53	34	15	0	20	2.65	-1.8 + 0.8	F	20.0	1426.5	1537	48.8	11698	3147	0.14	14844	1.26	1.26	1.26
E13	B	53	34	15	0	20	2.65	-1.8 + 0.8	F	9.6	0.0	1060	28.3	7316	3748	0.27	11063	1.40	1.25	1.29
E14	B	53	25	15	0	20	2.65	-1.8 + 0.8	F	32.0	3508.0	421	44.6	11337	943	0.06	12280	1.25	1.33	1.32
E15	B	53	25	15	0	20	2.65	-1.8 + 0.8	F	21.5	2575.4	423	45.4	13019	933	0.05	13952	1.27	1.27	1.27
E16	B	53	25	15	0	20	2.65	-1.8 + 0.8	F	16.2	1850.3	424	45.0	13086	943	0.04	14029	1.28	1.27	1.27
E17	B	53	25	15	0	20	2.65	-1.8 + 0.8	F	3.3	0.0	340	21.9	8722	1552	0.12	10274	1.45	1.25	1.27
F1	B	64	45	15	0	20	2.65	-1.8 + 0.8	F	11.1	0.9	1328	29.8	7468	4456	0.30	11925	1.36	1.22	1.26
F2	B	64	45	15	0	20	2.65	-1.8 + 0.8	F	24.6	177.9	3290	51.4	7718	6406	0.29	14124	1.23	1.24	1.24
F3	B	64	45	15	0	20	2.65	-1.8 + 0.8	F	30.6	884.1	3288	50.5	7145	6511	0.34	13656	1.25	1.23	1.24
F4	B	64	45	15	0	20	2.65	-1.8 + 0.8	F	26.1	522.9	3163	49.4	7742	6399	0.31	14141	1.26	1.24	1.25
F5	B	64	45	15	0	20	2.65	-1.8 + 0.8	F	20.3	1.2	2729	27.9	3664	9769	0.66	13433	1.25	1.22	1.24

D = 165mm; 15° cone

Test No.	D_i	D_o (mm)	D_u (mm)	α (deg.)	BI (mm)	P (kPa)	ρ_{ore} (kg/l)	d_{ore} (mm)	Med grade	C_{vf} (v/v%)	Q_O (l/hr ore)	Q_U (l/hr ore)	C_{mvu} (v/v%)	Q_{OS} (l/hr slurry)	Q_{US} (l/hr slurry)	R_m (v/v)	Q (l/hr)	$\rho_{UF(med)}$ (kg/l)	$\rho_{OF(med)}$ (kg/l)	ρ_{med} (kg/l)
F6	B	64	34	15	0	20	2.65	-1.8 + 0.8	F	13.3	1269.7	629	46.6	12968	1350	0.06	14318	1.28	1.25	1.25
F7	B	64	25	15	0	20	2.65	-1.8 + 0.8	F	15.2	1826.6	418	44.7	13829	935	0.04	14763	1.27	1.25	1.25
F8	B	64	25	15	0	20	2.65	-1.8 + 0.8	F	12.4	1346.0	432	45.2	13393	957	0.04	14349	1.29	1.26	1.26
F9	B	64	25	15	0	20	2.65	-1.8 + 0.8	F	2.2	0.0	249	19.5	10243	1275	0.09	11518	1.57	1.22	1.25
G1	B	64	45	15	0	20	2.65	-1.8 + 0.8	F	27.5	646.7	3265	50.6	7770	6453	0.31	14223	1.25	1.24	1.24
G2	B	64	34	15	0	20	2.65	-1.8 + 0.8	F	32.9	2096.3	2061	49.8	8498	4140	0.25	12638	1.25	1.24	1.24
G3	B	64	25	15	0	20	2.65	-1.8 + 0.8	F	21.4	2656.8	422	45.1	13442	937	0.05	14379	1.27	1.24	1.24
G4	B	64	20	15	0	20	2.65	-1.8 + 0.8	F	17.6	2437.0	286	42.9	14812	667	0.03	15479	1.26	1.24	1.24
G5	B	53	45	15	0	20	2.65	-1.8 + 0.8	F	29.6	884.3	3251	50.1	7473	6492	0.33	13965	1.25	1.24	1.25
G6	B	53	34	15	0	20	2.65	-1.8 + 0.8	F	23.1	1721.5	1683	48.5	11238	3471	0.16	14710	1.26	1.24	1.24
G7	B	53	25	15	0	20	2.65	-1.8 + 0.8	F	19.4	2434.3	453	45.5	13893	996	0.05	14889	1.26	1.23	1.23
G8	B	53	20	15	0	20	2.65	-1.8 + 0.8	F	27.4	3357.3	280	43.0	12646	651	0.04	13297	1.25	1.24	1.24
G9	B	40	45	15	0	20	2.65	-1.8 + 0.8	F	29.0	679.7	3382	49.5	7148	6839	0.35	13986	1.25	1.25	1.25
G10	B	40	34	15	0	20	2.65	-1.8 + 0.8	F	35.5	2541.6	1895	47.2	8467	4015	0.26	12483	1.26	1.25	1.25
G11	B	40	25	15	0	20	2.65	-1.8 + 0.8	F	35.6	3811.7	559	44.7	11040	1250	0.09	12290	1.25	1.26	1.26
G12	B	40	20	15	0	20	2.65	-1.8 + 0.8	F	35.4	3937.8	376	42.8	11302	878	0.06	12180	1.27	1.29	1.29
H1	B	64	25	15	0	20	2.65	-1.8 + 0.8	F	32.5	4191.0	408	44.9	13257	907	0.05	14164	1.29	1.27	1.27
H2	B	64	25	15	0	20	2.65	-1.8 + 0.8	F	25.7	3216.2	449	51.0	13368	881	0.04	14248	1.36	1.29	1.29
H3	B	64	25	15	0	20	2.65	-1.8 + 0.8	F	13.3	1554.0	452	47.6	14114	950	0.04	15064	1.33	1.29	1.29
H4	B	64	25	15	0	20	2.65	-1.8 + 0.8	F	9.2	958.2	437	47.0	14203	930	0.04	15133	1.34	1.29	1.29
H5	B	64	25	15	0	20	2.65	-1.8 + 0.8	F	5.2	311.9	446	46.0	13650	970	0.04	14620	1.36	1.29	1.29
H6	B	64	34	15	0	20	2.65	-1.8 + 0.8	F	23.1	2265.5	1218	49.2	12626	2474	0.11	15099	1.29	1.27	1.28
H7	B	64	34	15	0	20	2.65	-1.8 + 0.8	F	15.4	1720.8	663	49.9	14119	1329	0.05	15448	1.30	1.28	1.28
H8	B	64	34	15	0	20	2.65	-1.8 + 0.8	F	14.8	1587.6	673	49.1	13900	1370	0.05	15270	1.28	1.28	1.28
H9	B	64	34	15	0	20	2.65	-1.8 + 0.8	F	10.5	959.7	653	48.0	13949	1359	0.05	15308	1.31	1.28	1.29
H10	B	64	34	15	0	20	2.65	-1.8 + 0.8	F	11.3	981.8	675	49.0	13315	1377	0.05	14692	1.34	1.29	1.29

D = 165mm; 15° cone

Test No.	D_i	D_o (mm)	D_u (mm)	α (deg.)	BI (mm)	P (kPa)	ρ_{ore} (kg/l)	d_{ore} (mm)	Med grade	C_{vf} (v/v%)	Q_O (l/hr ore)	Q_U (l/hr ore)	C_{mvu} (v/v%)	Q_{OS} (l/hr slurry)	Q_{US} (l/hr slurry)	R_m (v/v)	Q (l/hr)	$\rho_{UF(med)}$ (kg/l)	$\rho_{OF(med)}$ (kg/l)	ρ_{med} (kg/l)
H11	B	64	34	15	0	20	2.65	-1.8 + 0.8	F	7.6	459.2	725	48.8	14081	1487	0.05	15569	1.33	1.29	1.29
H12	B	64	45	15	0	20	2.65	-1.8 + 0.8	F	29.7	1209.1	2934	50.3	8122	5836	0.30	13958	1.28	1.27	1.27
H13	B	64	45	15	0	20	2.65	-1.8 + 0.8	F	30.5	1062.2	3244	51.2	7785	6335	0.31	14120	1.28	1.27	1.27
H14	B	64	45	15	0	20	2.65	-1.8 + 0.8	F	24.4	338.5	3176	50.2	8075	6322	0.29	14397	1.28	1.27	1.28
H15	B	64	45	15	0	20	2.65	-1.8 + 0.8	F	26.5	545.1	3259	51.8	8084	6287	0.29	14371	1.28	1.27	1.27
I1	B	64	34	15	0	20	2.65	-1.8 + 0.8	F	14.7	1751.3	651	47.1	14924	1382	0.05	16305	1.32	1.29	1.29
I2	B	64	30	15	0	20	2.65	-1.8 + 0.8	F	15.3	1958.3	518	46.2	15096	1122	0.04	16218	1.33	1.29	1.29
I3	B	64	30	15	0	20	2.65	-1.8 + 0.8	F	15.6	1961.9	526	45.9	14844	1145	0.05	15990	1.33	1.29	1.30
I4	B	53	34	15	0	20	2.65	-1.8 + 0.8	F	16.8	1890.1	713	46.9	13996	1521	0.06	15516	1.33	1.30	1.30
I5	B	53	34	15	0	20	2.65	-1.8 + 0.8	F	13.2	1390.2	744	48.0	14560	1551	0.06	16112	1.33	1.30	1.30
I6	B	40	34	15	0	20	2.65	-1.8 + 0.8	F	16.8	1617.9	866	47.4	12935	1828	0.08	14763	1.33	1.30	1.30
I7	B	40	34	15	0	20	2.65	-1.8 + 0.8	F	17.7	1731.2	874	47.0	12884	1861	0.08	14745	1.32	1.29	1.30
I8	B	40	25	15	0	20	2.65	-1.8 + 0.8	F	17.0	1884.0	543	44.6	13018	1219	0.06	14238	1.33	1.30	1.30
J1	B	40	34	15	0	20	2.65	-1.8 + 0.8	F	12.6	721.0	953	47.1	11225	2025	0.09	13250	1.31	1.27	1.28
J2	B	40	34	15	0	20	2.65	-1.8 + 0.8	F	25.5	2188.2	1362	47.0	11022	2898	0.15	13919	1.27	1.26	1.27
J3	B	40	34	15	0	20	2.65	-1.8 + 0.8	F	25.8	1902.8	1682	46.3	10273	3632	0.19	13905	1.27	1.26	1.26
J4	B	40	34	15	0	20	2.65	-1.8 + 0.8	F	21.7	2116.4	848	46.1	11824	1838	0.09	13662	1.29	1.26	1.26
J5	B	40	45	15	0	20	2.65	-1.8 + 0.8	F	26.0	413.6	3356	49.9	7800	6727	0.31	14527	1.28	1.27	1.27
J6	B	40	30	15	0	20	2.65	-1.8 + 0.8	F	20.7	2185.7	676	45.5	12350	1485	0.07	13835	1.28	1.26	1.27
J7	B	40	30	15	0	20	2.65	-1.8 + 0.8	F	20.6	2176.7	692	45.5	12376	1520	0.08	13896	1.29	1.27	1.27
J8	B	64	30	15	0	20	2.65	-1.8 + 0.8	F	8.4	38.2	1306	48.1	13366	2715	0.10	16081	1.34	1.28	1.28
J9	B	64	30	15	0	20	2.65	-1.8 + 0.8	F	10.5	1052.9	541	46.3	14061	1169	0.05	15230	1.32	1.28	1.28
J10	B	64	30	15	0	20	2.65	-1.8 + 0.8	F	16.6	2077.5	527	46.4	14560	1134	0.05	15694	1.30	1.28	1.28
J11	B	64	25	15	0	20	2.65	-1.8 + 0.8	F	14.7	1901.6	421	45.2	14901	930	0.04	15832	1.31	1.28	1.28
J12	B	64	34	15	0	20	2.65	-1.8 + 0.8	F	12.4	1323.5	669	48.0	14667	1393	0.05	16060	1.30	1.28	1.28
J13	B	64	34	15	0	20	2.65	-1.8 + 0.8	F	16.8	1946.2	659	45.8	14094	1437	0.06	15531	1.29	1.28	1.28

D = 165mm; 15° cone

Test No.	D_i	D_o (mm)	D_u (mm)	α (deg.)	BI (mm)	P (kPa)	ρ_{ore} (kg/l)	d_{ore} (mm)	Med grade	C_{vf} (v/v%)	Q_O (l/hr ore)	Q_U (l/hr ore)	C_{mvu} (v/v%)	Q_{OS} (l/hr slurry)	Q_{US} (l/hr slurry)	R_m (v/v)	Q (l/hr)	$\rho_{UF(med)}$ (kg/l)	$\rho_{OF(med)}$ (kg/l)	ρ_{med} (kg/l)
K1	B	64	45	15	0	20	2.65	-1.8 + 0.8	M	30.3	839.3	3347	51.2	7281	6537	0.33	13818	1.31	1.25	1.27
K2	B	64	34	15	0	20	2.65	-1.8 + 0.8	M	31.7	3632.6	654	48.6	12169	1343	0.07	13512	1.36	1.27	1.28
K3	B	64	25	15	0	20	2.65	-1.8 + 0.8	M	36.1	4166.4	393	44.9	11771	877	0.06	12647	1.36	1.27	1.27
K4	B	40	25	15	0	20	2.65	-1.8 + 0.8	M	27.0	2851.4	543	45.1	11383	1204	0.07	12587	1.34	1.27	1.28
K5	B	40	34	15	0	20	2.65	-1.8 + 0.8	M	26.8	2566.1	832	46.9	10917	1772	0.10	12689	1.35	1.27	1.28
K6	B	40	45	15	0	20	2.65	-1.8 + 0.8	M	26.3	254.8	3509	50.5	7338	6951	0.33	14289	1.30	1.26	1.28
K7	B	64	45	15	0	20	2.65	-1.8 + 0.8	M	31.4	984.9	3258	50.2	7037	6490	0.35	13527	1.39	1.35	1.36
K8	B	64	34	15	0	20	2.65	-1.8 + 0.8	M	32.0	3607.7	607	47.3	11893	1283	0.08	13177	1.44	1.35	1.36
K9	B	64	34	15	0	20	2.65	-1.8 + 0.8	M	27.1	3536.9	619	47.4	14008	1306	0.06	15314	1.45	1.35	1.35
K10	B	64	34	15	0	20	2.65	-1.8 + 0.8	M	17.6	2291.8	662	47.5	15421	1393	0.05	16815	1.53	1.36	1.37
K11	B	64	25	15	0	20	2.65	-1.8 + 0.8	M	18.1	2161.0	407	46.4	13305	878	0.04	14183	1.51	1.37	1.37
K12	B	64	25	15	0	20	2.65	-1.8 + 0.8	M	15.5	2055.4	428	46.1	15083	928	0.04	16012	1.52	1.37	1.38
K13	B	64	25	15	0	20	2.65	-1.8 + 0.8	M	6.2	644.6	454	46.3	16627	981	0.03	17608	1.56	1.37	1.37
K14	B	64	45	15	0	20	2.65	-1.8 + 0.8	M	39.2	2452.7	2678	43.6	6953	6144	0.44	13097	1.53	1.72	1.64
K15	B	64	34	15	0	20	2.65	-1.8 + 0.8	M	11.3	1325.4	567	52.7	15736	1076	0.03	16812	1.65	1.39	1.40
K16	B	64	34	15	0	20	2.65	-1.8 + 0.8	M	29.4	4227.9	623	46.9	15168	1327	0.06	16495	1.61	1.49	1.50
K17	B	64	34	15	0	20	2.65	-1.8 + 0.8	M	10.7	1170.9	635	46.8	15552	1357	0.05	16909	1.64	1.51	1.51
K18	B	64	25	15	0	20	2.65	-1.8 + 0.8	M	25.1	3234.1	337	45.8	13464	736	0.04	14200	1.61	1.50	1.51
L1	B	64	25	15	0	25	2.65	-1.8 + 0.8	F	10.9	1273.7	450	44.9	14853	1002	0.04	15855	1.36	1.29	1.29
L2	B	64	25	15	0	29	2.65	-1.8 + 0.8	F	13.2	1708.1	477	45.1	15524	1056	0.04	16580	1.36	1.29	1.29
L3	B	64	34	15	0	25	2.65	-1.8 + 0.8	F	11.2	1083.0	702	47.4	14459	1479	0.05	15938	1.34	1.28	1.29
L4	B	64	34	15	0	29	2.65	-1.8 + 0.8	F	10.1	1033.0	731	47.9	15900	1528	0.05	17427	1.34	1.29	1.29
L5	B	64	45	15	0	20	2.65	-1.8 + 0.8	F	26.0	532.1	3205	53.5	8364	5996	0.26	14360	1.27	1.27	1.27
L6	B	64	45	15	0	20	2.65	-1.8 + 0.8	F	23.3	248.9	3187	50.5	8457	6313	0.28	14770	1.28	1.27	1.27
L7	B	64	45	15	0	20	2.65	-1.8 + 0.8	F	21.3	1.4	3033	31.0	4491	9790	0.60	14281	1.29	1.26	1.28
L8	B	64	45	15	0	20	2.65	-1.8 + 0.8	F	9.0	0.9	1174	22.2	7750	5300	0.35	13049	1.34	1.25	1.28

D = 165mm; 15° cone

Test No.	D_i	D_o (mm)	D_u (mm)	α (deg.)	BI (mm)	P (kPa)	ρ_{ore} (kg/l)	d_{ore} (mm)	Med grade	C_{vf} (v/v%)	Q_O (l/hr ore)	Q_U (l/hr ore)	C_{mvu} (v/v%)	Q_{OS} (l/hr slurry)	Q_{US} (l/hr slurry)	R_m (v/v)	Q (l/hr)	$\rho_{UF(med)}$ (kg/l)	$\rho_{OF(med)}$ (kg/l)	ρ_{med} (kg/l)
L9	B	64	40	15	0	20	2.65	-1.8 + 0.8	F	21.8	1087.5	2131	49.0	10426	4350	0.19	14776	1.28	1.28	1.28
L10	B	64	45	15	0	20	2.65	-1.8 + 0.8	F	27.2	812.9	3126	50.2	8274	6226	0.29	14500	1.38	1.38	1.38
L11	B	64	34	15	0	20	2.65	-1.8 + 0.8	F	34.7	4115.2	593	48.5	12337	1222	0.07	13559	1.40	1.37	1.38
L12	B	64	34	15	0	25	2.65	-1.8 + 0.8	F	30.2	3933.9	635	48.9	13836	1298	0.06	15135	1.40	1.38	1.38
L13	B	64	34	15	0	29	2.65	-1.8 + 0.8	F	12.0	1293.4	709	48.6	15235	1458	0.05	16693	1.44	1.39	1.39
L14	B	64	25	15	0	20	2.65	-1.8 + 0.8	F	23.7	2866.2	392	47.5	12911	825	0.04	13736	1.41	1.38	1.39
L15	B	64	25	15	0	25	2.65	-1.8 + 0.8	F	22.6	3094.6	408	46.4	14605	878	0.04	15483	1.41	1.39	1.39
L16	B	64	25	15	0	29	2.65	-1.8 + 0.8	F	10.9	1338.8	448	46.8	15431	958	0.03	16389	1.43	1.39	1.39
M1	B	64	45	15	0	20	2.65	-3 + 1	F	22.9	306.7	3031	51.3	8644	5908	0.26	14552	1.30	1.28	1.29
M2	B	64	45	15	0	20	2.65	-3 + 1	F	25.9	634.0	3009	51.2	8188	5878	0.28	14066	1.30	1.28	1.29
M3	B	64	34	15	0	20	2.65	-3 + 1	F	27.1	2981.1	700	51.0	12229	1371	0.07	13600	1.33	1.29	1.29
M4	B	64	34	15	0	25	2.65	-3 + 1	F	17.1	1932.3	694	50.2	13983	1383	0.05	15366	1.38	1.30	1.30
M5	B	64	25	15	0	20	2.65	-3 + 1	F	21.7	2553.3	406	47.7	12796	851	0.04	13647	1.36	1.30	1.30
M6	B	64	25	15	0	20	2.65	-3 + 1	F	23.8	2649.2	394	47.9	11976	823	0.04	12799	1.43	1.37	1.37
M7	B	64	34	15	0	29	2.65	-3 + 1	F	12.7	1439.9	692	50.8	15377	1363	0.05	16740	1.47	1.37	1.37
M8	B	64	34	15	0	25	2.65	-3 + 1	F	25.7	3108.2	680	50.1	13389	1357	0.06	14746	1.42	1.37	1.37
M9	B	64	34	15	0	20	2.65	-3 + 1	F	21.8	2319.6	637	50.1	12263	1271	0.06	13534	1.42	1.37	1.37
M10	B	64	45	15	0	20	2.65	-3 + 1	F	29.3	1018.2	2995	50.1	7730	5978	0.31	13709	1.38	1.36	1.37
M11	B	64	45	15	0	20	2.65	-3 + 1	F	27.4	678.7	3054	55.7	8144	5486	0.25	13630	1.51	1.49	1.50
M12	B	64	34	15	0	30	2.65	-3 + 1	F	24.8	3196.5	663	51.3	14261	1294	0.05	15555	1.54	1.50	1.50
M13	B	64	34	15	0	27	2.65	-3 + 1	F	27.4	3473.2	630	50.7	13731	1243	0.06	14974	1.54	1.49	1.50
M14	B	64	34	15	0	22	2.65	-3 + 1	F	23.1	2661.1	611	51.2	12953	1194	0.05	14147	1.54	1.51	1.51
M15	B	64	25	15	0	22	2.65	-3 + 1	F	29.2	3564.9	370	50.1	12745	738	0.04	13483	1.54	1.51	1.51
M16	B	64	20	15	0	22	2.65	-3 + 1	F	26.3	3383.2	215	47.0	13229	458	0.02	13687	1.55	1.51	1.51
M17	B	64	30	15	0	22	2.65	-3 + 1	F	24.0	2892.1	473	50.7	13067	932	0.04	13999	1.55	1.51	1.51
M18	B	64	40	15	0	22	2.65	-3 + 1	F	19.5	1051.9	1652	54.1	10818	3055	0.13	13873	1.53	1.51	1.51

D = 165mm; 15° cone

Test No.	D_i	D_o (mm)	D_u (mm)	α (deg.)	BI (mm)	P (kPa)	ρ_{ore} (kg/l)	d_{ore} (mm)	Med grade	C_{vf} (v/v%)	Q_O (l/hr ore)	Q_U (l/hr ore)	C_{mvu} (v/v%)	Q_{OS} (l/hr slurry)	Q_{US} (l/hr slurry)	R_m (v/v)	Q (l/hr)	$\rho_{UF(med)}$ (kg/l)	$\rho_{OF(med)}$ (kg/l)	ρ_{med} (kg/l)
N1	B	64	45	15	0	20	2.65	-3 + 1	M	30.0	718.9	3177	53.1	7024	5980	0.31	13004	1.35	1.27	1.29
N2	B	64	34	15	0	20	2.65	-3 + 1	M	30.5	3134.8	712	52.4	11271	1358	0.07	12629	1.39	1.28	1.29
N3	B	64	25	15	0	20	2.65	-3 + 1	M	29.1	3298.7	425	48.3	11917	881	0.05	12798	1.40	1.29	1.29
N4	B	64	25	15	0	20	2.65	-3 + 1	M	27.3	2995.1	407	48.4	11616	842	0.05	12458	1.50	1.37	1.38
N5	B	64	34	15	0	20	2.65	-3 + 1	M	28.6	2914.8	661	51.3	11200	1289	0.07	12489	1.50	1.37	1.38
N6	B	64	45	15	0	20	2.65	-3 + 1	M	25.4	277.0	3252	51.5	7603	6308	0.29	13910	1.42	1.36	1.38
N7	B	64	45	15	0	22	2.65	-3 + 1	M	40.1	1505.1	3253	56.9	6143	5716	0.35	11859	1.75	1.57	1.63
N8	B	64	34	15	0	22	2.65	-3 + 1	M	16.7	1963.7	596	46.4	14046	1286	0.05	15331	1.43	1.41	1.42
N9	B	64	25	15	0	22	2.65	-3 + 1	M	25.2	3116.6	366	48.3	13057	757	0.04	13814	1.59	1.48	1.49
O1	B	64	45	15	0	22	2.65	-1.8 + 0.8	F	32.6	1536.6	3063	49.2	7893	6228	0.33	14121	1.50	1.45	1.46
O2	B	64	34	15	0	22	2.65	-1.8 + 0.8	F	24.2	2865.8	538	47.7	12940	1128	0.06	14068	1.55	1.46	1.47
O3	B	64	25	15	0	22	2.65	-1.8 + 0.8	F	30.5	3768.6	358	46.4	12779	771	0.04	13550	1.56	1.46	1.47
O4	B	64	25	15	0	25	2.65	-1.8 + 0.8	F	15.7	1889.2	301	47.1	13292	639	0.03	13932	1.74	1.67	1.67
O5	B	64	34	15	0	25	2.65	-1.8 + 0.8	F	15.3	1686.4	468	48.0	13087	976	0.04	14062	1.73	1.66	1.67
O6	B	64	45	15	0	25	2.65	-1.8 + 0.8	F	26.2	855.1	2960	47.2	8319	6264	0.31	14583	1.68	1.65	1.66
P1	B	64	34	15	0	22	2.65	-1.8 + 0.8	C	30.6	3611.1	349	46.8	12191	745	0.04	12936	1.89	1.62	1.63
P2	B	64	34	15	0	27	2.65	-1.8 + 0.8	C	36.7	4867.9	362	47.0	13466	770	0.05	14237	1.93	1.62	1.63
P3	B	64	34	15	0	31	2.65	-1.8 + 0.8	C	40.0	5677.1	398	47.3	14333	840	0.05	15173	1.91	1.61	1.63
P4	B	64	25	15	0	22	2.65	-1.8 + 0.8	C	33.2	4034.4	229	45.8	12360	501	0.03	12861	1.91	1.62	1.63
P5	B	64	45	15	0	22	2.65	-3 + 1	C	28.6	722.7	3151	50.2	7263	6273	0.32	13535	1.73	1.58	1.63
P6	B	64	34	15	0	22	2.65	-3 + 1	C	28.1	3182.6	507	49.6	12087	1021	0.05	13108	1.83	1.62	1.63
P7	B	64	34	15	0	27	2.65	-3 + 1	C	29.3	3801.3	506	49.5	13654	1022	0.05	14676	1.86	1.61	1.62
P8	B	64	34	15	0	31	2.65	-3 + 1	C	35.2	5107.0	499	49.5	14908	1008	0.05	15916	1.88	1.60	1.61
P9	B	64	25	15	0	22	2.65	-3 + 1	C	24.1	2886.3	310	48.0	12639	644	0.03	13283	1.85	1.62	1.63
Q1	A	64	25	15	0	25	2.65	-1.8 + 0.8	F	15.3	2848.9	526	46.0	20950	1143	0.03	22094	1.49	1.37	1.38
Q2	A	64	34	15	0	25	2.65	-1.8 + 0.8	F	14.4	2401.1	803	47.3	20562	1699	0.05	22261	1.48	1.37	1.38

D = 165mm; 15° cone

Test No.	D_i	D_o (mm)	D_u (mm)	α (deg.)	Bl (mm)	P (kPa)	ρ_{ore} (kg/l)	d_{ore} (mm)	Med grade	C_{vf} (v/v%)	Q_O (l/hr ore)	Q_U (l/hr ore)	C_{mvu} (v/v%)	Q_{OS} (l/hr slurry)	Q_{US} (l/hr slurry)	R_m (v/v)	Q (l/hr)	$\rho_{UF(med)}$ (kg/l)	$\rho_{OF(med)}$ (kg/l)	ρ_{med} (kg/l)
Q3	A	64	45	15	0	25	2.65	-1.8 + 0.8	F	18.1	32.0	3923	47.6	13582	8240	0.24	21822	1.41	1.36	1.37
Q4	A	64	45	15	0	25	2.65	-1.8 + 0.8	F	18.5	196.2	3896	46.8	13790	8325	0.25	22115	1.50	1.47	1.48
Q5	A	64	34	15	0	25	2.65	-1.8 + 0.8	F	20.6	3570.1	744	46.4	19343	1602	0.05	20945	1.55	1.48	1.48
Q6	A	64	25	15	0	25	2.65	-1.8 + 0.8	F	17.8	3394.7	491	45.1	20788	1088	0.03	21876	1.57	1.48	1.48
Q7	A	64	25	15	0	25	2.65	-1.8 + 0.8	F	7.4	982.8	499	45.2	18807	1104	0.03	19911	1.75	1.69	1.69
Q8	A	64	34	15	0	25	2.65	-1.8 + 0.8	F	11.6	1601.8	793	46.4	18900	1710	0.05	20610	1.73	1.69	1.69
Q9	A	64	45	15	0	25	2.65	-1.8 + 0.8	F	19.8	525.7	3856	46.1	13820	8358	0.25	22179	1.71	1.69	1.69
Q10	A	53	45	15	0	25	2.65	-1.8 + 0.8	F	22.9	461.1	4425	46.1	11782	9597	0.31	21380	1.69	1.69	1.69
Q11	A	53	34	15	0	25	2.65	-1.8 + 0.8	F	21.6	3964.6	788	45.6	20252	1727	0.05	21979	1.73	1.69	1.69
Q12	A	53	25	15	0	25	2.65	-1.8 + 0.8	F	18.4	3500.3	508	44.4	20614	1146	0.04	21761	1.73	1.70	1.70
Q13	A	40	25	15	0	25	2.65	-1.8 + 0.8	F	16.8	2679.9	621	44.1	18270	1406	0.05	19676	1.73	1.70	1.70
Q14	A	40	34	15	0	25	2.65	-1.8 + 0.8	F	19.1	2637.1	1012	46.5	16914	2174	0.08	19088	1.73	1.70	1.71
Q15	A	40	45	15	0	25	2.65	-1.8 + 0.8	F	25.1	830.0	4523	46.1	11504	9814	0.33	21318	1.71	1.71	1.71
Q16	A	40	34	15	0	25	2.65	-5 + 3	F	15.5	2110.3	1126	46.9	18500	2401	0.07	20901	1.73	1.72	1.72
Q17	A	40	25	15	0	25	2.65	-5 + 3	F	20.5	2993.2	631	43.4	16220	1455	0.06	17675	1.73	1.71	1.72
Q18	A	64	25	15	0	25	2.65	-5 + 3	F	9.0	1301.3	524	44.4	19152	1179	0.04	20331	1.75	1.72	1.72
Q19	A	64	34	15	0	25	2.65	-5 + 3	F	13.0	1863.7	921	47.0	19448	1960	0.06	21408	1.74	1.72	1.72
R1	B	40	45	15	0	20	2.65	-1.8 + 0.8	C	34.7	857.2	3385	47.0	5013	7199	0.48	12211	1.34	1.25	1.29
R2	B	40	34	15	0	20	2.65	-1.8 + 0.8	C	33.7	3066.7	829	45.2	9728	1834	0.13	11562	1.41	1.28	1.30
R3	B	40	25	15	0	20	2.65	-1.8 + 0.8	C	32.3	3228.3	547	43.6	10439	1254	0.09	11692	1.43	1.28	1.30
R4	B	64	25	15	0	20	2.65	-1.8 + 0.8	C	21.0	2456.1	413	44.0	12736	937	0.05	13673	1.48	1.29	1.30
R5	B	64	34	15	0	20	2.65	-1.8 + 0.8	C	21.3	2249.4	670	47.2	12269	1421	0.07	13690	1.48	1.28	1.29
R6	B	64	45	15	0	20	2.65	-1.8 + 0.8	C	29.8	543.8	3481	49.2	6437	7074	0.38	13511	1.35	1.26	1.29
R7	B	64	45	15	0	20	2.65	-1.8 + 0.8	C	33.2	950.3	3439	48.9	6183	7039	0.41	13222	1.45	1.34	1.38
R8	B	64	34	15	0	20	2.65	-1.8 + 0.8	C	24.4	2608.9	655	47.0	11989	1393	0.07	13382	1.54	1.36	1.37
R9	B	64	25	15	0	20	2.65	-1.8 + 0.8	C	21.5	2555.0	419	44.6	12886	940	0.05	13826	1.55	1.36	1.37
R10	B	64	25	15	0	25	2.65	-1.8 + 0.8	C	12.5	1348.7	326	45.3	12729	720	0.03	13449	1.94	1.70	1.71
R11	B	64	34	15	0	25	2.65	-1.8 + 0.8	C	17.2	1853.3	499	45.8	12613	1090	0.05	13703	1.90	1.69	1.70
R12	B	64	45	15	0	25	2.65	-1.8 + 0.8	C	29.9	1292.5	3071	46.5	7983	6607	0.35	14590	1.78	1.65	1.70

7.2.2. Data for tests performed with 20° cone (cone A).

D = 165mm; 20° cone (cone A)

Test No.	D_i	D_o (mm)	D_u (mm)	α (deg.)	Bl (mm)	P (kPa)	ρ_{ore} (kg/l)	d_{ore} (mm)	Med grade	C_{vf} (v/v%)	Q_O (l/hr ore)	Q_U (l/hr ore)	C_{mvu} (v/v%)	Q_{OS} (l/hr slurry)	Q_{US} (l/hr slurry)	R_m (v/v)	Q (l/hr)	$\rho_{UF(med)}$ (kg/l)	$\rho_{OF(med)}$ (kg/l)	ρ_{med} (kg/l)
S8	B	40	45	20	200	22	2.65	-1.8 + 0.8	M	33.0	351.8	3506	50.1	4697	6999	0.45	11696	1.27	1.28	1.28
S9	B	53	45	20	200	20	2.65	-1.8 + 0.8	M	31.2	123.9	3434	52.1	4825	6596	0.40	11421	1.27	1.28	1.28
S10	B	64	45	20	200	20	2.65	-1.8 + 0.8	M	30.9	192.1	3307	48.3	4460	6848	0.45	11307	1.27	1.28	1.27
T1	B	64	45	20	0	20	2.65	-1.8 + 0.8	M	26.6	327.5	3017	50.7	6611	5956	0.32	12567	1.30	1.25	1.27
T2	B	64	34	20	0	20	2.65	-1.8 + 0.8	M	25.7	1384.6	1644	46.8	8273	3511	0.21	11784	1.30	1.25	1.26
T3	B	64	25	20	0	20	2.65	-1.8 + 0.8	M	24.2	2030.2	773	46.5	9898	1662	0.10	11561	1.33	1.29	1.29
T4	B	64	25	20	200	20	2.65	-1.8 + 0.8	M	19.6	1604.9	801	45.4	10499	1763	0.10	12262	1.30	1.28	1.28
T5	B	64	34	20	200	20	2.65	-1.8 + 0.8	M	21.6	776.0	1937	57.0	9178	3400	0.15	12577	1.32	1.24	1.25
T6	B	64	45	20	200	20	2.65	-1.8 + 0.8	M	35.5	845.7	3307	45.9	4506	7207	0.52	11713	1.24	1.31	1.27
U1	B	64	34	20	200	20	2.65	-1.8 + 0.8	M	22.5	789.0	1749	49.0	7734	3570	0.21	11304	1.29	1.27	1.27
U2	B	64	25	20	200	20	2.65	-1.8 + 0.8	M	19.0	1350.5	856	47.0	9770	1820	0.10	11590	1.29	1.27	1.27
U3	B	64	25	20	200	25	2.65	-1.8 + 0.8	M	16.1	1257.4	854	46.4	11268	1843	0.09	13111	1.41	1.36	1.36
U4	B	64	25	20	200	30	2.65	-1.8 + 0.8	M	16.1	1540.9	855	45.9	13040	1864	0.08	14904	1.43	1.36	1.36
U5	B	64	34	20	200	25	2.65	-1.8 + 0.8	M	17.2	477.4	1735	48.7	9274	3565	0.17	12839	1.39	1.36	1.36
U6	B	64	34	20	200	30	2.65	-1.8 + 0.8	M	18.0	803.1	1803	48.9	10806	3684	0.16	14489	1.41	1.36	1.37
U7	B	64	45	20	200	20	2.65	-1.8 + 0.8	M	33.5	25.5	3364	54.2	3916	6208	0.42	10124	1.37	1.35	1.36
V1	B	64	25	20	0	25	2.65	-1.8 + 0.8	M	16.3	1119.8	839	46.5	10180	1804	0.10	11984	1.39	1.28	1.29
V2	B	64	34	20	0	25	2.65	-1.8 + 0.8	M	20.5	664.8	1740	48.0	8134	3623	0.20	11757	1.36	1.27	1.29
V3	B	64	45	20	0	25	2.65	-1.8 + 0.8	M	34.3	742.1	3268	49.8	5119	6564	0.43	11683	1.32	1.26	1.28
V4	B	64	45	20	0	25	2.65	-1.8 + 0.8	M	33.2	572.3	3276	48.8	4886	6709	0.44	11596	1.39	1.34	1.36
V5	B	64	34	20	0	25	2.65	-1.8 + 0.8	M	28.0	1471.9	1775	49.9	8047	3560	0.21	11607	1.43	1.36	1.37
V6	B	64	25	20	0	25	2.65	-1.8 + 0.8	M	21.8	1795.8	838	46.5	10263	1801	0.10	12064	1.44	1.36	1.37
X1	B	64	45	20	0	30	2.65	-1.8 + 0.8	F	31.5	798.2	3598	50.7	6867	7096	0.37	13963	1.30	1.27	1.28
X2	B	64	34	20	0	25	2.65	-1.8 + 0.8	F	26.9	1079.5	2032	46.3	7157	4390	0.28	11546	1.29	1.27	1.27
X3	B	64	34	20	0	30	2.65	-1.8 + 0.8	F	26.3	1779.0	2145	47.5	10434	4511	0.21	14946	1.30	1.27	1.27
X4	B	64	34	20	0	36	2.65	-1.8 + 0.8	F	20.4	1139.0	2267	47.7	11911	4747	0.19	16658	1.31	1.27	1.28

D = 165mm; 20° cone (cone A)

Test No.	D_i	D_o (mm)	D_u (mm)	α (deg.)	BI (mm)	P (kPa)	ρ_{ore} (kg/l)	d_{ore} (mm)	Med grade	C_{vf} (v/v%)	Q_O (l/hr ore)	Q_U (l/hr ore)	C_{mvu} (v/v%)	Q_{OS} (l/hr slurry)	Q_{US} (l/hr slurry)	R_m (v/v)	Q (l/hr)	$\rho_{UF(med)}$ (kg/l)	$\rho_{OF(med)}$ (kg/l)	ρ_{med} (kg/l)
X5	B	64	25	20	0	25	2.65	-1.8 + 0.8	F	16.8	1193.6	874	43.3	10263	2015	0.11	12279	1.33	1.28	1.29
X6	B	64	25	20	0	30	2.65	-1.8 + 0.8	F	15.1	1303.6	933	43.1	12630	2165	0.10	14795	1.34	1.29	1.29
X7	B	64	25	20	0	36	2.65	-1.8 + 0.8	F	10.9	777.1	980	42.9	13790	2284	0.09	16073	1.36	1.28	1.29
X8	B	64	25	20	0	29	2.65	-1.8 + 0.8	F	15.3	987.9	778	44.5	9792	1750	0.10	11542	1.70	1.65	1.66
X9	B	64	25	20	0	35	2.65	-1.8 + 0.8	F	26.2	3006.4	841	47.6	12929	1767	0.09	14696	1.77	1.53	1.55
X10	B	64	25	20	0	42	2.65	-1.8 + 0.8	F	27.5	3731.1	824	44.2	14681	1864	0.09	16545	1.60	1.52	1.52
X11	B	64	34	20	0	29	2.65	-1.8 + 0.8	F	20.3	731.3	1903	46.4	8877	4099	0.21	12977	1.53	1.52	1.52
X12	B	64	34	20	0	35	2.65	-1.8 + 0.8	F	19.0	963.3	2017	46.4	11301	4350	0.18	15651	1.55	1.51	1.52
X13	B	64	34	20	0	42	2.65	-1.8 + 0.8	F	19.4	1178.4	2038	45.8	12105	4448	0.18	16552	1.65	1.52	1.54
X14	B	64	45	20	0	35	2.65	-1.8 + 0.8	F	28.6	973.8	3269	46.5	7781	7036	0.36	14817	1.51	1.50	1.50
X15	B	64	45	20	0	39	2.65	-1.8 + 0.8	F	27.2	1424.7	3028	40.9	8962	7407	0.37	16368	1.45	1.71	1.61
X16	B	64	34	20	0	33	2.65	-1.8 + 0.8	F	24.9	1764.2	1556	44.9	9854	3469	0.19	13323	1.73	1.73	1.73
X17	B	64	34	20	0	39	2.65	-1.8 + 0.8	F	26.0	2298.6	1535	45.4	11367	3384	0.17	14751	1.74	1.77	1.76
X18	B	64	34	20	0	47	2.65	-1.8 + 0.8	F	27.8	3008.5	1644	44.9	13065	3661	0.17	16727	1.74	1.74	1.74
X19	B	64	25	20	0	33	2.65	-1.8 + 0.8	F	27.0	2785.8	709	43.4	11334	1634	0.10	12968	1.73	1.74	1.74
X20	B	64	25	20	0	39	2.65	-1.8 + 0.8	F	25.6	3087.9	709	46.1	13317	1538	0.07	14856	1.86	1.76	1.77
X21	B	64	25	20	0	47	2.65	-1.8 + 0.8	F	25.4	3466.7	722	43.3	14836	1669	0.08	16505	1.75	1.75	1.75
Y1	B	53	45	20	0	30	2.65	-1.8 + 0.8	F	30.4	1026.7	3345	46.9	7241	7129	0.38	14370	1.30	1.28	1.29
Y2	B	53	34	20	0	25	2.65	-1.8 + 0.8	F	29.4	1789.9	1915	46.9	8532	4081	0.24	12612	1.30	1.27	1.28
Y3	B	53	34	20	0	30	2.65	-1.8 + 0.8	F	25.2	1769.8	1950	44.8	10420	4352	0.22	14772	1.30	1.28	1.28
Y4	B	53	34	20	0	36	2.65	-1.8 + 0.8	F	21.5	1294.8	2125	45.2	11187	4703	0.21	15890	1.32	1.29	1.29
Y5	B	53	25	20	0	25	2.65	-1.8 + 0.8	F	16.5	1235.6	879	44.4	10816	1979	0.10	12795	1.33	1.29	1.30
Y6	B	53	25	20	0	30	2.65	-1.8 + 0.8	F	18.4	1743.8	913	43.7	12320	2086	0.10	14407	1.34	1.29	1.30
Y7	B	53	25	20	0	36	2.65	-1.8 + 0.8	F	23.1	2526.1	943	43.2	12823	2182	0.11	15005	1.35	1.29	1.30
Y8	B	40	25	20	0	25	2.65	-1.8 + 0.8	F	28.9	2267.8	929	42.8	8905	2169	0.16	11073	1.32	1.29	1.30
Y9	B	40	25	20	0	30	2.65	-1.8 + 0.8	F	24.5	2285.5	1008	42.9	11091	2347	0.13	13438	1.33	1.30	1.30

D = 165mm; 20° cone (cone A)

Test No.	D_i	D_o (mm)	D_u (mm)	α (deg.)	BI (mm)	P (kPa)	ρ_{ore} (kg/l)	d_{ore} (mm)	Med grade	C_{vf} (v/v%)	Q_O (l/hr ore)	Q_U (l/hr ore)	C_{mvu} (v/v%)	Q_{OS} (l/hr slurry)	Q_{US} (l/hr slurry)	R_m (v/v)	Q (l/hr)	$\rho_{UF(med)}$ (kg/l)	$\rho_{OF(med)}$ (kg/l)	ρ_{med} (kg/l)
Y10	B	40	25	20	0	36	2.65	-1.8 + 0.8	F	22.6	2267.0	1098	43.8	12382	2505	0.12	14887	1.33	1.29	1.29
Y11	B	40	34	20	0	25	2.65	-1.8 + 0.8	F	23.2	918.2	1967	45.0	8088	4375	0.25	12462	1.30	1.29	1.29
Y12	B	40	34	20	0	30	2.65	-1.8 + 0.8	F	22.5	1033.9	2145	45.6	9402	4703	0.23	14105	1.31	1.29	1.29
Y13	B	40	34	20	0	36	2.65	-1.8 + 0.8	F	24.0	1485.7	2255	45.3	10622	4972	0.23	15593	1.31	1.29	1.29
Y14	B	40	40	20	0	25	2.65	-1.8 + 0.8	F	29.9	984.5	2624	47.2	6521	5556	0.35	12077	1.30	1.28	1.29
Y15	B	40	40	20	0	30	2.65	-1.8 + 0.8	F	27.6	1136.6	2772	46.0	8130	6033	0.32	14162	1.30	1.29	1.29
Y16	B	40	40	20	0	36	2.65	-1.8 + 0.8	F	26.4	1201.6	2876	45.6	9153	6311	0.30	15464	1.30	1.30	1.30
Y17	A	64	34	20	0	25	2.65	-1.8 + 0.8	F	22.3	2523.9	1977	46.4	15896	4266	0.15	20161	1.31	1.31	1.31
Y18	A	64	34	20	0	30	2.65	-1.8 + 0.8	F	10.9	121.6	2136	45.6	16109	4683	0.14	20793	1.33	1.31	1.31
Y19	A	64	25	20	0	25	2.65	-1.8 + 0.8	F	10.4	1120.9	937	44.5	17717	2107	0.07	19824	1.34	1.34	1.34
Y20	A	64	25	20	0	30	2.65	-1.8 + 0.8	F	13.0	1652.0	1104	46.4	18749	2379	0.07	21128	1.36	1.34	1.34
Y21	A	40	25	20	0	25	2.65	-1.8 + 0.8	F	13.6	1428.4	1134	43.1	16269	2632	0.09	18901	1.32	1.31	1.31
Y22	A	40	25	20	0	30	2.65	-1.8 + 0.8	F	15.7	1881.5	1276	44.2	17234	2888	0.10	20122	1.34	1.32	1.32
Y23	A	40	34	20	0	25	2.65	-1.8 + 0.8	F	25.2	2517.6	2399	47.0	14422	5105	0.19	19527	1.31	1.31	1.31

7.2.3. Data for tests performed with 20° cone (cone B).

D = 165mm; 20° cone (cone B)

Test No.	D_i	D_o (mm)	D_u (mm)	α (deg.)	Bl (mm)	P (kPa)	ρ_{ore} (kg/l)	d_{ore} (mm)	Med grade	C_{vf} (v/v%)	Q_O (l/hr ore)	Q_U (l/hr ore)	C_{mvu} (v/v%)	Q_{OS} (l/hr slurry)	Q_{US} (l/hr slurry)	R_m (v/v)	Q (l/hr)	$\rho_{UF(med)}$ (kg/l)	$\rho_{OF(med)}$ (kg/l)	ρ_{med} (kg/l)
S1	B	40	45	20	200	20	2.65	-1.8 + 0.8	F	31.28	391.92	4099.59	47.45	5720.51	8639.24	0.46	14359.75	1.28	1.27	1.28
S2	B	64	45	20	200	20	2.65	-1.8 + 0.8	F	32.32	126.29	3817.91	47.40	4148.89	8054.29	0.51	12203.18	1.29	1.29	1.29
S3	B	64	45	20	200	20	2.65	-1.8 + 0.8	F	34.19	253.23	3728.38	48.84	4010.80	7634.30	0.51	11645.10	1.39	1.38	1.39
S4	B	53	45	20	200	20	2.65	-1.8 + 0.8	F	31.01	183.47	3770.21	47.38	4791.36	7957.44	0.48	12748.80	1.37	1.38	1.38
S5	B	40	45	20	200	20	2.65	-1.8 + 0.8	F	35.74	212.02	4004.94	49.78	3752.83	8044.65	0.53	11797.48	1.38	1.38	1.38
S6	B	64	45	20	200	22	2.65	-1.8 + 0.8	F	35.49	432.59	3801.22	49.91	4313.84	7615.73	0.50	11929.57	1.47	1.49	1.48
S7	B	64	45	20	200	30	2.65	-1.8 + 0.8	F	29.05	360.68	3566.04	47.56	6019.54	7498.18	0.41	13517.72	1.65	1.67	1.66

7.2.4. Data for tests performed with the 350mm cyclone.

D = 350mm; D_i = 70mm; D_o = 151mm; $\alpha = 20^o$; Bl = None.
Medium grade = F; Ore = Silica (2.65kg/l); d_{ore} = -5+3mm

Test No.	D_u (mm)	ρ_{med} (kg/l)	P (kPa)	Q_{UM} (kg/s ore)	STD Dev (kg/s)	Q_{UM} (l/hr ore)
09-4	100	1.5	70	12.43	0.04	16887
09-5	100	1.5	90	12.41	0.04	16860
09-6	100	1.3	65	12.63	0.00	17160
09-7	90	1.7	80	9.92	0.19	13477
09-8	90	1.7	100	10.00	0.39	13587
09-10	90	1.5	70	10.64	0.34	14452
09-11	90	1.5	90	11.85	0.16	16101
09-13	90	1.3	65	9.75	0.34	13244
09-16	75	1.7	80	8.04	0.01	10923
09-19	75	1.5	70	8.75	0.29	11884
09-22	75	1.3	65	8.21	0.08	11154
09-23	75	1.3	70	8.96	0.65	12173
09-25	60	1.7	80	4.82	0.11	6548
09-28	60	1.5	70	5.69	0.02	7731
09-29	60	1.5	90	7.08	0.30	9615
09-30	60	1.5	60	5.37	0.24	7298
09-31	60	1.3	60	4.86	0.09	6599
09-32	60	1.3	80	5.96	0.02	8097
09-33	60	1.3	70	5.69	0.77	7727

7.3. Appendix C. Raw Data and Experimental Conditions

7.3.1. Raw data for tests performed with 15° cone.

D = 165mm; 15° cone

										Floats				Sinks			
Test No.	D_i	D_o (mm)	D_u (mm)	α (deg.)	Bl (mm)	P (kPa)	ρ_{ore} (kg/l)	d_{ore} (mm)	Med grade	Flow-rate (kg/s)	ρ_{slurry} (kg/l)	C_{vo} (v/v%)	ρ_{medium} (kg/l)	Flow-rate (kg/s)	ρ_{slurry} (kg/l)	C_{vu} (v/v%)	ρ_{medium} (kg/l)
A1	B	64	45	15	0	20	2.65	-1.8 + 0.8	F	2.67	1.20	0.00	1.20	1.14	1.79	1.64	1.77
A2	B	64	45	15	0	25	2.65	-1.8 + 0.8	F	2.93	1.18	0.00	1.18	1.20	1.91	3.21	1.88
A3	B	64	45	15	0	30	2.65	-1.8 + 0.8	F	3.45	1.17	0.00	1.18	1.30	2.02	3.36	2.15
A4	B	64	34	15	0	30	2.65	-1.8 + 0.8	F	3.61	1.18	0.00	1.17	1.11	2.19	5.71	2.00
A5	B	64	45	15	0	20	2.65	-1.8 + 0.8	F	3.22	1.39	0.00	1.39	1.36	1.92	1.14	1.90
A6	B	64	45	15	0	25	2.65	-1.8 + 0.8	F	3.55	1.39	0.00	1.37	1.41	1.99	0.31	1.97
A7	B	64	45	15	0	30	2.65	-1.8 + 0.8	F	4.06	1.38	0.00	1.38	1.55	2.11	4.04	2.06
A8	B	64	45	15	0	20	2.65	-1.8 + 0.8	F	3.61	1.58	0.00	1.59	1.43	1.94	0.12	1.95
A9	B	64	45	15	0	25	2.65	-1.8 + 0.8	F	4.25	1.59	0.00	1.59	1.50	2.04	0.01	2.04
A10	B	64	45	15	0	30	2.65	-1.8 + 0.8	F	4.57	1.60	0.00	1.61	1.58	2.10	1.91	2.10
A11	B	64	20	15	0	20	2.65	-1.8 + 0.8	F	3.63	1.13	0.00	1.17	0.81	1.98	13.42	1.73
A12	B	64	34	15	0	20	2.65	-1.8 + 0.8	F	3.34	1.21	0.00	1.20	1.49	1.95	25.69	1.88
A13	B	40	20	15	0	20	2.65	-1.8 + 0.8	F	2.08	1.19	0.00	1.18	0.70	2.42	6.69	2.37
A14	B	40	34	15	0	20	2.65	-1.8 + 0.8	F	1.54	1.15	0.00	1.15	1.46	1.57	1.33	1.54
A15	B	40	45	15	0	20	2.65	-1.8 + 0.8	F	0.88	1.18	0.00	1.18	2.45	1.43	4.50	1.38
A16	B	53	20	15	0	20	2.65	-1.8 + 0.8	F	2.89	1.20	0.00	1.20	0.76	2.17	3.80	2.08
A17	B	53	34	15	0	20	2.65	-1.8 + 0.8	F	2.32	1.16	0.00	1.15	1.16	1.81	9.60	1.73
A18	B	53	45	15	0	20	2.65	-1.8 + 0.8	F	2.05	1.16	0.00	1.16	1.56	1.66	2.28	1.64

NB: A-inlet – 70x25 mm^2 and B-inlet – 70x10mm^2.

D = 165mm; 15° cone

										Floats				Sinks			
Test No.	D_i	D_o (mm)	D_u (mm)	α (deg.)	Bl (mm)	P (kPa)	ρ_{ore} (kg/l)	d_{ore} (mm)	Med grade	Flow-rate (kg/s)	ρ_{slurry} (kg/l)	C_{vo} (v/v%)	ρ_{medium} (kg/l)	Flow-rate (kg/s)	ρ_{slurry} (kg/l)	C_{vu} (v/v%)	ρ_{medium} (kg/l)
B1	B	53	45	15	0	20	2.65	-1.8 + 0.8	F	2.35	1.15	0.00	1.15	1.63	1.61	3.99	1.56
B2	B	53	45	15	0	20	2.65	-1.8 + 0.8	F	2.34	1.15	0.00	1.15	1.71	1.63	6.25	1.55
B3	B	53	45	15	0	20	2.65	-1.8 + 0.8	F	2.32	1.16	0.01	1.15	1.76	1.66	8.67	1.56
B4	B	53	45	15	0	20	2.65	-1.8 + 0.8	F	2.47	1.16	0.00	1.16	1.99	1.68	10.58	1.55
B5	B	53	45	15	0	20	2.65	-1.8 + 0.8	F	2.37	1.16	0.01	1.16	1.94	1.69	11.82	1.55
B6	B	53	45	15	0	20	2.65	-1.8 + 0.8	F	2.34	1.16	0.01	1.16	2.05	1.69	12.82	1.54
B7	B	53	45	15	0	20	2.65	-1.8 + 0.8	F	2.35	1.15	0.02	1.15	2.17	1.73	16.42	1.54
B8	B	53	45	15	0	20	2.65	-1.8 + 0.8	F	2.31	1.18	0.02	1.18	2.77	1.77	25.32	1.46
C1	B	64	45	15	0	20	2.65	-1.8 + 0.8	F	2.72	1.19	0.00	1.19	1.62	1.79	17.33	1.61
C2	B	64	45	15	0	20	2.65	-1.8 + 0.8	F	2.53	1.18	0.00	1.18	2.06	1.78	22.39	1.53
C3	B	64	45	15	0	20	2.65	-1.8 + 0.8	F	2.55	1.19	0.00	1.19	2.17	1.75	20.41	1.52
C4	B	64	45	15	0	20	2.65	-1.8 + 0.8	F	2.11	1.19	0.00	1.19	2.86	1.75	25.34	1.44
C5	B	64	45	15	0	20	2.65	-1.8 + 0.8	F	1.78	1.20	0.00	1.20	3.33	1.76	29.38	1.39
C6	B	64	45	15	0	20	2.65	-1.8 + 0.8	F	1.07	1.22	0.00	1.22	4.38	1.52	17.01	1.29
C7	B	64	34	15	0	20	2.65	-1.8 + 0.8	F	3.33	1.19	0.00	1.19	1.04	1.99	13.65	1.88
C8	B	64	34	15	0	20	2.65	-1.8 + 0.8	F	3.32	1.18	0.00	1.18	1.06	2.01	13.72	1.91
C9	B	64	34	15	0	20	2.65	-1.8 + 0.8	F	3.28	1.19	0.00	1.19	1.22	2.02	21.86	1.84
C10	B	64	25	15	0	20	2.65	-1.8 + 0.8	F	3.47	1.21	0.00	1.21	1.00	2.13	30.80	1.89
C11	B	64	25	15	0	20	2.65	-1.8 + 0.8	F	3.49	1.21	0.00	1.21	0.91	2.14	26.23	1.96

D = 165mm; 15° cone

										Floats				Sinks			
Test No.	D_i	D_o (mm)	D_u (mm)	α (deg.)	Bl (mm)	P (kPa)	ρ_{ore} (kg/l)	d_{ore} (mm)	Med grade	Flow-rate (kg/s)	ρ_{slurry} (kg/l)	C_{vo} (v/v%)	ρ_{medium} (kg/l)	Flow-rate (kg/s)	ρ_{slurry} (kg/l)	C_{vu} (v/v%)	ρ_{medium} (kg/l)
D1	B	53	45	15	0	20	2.65	-1.8 + 0.8	F	2.13	1.14	0.00	1.14	1.86	1.68	14.58	1.52
D2	B	53	45	15	0	20	2.65	-1.8 + 0.8	F	2.08	1.14	0.00	1.14	2.00	1.72	17.15	1.52
D3	B	53	45	15	0	20	2.65	-1.8 + 0.8	F	2.06	1.14	0.00	1.14	2.17	1.66	14.10	1.50
D4	B	53	45	15	0	20	2.65	-1.8 + 0.8	F	2.05	1.15	0.00	1.15	2.54	1.70	22.60	1.42
D5	B	53	45	15	0	20	2.65	-1.8 + 0.8	F	1.95	1.15	0.00	1.15	2.80	1.78	28.37	1.43
D6	B	53	45	15	0	20	2.65	-1.8 + 0.8	F	1.12	1.19	0.00	1.19	3.84	1.53	17.71	1.29
D7	B	53	34	15	0	20	2.65	-1.8 + 0.8	F	4.54	1.31	3.40	1.26	0.88	1.98	45.31	1.42
D8	B	53	34	15	0	20	2.65	-1.8 + 0.8	F	2.53	1.16	0.00	1.16	1.56	1.75	15.81	1.58
D9	B	53	34	15	0	20	2.65	-1.8 + 0.8	F	2.52	1.15	0.00	1.15	1.28	1.78	10.47	1.68
D10	B	53	34	15	0	20	2.65	-1.8 + 0.8	F	2.60	1.14	0.00	1.14	1.22	1.79	6.77	1.73
D11	B	53	25	15	0	20	2.65	-1.8 + 0.8	F	2.82	1.17	0.00	1.17	0.99	2.02	21.87	1.84
E1	B	53	45	15	0	20	2.65	-1.8 + 0.8	F	2.14	1.20	0.00	1.20	1.89	1.52	10.65	1.39
E2	B	53	45	15	0	20	2.65	-1.8 + 0.8	F	0.88	1.26	0.08	1.26	4.85	1.64	27.49	1.26
E3	B	53	45	15	0	20	2.65	-1.8 + 0.8	F	2.93	1.32	4.45	1.26	3.41	1.97	51.01	1.27
E4	B	53	45	15	0	20	2.65	-1.8 + 0.8	F	2.68	1.35	6.44	1.26	3.59	1.96	50.40	1.26
E5	B	53	45	15	0	20	2.65	-1.8 + 0.8	F	3.04	1.35	6.90	1.25	3.35	1.96	50.50	1.26
E6	B	53	45	15	0	20	2.65	-1.8 + 0.8	F	3.04	1.34	4.99	1.27	3.37	1.98	51.26	1.27
E7	B	53	45	15	0	20	2.65	-1.8 + 0.8	F	2.68	1.27	0.92	1.26	3.54	1.97	50.41	1.27
E8	B	53	45	15	0	20	2.65	-1.8 + 0.8	F	1.17	1.25	0.08	1.25	4.78	1.72	32.81	1.27
E9	B	53	34	15	0	20	2.65	-1.8 + 0.8	F	4.82	1.38	10.81	1.23	1.14	1.97	49.40	1.31
E10	B	53	34	15	0	20	2.65	-1.8 + 0.8	F	3.97	1.53	19.30	1.26	2.22	1.92	47.43	1.26
E11	B	53	34	15	0	20	2.65	-1.8 + 0.8	F	3.63	1.62	26.48	1.25	2.19	1.93	47.84	1.27

D = 165mm; 15° cone

										Floats				Sinks			
Test No.	D_i	D_o (mm)	D_u (mm)	α (deg.)	Bl (mm)	P (kPa)	ρ_{ore} (kg/l)	d_{ore} (mm)	Med grade	Flow-rate (kg/s)	ρ_{slurry} (kg/l)	C_{vo} (v/v%)	ρ_{medium} (kg/l)	Flow-rate (kg/s)	ρ_{slurry} (kg/l)	C_{vu} (v/v%)	ρ_{medium} (kg/l)
E12	B	53	34	15	0	20	2.65	-1.8 + 0.8	F	4.64	1.43	12.19	1.26	1.70	1.94	48.85	1.26
E13	B	53	34	15	0	20	2.65	-1.8 + 0.8	F	2.54	1.25	0.00	1.25	1.82	1.75	28.28	1.40
E14	B	53	25	15	0	20	2.65	-1.8 + 0.8	F	5.46	1.74	30.94	1.33	0.49	1.88	44.58	1.25
E15	B	53	25	15	0	20	2.65	-1.8 + 0.8	F	5.57	1.54	19.78	1.27	0.49	1.90	45.38	1.27
E16	B	53	25	15	0	20	2.65	-1.8 + 0.8	F	5.32	1.46	14.14	1.27	0.50	1.90	45.00	1.28
E17	B	53	25	15	0	20	2.65	-1.8 + 0.8	F	3.03	1.25	0.00	1.25	0.74	1.71	21.93	1.45
F1	B	64	45	15	0	20	2.65	-1.8 + 0.8	F	2.53	1.22	0.01	1.22	2.16	1.74	29.81	1.36
F2	B	64	45	15	0	20	2.65	-1.8 + 0.8	F	2.74	1.28	2.31	1.24	3.48	1.96	51.36	1.23
F3	B	64	45	15	0	20	2.65	-1.8 + 0.8	F	2.80	1.41	12.37	1.23	3.54	1.96	50.51	1.25
F4	B	64	45	15	0	20	2.65	-1.8 + 0.8	F	2.88	1.34	6.75	1.24	3.47	1.95	49.44	1.26
F5	B	64	45	15	0	20	2.65	-1.8 + 0.8	F	1.24	1.22	0.03	1.22	4.46	1.64	27.94	1.25
F6	B	64	34	15	0	20	2.65	-1.8 + 0.8	F	5.01	1.39	9.79	1.25	0.72	1.92	46.59	1.28
F7	B	64	25	15	0	20	2.65	-1.8 + 0.8	F	5.50	1.43	13.21	1.25	0.49	1.89	44.73	1.27
F8	B	64	25	15	0	20	2.65	-1.8 + 0.8	F	5.20	1.40	10.05	1.26	0.51	1.90	45.16	1.29
F9	B	64	25	15	0	20	2.65	-1.8 + 0.8	F	3.48	1.22	0.00	1.22	0.63	1.78	19.55	1.57
G1	B	64	45	15	0	20	2.65	-1.8 + 0.8	F	2.92	1.35	8.32	1.24	3.51	1.96	50.60	1.25
G2	B	64	34	15	0	20	2.65	-1.8 + 0.8	F	3.74	1.59	24.67	1.24	2.24	1.95	49.79	1.25
G3	B	64	25	15	0	20	2.65	-1.8 + 0.8	F	5.68	1.52	19.76	1.24	0.49	1.89	45.08	1.27
G4	B	64	20	15	0	20	2.65	-1.8 + 0.8	F	6.07	1.48	16.45	1.24	0.34	1.86	42.89	1.26
G5	B	53	45	15	0	20	2.65	-1.8 + 0.8	F	2.92	1.41	11.83	1.24	3.52	1.95	50.07	1.25
G6	B	53	34	15	0	20	2.65	-1.8 + 0.8	F	4.54	1.46	15.32	1.24	1.86	1.93	48.49	1.26
G7	B	53	25	15	0	20	2.65	-1.8 + 0.8	F	5.72	1.48	17.52	1.23	0.52	1.89	45.53	1.26

D = 165mm; 15° cone

										Floats				Sinks			
Test No.	D_i	D_o (mm)	D_u (mm)	α (deg.)	Bl (mm)	P (kPa)	ρ_{ore} (kg/l)	d_{ore} (mm)	Med grade	Flow-rate (kg/s)	ρ_{slurry} (kg/l)	C_{vo} (v/v%)	ρ_{medium} (kg/l)	Flow-rate (kg/s)	ρ_{slurry} (kg/l)	C_{vu} (v/v%)	ρ_{medium} (kg/l)
G8	B	53	20	15	0	20	2.65	-1.8 + 0.8	F	5.67	1.61	26.55	1.24	0.34	1.85	42.98	1.25
G9	B	40	45	15	0	20	2.65	-1.8 + 0.8	F	2.75	1.38	9.51	1.25	3.69	1.94	49.46	1.25
G10	B	40	34	15	0	20	2.65	-1.8 + 0.8	F	3.93	1.67	30.02	1.25	2.14	1.91	47.20	1.26
G11	B	40	25	15	0	20	2.65	-1.8 + 0.8	F	5.33	1.74	34.53	1.26	0.65	1.88	44.74	1.25
G12	B	40	20	15	0	20	2.65	-1.8 + 0.8	F	5.55	1.77	34.84	1.29	0.45	1.86	42.82	1.27
H1	B	64	25	15	0	20	2.65	-1.8 + 0.8	F	6.29	1.71	31.61	1.27	0.48	1.90	44.93	1.29
H2	B	64	25	15	0	20	2.65	-1.8 + 0.8	F	6.00	1.62	24.06	1.29	0.49	2.02	50.98	1.36
H3	B	64	25	15	0	20	2.65	-1.8 + 0.8	F	5.64	1.44	11.01	1.29	0.52	1.96	47.62	1.33
H4	B	64	25	15	0	20	2.65	-1.8 + 0.8	F	5.46	1.38	6.75	1.29	0.50	1.95	47.01	1.34
H5	B	64	25	15	0	20	2.65	-1.8 + 0.8	F	5.01	1.32	2.28	1.29	0.53	1.95	46.04	1.36
H6	B	64	34	15	0	20	2.65	-1.8 + 0.8	F	5.33	1.52	17.94	1.27	1.35	1.96	49.25	1.29
H7	B	64	34	15	0	20	2.65	-1.8 + 0.8	F	5.67	1.44	12.19	1.28	0.73	1.97	49.85	1.30
H8	B	64	34	15	0	20	2.65	-1.8 + 0.8	F	5.55	1.44	11.42	1.28	0.74	1.95	49.12	1.28
H9	B	64	34	15	0	20	2.65	-1.8 + 0.8	F	5.34	1.38	6.88	1.28	0.74	1.95	48.03	1.31
H10	B	64	34	15	0	20	2.65	-1.8 + 0.8	F	5.14	1.39	7.37	1.29	0.76	1.98	49.00	1.34
H11	B	64	34	15	0	20	2.65	-1.8 + 0.8	F	5.21	1.33	3.26	1.29	0.82	1.98	48.76	1.33
H12	B	64	45	15	0	20	2.65	-1.8 + 0.8	F	3.32	1.47	14.89	1.27	3.19	1.97	50.28	1.28
H13	B	64	45	15	0	20	2.65	-1.8 + 0.8	F	3.15	1.46	13.64	1.27	3.49	1.98	51.20	1.28
H14	B	64	45	15	0	20	2.65	-1.8 + 0.8	F	2.99	1.33	4.19	1.27	3.46	1.97	50.24	1.28
H15	B	64	45	15	0	20	2.65	-1.8 + 0.8	F	3.07	1.37	6.74	1.27	3.47	1.99	51.84	1.28
I1	B	64	34	15	0	20	2.65	-1.8 + 0.8	F	6.02	1.45	11.74	1.29	0.75	1.95	47.08	1.32
I2	B	64	30	15	0	20	2.65	-1.8 + 0.8	F	6.15	1.47	12.97	1.29	0.60	1.94	46.20	1.33

D = 165mm; 15° cone

										Floats				Sinks			
Test No.	D_i	D_o (mm)	D_u (mm)	α (deg.)	Bl (mm)	P (kPa)	ρ_{ore} (kg/l)	d_{ore} (mm)	Med grade	Flow-rate (kg/s)	ρ_{slurry} (kg/l)	C_{vo} (v/v%)	ρ_{medium} (kg/l)	Flow-rate (kg/s)	ρ_{slurry} (kg/l)	C_{vu} (v/v%)	ρ_{medium} (kg/l)
I3	B	64	30	15	0	20	2.65	-1.8 + 0.8	F	6.07	1.47	13.22	1.29	0.62	1.93	45.94	1.33
I4	B	53	34	15	0	20	2.65	-1.8 + 0.8	F	5.76	1.48	13.50	1.30	0.82	1.95	46.88	1.33
I5	B	53	34	15	0	20	2.65	-1.8 + 0.8	F	5.76	1.42	9.55	1.30	0.85	1.96	47.98	1.33
I6	B	40	34	15	0	20	2.65	-1.8 + 0.8	F	5.27	1.47	12.51	1.30	0.99	1.95	47.39	1.33
I7	B	40	34	15	0	20	2.65	-1.8 + 0.8	F	5.28	1.48	13.44	1.29	1.01	1.94	46.97	1.32
I8	B	40	25	15	0	20	2.65	-1.8 + 0.8	F	5.41	1.50	14.47	1.30	0.65	1.92	44.55	1.33
J1	B	40	34	15	0	20	2.65	-1.8 + 0.8	F	4.25	1.36	6.42	1.27	1.09	1.94	47.06	1.31
J2	B	40	34	15	0	20	2.65	-1.8 + 0.8	F	4.71	1.54	19.85	1.26	1.55	1.92	47.00	1.27
J3	B	40	34	15	0	20	2.65	-1.8 + 0.8	F	4.32	1.52	18.52	1.26	1.93	1.91	46.31	1.27
J4	B	40	34	15	0	20	2.65	-1.8 + 0.8	F	4.96	1.51	17.90	1.26	0.98	1.92	46.15	1.29
J5	B	40	45	15	0	20	2.65	-1.8 + 0.8	F	2.90	1.34	5.30	1.27	3.67	1.96	49.89	1.28
J6	B	40	30	15	0	20	2.65	-1.8 + 0.8	F	5.18	1.51	17.70	1.26	0.79	1.90	45.53	1.28
J7	B	40	30	15	0	20	2.65	-1.8 + 0.8	F	5.20	1.51	17.59	1.27	0.81	1.91	45.54	1.29
J8	B	64	30	15	0	20	2.65	-1.8 + 0.8	F	4.75	1.28	0.29	1.28	1.49	1.97	48.09	1.34
J9	B	64	30	15	0	20	2.65	-1.8 + 0.8	F	5.41	1.38	7.49	1.28	0.63	1.94	46.30	1.32
J10	B	64	30	15	0	20	2.65	-1.8 + 0.8	F	5.97	1.47	14.27	1.28	0.61	1.93	46.44	1.30
J11	B	64	25	15	0	20	2.65	-1.8 + 0.8	F	6.02	1.46	12.76	1.28	0.49	1.92	45.25	1.31
J12	B	64	34	15	0	20	2.65	-1.8 + 0.8	F	5.71	1.40	9.02	1.28	0.75	1.95	48.02	1.30
J13	B	64	34	15	0	20	2.65	-1.8 + 0.8	F	5.76	1.47	13.81	1.28	0.76	1.91	45.83	1.29
K1	B	64	45	15	0	20	2.65	-1.8 + 0.8	M	2.86	1.41	11.53	1.25	3.63	2.00	51.20	1.31
K2	B	64	34	15	0	20	2.65	-1.8 + 0.8	M	5.69	1.68	29.85	1.27	0.74	1.99	48.65	1.36
K3	B	64	25	15	0	20	2.65	-1.8 + 0.8	M	5.75	1.76	35.40	1.27	0.47	1.94	44.86	1.36

D = 165mm; 15° cone

										Floats				Sinks			
Test No.	D_i	D_o (mm)	D_u (mm)	α (deg.)	Bl (mm)	P (kPa)	ρ_{ore} (kg/l)	d_{ore} (mm)	Med grade	Flow-rate (kg/s)	ρ_{slurry} (kg/l)	C_{vo} (v/v%)	ρ_{medium} (kg/l)	Flow-rate (kg/s)	ρ_{slurry} (kg/l)	C_{vu} (v/v%)	ρ_{medium} (kg/l)
K4	B	40	25	15	0	20	2.65	-1.8 + 0.8	M	5.12	1.62	25.05	1.27	0.65	1.93	45.06	1.34
K5	B	40	34	15	0	20	2.65	-1.8 + 0.8	M	4.84	1.60	23.51	1.27	0.96	1.96	46.91	1.35
K6	B	40	45	15	0	20	2.65	-1.8 + 0.8	M	2.67	1.31	3.47	1.26	3.83	1.98	50.48	1.30
K7	B	64	45	15	0	20	2.65	-1.8 + 0.8	M	2.99	1.53	14.00	1.35	3.65	2.02	50.20	1.39
K8	B	64	34	15	0	20	2.65	-1.8 + 0.8	M	5.77	1.75	30.33	1.35	0.72	2.01	47.30	1.44
K9	B	64	34	15	0	20	2.65	-1.8 + 0.8	M	6.52	1.68	25.25	1.35	0.73	2.02	47.42	1.45
K10	B	64	34	15	0	20	2.65	-1.8 + 0.8	M	6.66	1.55	14.86	1.36	0.80	2.06	47.52	1.53
K11	B	64	25	15	0	20	2.65	-1.8 + 0.8	M	5.82	1.58	16.24	1.37	0.50	2.04	46.38	1.51
K12	B	64	25	15	0	20	2.65	-1.8 + 0.8	M	6.49	1.55	13.63	1.37	0.53	2.04	46.13	1.52
K13	B	64	25	15	0	20	2.65	-1.8 + 0.8	M	6.54	1.42	3.88	1.37	0.56	2.07	46.31	1.56
K14	B	64	45	15	0	20	2.65	-1.8 + 0.8	M	3.96	2.05	35.27	1.72	3.44	2.02	43.59	1.53
K15	B	64	34	15	0	20	2.65	-1.8 + 0.8	M	6.53	1.49	8.42	1.39	0.65	2.18	52.73	1.65
K16	B	64	34	15	0	20	2.65	-1.8 + 0.8	M	7.65	1.82	27.87	1.49	0.77	2.10	46.94	1.61
K17	B	64	34	15	0	20	2.65	-1.8 + 0.8	M	6.88	1.59	7.53	1.51	0.80	2.11	46.81	1.64
K18	B	64	25	15	0	20	2.65	-1.8 + 0.8	M	6.65	1.78	24.02	1.50	0.43	2.08	45.76	1.61
L1	B	64	25	15	0	25	2.65	-1.8 + 0.8	F	5.79	1.40	8.58	1.29	0.54	1.94	44.94	1.36
L2	B	64	25	15	0	29	2.65	-1.8 + 0.8	F	6.20	1.44	11.00	1.29	0.57	1.94	45.14	1.36
L3	B	64	34	15	0	25	2.65	-1.8 + 0.8	F	5.57	1.39	7.49	1.28	0.81	1.96	47.44	1.34
L4	B	64	34	15	0	29	2.65	-1.8 + 0.8	F	6.07	1.37	6.50	1.29	0.84	1.97	47.88	1.34
L5	B	64	45	15	0	20	2.65	-1.8 + 0.8	F	3.15	1.36	6.36	1.27	3.35	2.01	53.45	1.27
L6	B	64	45	15	0	20	2.65	-1.8 + 0.8	F	3.08	1.31	2.94	1.27	3.46	1.97	50.48	1.28
L7	B	64	45	15	0	20	2.65	-1.8 + 0.8	F	1.57	1.26	0.03	1.26	4.66	1.71	30.99	1.29

D = 165mm; 15° cone

										Floats				Sinks			
Test No.	D_i	D_o (mm)	D_u (mm)	α (deg.)	Bl (mm)	P (kPa)	ρ_{ore} (kg/l)	d_{ore} (mm)	Med grade	Flow-rate (kg/s)	ρ_{slurry} (kg/l)	C_{vo} (v/v%)	ρ_{medium} (kg/l)	Flow-rate (kg/s)	ρ_{slurry} (kg/l)	C_{vu} (v/v%)	ρ_{medium} (kg/l)
L8	B	64	45	15	0	20	2.65	-1.8 + 0.8	F	2.69	1.25	0.01	1.25	2.40	1.63	22.16	1.34
L9	B	64	40	15	0	20	2.65	-1.8 + 0.8	F	4.11	1.42	10.43	1.28	2.36	1.95	48.99	1.28
L10	B	64	45	15	0	20	2.65	-1.8 + 0.8	F	3.45	1.50	9.82	1.38	3.49	2.02	50.21	1.38
L11	B	64	34	15	0	20	2.65	-1.8 + 0.8	F	6.17	1.80	33.36	1.37	0.68	2.01	48.51	1.40
L12	B	64	34	15	0	25	2.65	-1.8 + 0.8	F	6.69	1.74	28.43	1.38	0.73	2.01	48.88	1.40
L13	B	64	34	15	0	29	2.65	-1.8 + 0.8	F	6.34	1.50	8.49	1.39	0.82	2.03	48.61	1.44
L14	B	64	25	15	0	20	2.65	-1.8 + 0.8	F	5.97	1.67	22.20	1.38	0.46	2.00	47.54	1.41
L15	B	64	25	15	0	25	2.65	-1.8 + 0.8	F	6.73	1.66	21.19	1.39	0.48	1.99	46.44	1.41
L16	B	64	25	15	0	29	2.65	-1.8 + 0.8	F	6.43	1.50	8.68	1.39	0.53	2.00	46.78	1.43
M1	B	64	45	15	0	20	2.65	-3 + 1	F	3.19	1.33	3.55	1.28	3.27	1.99	51.31	1.30
M2	B	64	45	15	0	20	2.65	-3 + 1	F	3.16	1.39	7.74	1.28	3.25	1.99	51.19	1.30
M3	B	64	34	15	0	20	2.65	-3 + 1	F	5.51	1.62	24.38	1.29	0.76	2.00	51.02	1.33
M4	B	64	34	15	0	25	2.65	-3 + 1	F	5.76	1.48	13.82	1.30	0.78	2.02	50.20	1.38
M5	B	64	25	15	0	20	2.65	-3 + 1	F	5.57	1.57	19.95	1.30	0.47	1.98	47.69	1.36
M6	B	64	25	15	0	20	2.65	-3 + 1	F	5.50	1.65	22.12	1.37	0.46	2.01	47.93	1.43
M7	B	64	34	15	0	29	2.65	-3 + 1	F	6.36	1.49	9.36	1.37	0.78	2.07	50.77	1.47
M8	B	64	34	15	0	25	2.65	-3 + 1	F	6.19	1.66	23.21	1.37	0.77	2.04	50.09	1.42
M9	B	64	34	15	0	20	2.65	-3 + 1	F	5.48	1.61	18.92	1.37	0.72	2.04	50.13	1.42
M10	B	64	45	15	0	20	2.65	-3 + 1	F	3.29	1.53	13.17	1.36	3.35	2.02	50.09	1.38
M11	B	64	45	15	0	20	2.65	-3 + 1	F	3.60	1.59	8.33	1.49	3.27	2.14	55.67	1.51
M12	B	64	34	15	0	30	2.65	-3 + 1	F	6.96	1.76	22.41	1.50	0.76	2.11	51.28	1.54
M13	B	64	34	15	0	27	2.65	-3 + 1	F	6.81	1.79	25.29	1.49	0.73	2.10	50.70	1.54

D = 165mm; 15° cone

										Floats				Sinks			
Test No.	D_i	D_o (mm)	D_u (mm)	α (deg.)	Bl (mm)	P (kPa)	ρ_{ore} (kg/l)	d_{ore} (mm)	Med grade	Flow-rate (kg/s)	ρ_{slurry} (kg/l)	C_{vo} (v/v%)	ρ_{medium} (kg/l)	Flow-rate (kg/s)	ρ_{slurry} (kg/l)	C_{vu} (v/v%)	ρ_{medium} (kg/l)
M14	B	64	34	15	0	22	2.65	-3 + 1	F	6.26	1.74	20.54	1.51	0.70	2.11	51.17	1.54
M15	B	64	25	15	0	22	2.65	-3 + 1	F	6.46	1.83	27.97	1.51	0.43	2.09	50.12	1.54
M16	B	64	20	15	0	22	2.65	-3 + 1	F	6.62	1.80	25.57	1.51	0.26	2.06	47.02	1.55
M17	B	64	30	15	0	22	2.65	-3 + 1	F	6.39	1.76	22.13	1.51	0.55	2.11	50.75	1.55
M18	B	64	40	15	0	22	2.65	-3 + 1	F	4.87	1.62	9.72	1.51	1.81	2.14	54.07	1.53
N1	B	64	45	15	0	20	2.65	-3 + 1	M	2.75	1.41	10.23	1.27	3.39	2.04	53.12	1.35
N2	B	64	34	15	0	20	2.65	-3 + 1	M	5.21	1.66	27.81	1.28	0.77	2.05	52.43	1.39
N3	B	64	25	15	0	20	2.65	-3 + 1	M	5.50	1.66	27.68	1.29	0.49	2.00	48.27	1.40
N4	B	64	25	15	0	20	2.65	-3 + 1	M	5.50	1.70	25.78	1.37	0.48	2.06	48.37	1.50
N5	B	64	34	15	0	20	2.65	-3 + 1	M	5.29	1.70	26.02	1.37	0.75	2.09	51.30	1.50
N6	B	64	45	15	0	20	2.65	-3 + 1	M	2.97	1.41	3.64	1.36	3.60	2.05	51.55	1.42
N7	B	64	45	15	0	22	2.65	-3 + 1	M	3.14	1.84	24.50	1.57	3.59	2.26	56.91	1.75
N8	B	64	34	15	0	22	2.65	-3 + 1	M	6.19	1.59	13.98	1.41	0.71	2.00	46.37	1.43
N9	B	64	25	15	0	22	2.65	-3 + 1	M	6.39	1.76	23.87	1.48	0.44	2.10	48.35	1.59
O1	B	64	45	15	0	22	2.65	-1.8 + 0.8	F	3.69	1.68	19.47	1.45	3.57	2.06	49.19	1.50
O2	B	64	34	15	0	22	2.65	-1.8 + 0.8	F	6.20	1.72	22.15	1.46	0.65	2.08	47.69	1.55
O3	B	64	25	15	0	22	2.65	-1.8 + 0.8	F	6.44	1.81	29.49	1.46	0.44	2.07	46.44	1.56
O4	B	64	25	15	0	25	2.65	-1.8 + 0.8	F	6.67	1.81	14.21	1.67	0.39	2.17	47.06	1.74
O5	B	64	34	15	0	25	2.65	-1.8 + 0.8	F	6.50	1.79	12.89	1.66	0.59	2.17	48.00	1.73
O6	B	64	45	15	0	25	2.65	-1.8 + 0.8	F	4.06	1.76	10.28	1.65	3.73	2.14	47.25	1.68
P1	B	64	34	15	0	22	2.65	-1.8 + 0.8	C	6.52	1.93	29.62	1.62	0.47	2.25	46.83	1.89
P2	B	64	34	15	0	27	2.65	-1.8 + 0.8	C	7.45	1.99	36.15	1.62	0.48	2.27	46.96	1.93

D = 165mm; 15° cone

										Floats				Sinks			
Test No.	D_i	D_o (mm)	D_u (mm)	α (deg.)	Bl (mm)	P (kPa)	ρ_{ore} (kg/l)	d_{ore} (mm)	Med grade	Flow-rate (kg/s)	ρ_{slurry} (kg/l)	C_{vo} (v/v%)	ρ_{medium} (kg/l)	Flow-rate (kg/s)	ρ_{slurry} (kg/l)	C_{vu} (v/v%)	ρ_{medium} (kg/l)
P3	B	64	34	15	0	31	2.65	-1.8 + 0.8	C	8.06	2.02	39.61	1.61	0.53	2.26	47.33	1.91
P4	B	64	25	15	0	22	2.65	-1.8 + 0.8	C	6.73	1.96	32.64	1.62	0.31	2.25	45.76	1.91
P5	B	64	45	15	0	22	2.65	-3 + 1	C	3.40	1.69	9.95	1.58	3.82	2.19	50.24	1.73
P6	B	64	34	15	0	22	2.65	-3 + 1	C	6.35	1.89	26.33	1.62	0.63	2.24	49.64	1.83
P7	B	64	34	15	0	27	2.65	-3 + 1	C	7.20	1.90	27.84	1.61	0.64	2.25	49.50	1.86
P8	B	64	34	15	0	31	2.65	-3 + 1	C	8.12	1.96	34.26	1.60	0.63	2.26	49.48	1.88
P9	B	64	25	15	0	22	2.65	-3 + 1	C	6.51	1.85	22.84	1.62	0.40	2.23	48.04	1.85
Q1	A	64	25	15	0	25	2.65	-1.8 + 0.8	F	9.00	1.55	13.60	1.37	0.64	2.02	45.99	1.49
Q2	A	64	34	15	0	25	2.65	-1.8 + 0.8	F	8.70	1.52	11.68	1.37	0.96	2.03	47.26	1.48
Q3	A	64	45	15	0	25	2.65	-1.8 + 0.8	F	5.15	1.37	0.24	1.36	4.58	2.00	47.61	1.41
Q4	A	64	45	15	0	25	2.65	-1.8 + 0.8	F	5.70	1.49	1.42	1.47	4.71	2.04	46.79	1.50
Q5	A	64	34	15	0	25	2.65	-1.8 + 0.8	F	9.11	1.70	18.46	1.48	0.92	2.06	46.42	1.55
Q6	A	64	25	15	0	25	2.65	-1.8 + 0.8	F	9.65	1.67	16.33	1.48	0.62	2.06	45.15	1.57
Q7	A	64	25	15	0	25	2.65	-1.8 + 0.8	F	9.10	1.74	5.23	1.69	0.66	2.15	45.18	1.75
Q8	A	64	34	15	0	25	2.65	-1.8 + 0.8	F	9.31	1.77	8.47	1.69	1.02	2.15	46.37	1.73
Q9	A	64	45	15	0	25	2.65	-1.8 + 0.8	F	6.62	1.73	3.80	1.69	4.98	2.14	46.14	1.71
Q10	A	53	45	15	0	25	2.65	-1.8 + 0.8	F	5.66	1.73	3.91	1.69	5.69	2.13	46.11	1.69
Q11	A	53	34	15	0	25	2.65	-1.8 + 0.8	F	10.55	1.88	19.58	1.69	1.03	2.15	45.65	1.73
Q12	A	53	25	15	0	25	2.65	-1.8 + 0.8	F	10.64	1.86	16.98	1.70	0.68	2.14	44.35	1.73
Q13	A	40	25	15	0	25	2.65	-1.8 + 0.8	F	9.35	1.84	14.67	1.70	0.83	2.13	44.13	1.73
Q14	A	40	34	15	0	25	2.65	-1.8 + 0.8	F	8.70	1.85	15.59	1.70	1.30	2.16	46.54	1.73
Q15	A	40	45	15	0	25	2.65	-1.8 + 0.8	F	5.67	1.77	7.21	1.71	5.84	2.14	46.09	1.71

D = 165mm; 15° cone

										Floats				Sinks			
Test No.	D_i	D_o (mm)	D_u (mm)	α (deg.)	Bl (mm)	P (kPa)	ρ_{ore} (kg/l)	d_{ore} (mm)	Med grade	Flow-rate (kg/s)	ρ_{slurry} (kg/l)	C_{vo} (v/v%)	ρ_{medium} (kg/l)	Flow-rate (kg/s)	ρ_{slurry} (kg/l)	C_{vu} (v/v%)	ρ_{medium} (kg/l)
Q16	A	40	34	15	0	25	2.65	-5 + 3	F	9.39	1.83	11.41	1.72	1.44	2.16	46.88	1.73
Q17	A	40	25	15	0	25	2.65	-5 + 3	F	8.50	1.89	18.45	1.71	0.86	2.13	43.38	1.73
Q18	A	64	25	15	0	25	2.65	-5 + 3	F	9.50	1.79	6.79	1.72	0.70	2.15	44.44	1.75
Q19	A	64	34	15	0	25	2.65	-5 + 3	F	9.76	1.81	9.58	1.72	1.18	2.17	46.99	1.74
R1	B	40	45	15	0	20	2.65	-1.8 + 0.8	C	2.07	1.49	17.10	1.25	3.92	1.96	47.02	1.34
R2	B	40	34	15	0	20	2.65	-1.8 + 0.8	C	4.63	1.71	31.52	1.28	1.00	1.97	45.19	1.41
R3	B	40	25	15	0	20	2.65	-1.8 + 0.8	C	4.95	1.71	30.93	1.28	0.68	1.96	43.60	1.43
R4	B	64	25	15	0	20	2.65	-1.8 + 0.8	C	5.49	1.55	19.29	1.29	0.52	2.00	44.04	1.48
R5	B	64	34	15	0	20	2.65	-1.8 + 0.8	C	5.22	1.53	18.33	1.28	0.80	2.03	47.18	1.48
R6	B	64	45	15	0	20	2.65	-1.8 + 0.8	C	2.46	1.38	8.45	1.26	3.91	1.99	49.21	1.35
R7	B	64	45	15	0	20	2.65	-1.8 + 0.8	C	2.64	1.54	15.37	1.34	3.98	2.03	48.86	1.45
R8	B	64	34	15	0	20	2.65	-1.8 + 0.8	C	5.45	1.64	21.76	1.36	0.80	2.06	47.05	1.54
R9	B	64	25	15	0	20	2.65	-1.8 + 0.8	C	5.79	1.62	19.83	1.36	0.53	2.04	44.59	1.55
R10	B	64	25	15	0	25	2.65	-1.8 + 0.8	C	6.37	1.80	10.60	1.70	0.45	2.26	45.34	1.94
R11	B	64	34	15	0	25	2.65	-1.8 + 0.8	C	6.42	1.83	14.69	1.69	0.68	2.24	45.78	1.90
R12	B	64	45	15	0	25	2.65	-1.8 + 0.8	C	4.02	1.81	16.19	1.65	4.01	2.18	46.48	1.78

7.3.2. Raw data for tests performed with cone A.

D = 165mm; 20°cone (Cone A)

										Floats				Sinks			
Test No.	D_i	D_o (mm)	D_u (mm)	α (deg.)	Bl (mm)	P (kPa)	ρ_{ore} (kg/l)	d_{ore} (mm)	Med grade	Flow-rate (kg/s)	ρ_{slurry} (kg/l)	C_{vo} (v/v%)	ρ_{medium} (kg/l)	Flow-rate (kg/s)	ρ_{slurry} (kg/l)	C_{vu} (v/v%)	ρ_{medium} (kg/l)
S8	B	40	45	20	200	22	2.65	-1.8 + 0.8	M	1.77	1.32	2.57	1.28	3.65	1.99	52.06	1.27
S9	B	53	45	20	200	20	2.65	-1.8 + 0.8	M	1.66	1.34	4.31	1.28	3.69	1.94	48.29	1.27
S10	B	64	45	20	200	20	2.65	-1.8 + 0.8	M	1.80	1.38	7.49	1.28	3.81	1.96	50.09	1.27
T1	B	64	45	20	0	20	2.65	-1.8 + 0.8	M	2.42	1.32	4.95	1.25	3.28	1.98	50.66	1.30
T2	B	64	34	20	0	20	2.65	-1.8 + 0.8	M	3.42	1.49	16.74	1.25	1.88	1.93	46.82	1.30
T3	B	64	25	20	0	20	2.65	-1.8 + 0.8	M	4.30	1.57	20.51	1.29	0.90	1.94	46.51	1.33
T4	B	64	25	20	200	20	2.65	-1.8 + 0.8	M	4.35	1.49	15.29	1.28	0.94	1.91	45.42	1.30
T5	B	64	34	20	200	20	2.65	-1.8 + 0.8	M	3.46	1.36	8.46	1.24	1.96	2.08	56.99	1.32
T6	B	64	45	20	200	20	2.65	-1.8 + 0.8	M	1.95	1.56	18.77	1.31	3.77	1.89	45.89	1.24
U1	B	64	34	20	200	20	2.65	-1.8 + 0.8	M	3.03	1.41	10.20	1.27	1.94	1.96	48.99	1.29
U2	B	64	25	20	200	20	2.65	-1.8 + 0.8	M	3.96	1.46	13.82	1.27	0.98	1.93	47.04	1.29
U3	B	64	25	20	200	25	2.65	-1.8 + 0.8	M	4.69	1.50	11.16	1.36	1.02	1.98	46.35	1.41
U4	B	64	25	20	200	30	2.65	-1.8 + 0.8	M	5.47	1.51	11.82	1.36	1.03	1.99	45.87	1.43
U5	B	64	34	20	200	25	2.65	-1.8 + 0.8	M	3.67	1.43	5.15	1.36	1.98	2.00	48.67	1.39
U6	B	64	34	20	200	30	2.65	-1.8 + 0.8	M	4.37	1.46	7.43	1.36	2.06	2.02	48.95	1.41
U7	B	64	45	20	200	20	2.65	-1.8 + 0.8	M	1.48	1.36	0.65	1.35	3.56	2.06	54.18	1.37
V1	B	64	25	20	0	25	2.65	-1.8 + 0.8	M	4.05	1.43	11.00	1.28	0.99	1.98	46.52	1.39
V2	B	64	34	20	0	25	2.65	-1.8 + 0.8	M	3.13	1.39	8.17	1.27	1.99	1.98	48.04	1.36
V3	B	64	45	20	0	25	2.65	-1.8 + 0.8	M	2.08	1.46	14.50	1.26	3.61	1.98	49.79	1.32
V4	B	64	45	20	0	25	2.65	-1.8 + 0.8	M	2.03	1.50	11.71	1.34	3.73	2.00	48.83	1.39
V5	B	64	34	20	0	25	2.65	-1.8 + 0.8	M	3.56	1.59	18.29	1.36	2.01	2.04	49.86	1.43
V6	B	64	25	20	0	25	2.65	-1.8 + 0.8	M	4.51	1.58	17.50	1.36	1.00	2.00	46.50	1.44

D = 165mm; 20°cone (Cone A)

										Floats				Sinks			
Test No.	D_i	D_o (mm)	D_u (mm)	α (deg.)	Bl (mm)	P (kPa)	ρ_{ore} (kg/l)	d_{ore} (mm)	Med grade	Flow-rate (kg/s)	ρ_{slurry} (kg/l)	C_{vo} (v/v%)	ρ_{medium} (kg/l)	Flow-rate (kg/s)	ρ_{slurry} (kg/l)	C_{vu} (v/v%)	ρ_{medium} (kg/l)
X1	B	64	45	20	0	30	2.65	-1.8 + 0.8	F	2.73	1.43	11.62	1.27	3.91	1.98	50.70	1.30
X2	B	64	34	20	0	25	2.65	-1.8 + 0.8	F	2.93	1.48	15.08	1.27	2.34	1.92	46.28	1.29
X3	B	64	34	20	0	30	2.65	-1.8 + 0.8	F	4.36	1.50	17.05	1.27	2.43	1.94	47.54	1.30
X4	B	64	34	20	0	36	2.65	-1.8 + 0.8	F	4.64	1.40	9.56	1.27	2.57	1.95	47.75	1.31
X5	B	64	25	20	0	25	2.65	-1.8 + 0.8	F	4.11	1.44	11.63	1.28	1.06	1.90	43.35	1.33
X6	B	64	25	20	0	30	2.65	-1.8 + 0.8	F	5.00	1.43	10.32	1.29	1.15	1.91	43.09	1.34
X7	B	64	25	20	0	36	2.65	-1.8 + 0.8	F	5.21	1.36	5.64	1.28	1.21	1.91	42.93	1.36
X8	B	64	25	20	0	29	2.65	-1.8 + 0.8	F	4.77	1.75	10.09	1.65	1.03	2.12	44.48	1.70
X9	B	64	25	20	0	35	2.65	-1.8 + 0.8	F	6.42	1.79	23.25	1.53	1.07	2.19	47.61	1.77
X10	B	64	25	20	0	42	2.65	-1.8 + 0.8	F	7.36	1.80	25.41	1.52	1.07	2.06	44.22	1.60
X11	B	64	34	20	0	29	2.65	-1.8 + 0.8	F	3.97	1.61	8.24	1.52	2.34	2.05	46.41	1.53
X12	B	64	34	20	0	35	2.65	-1.8 + 0.8	F	5.06	1.61	8.52	1.51	2.49	2.06	46.37	1.55
X13	B	64	34	20	0	42	2.65	-1.8 + 0.8	F	5.48	1.63	9.74	1.52	2.61	2.11	45.82	1.65
X14	B	64	45	20	0	35	2.65	-1.8 + 0.8	F	3.55	1.64	12.52	1.50	3.99	2.04	46.46	1.51
X15	B	64	45	20	0	39	2.65	-1.8 + 0.8	F	4.62	1.86	15.90	1.71	4.00	1.94	40.88	1.45
X16	B	64	34	20	0	33	2.65	-1.8 + 0.8	F	5.19	1.89	17.90	1.73	2.06	2.14	44.86	1.73
X17	B	64	34	20	0	39	2.65	-1.8 + 0.8	F	6.14	1.94	20.22	1.77	2.02	2.15	45.37	1.74
X18	B	64	34	20	0	47	2.65	-1.8 + 0.8	F	7.06	1.95	23.03	1.74	2.18	2.15	44.90	1.74
X19	B	64	25	20	0	33	2.65	-1.8 + 0.8	F	6.18	1.96	24.58	1.74	0.97	2.13	43.41	1.73
X20	B	64	25	20	0	39	2.65	-1.8 + 0.8	F	7.28	1.97	23.19	1.76	0.95	2.23	46.12	1.86
X21	B	64	25	20	0	47	2.65	-1.8 + 0.8	F	8.07	1.96	23.37	1.75	0.99	2.14	43.29	1.75

D = 165mm; 20°cone (Cone A)

										Floats				Sinks			
Test No.	D_i	D_o (mm)	D_u (mm)	α (deg.)	BI (mm)	P (kPa)	ρ_{ore} (kg/l)	d_{ore} (mm)	Med grade	Flow-rate (kg/s)	ρ_{slurry} (kg/l)	C_{vo} (v/v%)	ρ_{medium} (kg/l)	Flow-rate (kg/s)	ρ_{slurry} (kg/l)	C_{vu} (v/v%)	ρ_{medium} (kg/l)
Y1	B	53	45	20	0	30	2.65	-1.8 + 0.8	F	2.96	1.47	14.18	1.28	3.83	1.93	46.92	1.30
Y2	B	53	34	20	0	25	2.65	-1.8 + 0.8	F	3.70	1.56	20.98	1.27	2.19	1.93	46.93	1.30
Y3	B	53	34	20	0	30	2.65	-1.8 + 0.8	F	4.37	1.51	16.99	1.28	2.30	1.91	44.81	1.30
Y4	B	53	34	20	0	36	2.65	-1.8 + 0.8	F	4.49	1.44	11.57	1.29	2.51	1.92	45.18	1.32
Y5	B	53	25	20	0	25	2.65	-1.8 + 0.8	F	4.35	1.45	11.42	1.29	1.05	1.92	44.40	1.33
Y6	B	53	25	20	0	30	2.65	-1.8 + 0.8	F	5.08	1.48	14.15	1.29	1.11	1.91	43.74	1.34
Y7	B	53	25	20	0	36	2.65	-1.8 + 0.8	F	5.55	1.56	19.70	1.29	1.16	1.91	43.22	1.35
Y8	B	40	25	20	0	25	2.65	-1.8 + 0.8	F	4.06	1.64	25.47	1.29	1.14	1.89	42.85	1.32
Y9	B	40	25	20	0	30	2.65	-1.8 + 0.8	F	4.86	1.58	20.61	1.30	1.24	1.90	42.93	1.33
Y10	B	40	25	20	0	36	2.65	-1.8 + 0.8	F	5.28	1.54	18.31	1.29	1.33	1.91	43.81	1.33
Y11	B	40	34	20	0	25	2.65	-1.8 + 0.8	F	3.24	1.44	11.35	1.29	2.32	1.91	44.97	1.30
Y12	B	40	34	20	0	30	2.65	-1.8 + 0.8	F	3.76	1.44	11.00	1.29	2.51	1.92	45.60	1.31
Y13	B	40	34	20	0	36	2.65	-1.8 + 0.8	F	4.36	1.48	13.99	1.29	2.65	1.92	45.35	1.31
Y14	B	40	40	20	0	25	2.65	-1.8 + 0.8	F	2.70	1.49	15.10	1.28	2.99	1.94	47.23	1.30
Y15	B	40	40	20	0	30	2.65	-1.8 + 0.8	F	3.34	1.48	13.98	1.29	3.21	1.92	45.96	1.30
Y16	B	40	40	20	0	36	2.65	-1.8 + 0.8	F	3.75	1.47	13.13	1.30	3.36	1.92	45.58	1.30
Y17	A	64	34	20	0	25	2.65	-1.8 + 0.8	F	6.72	1.52	15.88	1.31	2.29	1.93	46.36	1.31
Y18	A	64	34	20	0	30	2.65	-1.8 + 0.8	F	5.89	1.32	0.75	1.31	2.52	1.93	45.62	1.33
Y19	A	64	25	20	0	25	2.65	-1.8 + 0.8	F	6.99	1.42	6.33	1.34	1.12	1.92	44.46	1.34
Y20	A	64	25	20	0	30	2.65	-1.8 + 0.8	F	7.60	1.46	8.81	1.34	1.30	1.96	46.41	1.36
Y21	A	40	25	20	0	25	2.65	-1.8 + 0.8	F	6.46	1.43	8.78	1.31	1.39	1.89	43.09	1.32
Y22	A	40	25	20	0	30	2.65	-1.8 + 0.8	F	7.00	1.46	10.92	1.32	1.54	1.92	44.17	1.34
Y23	A	40	34	20	0	25	2.65	-1.8 + 0.8	F	6.17	1.54	17.46	1.31	2.75	1.94	47.00	1.31

7.3.3. Raw data for cyclone operating with cone B.

D = 165mm; 20°cone (Cone B)

										Floats				Sinks			
Test No.	D_i	D_o (mm)	D_u (mm)	α (deg.)	Bl (mm)	P (kPa)	ρ_{ore} (kg/l)	d_{ore} (mm)	Med grade	Flow-rate (kg/s)	ρ_{slurry} (kg/l)	C_{vo} (v/v%)	ρ_{medium} (kg/l)	Flow-rate (kg/s)	ρ_{slurry} (kg/l)	C_{vu} (v/v%)	ρ_{medium} (kg/l)
S1	B	40	45	20	200	20	2.65	-1.8 + 0.8	F	2.17	1.37	6.85	1.27	4.64	1.93	47.45	1.28
S2	B	64	45	20	200	20	2.65	-1.8 + 0.8	F	1.54	1.33	3.04	1.29	4.33	1.93	47.40	1.29
S3	B	64	45	20	200	20	2.65	-1.8 + 0.8	F	1.62	1.46	6.31	1.38	4.26	2.01	48.84	1.39
S4	B	53	45	20	200	20	2.65	-1.8 + 0.8	F	1.90	1.43	3.83	1.38	4.37	1.98	47.38	1.37
S5	B	40	45	20	200	20	2.65	-1.8 + 0.8	F	1.52	1.45	5.65	1.38	4.49	2.01	49.78	1.38
S6	B	64	45	20	200	22	2.65	-1.8 + 0.8	F	1.92	1.60	10.03	1.49	4.36	2.06	49.91	1.47
S7	B	64	45	20	200	30	2.65	-1.8 + 0.8	F	2.89	1.73	5.99	1.67	4.43	2.13	47.56	1.65